Vrije Universiteit Brussel

Faculteit Wetenschappen en Bio-ingenieurswetenschappen
Departement Natuurkunde

Unconventional signatures of supersymmetry

Karen De Causmaecker

Promotor
Prof. Dr. Jorgen D'Hondt

Proefschrift ingediend met het oog op het behalen van de academische graad Doctor in de Wetenschappen

Augustus 2016

Doctoral examination commission:

Prof. Dr. Nick van Eijndhoven (Vrije Universiteit Brussel, *chair*)
Prof. Dr. Freya Blekman (Vrije Universiteit Brussel, *secretary*)
Prof. Dr. Jorgen D'Hondt (Vrije Universiteit Brussel, *promotor*)
Prof. Dr. Alberto Mariotti (Vrije Universiteit Brussel)
Prof. Dr. Kentarou Mawatari (LPSC, Grenoble)
Prof. Dr. Benjamin Fuks (LPTHE, Paris)
Prof. Dr. Fabio Maltoni (CP3, Louvain)
Prof. Dr. Ann Dooms (Vrije Universiteit Brussel)

Contents

Introduction

Even though we live our daily life at a scale of roughly 10^{-3} to 10^{3} meter, scientific research has opened up a much wider range of scales. Cosmology allows us to get an idea of the universe at scales of $\mathcal{O}(10^{26})$ m while particle colliders, like the Large Hadron Collider (LHC) at the CERN laboratory in Geneva, search for the fundamental building blocks of Nature at a scale of $\mathcal{O}(10^{-16})$ m. Needless to say, there still remain a lot of unanswered questions in both directions. This thesis aims at answering at least some of the remaining open questions within reach of the LHC.

The Standard Model (SM) of particle physics describes the known elementary particles and their interactions and is a very successful theory as it agrees to a very large extent with the experimental data. However, as we will see, the SM is not entirely satisfactory. It covers only about 5% of the energy and matter content in the universe, the remaining 95% is made of dark matter/energy and cannot be explained within the SM. Additionally, the SM does not include gravity, it is described by many free, unpredicted parameters and exhibits an undesirable sensitivity with respect to some of these. We hence expect the SM to be a low-energy version of a more fundamental theory which is valid up to much higher energy scales or, equivalently, much smaller distance scales.

Supersymmetry (SUSY), a symmetry relating fermions and bosons, is an attractive candidate for this more fundamental theory. It offers a candidate for dark matter and local supersymmetry is a way to incorporate gravity. SUSY has already been searched for for a long time, but up to now, it has not been experimentally observed. Most of the studies are however based on minimal versions of SUSY and it is very well possible that a signal evaded our attention. To get a comprehensive overview, it is therefore important to also study less straightforward, unconventional signatures of SUSY at the LHC. This thesis takes us along this road and investigates to which extent deviations from the minimal versions of SUSY are still allowed by experiment and how they could change the limits on supersymmetry.

This is a very broad subject, ranging from the theoretical formulation and experimental data analysis to the phenomenological research establishing the connection between theory and experiment. In this work, we adopt the phenomenological approach, we will use the experimental results and interpret them

in terms of non-minimal supersymmetric theories by means of phenomenological tools which are developed within the community. These tools are important as they facilitate the calculations and make them less error prone, the work presented here also contributed to their development.

This thesis is divided into two parts. Part I introduces the relevant theoretical, experimental and phenomenological background briefly mentioning my own contribution to tool development, *i.e.* ASperGe, published in

- A. Alloul, J. D'Hondt, K. De Causmaecker, B. Fuks and M. Rausch de Traubenberg, *Automated mass spectrum generation for new physics*, *Eur. Phys. J.* **C73** (2013) 2325, [arxiv:1301.5932]

while Part II is devoted to the investigation of three specific scenarios of non-minimal supersymmetry and is based on the following publications

- R. Argurio, K. De Causmaecker, G. Ferretti, A. Mariotti, K. Mawatari and Y. Takaesu, *Collider signatures of goldstini in gauge mediation*, *JHEP* **06** (2012) 096, [arxiv:1112.5058]

- J. D'Hondt, K. De Causmaecker, B. Fuks, A. Mariotti, K. Mawatari, C. Petersson and D. Redigolo, *Multilepton signals of gauge mediated supersymmetry breaking at the LHC*, *Phys. Lett.* **B731** (2014) 7-12, [arxiv:1310.0018]

- K. De Causmaecker, B. Fuks, B. Herrmann, F. Mahmoudi, B. O'Leary, W. Porod, S. Sekmen and N. Strobbe, *General squark flavour mixing: constraints phenomenology and benchmarks*, *JHEP* **11** (2015) 125, [arxiv:1509.05414].

In preparation of the last publication, I also contributed to the proceedings of the Les Houches workshop

- G. Brooijmans et al., *Les Houches 2013: Physics at TeV Colliders: New Physics Working Group Report*, (2014), [arxiv:1405.1617]

but the work presented there will not be discussed in detail in this thesis.

Part I

Setting the stage

In the first half of this work, we introduce all the concepts and ideas needed to further understand the more specific projects detailed in Part II. In chapter 1 we start by introducing the Standard Model. We explain the basic concepts of quantum field theory and show how these are used within the SM to describe all the known fundamental particles and their interactions. We show that the SM is a very successful theory which agrees very well with experiment, but we also see that it has its shortcomings. This motivates us to look for physics beyond the SM.

In chapter 2 we explain how supersymmetry can solve some of the problems of the SM. We construct the Minimal Supersymmetric Standard Model, the MSSM, and explain that the experimental signatures within the MSSM are largely determined by the lightest supersymmetric particles. Consequently, collider searches for supersymmetry are now mainly based on simplified models, models in which only a couple of supersymmetric particles have a mass low enough to be accessible at colliders. We then show that the most straightforward collider searches for supersymmetric particles did not yield any positive results up to now and, consequently, minimal realisations of SUSY become less and less likely.

In the first two chapters, we already touch upon the experimental constraints on the SM and SUSY, but we do it only briefly. A more thorough treatment of the experimental side of this work is provided in chapter 3. We introduce the basics of collider physics, we mention the differences between lepton and hadron colliders and briefly explain how detectors work. We then move on to simulation tools for colliders. We explain and illustrate every step in the phenomenological chain, starting from extracting the Feynman rules from a quantum field theory to simulating high-energy collisions, detector simulation and recasting the experimental analyses.

Chapter 1

The Standard Model

Elementary particle physics aims at answering the question 'What is matter made of and how does it interact?' Despite the versatility of matter in the universe, it turns out that the basic constituents of all matter can be brought back to a rather small number of elementary particles. The Standard Model (SM) of particle physics describes all the known elementary particles and their interactions. It is a very successful theory as it describes very well most experimental observations up to now.

After describing the fundamental particles and forces of the SM in section 1.1, we introduce the basics of quantum field theory in section 1.2 while the theoretical formulation of the Standard Model is provided in section 1.3. In section 1.4 we then explain why the SM is a successful theory and in section 1.5 we explain where the SM falls short.

1.1 The SM particles and forces

As far as we know now, all matter is built from a finite number of fundamental particles largely divided in two groups according to their spin. Fermions have half-integer spin while bosons carry integer spin. Quarks and leptons are spin-1/2 fermions while the gauge bosons, which mediate the forces, are spin-1 bosons. The recently discovered Brout-Englert-Higgs boson is the only known spin-0 boson, also called a scalar particle, and is responsible for the mass of all aforementioned particles. All the known particles and their properties are displayed in figure 1.1. The quarks and leptons each come in three families, flavours or generations and are known to interact through the three fundamental forces: the electromagnetic force, mediated by the photon, the weak nuclear force mediated by the W and Z bosons and the strong nuclear force mediated by the gluon.

The elementary particles of the Standard Model interact at small distance scales and their energy is typically higher or comparable to their masses. The

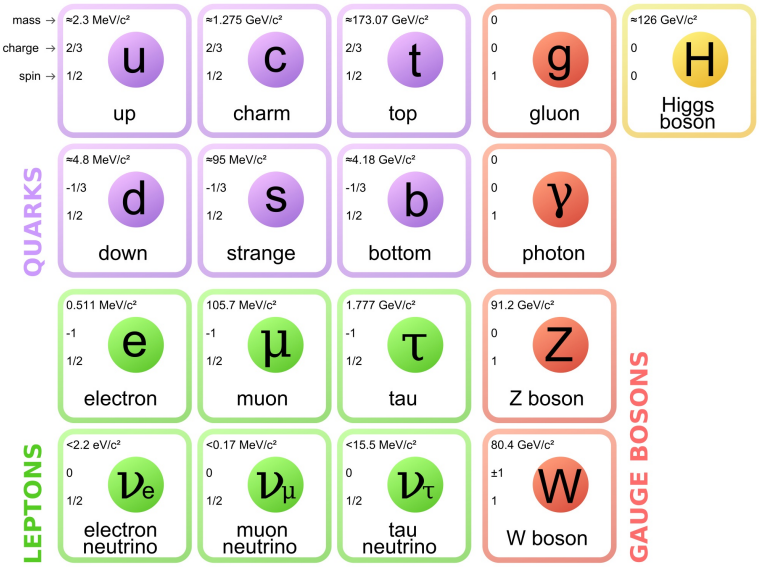

Figure 1.1: The particle content of the SM. Figure taken from [1].

physics describing their motion and interactions therefore has to incorporate quantum mechanics as well as the theory of special relativity, this is achieved in quantum field theory (QFT). Before further describing the SM, we will first briefly introduce a couple of aspects of QFT relevant for this work.

1.2 Aspects of quantum field theory

1.2.1 Particles, fields and the Lagrangian density

In quantum field theory, particles are represented by fields. In case of a scalar field, the value taken by the field, is related to its deviation from its equilibrium state and is hence naturally small. The field can be excited resulting in waves of which the momentum can only take discrete values, the momentum is quantized. These discrete excitations correspond to the particles we observe. The way the particles propagate and interact, is fully determined by the action S which is defined as the integral over space-time d^4x of the Lagrangian density $\mathcal{L}$, a function of the fields, as

$$S = \int \mathcal{L}\, d^4x. \tag{1.1}$$

The physical behaviour of the fields can be derived from minimizing the action. The symmetries of Nature have to be reflected in our action and Lagrangian density. From the theory of special relativity, we know that all physics should be invariant under the space-time transformations of the Lorentz group, which include for example rotations of the space coordinates or Lorentz boosts. Conse-

quently, S and $\mathcal{L}$ have to be invariant under the transformations of the Lorentz group. For a complex scalar field ϕ, the Lagrangian density can for example be given by

$$\mathcal{L} = \partial_\mu \phi (\partial^\mu \phi)^* - m^2 \phi \phi^* \tag{1.2}$$

where ∂_μ indicates the derivative with respect to the space-time coordinates $x^\mu = (t, x, y, z)$ and contracting the Lorentz-indices μ insures Lorentz invariance.[1] The first term is the kinetic term and is related to the propagation of the field while the second term describes the mass of the field. The scalar field has to minimize S which will be the case if ϕ satisfies the Euler-Lagrange equation

$$\partial_\mu \left(\frac{\delta \mathcal{L}}{\delta(\partial_\mu \phi)} \right) - \frac{\delta \mathcal{L}}{\delta \phi} = 0. \tag{1.3}$$

The Euler-Lagrange equation of our complex scalar field, the Klein-Gordon equation, is given by

$$\partial_\mu \partial^\mu \phi + m^2 \phi = 0 \tag{1.4}$$

and is called the equation of motion of the field. We already introduced Lorentz invariance as an example of the importance of symmetries, in the next section 1.2.2 we will see that symmetries are also crucial to describe forces in QFT.

1.2.2 Symmetries and interactions

Our example in section 1.2.1 only included one non-interacting scalar field. To incorporate forces in our model, we will need to introduce a space-time dependent, local, symmetry. Let us consider a massless complex scalar field ϕ with Lagrangian density

$$\mathcal{L}_\phi^{\text{global}} = \partial_\mu \phi (\partial^\mu \phi)^* \equiv |\partial_\mu \phi|^2. \tag{1.5}$$

This Lagrangian does not change under the U(1) transformation $\phi \to e^{i\alpha}\phi$, U(1) is a symmetry of our model. U(1) is the symmetry group of rotations in the complex plane and is only a symmetry of our model if the angle of the rotation α is independent of space-time. We say that U(1) is a global symmetry of the theory. If we want our Lagrangian to be invariant under a local U(1) transformation $\phi \to e^{i\alpha(x)}\phi$, where the parameter of the symmetry transformation, $\alpha(x)$, now depends on the space-time coordinates, we have to modify the Lagrangian density to

$$\begin{aligned} \mathcal{L}_\phi^{\text{local}} &= |D_\mu \phi|^2 \equiv |\partial_\mu \phi + igA_\mu \phi|^2 \\ &= |\partial_\mu \phi|^2 + igA_\mu \left(\phi \partial^\mu \phi^* - \phi^* \partial^\mu \phi\right) + g^2 A_\mu A^\mu |\phi|^2 \end{aligned} \tag{1.6}$$

where we introduced a vector field A_μ and the covariant derivative $D_\mu = \partial_\mu + igA_\mu$. The coupling constant g indicates how strongly A_μ couples to ϕ. For $\mathcal{L}_\phi^{\text{local}}$

[1] More details on Lorentz invariance and the conventions adopted in this thesis can be found in appendix A and in particular section A.1.

to be invariant under the local U(1) transformation, A_μ is required to transform as $A_\mu \to A_\mu - \frac{1}{g}\partial_\mu \alpha(x)$. Promoting a global to a local symmetry is referred to as gauging the symmetry and the vector field A_μ is accordingly called the gauge boson. Local U(1) invariance further allows us to write the kinetic term for the gauge boson as

$$\mathcal{L}_A = -\frac{1}{4} F_{\mu\nu} F^{\mu\nu} \tag{1.7}$$

where $F_{\mu\nu} = \partial_\mu A_\nu - \partial_\nu A_\mu$ is the field strength tensor. A mass term $\frac{1}{2} m_A^2 A_\mu A^\mu$ for the gauge boson is however not allowed.

Starting from a non-interacting complex scalar field, we saw that gauging a symmetry naturally leads to the introduction of a massless gauge boson, introducing interaction terms between the complex field and the gauge boson (the last two terms in (1.6)) and, as such, the particles from the scalar field also interact with themselves by exchanging gauge bosons.

The way of gauging the symmetry we explained up to now is sufficient to model the electromagnetic force with the photon as its massless mediator, but to explain massive gauge bosons, such as the W and Z bosons of the weak nuclear force, we will need another mechanism: spontaneous symmetry breaking.

1.2.3 Spontaneous symmetry breaking

The U(1) symmetry allows us to extend the Lagrangian density (1.6) to

$$\mathcal{L} = |D_\mu \phi|^2 - \frac{1}{4} F_{\mu\nu} F^{\mu\nu} - V(\phi) \tag{1.8}$$

with the scalar potential $V(\phi) = -\mu^2 |\phi|^2 + \lambda |\phi|^4$. The state with lowest energy, the equilibrium or vacuum state, corresponds to the minimum of the scalar potential where the field ϕ takes on its vacuum expectation value (vev) $\langle \phi \rangle$. Requiring the vacuum to be bounded from below implies that λ always has to be positive. The vev then solely depends on the sign of μ^2:

- If $\mu^2 < 0$, $\langle \phi \rangle = 0$
- If $\mu^2 > 0$, $|\langle \phi \rangle| = \frac{\mu}{\sqrt{2\lambda}} \equiv \frac{v}{\sqrt{2}}$ corresponding to an infinite number of degenerate vacua $\langle \phi \rangle = \frac{v}{\sqrt{2}} e^{i\theta}$ where θ is an arbitrary phase.

This is illustrated in figure 1.2. When $\mu^2 > 0$, ϕ effectively fluctuates around the vev and since the fields are defined as fluctuations around their equilibrium value, we have to redefine the field and expand ϕ around its vev instead of zero. Since all vacua are equivalent, we can *e.g.* choose $\langle \phi \rangle = v/\sqrt{2}$ and expand ϕ as

$$\phi(x) = \frac{1}{\sqrt{2}} \left(v + \eta(x) \right) e^{i\xi(x)/v} \tag{1.9}$$

$$\simeq \frac{1}{\sqrt{2}} \left(v + \eta(x) + i\xi(x) \right). \tag{1.10}$$

The Lagrangian density of the scalar field then becomes

$$|D_\mu\phi|^2 - V(\phi) = \frac{1}{2}\partial_\mu\eta\partial^\mu\eta - \mu^2\eta^2 + \frac{1}{2}\partial_\mu\xi\partial^\mu\xi + gvA_\mu\partial^\mu\xi + \frac{1}{2}(gv)^2 A_\mu A^\mu + (\text{terms cubic and quartic in the fields}). \tag{1.11}$$

Even though the original U(1) symmetry is still there, it is no longer apparent in the Lagrangian density: the vacuum has broken the symmetry. If a theory is invariant under a symmetry but the vacuum state is not, the symmetry is said to be spontaneously broken.

In the Lagrangian density (1.11) we observe a massless boson, ξ. This is in accordance with Goldstone's theorem [2] which tells us there will be a massless Goldstone boson for every spontaneously broken generator of a symmetry. As we can see in the third term in equation (1.11), the Goldstone boson ξ couples to the gauge boson, However, if we use gauge freedom and go to unitary gauge by applying a gauge transformation with $\alpha = -\xi/v$, equation (1.11) modifies the Lagrangian to

$$|D_\mu\phi|^2 - V(\phi) = \frac{1}{2}\partial_\mu\eta\partial^\mu\eta - \mu^2\eta^2 + \frac{1}{2}(gv)^2 A_\mu A^\mu + (\text{terms cubic and quartic in the fields}) \tag{1.12}$$

and we see that the Goldstone boson has been removed from the theory. Since it can be removed by using the gauge freedom, the Goldstone boson is not a physical particle. η, on the contrary, is a physical massive scalar and, most importantly, we see that spontaneous breaking of the symmetry generated a mass term for the gauge boson. This mechanism to generate masses for the gauge bosons is called the Brout-Englert-Higgs mechanism and was proposed by Brout and Englert [3] and independently by Higgs [4, 5] and Guralnik, Hagen and Kibble [6] in 1964.

In our example, we introduced an interaction by gauging a global U(1) symmetry and we gave mass to the mediator by breaking the symmetry spontaneously. The electromagnetic and weak and strong nuclear forces of the SM are described in an analogous way, but since the SM gauge groups are somewhat more complicated, we will first introduce some basics of group theory that will be of help later.

1.2.4 Basics of group theory

Generally speaking, a group is defined as a set of elements for which we can define a group product $\times$ such that, if A and B are elements of the group, their product $A \times B$ is again an element of the group. If A, B and C are elements of the group, we have $(A \times B) \times C = A \times (B \times C) = A \times B \times C$, the identity operation 1 is an element of the group and for every element A there exists an inverse A^{-1} which is also part of the group so that $A \times A^{-1} = A^{-1} \times A = 1$.

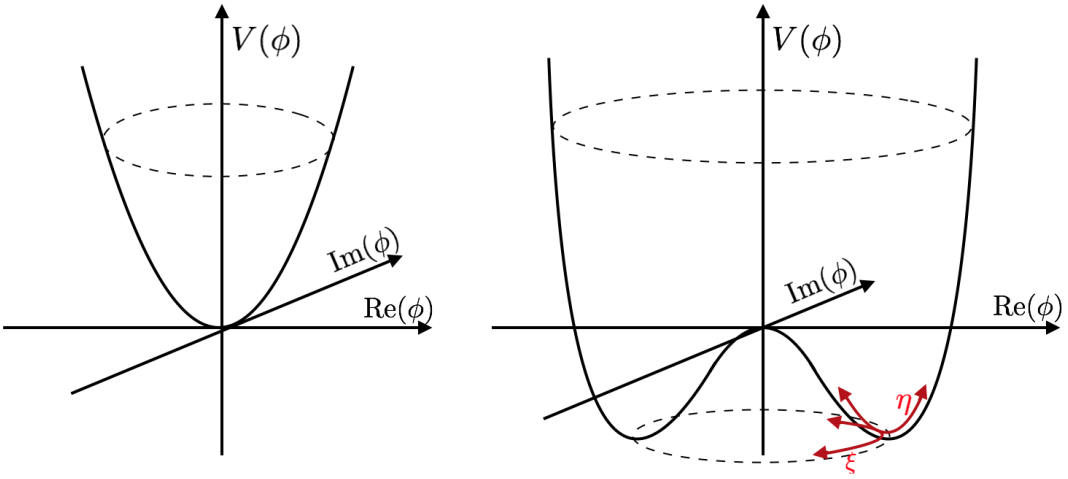

Figure 1.2: The scalar potential $V(\phi)$. The left shows a symmetry-conserving potential with one global minimum corresponding to the case where $\mu^2 < 0$. The potential on the right breaks the symmetry spontaneously resulting in a circle of degenerate minima, corresponding to $\mu^2 > 0$.

A linear representation D of a group maps every group element to a linear transformation in a vector space: an n-dimensional linear representation corresponds to a set of $n \times n$ matrices acting on an n-dimensional vector space. The vector space is called the representation space or, also, simply the representation. The $n \times n$ matrices together with matrix multiplication fulfil all the requirements to be called a group, *i.e.* the mapping of the group to the linear representation preserves the group structure and is a homomorphism. If the mapping also has a homomorphic inverse, it is called an isomorphism and the corresponding representation is referred to as a faithful representation. An n-dimensional representation and its complex conjugate are respectively denoted by $\mathbf{n}$ and $\bar{\mathbf{n}}$ and the smallest faithful representation is called the fundamental representation.

The groups most commonly encountered in high-energy particle physics are Lie groups. Lie groups have an infinite number of group elements $g(\alpha)$ which depend smoothly on a finite set of continuous parameters $\alpha \in \mathbb{R}^m$. Since they form a group, there has to be a composition law ϕ which combines every two elements α and β of the Lie group as

$$\gamma = \phi(\alpha; \beta) \tag{1.13}$$

where γ is again a group element. Similarly, we can find a function ψ relating α to its inverse group element $\bar{\alpha}$ as

$$\bar{\alpha} = \psi(\alpha). \tag{1.14}$$

For the group to be a Lie group, the composition law ϕ as well as the inverse ψ have to be differentiable to all orders.

Due to the aforementioned differentiability, for small $\delta\alpha$, we can Taylor expand $D(\delta\alpha)$ around the identity as[2]

$$D(\delta\alpha) = D(0) + i\delta\alpha^a \left.\frac{\partial D(\alpha)}{\partial \alpha^a}\right|_{\alpha=0} + \dots \tag{1.15}$$

We can always parametrize the Lie group such that $g(0)$ is the identity element of the group so that in any linear representation $D(0) = \mathbb{1}$. If we further define the generators of the Lie group as $T^a \equiv \left.\frac{\partial D(\alpha)}{\partial \alpha^a}\right|_{\alpha=0}$, we can rewrite the above as

$$D(\delta\alpha) = \mathbb{1} + i\delta\alpha^a T^a + \dots \tag{1.16}$$

which then, for finite α, allows us to obtain the representation in terms of the generators as

$$D(\alpha) = \lim_{k\to\infty} \left(\mathbb{1} + i\frac{\alpha^a T^a}{k}\right)^k = e^{i\alpha^a T^a}. \tag{1.17}$$

If we require that the elements $D(\alpha)$ form a group, we find that the generators have to satisfy the commutation relations

$$[T^a, T^b] = f^{abc} T^c \tag{1.18}$$

where f^{abc} is the structure constant. This shows that generators of a Lie group define an algebra structure, the Lie algebra. From equation (1.18) we also find the Jacobi identity

$$[T^a, [T^b, T^c]] + [T^b, [T^c, T^a]] + [T^c, [T^a, T^b]] = 0. \tag{1.19}$$

It is now straightforward to show that $(T^a)_{bc} = f^{abc}$ fulfils the commutation relation as well as the Jacobi identity. The structure constants therefore also form a Lie algebra and the corresponding representation of the Lie group is called the adjoint representation.

The gauge groups of the Standard Model are based on two kinds of Lie groups: the group of the unitary $n \times n$ matrices U(n) and the special unitary group of unitary $n \times n$ matrices with determinant 1, SU(n). U(n) and SU(n) have respective group-dimensions n^2 and $n^2 - 1$. The fundamental representation is n-dimensional in both cases and the dimension of the adjoint representation is equal to the dimension of the group.

According to their interactions, the fields of the SM particles are then ordered within the representations of the gauge groups, more specifically, they span the vector space of the representation. If a particle is not charged under one of the gauge groups, it will transform according to the singlet representation **1**. For example, the leptons are singlets under the gauge group of the strong interaction. We can now apply the ideas we explained before and write down the Lagrangian density of the Standard Model.

[2]We adopt the Einstein summation convention and sum implicitly over a repeated upper- and lower-index. However, since we restrict ourselves to compact algebras, the position of the index does not matter here and we simply sum over repeated indices.

1.3 The Standard Model

1.3.1 The SM Lagrangian density

The Standard Model is based on the gauge groups $\mathrm{SU}(3)_c$, $\mathrm{SU}(2)_L$ and $\mathrm{U}(1)_Y$. The electromagnetic and weak forces are unified in the electroweak theory based on the $\mathrm{SU}(2)_L \times \mathrm{U}(1)_Y$ symmetry that was formulated in the 60's by Glashow [7], Weinberg [8] and Salam [9]. Around the same time, Gell-Mann came up with the quark model [10,11] which, together with the work of Gross and Wilczek [12–14] and Politzer [15,16] in the 70's, laid the foundations for quantum chromodynamics (QCD), the quantum field theory based on the gauge group $\mathrm{SU}(3)_c$ describing the strong interactions. The subscripts indicate that the strong interaction couples with a colour charge (c), $\mathrm{SU}(2)_L$ couples only to left-handed particles and the coupling to $\mathrm{U}(1)_Y$ is determined by the hypercharge Y of the particle.

We denote the coupling strengths of $\mathrm{SU}(3)_c$, $\mathrm{SU}(2)_L$ and $\mathrm{U}(1)_Y$ respectively by g_s, g and g' while T^A, T^I and Y represent the respective generators of the fundamental representation.[3] The covariant derivative of a field transforming under the fundamental representation of all gauge groups of the SM, like the left-handed quarks, is then generally given by

$$D_\mu = \partial_\mu + ig_s G_\mu^A T^A + igW_\mu^I T^I + ig' B_\mu Y \tag{1.20}$$

where $A = 1 \ldots 8$ and $I = 1 \ldots 3$ denote the indices of adjoint representations of the strong and weak interaction. If a field transforms as a singlet under a certain gauge group, the generator is zero and the corresponding term in the covariant derivative will drop out. The covariant derivative of the SM quarks, leptons and scalars can hence be derived based on the transformation properties of the fields given in table 1.1.

The field strength tensor for the $\mathrm{U}(1)_Y$ gauge field is given by

$$B_{\mu\nu} = \partial_\mu B_\nu - \partial_\nu B_\mu. \tag{1.21}$$

For non-abelian gauge groups, the structure constant enters in the field strength tensor. The field strength tensor of the $\mathrm{SU}(3)_c$ gauge field is given by

$$G_{\mu\nu}^A = \partial_\mu G_\nu^A - \partial_\nu G_\mu^A - g_s f^{ABC} G_\mu^B G_\nu^C \tag{1.22}$$

while the one of $\mathrm{SU}(2)_L$ reads

$$W_{\mu\nu}^I = \partial_\mu W_\nu^I - \partial_\nu W_\mu^I - g\epsilon^{IJK} W_\mu^J W_\nu^K. \tag{1.23}$$

Finally, we define $\not{D} = D_\mu \gamma^\mu$ and $\bar{\psi} = \psi^\dagger \gamma^0$ where ψ is a Dirac spinor. This allows us to write the SM Lagrangian density as

[3] The generators are given by $T^A = \lambda^A/2$ and $T^I = \sigma^I/2$ where λ^A are the Gell-Mann matrices and σ^I the Pauli matrices which can be found in appendix A.

Field	Spin	$SU(3)_c$	$SU(2)_L$	Y	T^3	Q
$q = \begin{pmatrix} u_L \\ d_L \end{pmatrix}$	1/2	**3**	**2**	1/6	$\begin{pmatrix} 1/2 \\ -1/2 \end{pmatrix}$	$\begin{pmatrix} +2/3 \\ -1/3 \end{pmatrix}$
u_R	1/2	**3**	**1**	2/3	0	+2/3
d_R	1/2	**3**	**1**	−1/3	0	−1/3
$l = \begin{pmatrix} \nu_L \\ e_L \end{pmatrix}$	1/2	**1**	**2**	−1/2	$\begin{pmatrix} 1/2 \\ -1/2 \end{pmatrix}$	$\begin{pmatrix} 0 \\ -1 \end{pmatrix}$
e_R	1/2	**1**	**1**	−1	0	−1
$\phi = \begin{pmatrix} \phi_+ \\ \phi_0 \end{pmatrix}$	0	**1**	**2**	1/2	$\begin{pmatrix} 1/2 \\ -1/2 \end{pmatrix}$	$\begin{pmatrix} +1 \\ 0 \end{pmatrix}$
G^A_μ	1	**8**	**1**	0	-	-
W^I_μ	1	**1**	**3**	0	-	-
B_μ	1	**1**	**1**	0	-	-

Table 1.1: The fields of the SM and their transformation properties under the SM gauge groups. The electric charge is given by $Q = T_3 + Y$. Only the indices of the adjoint representations are written explicitly, $A = 1 \dots 8$ and $I = 1 \dots 3$ respectively run over the generators of the strong and weak interaction.

$$\mathcal{L}_{SM} = \mathcal{L}_F + \mathcal{L}_V + \mathcal{L}_S + \mathcal{L}_Y \tag{1.24}$$

where the first term involves the fermions

$$\mathcal{L}_F = \bar{q} i \not{D} q + \bar{u}_R i \not{D} u_R + \bar{d}_R i \not{D} d_R + \bar{l} i \not{D} l + \bar{e}_R i \not{D} e_R, \tag{1.25}$$

the second the gauge bosons

$$\mathcal{L}_V = -\frac{1}{4} G^A_{\mu\nu} G^{A\mu\nu} - \frac{1}{4} W^I_{\mu\nu} W^{I\mu\nu} - \frac{1}{4} B_{\mu\nu} B^{\mu\nu} \tag{1.26}$$

and the third the scalar doublet

$$\mathcal{L}_S = (D_\mu \phi)^\dagger (D^\mu \phi) + \mu^2 \phi^\dagger \phi - \lambda (\phi^\dagger \phi)^2. \tag{1.27}$$

In the previous equations, the generation, colour and $SU(2)_L$ indices were implicit. However, it is instructive to write the generation indices explicitly now. Using the representation for the generators of $SU(2)_L$ where $T^I = \frac{\sigma^I}{2}$ with

$$\sigma^1 = \begin{pmatrix} 0 & 1 \\ 1 & 0 \end{pmatrix}, \quad \sigma^2 = \begin{pmatrix} 0 & -i \\ i & 0 \end{pmatrix}, \quad \sigma^3 = \begin{pmatrix} 1 & 0 \\ 0 & -1 \end{pmatrix} \tag{1.28}$$

we can define $\tilde{\phi} = i\sigma^2 \phi^*$ which transforms according to the fundamental representation of $SU(2)_L$ but has hypercharge $-\frac{1}{2}$. This allows us to write the last

term which contains interactions between the scalar doublet and the fermions, known as Yukawa interactions

$$\mathcal{L}_Y = -[\bar{q}^i \lambda^u_{ij} u^j_R \tilde{\phi} + \bar{q}^i \lambda^d_{ij} d^j_R \phi + \bar{l}^i \lambda^l_{ij} e^j_R \phi + \text{h.c.}] \tag{1.29}$$

where i and $j = 1 \dots 3$ denote the generation indices. The Yukawa coupling matrices λ^u, λ^d and λ^l are each 3×3 matrices in generation space.

In the following we will see how the gauge bosons acquire mass through the Brout-Englert-Higgs mechanism while mass terms for the fermions are generated through the Yukawa couplings.

1.3.2 Massive gauge bosons and the Brout-Englert-Higgs mechanism

Let us have a closer look at the Lagrangian density of the scalar doublet in equation (1.27). When $\mu^2 > 0$, the scalar potential breaks the $\mathrm{SU}(2)_L \times \mathrm{U}(1)_Y$ symmetry spontaneously to $\mathrm{U}(1)_{\mathrm{em}}$ which, analogously to the discussion in section 1.2.3, generates mass terms for the gauge bosons of the weak interaction. The photon remains massless due to the remaining $\mathrm{U}(1)_{\mathrm{em}}$. We choose

$$\langle \phi \rangle = \frac{1}{\sqrt{2}} \begin{pmatrix} 0 \\ v \end{pmatrix} \tag{1.30}$$

where again $v = \frac{\mu}{\sqrt{\lambda}}$. In unitary gauge we expand the scalar doublet around its vev as

$$\phi = \frac{1}{\sqrt{2}} \begin{pmatrix} 0 \\ v + h(x) \end{pmatrix} \tag{1.31}$$

and substitute this in the Lagrangian density. Through a calculation analogous to the discussion in section 1.2.3, which will not be detailed here, we can find the mass terms of the gauge bosons. Suppose we work in the basis (1.28) of the $\mathrm{SU}(2)_L$ generators. W^3_μ and B_μ appear not to be the mass eigenstates, the propagating fields are found by diagonalizing the mass matrix and are given by

$$\begin{pmatrix} Z_\mu \\ A_\mu \end{pmatrix} = \begin{pmatrix} \cos\theta_w & -\sin\theta_w \\ \sin\theta_w & \cos\theta_w \end{pmatrix} \begin{pmatrix} W^3_\mu \\ B_\mu \end{pmatrix} \tag{1.32}$$

where $\sin\theta_W = \frac{g'}{\sqrt{g^2+g'^2}}$. Z_μ and A_μ correspond respectively to the Z boson of the weak interaction and the photon mediating the electromagnetic force. The $W^\pm_\mu$ boson is a linear combination of W^1_μ and W^2_μ and is given by

$$W^\pm_\mu = \frac{1}{\sqrt{2}} \left(W^1_\mu \mp i W^2_\mu \right). \tag{1.33}$$

The covariant derivative in terms of the propagating fields, is then given by

$$D_\mu = \partial_\mu + ig_s G_\mu^A T^A + ig\frac{1}{\sqrt{2}}\left(W_\mu^+\sigma^+ + W_\mu^-\sigma^-\right) + i\frac{Z_\mu}{\sqrt{g^2+g'^2}}\left(g^2\frac{\sigma^3}{2} - g'^2 Y\right) + \frac{igg'}{\sqrt{g^2+g'^2}}A_\mu\left(\frac{\sigma^3}{2}+Y\right) \tag{1.34}$$

with

$$\sigma^+ \equiv \frac{1}{\sqrt{2}}(\sigma^1 + i\sigma^2) = \sqrt{2}\begin{pmatrix}0 & 1\\ 0 & 0\end{pmatrix}, \tag{1.35}$$

$$\sigma^- \equiv \frac{1}{\sqrt{2}}(\sigma^1 - i\sigma^2) = \sqrt{2}\begin{pmatrix}0 & 0\\ 1 & 0\end{pmatrix}. \tag{1.36}$$

The photon is massless and the masses of the gauge bosons of the weak interaction are given by

$$m_W = \left|\frac{gv}{2}\right|, \qquad m_Z = \frac{m_W}{\cos\theta_W}. \tag{1.37}$$

From the covariant derivative, it is clear that the coupling strength of the photon to the field on which the derivative is acting is proportional to $\sigma^3/2+Y = T^3+Y$. We identify the unit of electric charge as

$$e = \frac{gg'}{\sqrt{g^2+g'^2}} \tag{1.38}$$

so that the electric charge of the field is given by $Q = T^3 + Y$. Q as well as T^3 and Y are shown in table 1.1.

1.3.3 Massive fermions and the CKM-matrix

Spontaneous symmetry breaking also gives mass to the SM fermions. Substituting the vev of the scalar doublet $\langle\phi\rangle = \frac{1}{\sqrt{2}}\begin{pmatrix}0\\ v\end{pmatrix}$ in the Yukawa couplings (1.29) yields the mass terms

$$\mathcal{L}_{mass} = -\left[\frac{v}{\sqrt{2}}\lambda^u_{ij}\bar{u}^i_L u^j_R + \frac{v}{\sqrt{2}}\lambda^d_{ij}\bar{d}^i_L d^j_R + \frac{v}{\sqrt{2}}\lambda^l_{ij}\bar{e}^i_L e^j_R + \text{h.c.}\right] \tag{1.39}$$

so that the mass matrices are given by $\frac{v}{\sqrt{2}}\lambda^{u,d,l}$. To find the propagating fields, we have to diagonalize the mass matrices. We focus first on the quark sector. Applying the unitary transformations

$$u_L \to V_{u_L}u_L, \quad u_R \to V_{u_R}u_R, \quad d_L \to V_{d_L}d_L, \quad d_R \to V_{d_R}d_R \tag{1.40}$$

on the quark fields changes the mass matrices to

$$\frac{v}{\sqrt{2}}\lambda^u \quad \to \quad \frac{v}{\sqrt{2}}\left(V^\dagger_{u_L}\lambda^u V_{u_R}\right) \equiv \frac{v}{\sqrt{2}}\lambda'^u \tag{1.41}$$

and analogously for the down-type mass matrix, where the transformation matrices can be chosen such that the λ' matrices are real, diagonal and positive. Since the right-handed quarks are singlets under $\mathrm{SU}(2)_L$, their kinetic term and gauge interactions are given by

$$\bar{u}_R i \not{D} u_R = \bar{u}_R i \left(\not{\partial} + i g_s \not{G}^A T^A + \frac{2}{3} i g' \not{B} \right) u_R \tag{1.42}$$

which is diagonal in flavour space and hence invariant under (1.40).

The same holds for the kinetic term and the couplings to G^A_μ, A_μ and Z_μ of the left-handed fields. However, since $\sigma^\pm$ have off-diagonal terms, the interactions with $W^\pm_\mu$ do change the flavour of the quarks so that transforming to the mass eigenbasis of the quarks yields

$$\frac{ig}{\sqrt{2}} \left(\bar{u}_L \not{W}^+ d_L + \text{h.c.} \right) \quad \rightarrow \quad \frac{ig}{\sqrt{2}} \left(\bar{u}_L \not{W}^+ \left(V^\dagger_{u_L} V_{d_L} \right) d_L + \text{h.c.} \right). \tag{1.43}$$

The matrix $V^\dagger_{u_L} V_{d_L}$ is called the Cabibbo–Kobayashi–Maskawa matrix V_{CKM}, the CKM-matrix for short [17, 18]. Since V_{CKM} is a 3×3 unitary matrix, it can be parametrized by 3 real parameters and 6 phases of which 5 phases can be removed by redefining the fields leaving us with 3 real parameters and 1 phase.

Since there are no right-handed neutrinos in the SM, the lepton sector is simplified with respect to the quark sector. Similarly to the quark sector, we can diagonalize the lepton mass matrix $\frac{v}{\sqrt{2}} \lambda^l$ by applying the unitary transformation

$$e_L \rightarrow V_{e_L} e_L, \quad e_R \rightarrow V_{e_R} e_R. \tag{1.44}$$

Since there is no mass term for the neutrino fields to be diagonalized, we are free to also transform the left-handed neutrino as

$$\nu_L \rightarrow V_{e_L} \nu_L \tag{1.45}$$

which yields the interaction terms diagonal in the generations. We hence do not have a lepton analogue of the CKM-matrix in the SM and, therefore, there are no generation-changing processes in the lepton sector.

The Standard Model does not contain right-handed neutrinos since there is no compelling evidence for their existence. However, as we will see in section 1.5, neutrinos have been observed to oscillate which implies they should have a small but non-zero mass. The precise origin of these masses is yet unclear, but right-handed neutrinos could play a crucial role in explaining them. If we would include right-handed neutrinos, the lepton sector would have a mixing matrix similar to the CKM-matrix for the quarks. This matrix is called the Pontecorvo-Maki-Nakagawa-Sakata matrix, or the PMNS-matrix for short [19, 20].

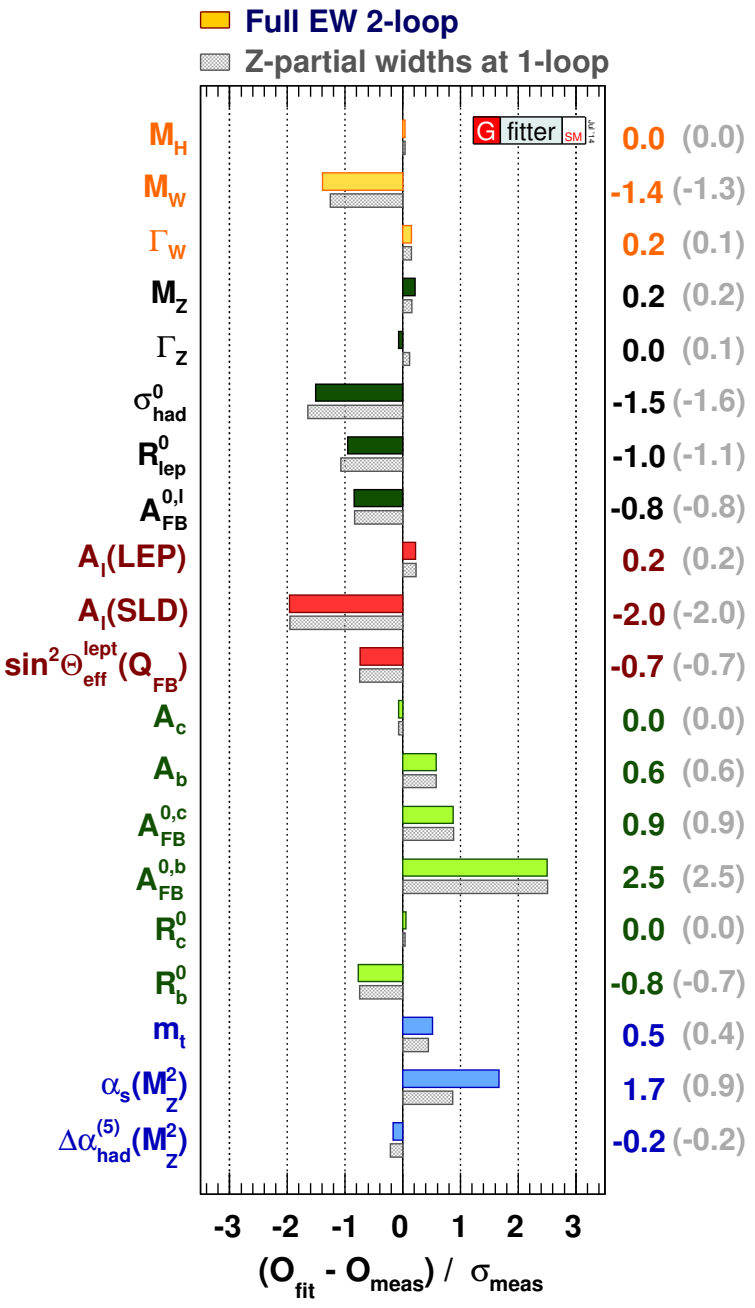

Figure 1.3: Comparison of the results from the electroweak precision fit with the direct measurements in units of the experimental uncertainty σ_{meas}. Figure taken from [21]

.

1.4 Successes of the Standard Model

Up to now we mainly constructed the Standard Model on theoretical grounds but the Standard Model is not merely a theoretical construction, it has been tested experimentally to a very high precision and has shown to perform very well.

The most recent success of the Standard Model is without doubt the discovery of the Brout-Englert-Higgs boson with a mass of 125 GeV by the CMS and ATLAS Collaborations at the Large Hadron Collider.[4] The discovery was announced on the 4th of July 2012 [22, 23] and one year later in 2013, François Englert and Peter Higgs were awarded the Nobel Prize in Physics for their theoretical discovery of the Brout-Englert-Higgs mechanism in 1964 [24]. With the Brout-Englert-Higgs boson, all the particles of the Standard Model have been experimentally observed.

If we do not include right-handed neutrinos, the Standard Model has 19 free parameters to be measured which have to be consistent with all the experimental data. Electroweak precision observables allow us to probe energy scales that are otherwise hard to reach. They have been measured precisely at lepton colliders such as LEP and SLC[5] and can be used to fit the SM parameters related to the electroweak sector. An example of the electroweak precision fit by the GFitter group [25] is shown in figure 1.3. The figure shows for each measurement in the list how many standard deviations σ_{meas} the SM prediction deviates from the measurement. All observables fall within $3\sigma_{\text{meas}}$ and we can conclude that the SM describes the data very well.

Also the flavour sector is very sensitive to new physics and fitting flavour observables similarly leads to a fit of the flavour sector of the SM, in particular the CKM-matrix. In the Wolfenstein parametrization [27], the CKM-matrix is parametrized by four parameters λ, A, $\bar{\rho}$ and $\bar{\eta}$. Figure 1.4 shows the experimental constraints in the plane of $\bar{\eta}$ and $\bar{\rho}$ as obtained by the CKMFitter group [28]. The coloured regions show the regions consistent with the indicated measurement at 95% confidence level. All allowed regions overlap leading to the global fit region indicated in red and showing that Standard Model is in good agreement with the experimental data.

1.5 Where the Standard Model falls short

Despite its successes, we know that the SM is not sufficient when we go to, for example, the Planck scale. The SM is expected to be an effective theory, a

[4] CMS and ATLAS are the two general-purpose experiments at the Large Hadron Collider (LHC), a proton-proton collider in Switzerland. The LHC as well as its experiments will be introduced in chapter 3.

[5] We will explain in chapter 3 why lepton colliders are better suited for precision measurements than hadron colliders.

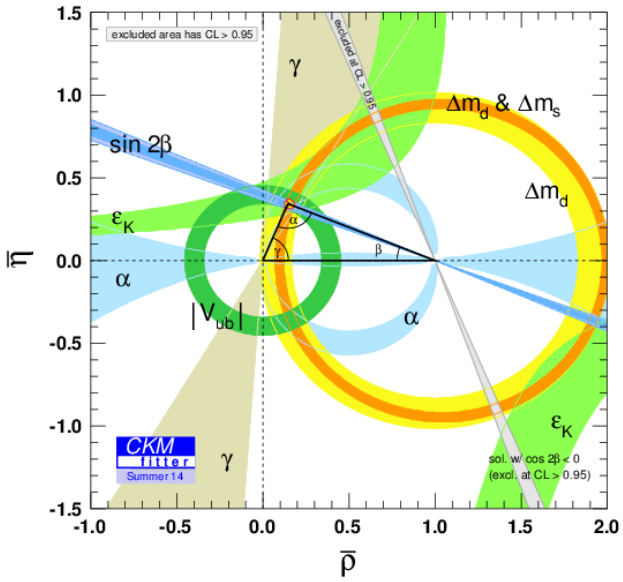

Figure 1.4: Constraints on the parameters $\bar{\rho}$ and $\bar{\eta}$ resulting from the global SM CKM-fit. The regions outside the coloured regions are excluded at 95% Confidence Level. Figure taken from [26].

theory in which the heaviest particles are integrated out, which describes low-energy effects well but yet will break down at higher energy scales. There are many open questions leading to the assumption that there must be something more, we will briefly discuss a couple of them below. One of them, the fine-tuning problem, is discussed in more detail in section 1.5.1.

Gravity

Gravity, one of the four fundamental forces, is not included in the SM since no consistent quantum theory of gravity has been formulated yet. We hence know that the SM has to break down at the scale where quantum gravitational effects become important, namely, when the Compton wavelength $\frac{h}{mc}$ of a mass m becomes comparable to its Schwarzschild radius $\frac{2Gm}{c^2}$. h denotes Planck's constant, c the velocity of light and G the gravitational constant. We hence know that new physics will have to enter at the Planck scale,

$$M_{\mathrm{P}} \sim \sqrt{\frac{hc}{2G}} \sim 10^{19}\,\mathrm{GeV}/c^2. \tag{1.46}$$

The huge energy range between the weak scale $\mathcal{O}(10^2\,\mathrm{GeV})$ and the Planck scale does not only suggest there must be some other physics in between, it is also at the origin of the fine-tuning problem which will be discussed in section 1.5.1.

Dark matter and dark energy

A careful study of the velocity of visible objects like stars or gas clouds within galaxies [29, 30] shows that they move faster than one would expect by taking into account the gravitational interactions of visible objects. This problem can be solved if we assume there is also matter that does not interact with photons, dark matter. This is only one of the experimental indications for the existence of dark matter in the universe. The latest results from the Planck space observatory [31] have led to the conclusion that only 5% of all the energy and mass present in the universe is described by the SM. Of the remaining 95%, about 26% consists of dark matter while dark energy makes up for the remaining 69%. Neutrinos could contribute to the dark matter density, but it has been shown [27] that their relic density cannot be large enough to account for the all the dark matter. The SM does not provide any other particle that could be a dark matter candidate, nor does the model provide any explanation for dark energy.

Neutrino oscillations

The Super-Kamiokande [32] and SNO [33] experiments studied respectively atmospheric and solar neutrinos and were the first experiments to show that neutrinos can change flavour over time, they oscillate. This can only be explained if they differ in mass, however, neutrinos are assumed massless in the SM. To explain neutrino oscillations, we will have to extend the SM.

Free parameters in the SM

The 19 free parameters of the SM are the gauge coupling strengths g_s, g and g', the parameters μ^2 and λ from the scalar potential, 6 quark masses, 3 real parameters and 1 phase from the CKM-matrix, 3 masses for the leptons and the θ_{QCD} parameter.[6] Adding up to 19 parameters which all have to be measured experimentally. We already showed in section 1.4 that the measurements lead to consistent results and therefore, in itself, there is not really a problem with the SM in itself. However, it does give the impression that there is another theory behind the SM governing the parameter values and it would be aesthetically much more appealing if they all could be calculated from first principles.

Fermions: families and mass hierarchy

Electroweak precision measurements studying the production and decay of the Z boson [35] show that there are exactly three generations of fermions with a neutrino with mass lower than half the Z-boson mass. Moreover, fruitless collider

[6] We can add a CP-violating term proportional to $\theta_{\text{QCD}} F^A_{\mu\nu} \widetilde{F}^{\mu\nu A}$ to the SM Lagrangian density and its coefficient θ_{QCD} is a free parameter. More information about this term can for example be found in [34].

searches for fourth generation quarks (see *e.g.* [36,37]) together with the discovery of the Brout-Englert-Higgs boson with a mass of about 125 GeV, imply that a fourth generation of SM-like chiral quarks is considered to be ruled out [38].[7]

The SM therefore appears to have three generations of fermions. Naturally we can ask ourselves the question 'Why three families and not more or less?' Moreover the fermion masses span a huge range, the mass of the top quark, 173 GeV, is about five orders of magnitude larger than the mass of electron which amounts to 0.511 MeV and the neutrino masses are even lower. The SM does not offer any clue why. This is known as the fermionic mass hierarchy problem.

Gauge coupling unification

Even though the electromagnetic and strong and weak nuclear forces are well described as gauge theories within the Standard Model, we do need three different, independent gauge groups, each with their own coupling constant, which makes the overall SM gauge structure rather complicated. However, the values of the couplings constants evolve depending on the energy scale and the SM gauge couplings can be shown to almost unify at a scale of order 10^{16} GeV, the scale of grand unification [39]. If the gauge couplings are equal, it might be possible to unify the SM gauge symmetry groups into one, larger symmetry group. Such a scenario is referred to as a Grand Unified Theory (GUT) and would considerably simplify the SM gauge structure. However, within the Standard Model the gauge couplings, do not exactly unify and for grand unification to take place, new physics would have to enter in between the electroweak scale and the scale of grand unification.

1.5.1 The fine-tuning problem

The fine-tuning problem concerns the sensitivity of the mass m_h of the Brout-Englert-Higgs boson h to quantum corrections. Suppose we have N_f Dirac fermions f with mass m_f which couple to h as $-\lambda_f \bar{f} f h$. The one-loop contribution of the fermion to m_h due to the fermions is shown in figure 1.5 and leads to a correction of m_h^2 given by [40]

$$\Delta m_h^2 = \frac{\lambda_f^2 N_f}{8\pi^2}\left[-\Lambda^2 + 6m_f^2 \log\frac{\Lambda}{m_f} - 2m_f^2\right] + \mathcal{O}\left(\frac{1}{\Lambda^2}\right) \tag{1.47}$$

where we introduced a cutoff Λ on the momentum to regulate the loop-integral. The correction depends quadratically on

the scale where we expect new physics to enter and for $\Lambda \to \infty$ it diverges quadratically. Naturally we would expect m_h to be roughly of the same order

[7] However, searches for exotic non-chiral types of quarks like vector-like quarks are still ongoing. They couple differently to the BEH-boson and therefore evade many of the constraints on chiral fourth generation quarks.

of magnitude as its quantum corrections. However, $\Lambda = M_{\mathrm{P}} \sim 10^{19}\,\mathrm{GeV}$ implies that Δm_h^2 is more than 30 orders of magnitude larger than $m_h^2 \sim 10^4\,\mathrm{GeV}^2$. This would imply that some of the parameters within the Standard Model would have to be fine-tuned to $\mathcal{O}(10^{-30})$ to achieve the cancellation required to get a reasonable value for m_h. Technically this is possible, but it seems very unnatural and the theory would be more reliable if there would be another way to remove the divergences.

This is for example the case for the fermions and gauge bosons of the SM where symmetry ensures that both are stable under quantum corrections. A non-zero fermion mass m_f breaks chiral symmetry which would be restored if $m_f \to 0$. As a consequence, the quantum corrections to m_f depend only logarithmically on Λ and are proportional to m_f. Similarly, an explicit gauge boson mass term would break local gauge symmetry which also restricts the quantum corrections to its mass and no quadratic divergences appear. In the SM, the fine-tuning problem only occurs for in the case of the Brout-Englert-Higgs boson since its mass is not protected by any symmetry.

However, suppose we add N_s complex scalars s with mass m_s which couples to h through $-\lambda_s |h|^2 |s|^2$ and $-\lambda_s v h |s|^2$. The one-loop contributions of the scalar to h are shown in figure 1.6 and can be calculated as

$$\Delta m_h^2 = \frac{\lambda_s N_s}{16\pi^2}\left[\Lambda^2 - 2m_s^2 \log\left(\frac{\Lambda}{m_s}\right)\right] - \frac{\lambda_s^2 N_s}{16\pi^2} v^2 \left[-1 + 2\log\left(\frac{\Lambda}{m_s}\right)\right] + \mathcal{O}\left(\frac{1}{\Lambda^2}\right). \tag{1.48}$$

This correction depends again quadratically on Λ. However, if we assume $\lambda_f^2 = \lambda_s$ and $N_s = 2N_f$, the total correction to m_h is given by

$$\Delta m_h^2 = \frac{\lambda_f^2 N_f}{4\pi^2}\left[(m_f^2 - m_s^2)\log\left(\frac{\Lambda}{m_s}\right) + 3m_f^2 \log\left(\frac{m_s}{m_f}\right)\right] + \mathcal{O}\left(\frac{1}{\Lambda^2}\right) \tag{1.49}$$

which is no longer quadratically divergent. A logarithmic divergence remains, but is relatively small and even disappears if $m_s = m_f$. A symmetry between bosons and fermions could hence solve the fine-tuning problem as long as $m_s \approx m_f$. As we will see in the next chapter, this is exactly what is done in supersymmetry. However, we know from experiment that $m_s \gg m_f$ and a certain amount of fine-tuning will remain. In the next chapter, we will introduce a measure for the level of fine-tuning in a theory and we will discuss how much fine-tuning we consider to be acceptable.

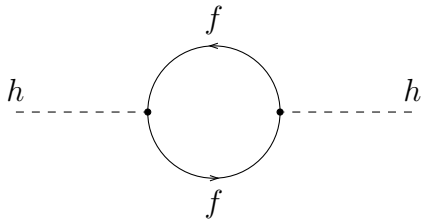

Figure 1.5: One-loop correction of a fermion to m_h.

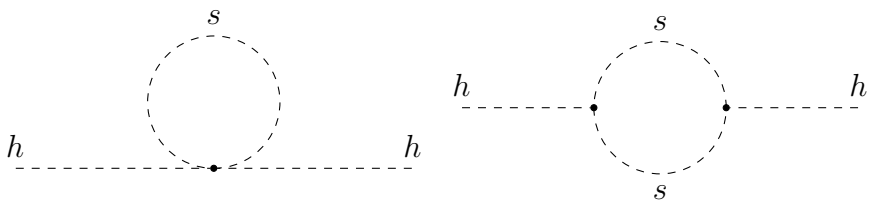

Figure 1.6: One-loop correction of a scalar to m_h.

Chapter 2

Supersymmetry

Supersymmetry is a symmetry connecting fermions and bosons which, as was shown in the previous chapter, is exactly what is needed to solve the fine-tuning problem of the Standard Model. In addition to solving, or at least softening, the fine-tuning problem, SUSY can also naturally improve the unification of the SM gauge couplings at the scale of grand unification, as is for example the case for the Minimal Supersymmetric Standard Model (MSSM).

In section 2.1 of this chapter we will introduce supersymmetry and describe how we can construct a supersymmetric model. In section 2.2 we will then use the SUSY formalism to introduce the Minimal Supersymmetric Standard Model, the MSSM, and in section 2.3 we explain how supersymmetry can be broken. In section 2.4 we explain what is the current status of SUSY given the lack of any experimental confirmation so far.

2.1 Supersymmetry in a nutshell

Supersymmetry is a symmetry relating particles of integer spin to particles with half-integer spin, differing in spin by $\frac{1}{2}$. A generator Q of supersymmetry changing bosons in fermions and vice versa,

$$Q\,|\text{fermion}\rangle = |\text{boson}\rangle \quad \text{and} \quad Q\,|\text{boson}\rangle = |\text{fermion}\rangle\,, \tag{2.1}$$

therefore has to be an anticommuting spin-$\frac{1}{2}$ spinor. As we will see below, in supersymmetry it is convenient to describe spin-$\frac{1}{2}$ particles with two-component Weyl spinors instead of the four-component Dirac spinors. The generators Q_α and $Q^\dagger_{\dot\alpha}$ are respectively a left-handed and a right-handed Weyl spinor, where $\alpha = 1, 2$ and $\dot\alpha = 1, 2$ (and generally the first letters of the Greek alphabet) denote the corresponding Weyl-spinor indices. In the following, we will restrict ourselves to $N = 1$ supersymmetry where we have only one set of supersymmetric generators Q.

2.1.1 The SUSY algebra

Since supersymmetry changes the spin of a field, it modifies its properties under the symmetry group describing space-time symmetries, the Poincaré group. Q can hence not commute with all the generators of the Poincaré group (*i.e.* the generators of the translations, P_μ, and Lorentz transformations, $M_{\mu\nu}$) and this constraint strongly limits the possibilities to incorporate supersymmetry in a quantum field theory.

In particular, Coleman and Mandula [41] showed that the Poincaré group cannot mix non-trivially with any other bosonic symmetry group of the theory, they should commute. Haag, Lopuszanski and Sohnius [42] extended this theorem to include fermionic generators, like the generators of supersymmetry Q, as well. It turned out that, whereas all the symmetry groups we encountered up to now were determined by a Lie algebra which imposes commutation relations on its generators, supersymmetry has to obey a Lie superalgebra which contains anticommutation as well. The Lie superalgebra is given by

$$\{Q_\alpha, Q^\dagger_{\dot\beta}\} = 2\,(\sigma^\mu)_{\alpha\dot\beta}\,P_\mu \tag{2.2}$$

$$\{Q_\alpha, Q_\beta\} = \{Q^\dagger_{\dot\alpha}, Q^\dagger_{\dot\beta}\} = 0 \tag{2.3}$$

$$[Q_\alpha, P_\mu] = [Q^\dagger_{\dot\alpha}, P_\mu] = 0 \tag{2.4}$$

$$[Q_\alpha, M_{\mu\nu}] = -\frac{1}{2}\,(\sigma_{\mu\nu})_\alpha{}^\beta\,Q_\beta \tag{2.5}$$

$$[Q^\dagger_{\dot\alpha}, M_{\mu\nu}] = \frac{1}{2}\,(\bar\sigma_{\mu\nu})_{\dot\alpha}{}^{\dot\beta}\,Q^\dagger_{\dot\beta} \tag{2.6}$$

where $\sigma^\mu = (1, \sigma^i)$ and $\bar\sigma^\mu = (1, -\sigma^i)$. The Pauli matrices σ^i with $i = 1, 2, 3$ and $\sigma^{\mu\nu}$ and $\bar\sigma^{\mu\nu}$ are defined in appendix A. The (anti-)commutation relations (2.2)-(2.6) together with Poincaré algebra[1] not mentioned here, forms the complete $N = 1$ SUSY algebra.

2.1.2 Supermultiplets

A set of particles that are transformed into each other by SUSY transformations and make up an irreducible representation of the SUSY algebra, form a supermultiplet. From the anti-commutation relation (2.2) it can be seen (see for example [39]) that each supermultiplet contains an equal number of fermionic and bosonic degrees of freedom. Moreover, since the SUSY generators commute with all the generators of the SM gauge groups as well as with P^2, all particles in the same supermultiplet will have the same quantum numbers under the SM gauge groups as well as the same masses.

Since we have not detected any supersymmetric particle yet, it is clear that in reality, they do not have the same masses. This, however, does not per se

[1] The Poincaré algebra can for example be found in [43].

exclude SUSY, a difference in mass between the Standard Model particles and their superpartners can still occur when SUSY is broken. We will discuss this in more detail in section 2.3,

For our purposes, two kinds of supermultiplets are sufficient:

- The chiral supermultiplet (ψ, ϕ, F) is composed of a left-handed Weyl fermion ψ, a complex scalar ϕ and an auxiliary, non-propagating, complex scalar field F.
- The vector or gauge supermultiplet (A_μ, λ, D) consists of a massless spin-1 vector boson A_μ, a massless spin-$\frac{1}{2}$ Majorana Weyl fermion λ and an auxiliary, non-propagating, real scalar field D.

By construction, the number of bosonic and fermionic degrees of freedom in each supermultiplet has to be equal for real or on-shell particles as well as for virtual or off-shell particles. In a chiral supermultiplet, ϕ and F each have 2 off-shell degrees of freedom, while ψ has 2 complex components corresponding to 4 off-shell degrees of freedom. In a vector supermultiplet on the other hand, A_μ, λ and D respectively have 3, 4 and 1 off-shell degrees of freedom. Off-shell, a chiral and vector supermultiplet therefore each have 4 bosonic and 4 fermionic degrees of freedom. If supersymmetry is preserved, the auxiliary fields F and D will vanish if we go on-shell. The number of bosonic and fermionic degrees of freedom will however stay equal since ψ, λ and A_μ will all lower their degrees of freedom to 2 when they are on-shell.

2.1.3 A general supersymmetric Lagrangian

The Lagrangian density of a general, renormalizable, supersymmetric model containing n chiral and m vector supermultiplets, can be written as

$$\mathcal{L}_{\text{SUSY}} = \mathcal{L}_{\text{sg}} + \mathcal{L}_{\text{W}} - V_\phi. \tag{2.7}$$

The first term in the Lagrangian density contains, among others, the kinetic terms of all the fields and is obtained from requiring gauge invariance and invariance under supersymmetry. It is given by

$$\mathcal{L}_{\text{sg}} = \sum_{j=1}^{n} \left[|D_\mu \phi_j|^2 + \bar{\psi}_j i \not{D} \psi_j \right] + \sum_{k=1}^{m} \left[\bar{\lambda}_k^{a_k} i \not{D} \lambda_k^{a_k} - \frac{1}{4} \left(V_{\mu\nu}\right)_k^{a_k} \left(V^{\mu\nu}\right)_k^{a_k} \right] - \left[\sqrt{2} \sum_{j,k} g_k \left(\phi_j^* T_k^{a_k} \psi_j \right) \lambda_k^{a_k} + \text{h.c.} \right] \tag{2.8}$$

where, in addition to the sum over the supermultiplets which is written explicitly, we also sum over the adjoint indices a_k corresponding to the gauge group of the

vector supermultiplet. $V_{\mu\nu}$ denotes the field-strength tensor of the vector field of the vector supermultiplet.

The second term of equation (2.7) contains SUSY-invariant interaction terms and is completely determined by the superpotential W, a holomorphic function of the complex scalar fields with mass dimension 3 which is at most cubic in the fields. In its most general form, the superpotential is given by

$$W_\phi(\phi) = L^i\phi_i + \frac{1}{2}M^{ij}\phi_i\phi_j + \frac{1}{6}y^{ijk}\phi_i\phi_j\phi_k \tag{2.9}$$

where, since ϕ has mass dimension 1, L^i, M^{ij} and y^{ijk} are constants of respective mass dimension 2, 1 and 0. The second part of the Lagrangian is then given by

$$\mathcal{L}_{\mathrm{W}} = -\frac{1}{2}\sum_{i,j=1}^{n}\psi_i\psi_j\frac{\partial^2 W_\phi}{\partial\phi_i\partial\phi_j} + \mathrm{h.c.} \tag{2.10}$$

Finally, the scalar potential V_ϕ can be expressed in function of the auxiliary fields as

$$V_\phi = \sum_{i=1}^{n}|F_i|^2 + \frac{1}{2}\sum_{k=1}^{m}g_k^2 D_k^{a_k}D_k^{a_k}. \tag{2.11}$$

We can, however, always replace F and D by their equations of motion

$$F_i = \frac{\partial W_\phi}{\partial\phi_i} \qquad \text{and} \qquad D_G^a = \sum_i(\phi_i^* T_G^a\phi_i) \tag{2.12}$$

such that the scalar potential indeed only depends on the scalar fields of the chiral supermultiplets.

As soon as we fix the chiral and vector superfields and their representation under the gauge groups, the only freedom when writing down a renormalizable, supersymmetric and gauge-invariant Lagrangian density, is the choice of the superpotential (2.9). All the other terms in the Lagrangian are completely determined by requiring gauge invariance and invariance under SUSY.[2]

2.2 The Minimal Supersymmetric Standard Model

The Minimal Supersymmetric Standard Model, the MSSM for short, is the minimal way to accommodate the Standard Model in a supersymmetric theory. All the SM particles fit into a chiral or vector supermultiplet and hence all have a partner with spin differing by $\frac{1}{2}$. The superpartner of a SM particle is always denoted with a tilde. In the following, we will always assume the auxiliary fields F and D have been replaced in function of the other fields by their equations of motion.

[2]This is the case since we assume a canonical Kähler and renormalizability.

2.2.1 The particle content of the MSSM

The particle content of the MSSM and their representations under the SM gauge groups are shown in tables 2.1 and 2.2.

The matter sector of the SM, the quarks and leptons, fit into chiral supermultiplets and their scalar superpartners are respectively called squarks and sleptons. Each quark and lepton is described by a left-handed as well as a right-handed Weyl fermion and therefore, each has two superpartners. Since chiral supermultiplets only contain left-handed Weyl fermions, it is the conjugate of the right-handed Weyl spinors that occurs in the chiral supermultiplets. For example, the up-type quark comes in two chiral supermultiplets $(u_L, \widetilde{u}_L)$ and $(u_R^c, \widetilde{u}_R^*)$.

The gauge bosons are best accommodated in vector multiplets. Since their SUSY partners have to carry the same quantum numbers, the corresponding Weyl fermions, referred to as gauginos, have to transform according to the adjoint representation of the gauge group as well. The superpartners of the gluon g_μ, the $\mathrm{SU(2)_L}$ gauge bosons W_μ and the $\mathrm{U(1)_Y}$ gauge boson B_μ are respectively called the gluino $\widetilde{g}$, the winos $\widetilde{W}$ and the bino $\widetilde{B}$.

As for the scalar sector of the SM, the most straightforward choice is to embed the Higgs doublet in a chiral supermultiplet, the corresponding Weyl fermion is then called the higgsino. However, the presence of only one higgsino would imply that perturbation theory does not conserve gauge invariance, in other words, our supersymmetric theory would contain gauge-anomalies. Within the MSSM this problem is solved by introducing a second chiral supermultiplet for the Higgs sector, with opposite hypercharge.[3] We then have two scalar doublets, one, H_u, gives mass to the up-type quarks while the other, H_d, gives mass to the down-type quarks. The corresponding hissginos are denoted as $\widetilde{H}_u$ and $\widetilde{H}_d$.

2.2.2 The MSSM Lagrangian

As was shown in section 2.1.3, once the particles and supermultiplets are fixed, the Lagrangian density of a renormalizable supersymmetric theory is fully determined by the superpotential. The most general superpotential for the MSSM would however lead to baryon number (B) or lepton number (L) violation which is strongly constrained by experiment. In the Standard Model B and L are accidental symmetries, but in the MSSM we can impose the conservation of B and L by imposing and additional, discrete symmetry called R-parity defined as

$$R = (-1)^{2S+3B+L} \tag{2.13}$$

[3]The condition for the cancellation of the gauge anomalies is $\mathrm{Tr}[T_3^2 Y] = \mathrm{Tr}[Y^3] = 0$ where the traces run over all the left-handed Weyl fermions. If we add one Higgs supermultiplet, the contribution from the corresponding higgsino can be cancelled by adding a second higgsino with opposite hypercharge as is done in the MSSM.

spin 0	spin $\frac{1}{2}$	$SU(3)_c$	$SU(2)_L$	$U(1)_Y$
$\widetilde{q} = \begin{pmatrix} \widetilde{u}_L \\ \widetilde{d}_L \end{pmatrix}$	$q = \begin{pmatrix} u_L \\ d_L \end{pmatrix}$	$\mathbf{3}$	$\mathbf{2}$	$\frac{1}{6}$
$\widetilde{u}_R^*$	u_R^c	$\bar{\mathbf{3}}$	$\mathbf{1}$	$-\frac{2}{3}$
$\widetilde{d}_R^*$	d_R^c	$\bar{\mathbf{3}}$	$\mathbf{1}$	$\frac{1}{3}$
$\widetilde{l} = \begin{pmatrix} \widetilde{\nu}_L \\ \widetilde{e}_L \end{pmatrix}$	$l = \begin{pmatrix} \nu_L \\ e_L \end{pmatrix}$	$\mathbf{1}$	$\mathbf{2}$	$-\frac{1}{2}$
$\widetilde{e}_R^*$	e_R^c	$\mathbf{1}$	$\mathbf{1}$	1
$H_u = \begin{pmatrix} H_u^+ \\ H_u^0 \end{pmatrix}$	$\widetilde{H}_u = \begin{pmatrix} \widetilde{H}_u^+ \\ \widetilde{H}_u^0 \end{pmatrix}$	$\mathbf{1}$	$\mathbf{2}$	$\frac{1}{2}$
$H_d = \begin{pmatrix} H_d^0 \\ H_d^- \end{pmatrix}$	$\widetilde{H}_d = \begin{pmatrix} \widetilde{H}_d^0 \\ \widetilde{H}_d^- \end{pmatrix}$	$\mathbf{1}$	$\mathbf{2}$	$-\frac{1}{2}$

Table 2.1: The chiral supermultiplets describing the matter and Higgs sector of the MSSM. The first two columns on the right show their representation under $SU(3)_c$ and $SU(2)_L$ while the last column shows their U(1) hypercharge Y.

spin 1	spin $\frac{1}{2}$	$SU(3)_c$	$SU(2)_L$	$U(1)_Y$
g_μ	$\widetilde{g}$	$\mathbf{8}$	$\mathbf{1}$	0
W_μ	$\widetilde{W}$	$\mathbf{1}$	$\mathbf{3}$	0
B_μ	$\widetilde{B}$	$\mathbf{1}$	$\mathbf{1}$	0

Table 2.2: The same as for table 2.1 for the vector supermultiplets within the MSSM.

where S denotes the spin quantum number. The SM and SUSY particles respectively have R-parity 1 and -1. As a consequence, supersymmetric particles will always be produced in pairs and the lightest SUSY particle, the LSP, has to be stable. R-parity conservation therefore has important consequences for the phenomenology of supersymmetric theories.

The superpotential

The superpotential of the MSSM, assuming R-parity conservation and neglecting right-handed neutrinos is given by

$$W_{\text{MSSM}} = (y_u)_{ij}\, \widetilde{u}_R^{i\dagger} \widetilde{q}^j \cdot H_u - (y_d)_{ij}\, \widetilde{d}_R^{i\dagger} \widetilde{q}^j \cdot H_d - (y_e)_{ij}\, \widetilde{e}_R^{i\dagger} \widetilde{l}^j \cdot H_d + \mu H_u \cdot H_d \quad (2.14)$$

where the indices $i, j = 1 \ldots 3$ now run over the generation indices. The dimensionless Yukawa couplings y_u, y_d and y_e are 3×3 matrices in generation space, μ has mass dimension one and will appear in the mass matrices of the Higgses and higgsinos. Finally, the dot product stands for $\text{SU}(2)_L$ invariant products, for example

$$H_u \cdot H_d = \epsilon_{ab} H_u^a H_d^b = H_u^+ H_d^- - H_u^0 H_d^0 \quad (2.15)$$

where a and b are fundamental $\text{SU}(2)_L$ indices and $\epsilon_{12} = -\epsilon_{21} = 1$.

Soft SUSY-breaking terms

The particle content and superpotential of the MSSM we specified up to now, leads to a theory invariant under supersymmetry. As we mentioned earlier, since no SUSY particles are observed up to now, they have to be more massive than their SM partners and SUSY has to be broken. We postpone a discussion of how this breaking can be accomplished to section 2.3, for now we will suffice assuming that SUSY has been broken at an unspecified higher energy scale. At the low scale, this results in a set of effective couplings that explicitly break SUSY. Including all of them in the MSSM Lagrangian covers all possible SUSY-breaking mechanisms at the high scale.

As we do not want to reintroduce the fine-tuning problem described in section 1.5.1, we eliminate the couplings that could introduce quadratically divergent corrections to the scalar masses. Since the cut-off scale Λ_{UV} and a scalar mass m_s both have mass dimension one, any coupling giving rise to a correction $\Delta m_s^2 \sim \Lambda_{\text{UV}}^2$, is necessarily dimensionless. From this dimensional analysis, we conclude that SUSY-breaking terms involving couplings with a positive mass dimension will not reintroduce the fine-tuning problem, they are said to break SUSY only softly. The soft SUSY-breaking Lagrangian of the MSSM is given by

$$\mathcal{L}_{\text{soft}}^{\text{MSSM}} = \mathcal{L}_{\text{soft}}^{\text{gaugino}} + \mathcal{L}_{\text{soft}}^{\text{scalar}} + \mathcal{L}_{\text{soft}}^{\text{tri/bi}} \quad (2.16)$$

where the first term contains mass terms for the gauginos

$$\mathcal{L}_{\text{soft}}^{\text{gaugino}} = \frac{1}{2}\left[M_3\widetilde{g}\widetilde{g} + M_2\widetilde{W}\widetilde{W} + M_1\widetilde{B}\widetilde{B} + \text{h.c.}\right], \tag{2.17}$$

the second mass terms for the squarks, sleptons and the two scalar $\text{SU}(2)_L$ doublets

$$\begin{aligned}\mathcal{L}_{\text{soft}}^{\text{scalar}} = &-\left(M_{\tilde{Q}}^2\right)_{ij}\widetilde{q}^{i\dagger}\widetilde{q}^{j} - \left(M_{\tilde{U}}^2\right)_{ij}\widetilde{u}_R^{i\dagger}\widetilde{u}_R^{j} - \left(M_{\tilde{D}}^2\right)_{ij}\widetilde{d}_R^{i\dagger}\widetilde{d}_R^{j} \\ &- \left(M_{\tilde{L}}^2\right)_{ij}\widetilde{l}^{i\dagger}\widetilde{l}^{j} - \left(M_{\tilde{E}}^2\right)_{ij}\widetilde{e}_R^{i\dagger}\widetilde{e}_R^{j} - m_{H_u}^2 H_u^\dagger H_u - m_{H_d}^2 H_d^\dagger H_d\end{aligned} \tag{2.18}$$

and the third term represents tri- and bilinear couplings among the scalars

$$\begin{aligned}\mathcal{L}_{\text{soft}}^{\text{tri/bi}} = &-\left(T_u\right)_{ij}\tilde{u}_R^{i\dagger}\tilde{q}^{j}\cdot H_u + \left(T_d\right)_{ij}\tilde{d}_R^{i\dagger}\tilde{q}^{j}\cdot H_d \\ &+ \left(T_e\right)_{ij}\tilde{e}_R^{i\dagger}\tilde{l}^{j}\cdot H_d - bH_u\cdot H_d + \text{h.c.}\end{aligned} \tag{2.19}$$

where b has mass dimension two. The mass matrices $M_{\tilde{Q}}^2$, $M_{\tilde{U}}^2$, $M_{\tilde{D}}^2$, $M_{\tilde{L}}^2$ and $M_{\tilde{e}}^2$ as well as the trilinear couplings T_u, T_d and T_e are 3×3 matrices in family space.

2.2.3 Sparticle masses in the MSSM

Electroweak symmetry breaking in the MSSM

As in the SM (see section 1.3), the scalar potential breaks electroweak symmetry spontaneously which generates mass terms for the gauge bosons, the leptons and quarks. In the SM, there was only one scalar doublet to get a vev whereas SUSY contains many more scalar fields that could acquire a vev. A non-zero vev for a squark, for example, would however not be desirable as it would lead to a charge and colour-breaking vacuum state. We therefore assume that the Higgs doublets are the only fields with a vev. Gathering all terms contributing to the Higgs scalar potential from the Lagrangian discussed in the previous sections, we get

$$\begin{aligned}V = &\left(|\mu|^2 + m_{H_u}^2\right)\left(|H_u^0|^2 + |H_u^+|^2\right) + \left(|\mu|^2 + m_{H_d}^2\right)\left(|H_d^0|^2 + |H_d^-|^2\right) \\ &+ \left[b\left(H_u^+ H_d^- - H_u^0 H_d^0\right) + \text{h.c.}\right] \\ &+ \frac{1}{8}\left(g^2 + g'^2\right)\left(|H_u^0|^2 + |H_u^+|^2 - |H_d^0|^2 - |H_d^-|^2\right)^2 \\ &+ \frac{g^2}{2}\left|H_u^+ H_d^{0*} + H_u^0 H_d^{-*}\right|^2.\end{aligned} \tag{2.20}$$

We can always use the $\text{SU}(2)_L$ symmetry to rotate the Higgs doublet H_u such that the vev of the charged component is zero, $\langle H_u^+\rangle = 0$. If we impose this to be the minimum of the potential (2.20), we immediately find that also $\langle H_d^-\rangle = 0$. The minimum of the potential hence does not break charge conservation, only the neutral components of the Higgs doublets can acquire a vev

$$\langle H_u\rangle = \frac{1}{\sqrt{2}}\begin{pmatrix}0\\ v_u\end{pmatrix} \qquad \text{and} \qquad \langle H_d\rangle = \frac{1}{\sqrt{2}}\begin{pmatrix}v_d\\ 0\end{pmatrix} \tag{2.21}$$

and the ratio of their vevs defines $\tan\beta$ as

$$\tan\beta = \frac{v_u}{v_d}. \tag{2.22}$$

Since v_u and v_d are real and positive, $0 < \beta < \pi/2$. The masses of the Z and W bosons are given by

$$m_W = \frac{g\sqrt{v_u^2 + v_d^2}}{2}, \qquad m_Z = \frac{m_W}{\cos\theta_W}. \tag{2.23}$$

Comparing with the SM result (1.37), we see that v_u and v_d are related to the vev of the Standard Model scalar by

$$v = \sqrt{v_u^2 + v_d^2}. \tag{2.24}$$

The Higgs sector is defined by the parameters m_{H_u}, m_{H_d}, μ and b of the scalar potential (2.20) and two additional parameters specifying EWSB which can be chosen as (v_u, v_d) or $(\tan\beta, m_Z)$. However, the scalar potential (2.20) will only break electroweak symmetry if the potential has a minimum for $|H_{u,d}| \neq 0$. This imposes the following two constraints on the parameters

$$m_{H_u}^2 + |\mu|^2 - b\cot\beta - \frac{m_Z^2}{2}\cos(2\beta) = 0 \tag{2.25}$$

$$m_{H_d}^2 + |\mu|^2 - b\tan\beta + \frac{m_Z^2}{2}\cos(2\beta) = 0 \tag{2.26}$$

and allows to eliminate two of the six parameters of the Higgs sector in the MSSM. Since m_Z is experimentally measured, the Higgs sector is described by three parameters, that can for example be chosen to be $\tan\beta$, b and μ.

Higgs masses

The Higgs doublets of the MSSM are two $\mathrm{SU}(2)_L$ doublets, containing 4 complex or 8 real degrees of freedom. Similarly to the SM, 3 of them are absorbed by the longitudinal modes of the $W^\pm$ and the Z boson to make them massive. The remaining 5 degrees of freedom, mix to form the physical Higgs fields. We expand the Higgs doublets around their vacuum expectation value as

$$H_u = \begin{pmatrix} h_u^+ \\ \frac{1}{\sqrt{2}}(v_u + h_u^0 + ip_u^0) \end{pmatrix} \qquad \text{and} \qquad H_d = \begin{pmatrix} \frac{1}{\sqrt{2}}(v_d + h_d^0 + ip_d^0) \\ h_d^- \end{pmatrix}, \tag{2.27}$$

extract the mass matrices of the scalar fields $h_{u/d}^0$, the pseudoscalar $p_{u/d}^0$ and the charged fields $h_{u/d}^\pm$ and diagonalize them to come to the mass eigenstates. The pseudoscalar fields $p_{u/d}^0$ mix as

$$\begin{pmatrix} G^0 \\ A^0 \end{pmatrix} = \begin{pmatrix} \sin\beta & -\cos\beta \\ \cos\beta & \sin\beta \end{pmatrix} \begin{pmatrix} p_u^0 \\ p_d^0 \end{pmatrix} \tag{2.28}$$

to form the two neutral CP-odd pseudoscalar fields G^0 and A^0. G^0 remains massless while A^0 has mass

$$m_A^2 = \frac{2b}{\sin(2\beta)} = 2|\mu|^2 + m_{H_u}^2 + m_{H_d}^2. \tag{2.29}$$

This equation is often used to eliminate b in favour of m_A so that they can be used interchangeably to parametrize the Higgs sector. The charged components mix as

$$\begin{pmatrix} G^\pm \\ H^\pm \end{pmatrix} = \begin{pmatrix} \sin\beta & -\cos\beta \\ \cos\beta & \sin\beta \end{pmatrix} \begin{pmatrix} h_u^\pm \\ h_d^\pm \end{pmatrix} \tag{2.30}$$

where the $G^\pm$ are massless and the mass of $H^\pm$ is given by

$$m_{H^\pm}^2 = m_A^2 + m_W^2. \tag{2.31}$$

Note also that the mixing of the pseudoscalar fields in (2.28) and the charged fields in (2.30) is fully determined by the ratio of the vevs $\tan\beta = v_u/v_d$. Finally, the two scalar fields $h_{u/d}^0$ mix as

$$\begin{pmatrix} h^0 \\ H^0 \end{pmatrix} = \begin{pmatrix} \cos\alpha & -\sin\alpha \\ \sin\alpha & \cos\alpha \end{pmatrix} \begin{pmatrix} h_u^0 \\ h_d^0 \end{pmatrix} \tag{2.32}$$

where the mixing angle α can be found at tree level to be

$$\alpha = \frac{1}{2}\arctan\left(\frac{m_A^2 + m_Z^2}{m_A^2 - m_Z^2}\tan(2\beta)\right). \tag{2.33}$$

The mass of the two neutral CP-even scalar mass eigenstates h^0 and H^0 is given by

$$m_{h^0,H^0}^2 = \frac{1}{2}\left(m_A^2 + m_Z^2 \mp \sqrt{(m_A^2 - m_Z^2)^2 + 4m_Z^2 m_A^2 \sin^2(2\beta)}\right). \tag{2.34}$$

The three Goldstone bosons G^0 and $G^\pm$ give mass to the massive gauge bosons, through a calculation similar to the one in the Standard Model, we can obtain the W- and Z-boson masses given in (2.23).

Even though m_A, $m_{H^\pm}$ and m_{H^0} can in principle be arbitrarily high since they grow with $\frac{b}{\sin(2\beta)}$, the mass of the lightest Higgs boson is, at tree-level, bounded from above as

$$m_{h^0} < m_Z|\cos 2\beta| \tag{2.35}$$

which is clearly incompatible with the experimental observations (*cfr.* figure 1.1). This can however be solved when we include the quantum corrections. The lightest Higgs boson mass receives large quantum corrections, mainly from top and stop loops, which leads to a higher, more realistic, upper bound of the order $m_{h^0} \lesssim 135$ GeV [39].

Neutralino mixing

In electroweak symmetry breaking, the neutral higgsinos $\widetilde{H}_u^0$ and $\widetilde{H}_d^0$ will mix with the neutral electroweak gauginos $\widetilde{B}$ and $\widetilde{W}^3$ to form the mass eigenstates. If we work in the basis of the gauge eigenstates $(i\widetilde{B}, i\widetilde{W}^3, \widetilde{H}_d^0, \widetilde{H}_u^0)$ the mass matrix M_{χ^0} is given by

$$M_{\chi^0} = \begin{pmatrix} M_1 & 0 & -m_Z s_W c_\beta & m_Z s_W s_\beta \\ 0 & M_2 & m_Z c_W c_\beta & -m_Z c_W s_\beta \\ -m_Z s_W c_\beta & m_Z c_W c_\beta & 0 & -\mu \\ m_Z s_W s_\beta & -m_Z c_W s_\beta & -\mu & 0 \end{pmatrix} \tag{2.36}$$

where we defined $s_\beta \equiv \sin\beta$, $c_\beta \equiv \cos\beta$, $s_W \equiv \sin\theta_W$ and $c_W \equiv \cos\theta_W$. Following the SLHA convention [44], we absorbed the factors i in the gaugino fields to make sure the mass matrix is real and symmetric and can be diagonalized by a unitary transformation N

$$N^* M_{\chi^0} N^{-1} = \mathrm{diag}(m_{\chi_1^0}, m_{\chi_2^0}, m_{\chi_3^0}, m_{\chi_4^0}). \tag{2.37}$$

The mass eigenstates $\chi^0_{1,2,3,4}$ are referred to as neutralinos and are defined in order of increasing mass $m_{\chi_1^0} < m_{\chi_2^0} < m_{\chi_3^0} < m_{\chi_4^0}$. They are related to the interaction eigenstates by

$$\begin{pmatrix} \chi_1^0 \\ \chi_2^0 \\ \chi_3^0 \\ \chi_4^0 \end{pmatrix} = N \begin{pmatrix} i\widetilde{B} \\ i\widetilde{W}^3 \\ \widetilde{H}_d^0 \\ \widetilde{H}_u^0 \end{pmatrix}. \tag{2.38}$$

Generically speaking, the eigenvalues $m_{\chi_i^0}$ in equation (2.37) can be complex. We can however choose them to be non-negative and real by choosing the mixing matrix N accordingly and/or absorbing the complex phases in the fields χ_i^0. This implies that the mixing matrix N is in general complex.

Up to now, the neutralino fields were always expressed as two-component Majorana Weyl fermions. The four-component Majorana spinor $\Psi_{\chi_i^0}$ corresponding to a neutralino mass eigenstate χ_i^0 can be obtained as

$$\Psi_{\chi_i^0} = \begin{pmatrix} \chi_i^0 \\ \bar{\chi}_i^0 \end{pmatrix} \tag{2.39}$$

where $i = 1 \ldots 4$ and we suppressed the spinor indices. χ_i^0 is a left-handed Weyl fermion while $\bar{\chi}_i^0$ is right-handed.

Chargino mixing

Moving on to the charged fields, the charged higgsinos $\widetilde{H}_u^+$ and $\widetilde{H}_d^-$ will mix with the charged electroweak gauginos $\widetilde{W}^\pm$. Their mass term in the Lagrangian

density can be written as

$$\mathcal{L}_{\chi^\pm} = -\left(i\widetilde{W}^- \widetilde{H}_d^-\right) M_{\chi^\pm} \begin{pmatrix} i\widetilde{W}^+ \\ \widetilde{H}_u^+ \end{pmatrix} + \text{h.c.} \tag{2.40}$$

where the mass matrix reads

$$M_{\chi^\pm} = \begin{pmatrix} M_2 & \sqrt{2}s_\beta m_W \\ \sqrt{2}c_\beta m_W & \mu \end{pmatrix}. \tag{2.41}$$

This mass matrix is not necessarily hermitian and we need two unitary matrices U and V to diagonalize this matrix

$$U^* M_{\chi^\pm} V^{-1} = \text{diag}(m_{\chi_1^\pm}, m_{\chi_2^\pm}). \tag{2.42}$$

the mass eigenstates, the charginos $\chi_{1,2}^\pm$, are again defined in order of increasing mass, $m_{\chi_1^\pm} < m_{\chi_2^\pm}$. The transformation matrices U and V relate the charginos to the interaction eigenstates as

$$\begin{pmatrix} \chi_1^+ \\ \chi_2^+ \end{pmatrix} = V \begin{pmatrix} i\widetilde{W}^+ \\ \widetilde{H}_u^+ \end{pmatrix} \qquad \begin{pmatrix} \chi_1^- \\ \chi_2^- \end{pmatrix} = U \begin{pmatrix} i\widetilde{W}^- \\ \widetilde{H}_d^- \end{pmatrix} \tag{2.43}$$

and can be obtained by respectively diagonalizing $M_{\chi^\pm} M_{\chi^\pm}^\dagger$ and $M_{\chi^\pm}^\dagger M_{\chi^\pm}$. The masses of the charginos are given by

$$m^2_{\chi^\pm_{1,2}} = \frac{1}{2}\Big[|M_2|^2 + |\mu|^2 + 2m_W^2 \mp \sqrt{(|M_2|^2 + |\mu|^2 + 2m_W^2)^2 - 4|\mu M_2 - m_W^2 \sin(2\beta)|^2}\Big]. \tag{2.44}$$

Similarly to the case of the neutralinos, all the chargino fields are expressed as two-component Weyl fermions. The four-component Dirac spinor $\Psi_{\chi_i^\pm}$ corresponding to a chargino mass eigenstate $\chi_i^\pm$ can be obtained as

$$\Psi_{\chi_i^\pm} = \begin{pmatrix} \chi_i^\pm \\ \bar{\chi}_i^\mp \end{pmatrix} \tag{2.45}$$

where the spinor indices are suppressed and $i = 1, 2$. $\chi_i^\pm$ and $\bar{\chi}_i^\mp$ are a left- and righ-handed Weyl fermion respectively.

Mixing in the quark sector

As in the Standard Model, the Yukawa couplings will transform to mass terms for the quarks after EWSB which, as was described in section 1.3.3, can be diagonalized by applying the unitary transformations

$$u_L \to V_{u_L} u_L, \quad u_R \to V_{u_R} u_R, \quad d_L \to V_{d_L} d_L, \quad d_R \to V_{d_R} d_R \tag{2.46}$$

on the quark fields. Whereas the mass matrix of the quarks is determined solely by the Yukawa couplings, the mass matrix of the squarks also contains contributions from the soft breaking parameters and the D- and F-terms of the scalar potential (2.11). Even though the squark mass matrix will most likely not be diagonal in this basis, we can still align the squark fields to the SM fields and transform them as

$$\widetilde{u}_L \to V_{u_L}\widetilde{u}_L, \quad \widetilde{u}_R \to V_{u_R}\widetilde{u}_R, \quad \widetilde{d}_L \to V_{d_L}\widetilde{d}_L, \quad \widetilde{d}_R \to V_{d_R}\widetilde{d}_R. \tag{2.47}$$

In this basis, we can write the superpotential as

$$W_{\text{MSSM}} = (\widehat{y}_u)_{ij}\, \widetilde{u}_R^{i\dagger}\widetilde{q}^j \cdot H_u - \left(\widehat{y}_d V_{d_L}^\dagger V_{u_L}\right)_{ij} \widetilde{d}_R^{i\dagger}\widetilde{q}^j \cdot H_d + \dots \tag{2.48}$$

where ellipses denote the terms not related to the quark sector. In this equation we redefined the left-handed down-type (s)quark fields as

$$d_L \to V_{\text{CKM}} d_L, \quad \widetilde{d}_L \to V_{\text{CKM}}\widetilde{d}_L \quad \text{with} \quad V_{\text{CKM}} = V_{u_L}^\dagger V_{d_L} \tag{2.49}$$

and introduced the diagonal Yukawa matrices

$$\widehat{y}_u \equiv V_{u_R}^\dagger y_u V_{u_L}, \qquad \widehat{y}_d \equiv V_{d_R}^\dagger y_d V_{d_L}. \tag{2.50}$$

The squark basis defined by the redefinitions (2.47) and (2.49), is called the super-CKM basis [45]. If we further define

$$\widehat{M}_{\tilde{Q}}^2 \equiv V_{\text{CKM}} M_{\tilde{Q}}^2 V_{\text{CKM}}^\dagger \qquad \widehat{M}_{\tilde{U}}^2 \equiv V_{u_R}^\dagger M_{\tilde{U}}^2 V_{u_R} \qquad \widehat{M}_{\tilde{D}}^2 \equiv V_{d_R}^\dagger M_{\tilde{D}}^2 V_{d_R}$$

and

$$\widehat{T}_u \equiv V_{u_R}^\dagger T_u V_{u_L} \qquad \widehat{T}_d \equiv V_{d_R}^\dagger T_d V_{d_L},$$

the soft masses can be written as

$$\mathcal{L}_{\text{soft}}^{\text{scalar}} = -\left(V_{\text{CKM}}\widehat{M}_{\tilde{Q}}^2 V_{\text{CKM}}^\dagger\right)_{ij} \widetilde{q}^{i\dagger}\widetilde{q}^j - \left(\widehat{M}_{\tilde{U}}^2\right)_{ij} \widetilde{u}_R^{i\dagger}\widetilde{u}_R^j - \left(\widehat{M}_{\tilde{D}}^2\right)_{ij} \widetilde{d}_R^{i\dagger}\widetilde{d}_R^j + \dots$$

while the tri- and bilinear couplings among the scalars become

$$\mathcal{L}_{\text{soft}}^{\text{tri/bi}} = -\left(\widehat{T}_u\right)_{ij} \tilde{u}_R^{i\dagger}\tilde{q}^j \cdot H_u + \left(\widehat{T}_d V_{\text{CKM}}^\dagger\right)_{ij} \tilde{d}_R^{i\dagger}\tilde{q}^j \cdot H_d + \text{h.c.} + \dots \tag{2.51}$$

where the terms unrelated to the quark sector are again contained in the ellipses. Whereas the transformed Yukawa matrices $\widehat{y}$ are defined to be diagonal in this basis, this is does not necessarily hold for the soft masses $\widehat{M}$ and the trilinear couplings $\widehat{T}$.

In addition to the soft masses and the trilinear couplings, the scalar potential (2.11) will also contribute to the squark mass matrix. After EWSB, the F-term

$$\frac{1}{2}\sum_{i=1}^{m}|F_i|^2 = \frac{1}{2}\sum_{i=1}^{m}\left|\frac{\partial W_\phi}{\partial \phi_i}\right|^2 \tag{2.52}$$

contains the diagonal mass terms

$$(m_u^2)^{ij}\left(\widetilde{u}_L^{i\dagger}\widetilde{u}_L^j + \widetilde{u}_R^{i\dagger}\widetilde{u}_R^j\right) + (m_d^2)^{ij}\left(\widetilde{d}_L^{i\dagger}\widetilde{d}_L^j + \widetilde{d}_R^{i\dagger}\widetilde{d}_R^j\right) \tag{2.53}$$

as well as the left-right mixing terms

$$-\frac{\mu^*}{\tan\beta}m_u^{ij}\,\widetilde{u}_R^{i\dagger}\widetilde{u}_L^j - \mu^*\tan\beta\, m_d^{ij}\,\widetilde{d}_R^{i\dagger}\widetilde{d}_L^j + \text{h.c.} \tag{2.54}$$

where we defined the diagonal matrices

$$m_u = \frac{v_u}{\sqrt{2}}\widehat{y}_u = \frac{v\sin\beta}{\sqrt{2}}\widehat{y}_u \quad \text{and} \quad m_d = \frac{v_d}{\sqrt{2}}\widehat{y}_d = \frac{v\cos\beta}{\sqrt{2}}\widehat{y}_d. \tag{2.55}$$

The D-term

$$\frac{1}{2}\sum_{k=1}^{m} g_k^2 D_k^{a_k} D_k^{a_k} = \frac{1}{2}\sum_{k=1}^{m}\left[g_k^2\sum_i\left(\phi_i^* T_k^{a_k}\phi_i\right)\sum_j\left(\phi_j^* T_k^{a_k}\phi_j\right)\right], \tag{2.56}$$

on the other hand, contains terms with structure (squark)^2(Higgs)^2 which transform to mass terms for the squarks after EWSB. The D-term contributions to the squark mass matrix are diagonal in flavour and depend on the SU(2) and $\mathrm{U(1)_{em}}$ charge of the squarks as

$$D_{\tilde{q},L} = m_Z^2\left(T_{3q} - Q_q\sin^2\theta_W\right)\cos 2\beta \qquad \text{and} \qquad D_{\tilde{q},R} = m_Z^2 Q_q\sin^2\theta_W\cos 2\beta \tag{2.57}$$

where Q_q and T_{3q} (with $q = u, d$) are the electric charge and the weak isospin quantum numbers of the (s)quarks as were indicated in table 1.1 and 2.1.

In the super-CKM bases $(\tilde{u}_L, \tilde{c}_L, \tilde{t}_L, \tilde{u}_R, \tilde{c}_R, \tilde{t}_R)$ and $(\tilde{d}_L, \tilde{s}_L, \tilde{b}_L, \tilde{d}_R, \tilde{s}_R, \tilde{b}_R)$, the up- and down-type squark mass matrices $\mathcal{M}_{\tilde{u}}^2$ and $\mathcal{M}_{\tilde{d}}^2$ are given by

$$\mathcal{M}_{\tilde{u}}^2 = \begin{pmatrix} V_{\mathrm{CKM}}\widehat{M}_{\widetilde{Q}}^2 V_{\mathrm{CKM}}^\dagger + m_u^2 + D_{\tilde{u},L} & \frac{v_u}{\sqrt{2}}\widehat{T}_u^\dagger - m_u\frac{\mu}{\tan\beta} \\ \frac{v_u}{\sqrt{2}}\widehat{T}_u - m_u\frac{\mu^*}{\tan\beta} & \widehat{M}_{\widetilde{U}}^2 + m_u^2 + D_{\tilde{u},R} \end{pmatrix} \tag{2.58}$$

and

$$\mathcal{M}_{\tilde{d}}^2 = \begin{pmatrix} \widehat{M}_{\widetilde{Q}}^2 + m_d^2 + D_{\tilde{d},L} & \frac{v_d}{\sqrt{2}}\widehat{T}_d^\dagger - m_d\mu\tan\beta \\ \frac{v_d}{\sqrt{2}}\widehat{T}_d - m_d\mu^*\tan\beta & \widehat{M}_{\widetilde{D}}^2 + m_d^2 + D_{\tilde{d},R} \end{pmatrix} \tag{2.59}$$

respectively. They are both 6×6 matrices and all four terms in these matrices stand for a 3×3 matrix which is generally not diagonal. The mass matrix for the sleptons formulated in the super-PMNS basis is completely analogous.

2.2.4 The phenomenological MSSM

Even though the supersymmetric part of the MSSM based on the superpotential (2.14) does not introduce extra parameters, we do need no less than 105 new parameters [46] to specify the soft supersymmetry-breaking terms in equation (2.16). The parameter space of the full MSSM is therefore much larger than the 19-dimensional parameter space of the Standard Model. Experimental constraints however show that the soft SUSY-breaking terms can not be arbitrary.

One important set of constraints comes from the flavour observables involving flavour-changing neutral currents (FCNCs). FCNCs are processes connecting two flavours of the same charge, as for example in the decay $b \to s\gamma$, and are constrained by the experimental constraints on the rare decays of B-mesons or kaon mixing. In the Standard Model, flavour-changing neutral currents (FCNCs) only occur at the loop-level and are additionally suppressed by the GIM-mechanism [47]. Consequently, new physics could easily yield contributions comparable to the Standard Model predictions and given that the SM prediction is in good agreement with the data, flavour changing processes are strongly constrained by experiment. On the other hand, since the soft SUSY-breaking parameters are generally complex, they would also contribute to CP-violating effects. As these are also strongly constrained by experiment, the complex parts can not be chosen freely.

The flavour constraints are not naturally met within the formalism of supersymmetry and the problem of formulating a complete supersymmetric theory consistent with the flavour observables is referred to as the SUSY flavour problem. One way to solve the SUSY flavour problem, is to impose Minimal Flavour Violation (MFV). The MFV paradigm essentially assumes that all flavour- and CP-violating interactions are related to the structure of the Yukawa couplings. The flavour constraints and the validity of MFV will be studied in more detail later in chapter 6. In the following we will describe how we can restrict the parameter space of the MSSM to come to a more phenomenologically viable model, the phenomenological MSSM.

The parameter space of the phenomenological MSSM

The phenomenological MSSM, the pMSSM [48], reduces the parameter space of the MSSM based on phenomenological arguments. In the first place, undesirable flavour mixings and CP-violation are avoided by assuming MFV and we restrict the soft masses of the sfermions as well as the trilinear couplings to be real and diagonal. Assuming some more simplifications brings us to the following parameter space:

1. The soft masses are real and diagonal and the first generations are degen-

erate. The soft parameters in the squark sector then reduce to the set

$$\left(\widehat{M}_{\tilde{Q}}\right)_{11} = \left(\widehat{M}_{\tilde{Q}}\right)_{22} \equiv M_{\tilde{Q}_{1,2}} \qquad \left(\widehat{M}_{\tilde{Q}}\right)_{33} \equiv M_{\tilde{Q}_3} \tag{2.60}$$

$$\left(\widehat{M}_{\tilde{U}}\right)_{11} = \left(\widehat{M}_{\tilde{U}}\right)_{22} \equiv M_{\tilde{U}_{1,2}} \qquad \left(\widehat{M}_{\tilde{U}}\right)_{33} \equiv M_{\tilde{U}_3} \tag{2.61}$$

$$\left(\widehat{M}_{\tilde{D}}\right)_{11} = \left(\widehat{M}_{\tilde{D}}\right)_{22} \equiv M_{\tilde{D}_{1,2}} \qquad \left(\widehat{M}_{\tilde{D}}\right)_{33} \equiv M_{\tilde{D}_3} \tag{2.62}$$

while the soft masses of the sleptons are parametrized by

$$\left(\widehat{M}_{\tilde{L}}\right)_{11} = \left(\widehat{M}_{\tilde{L}}\right)_{22} \equiv M_{\tilde{L}_{1,2}} \qquad \left(\widehat{M}_{\tilde{L}}\right)_{33} \equiv M_{\tilde{L}_3} \tag{2.63}$$

$$\left(\widehat{M}_{\tilde{E}}\right)_{11} = \left(\widehat{M}_{\tilde{E}}\right)_{22} \equiv M_{\tilde{E}_{1,2}} \qquad \left(\widehat{M}_{\tilde{E}}\right)_{33} \equiv M_{\tilde{E}_3}. \tag{2.64}$$

The soft sfermion masses are therefore fully determined by 10 parameters.

2. The trilinear couplings are defined proportional to the diagonal Yukawa matrices as

$$\widehat{T}_u \equiv A_u\, \widehat{y}_u \qquad \widehat{T}_d \equiv A_d\, \widehat{y}_d \qquad \widehat{T}_e \equiv A_e\, \widehat{y}_e. \tag{2.65}$$

We then impose the matrices A to be real and, similar to the sfermion soft masses, we impose

$$\left(A_u\right)_{11} = \left(A_u\right)_{22} \equiv A_{u,c} \qquad \left(A_u\right)_{33} \equiv A_t \tag{2.66}$$

$$\left(A_d\right)_{11} = \left(A_d\right)_{22} \equiv A_{d,s} \qquad \left(A_d\right)_{33} \equiv A_b \tag{2.67}$$

$$\left(A_l\right)_{11} = \left(A_l\right)_{22} \equiv A_{e,\mu} \qquad \left(A_l\right)_{33} \equiv A_\tau \tag{2.68}$$

which leaves us with 6 parameters describing the trilinear couplings.

3. The gaugino soft masses also have to be real which adds 3 parameters, M_1, M_2 and M_3, to the parameter space.

4. Finally, the Higgs sector is described by 3 more parameters, m_A, $\tan\beta$ and μ, which we also impose to be real.

These assumptions define the 22-dimensional parameter space of the pMSSM. Compared to the 105-dimensional parameter space of the full MSSM, the pMSSM is clearly much more accessible for phenomenological studies.

We introduced the pMSSM based on pragmatic arguments at the low energy scale. From a theoretical point of view, however, these assumptions are still arbitrary. It would be much more satisfying if the observed structure in the soft SUSY-breaking Lagrangian could be explained from a SUSY-breaking mechanism taking place at a higher energy scale.

2.3 Mechanisms of SUSY breaking

If we want to break SUSY without reintroducing the fine-tuning problem, SUSY should be restored at an energy scale M_{SUSY} in between the electroweak scale ($\sim$ 100 GeV) and the GUT scale ($\sim 10^{16}$ GeV). This can be done by breaking SUSY spontaneously. We will first generally discuss SUSY breaking after which we will briefly introduce the most common mechanisms to break SUSY.

2.3.1 General aspects of supersymmetry breaking

Similarly to the breaking of electroweak symmetry in the Standard Model, supersymmetry is spontaneously broken if the Lagrangian density is still invariant under SUSY transformations, but the vacuum state $|\Omega\rangle$ is not or, equivalently, $Q_\alpha |\Omega\rangle \neq 0$ or $Q^\dagger_{\dot\alpha} |\Omega\rangle \neq 0$. From the SUSY algebra (2.2) we can infer that the energy $E = P^0$ is related to the generators as

$$E = P^0 = \frac{1}{4}\left(Q_1 Q_1^\dagger + Q_1^\dagger Q_1 + Q_2 Q_2^\dagger + Q_2^\dagger Q_2\right). \tag{2.69}$$

When SUSY is conserved, we have $E|\Omega\rangle = 0$ and the vacuum has zero energy. On the other hand, when SUSY is spontaneously broken, we have

$$\langle\Omega| E |\Omega\rangle = \frac{1}{4}\left(|Q_1^\dagger|\Omega\rangle|^2 + |Q_1|\Omega\rangle|^2 + |Q_2^\dagger|\Omega\rangle|^2 + |Q_2|\Omega\rangle|^2\right) > 0 \tag{2.70}$$

so that the energy of the vacuum state is always positive. SUSY is broken if and only if $E > 0$ and conserved if and only if $E = 0$, the energy of the vacuum state can therefore be seen as the order parameter of the breaking of the symmetry.

At the classical level, the only contribution to the vacuum energy comes from the scalar potential. Therefore we know that $\langle\Omega| V |\Omega\rangle \geq 0$. From equation (2.11), we then see that SUSY is spontaneously broken if an only if the expectation value of one of the auxiliary fields F_i or $D_k^{a_k}$ does not vanish in the vacuum.

The goldstino, local supersymmetry and the gravitino

Goldstone's theorem tells us that, when a global symmetry is broken, there will be a massless particle with the same quantum numbers as the broken generator. The spontaneous breaking of SUSY therefore leads to a massless neutral Goldstone Weyl fermion, referred to as the goldstino. The proof of the supersymmetric version of the Goldstone theorem can be found in [39].

If we promote supersymmetry from a global to a local symmetry, we will have to introduce a supersymmetric analogue for the gauge bosons we mentioned in section 1.2.2. Due to the fermionic nature of supersymmetry, we will instead need a 'gauge fermion' which is called the gravitino. In section 1.2.3 we saw how

spontaneous symmetry breaking can generate a mass term for the gauge boson through the Brout-Englert-Higgs mechanism. Similarly, when supersymmetry is broken spontaneously, the gravitino will absorb the goldstino through the super-Higgs mechanism and become massive.

Suppose the hidden sector contains an auxiliary field F which breaks local SUSY spontaneously by acquiring a non-zero vev $\langle F \rangle$. $\langle F \rangle$ then corresponds to the scale of SUSY breaking and the mass of the gravitino $m_{3/2}$ can be estimated as

$$m_{3/2} = \frac{\langle F \rangle}{\sqrt{3} M_P}. \tag{2.71}$$

The gravitino mass is zero if SUSY is unbroken, or equivalently $\langle F \rangle = 0$, or if gravity can be neglected $M_P \to \infty$.

The supertrace theorem

After spontaneously breaking SUSY, the masses of the particles in supermultiplets will no longer be degenerate. For a theory containing chiral as well as gauge supermultiplets, a relation between the tree-level masses can be obtained from the explicit calculation of the mass matrices. This is referred to as the supertrace theorem and relates the tree-level masses squared m_i^2 by

$$\sum_{i \in s} m_i^2 - 2 \sum_{i \in f} m_i^2 + 3 \sum_{i \in v} m_i^2 = 0 \tag{2.72}$$

where s, f and v respectively denote the scalars, Weyl fermions and vector bosons of the theory. As a consequence, the masses of the particles within the supermultiplets will be split around an average value related to the mass the particle would have had if SUSY were unbroken. This implies that at least part of the superpartners of the SM particles have masses below the SM ones which is clearly excluded by experiment. Accommodating spontaneous SUSY breaking at tree-level is therefore a non-trivial task and SUSY breaking will have to be accomplished radiatively or by introducing non-renormalizable terms.

Mediating SUSY breaking and the renormalization group equations

Supersymmetry breaking then occurs in a 'hidden sector' of particles that do not interact directly, or only very weakly, with the 'visible sector', the MSSM. Instead, messenger fields which interact with both sectors will be responsible for mediating SUSY breaking. The nature of the mediating interactions will determine the structure of the soft SUSY-breaking terms in the visible sector at the SUSY-breaking scale which is usually rather high. From these terms at the high scale, the UV, the parameters, masses and couplings at the low scale, the IR, have to be calculated.

The renormalization group equations (RGEs) are differential equations connecting the parameters at different energy scales and the variation of the parameters is referred to as the RG-running. The RGEs of the MSSM can for example be found in [39] and several publicly available software packages have been developed to calculate the RG-running and the mass spectrum of a SUSY theory, for example SOFTSUSY [49], SPheno [50] and SuSpect [51]. Once you specify the SUSY-breaking mechanism and the input variables at the high scale, the corresponding parameters at the low scale are automatically calculated.

There are several proposals of how supersymmetry breaking can be mediated to the visible sector. The two main mediation mechanisms, gravity- and gauge-mediated SUSY breaking, will be detailed in the following.

2.3.2 Gravity-mediated SUSY breaking

In gravity-mediated SUSY breaking (see *e.g.* [52]), SUSY breaking is mediated by gravitational interactions. Since no renormalizable quantum theory of gravity has been formulated yet, the interaction is implemented in the Lagrangian by means of non-renormalizable couplings. If SUSY is broken by the non-zero vacuum expectation value of an auxiliary scalar field $\langle F \rangle$, the soft masses should vanish if $\langle F \rangle = 0$. The same should hold if gravity would be decoupled ($M_P \to \infty$) and therefore we know that

$$m_{\text{soft}} \sim \frac{\langle F \rangle}{M_P}. \tag{2.73}$$

If the soft masses are to be of the order $\mathcal{O}(10^3)$ GeV, low enough not to reintroduce the fine-tuning problem again and high enough to match the current experimental limit, this implies that the scale of SUSY breaking $\sqrt{\langle F \rangle}$ should be of the order $\mathcal{O}(10^{10} - 10^{11})$ GeV. The gravitino mass (2.71) will be of order $\mathcal{O}(10^3)$ GeV. Since the coupling strength of the gravitino to SM particles is proportional to $(m_{3/2} M_P)^{-1}$, it typically interacts only very weakly unless the gravitino is very light. In gravity-mediated SUSY-breaking scenarios, the gravitino is typically too heavy to be observable at colliders.

The Constrained MSSM (CMSSM)

In gravity-mediated SUSY breaking, the SUSY flavour problem (as discussed in section 2.2.4) is not naturally solved. Instead, additional assumptions on the parameters have to be made which is, for example, done in the constrained MSSM (CMSSM). Motivated by the apparent unification of the gauge couplings at the GUT-scale, the CMSSM applies the following boundary conditions at the GUT-scale:

- The gaugino masses unify.
  $M_1 = M_2 = M_3 = m_{1/2}$

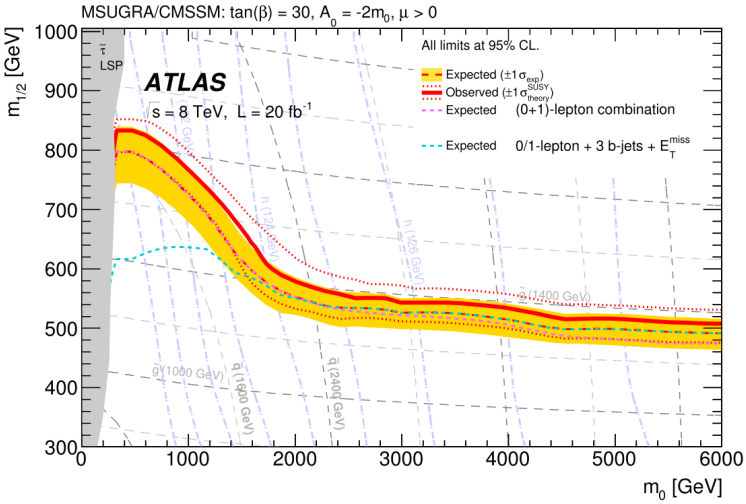

Figure 2.1: Exclusion limits at 95% Confidence Level for the 8 TeV analyses for mSUGRA/CMSSM. The limits are shown in the (m_0, $m_{1/2}$) plane, the other parameters are taken to be $\tan\beta = 30$, $A_0 = -2m_0$ and $\mu > 0$. The part of the parameter space underneath the curves is excluded. Figure taken from [53].

- The soft terms for the scalar masses are universal.
  $M_{\tilde{Q}^2} = M^2_{\tilde{U}} = M^2_{\tilde{D}} = M^2_{\tilde{L}} = M^2_{\tilde{E}} = m_0^2\mathbb{1}$ and $m^2_{H_u} = m^2_{H_d} = m_0^2$
- The trilinear couplings are defined by one parameter A_0.
  $T_u = A_0 y_u$, $T_d = A_0 y_d$ and $T_e = A_0 y_e$

The corresponding soft parameters at the weak scale are then obtained by running the parameters at the Planck scale down to the weak scale by solving the RGEs. In the Higgs sector, $\tan\beta$ is taken as an input parameter. Requiring that electroweak symmetry is broken successfully fixes b and $|\mu|$, leaving the sign of μ as a free input parameter (equations (2.25) and (2.26)). mSUGRA is therefore defined by only four parameters and a sign ($m_{1/2}$, m_0, A_0, $\tan\beta$ and sign(μ)) which makes the theory more accessible for phenomenological studies.

Experimental constraints on the CMSSM

How well does the CMSSM when we confront it with experiment? The most stringent constraints on the CMSSM parameter space come from collider experiments. We will introduce colliders later in chapter 3, for now we will suffice by stating the limits on the parameter space shown.

Figure 2.1 shows which part of the (m_0, $m_{1/2}$) plane is excluded by collider experiments, the part underneath the red curve is excluded at 95% Confidence Level. The remaining CMSSM parameters are related to the Higgs sector and are chosen as $\tan\beta = 30$, $A_0 = -2m_0$ and $\mu > 0$ which ensures the lightest Higgs

mass is around 125 GeV. The figure also shows the masses of the gluino and the squarks corresponding to the parameter points and we see that, within the CMSSM, gluinos and squarks are excluded to have masses lower than roughly 1.4 and 1.5 TeV respectively.

2.3.3 Gauge-mediated SUSY breaking

In gauge-mediated supersymmetry breaking (GMSB) [54] or its more general formulation, general gauge-mediation (GGM) [55], supersymmetry breaking is mainly communicated to the visible sector through messenger particles charged under the gauge interactions of the Standard Model. Since the SM gauge interactions are flavour universal, GMSB naturally solves the SUSY flavour problem mentioned in section 2.2.4. SUSY breaking is also mediated to the visible sector through the gravitational interactions, but these effects are subdominant with respect to the gauge interactions.

There are several ways to mediate SUSY breaking to the visible sector in gauge mediation. One possibility consists of introducing new messenger particles, chiral supermultiplets, which on the one hand couple to a SUSY-breaking vev $\langle F \rangle$ and, on the other hand, couple indirectly to the MSSM through the SM gauge interactions. The soft SUSY-breaking terms then arise from loop processes that will give rise to soft masses for the gauginos and sfermions of the order

$$m_{\text{soft}} \sim \frac{g^2}{(4\pi)^2} \frac{\langle F \rangle}{M_{\text{mess}}} \tag{2.74}$$

where g and M_{mess} respectively denote a gauge coupling strength and the characteristic scale of the messenger field. This equation behaves as expected: there are no soft terms if all the SM gauge couplings vanish, if there is no SUSY-breaking vev $\langle F \rangle = 0$ or if the messengers become infinitely heavy $M_{\text{mess}} \to \infty$. The contributions to the trilinear couplings are suppressed with respect to the other soft SUSY-breaking parameters and can be neglected.

If we assume $\sqrt{\langle F \rangle} \sim M_{\text{mess}}$, a SUSY-breaking scale as low as $\sqrt{\langle F \rangle} \sim 10^4$ GeV still results in a soft mass for the gluino at the experimental border of $\mathcal{O}(1\text{ TeV})$. The scale of supersymmetry breaking in GMSB can therefore be much lower than the SUSY-breaking scale in gravity-mediated SUSY breaking and the gravitino mass can be as low as $\mathcal{O}(\text{eV})$. Requiring on the other hand that gauge-mediating effects dominate over the effects of gravity mediation, gives an upper-limit on the gravitino mass of the order $\mathcal{O}(\text{GeV})$. As a result, in gauge mediation, the gravitino has a low mass of the order $\mathcal{O}(\text{eV} - \text{GeV})$ and will always be the lightest supersymmetric particle, the LSP.

Minimal gauge-mediated supersymmetry breaking (mGMSB)

In the simplest realization of gauge mediation, referred to as minimal GMSB (mGMSB), we only have one set of messenger chiral supermultiplets q, $\bar{q}$, l

and $\bar{l}$ respectively transforming under $\mathrm{SU}(3)_c \times \mathrm{SU}(2)_L \times \mathrm{U}(1)_Y$ as $(\mathbf{3}, \mathbf{1}, -1/3)$, $(\overline{\mathbf{3}}, \mathbf{1}, 1/3)$, $(\mathbf{1}, \mathbf{2}, 1/2)$ and $(\mathbf{1}, \mathbf{2}, -1/2)$. The messenger fields couple to a gauge-singlet chiral supermultiplet that breaks supersymmetry by means of non-zero vev $\langle F \rangle$ of its F-term. The scalar component of the SUSY-breaking multiplet also acquires a vev, generates the masses of the messenger fields and therefore determines the messenger scale M_{mess}. The soft masses of the gauginos then arise from interactions with the messenger fields at the one-loop order leading to gaugino soft masses given by

$$M_i(M_{\mathrm{mess}}) \approx \frac{\alpha_i(M_{\mathrm{mess}})}{4\pi}\Lambda \tag{2.75}$$

where we defined the effective SUSY-breaking scale $\Lambda \equiv \langle F \rangle / M_{\mathrm{mess}}$ and denoted the coupling strength of the i'th gauge group by α_i. The scalar fields, on the contrary, acquire their soft masses from the interactions with the messenger sector at the two-loop order. The soft mass of a scalar ϕ_i therefore reads

$$M^2_{\phi_i}(M_{\mathrm{mess}}) \approx 2\Lambda^2 \sum_{i=1}^{3} k_i \left(\frac{\alpha_i(M_{\mathrm{mess}})}{4\pi} \right)^2 \tag{2.76}$$

with $k_1 = 3Y^2/5$ where Y denotes the hypercharge, $k_2 = 3/4$ for $\mathrm{SU}(2)_L$ doublets and 0 for singlets and $k_3 = 4/3$ for colour triplets and 0 for colour singlets.

The soft masses in mGMSB are fully determined by the mass scale Λ and the messenger scale M_{mess}. We mentioned in section 2.2.3 that the Higgs sector of the MSSM is parametrized by 6 parameters: m_{H_u}, m_{H_d}, μ, b, $\tan\beta$ and v. The first two are fixed within mGMSB and further requiring EWSB (*cfr.* equations (2.25) and (2.26)) allows us to eliminate two more parameters, for example $|\mu|$ and b. Since v is experimentally known, we only need one parameters and a sign to parametrize the Higgs sector of the MSSM and the full mGMSB is parametrized by [56]

$$\tan\beta, \quad \Lambda, \quad \mathrm{sign}|\mu| \quad \text{and} \quad M_{\mathrm{mess}}. \tag{2.77}$$

Equations (2.75) and (2.76) imply that the ratios of the masses of the gauginos and scalars at the messenger scale are respectively given by

$$M_3 : M_2 : M_1 \simeq \alpha_3 : \alpha_2 : \alpha_1 \tag{2.78}$$

and

$$M^2_{\widetilde{Q}} : M^2_{\widetilde{L}} : M^2_{\widetilde{E}} \simeq \frac{4}{3}\alpha_3^2 : \frac{3}{4}\alpha_2^2 : \frac{3}{5}\alpha_1^2 \tag{2.79}$$

where $M^2_{\widetilde{Q}} \simeq M^2_{\widetilde{U}} \simeq M^2_{\widetilde{D}}$. We can also relate the scalar soft masses to the gaugino masses as

$$M^2_{\widetilde{Q}} \simeq \frac{8}{3}M_3^2 \qquad M^2_{\widetilde{L}} \simeq \frac{3}{2}M_2^2 \qquad M^2_{\widetilde{E}} \simeq \frac{6}{5}M_1^2. \tag{2.80}$$

If the messenger scale is well below the GUT-scale, we generally have $\alpha_3 \gg \alpha_2 > \alpha_1$ which implies that, at the messenger scale, the soft masses of the coloured

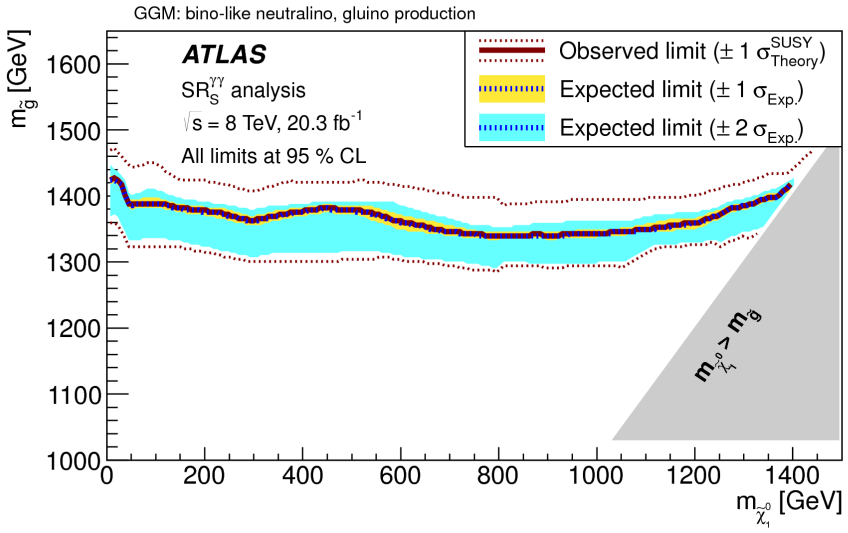

Figure 2.2: Exclusion limits in the gluino-bino mass plane for a scenario based on gauge mediation, the region underneath the red curve is excluded at 95% Confidence Level. Figure taken from [57].

superpartners are always the largest and the soft mass of the bino will be at the bottom of the mass spectrum. These tendencies are usually even enforced by the RG-evolution necessary to obtain the masses at the electroweak scale.

Experimental constraints on mGMSB

We can now use the above discussion about the mass spectrum in GMSB to interpret the exclusion plot shown in figure 2.2. This figure presents the limits on the pair-production of gluinos decaying to two quarks and the next-to-lightest supersymmetric particle, a bino-like neutralino, which will then decay to the gravitino LSP and a photon. The mass of the bino-like neutralino is shown on the horizontal axis while the vertical axis shows the mass of the gluino. Since everything underneath the red curve is excluded, we conclude that, in this scenario, the gluino mass has to be larger than 1.4 TeV. Using the aforementioned mass relations within mGMSB, we find that this limit on the gluino mass roughly corresponds to $\Lambda > 175$ TeV, $M_{\tilde{Q}} > 2.4$ TeV and $M_1 > 460$ GeV. The limits on the other sparticles can be computed analogously.[4]

[4] As a rule of thumb, the gauge coupling strengths at the electroweak scale are of the order $\alpha_3^{-1} \simeq 10$, $\alpha_2^{-1} \simeq 30$ and $\alpha_1^{-1} \simeq 60$.

2.4 The status of supersymmetry

In section 2.2.4 we defined the pMSSM as a phenomenologically more viable subset of the parameter space of the whole MSSM. In section 2.3.2 and 2.3.3 we then formulated two high-energy theories, mSUGRA and mGMSB, leading to phenomenologically acceptable and more accessible subsets of the parameter space of the (p)MSSM. We looked at the current experimental constraints and saw that within mSUGRA and mGMSB the masses of squarks and gluinos have to be higher than roughly $1.5 - 2.5$ TeV.

It is now worthwhile to come back to one of the main motivations for supersymmetry, the fine-tuning problem originating from the quadratic sensitivity of the Higgs boson mass to the scale of new physics. In the following we will quantify the level of fine-tuning and apply this to the simple models we constructed.

2.4.1 Naturalness

The level of fine-tuning in a model is related to a feeling of how natural a theory is and is therefore often referred to as the naturalness of the model. One way to quantify naturalness in SUSY, is based on the sensitivity of, for example, the mass of the Z boson, to the parameters a_i of the theory: a relative variation of a_i^2, $\delta a_i^2/a_i^2$, of a few percent should not result in a very large relative variation of m_Z^2, $\delta m_Z^2/m_Z^2$. More specifically, we can require the maximum of their ratio Δ defined as [58]

$$\Delta[a_i] = \left| \frac{a_i^2}{m_Z^2} \frac{\partial m_Z^2}{\partial a_i^2} \right| = \left| \frac{\partial \ln m_Z^2}{\partial \ln a_i^2} \right| \qquad \Delta = \max_i \Delta[a_i] \tag{2.81}$$

to be lower than a certain predefined value. There is however no unique way to define this sensitivity parameter, replacing a_i^2 with a_i in equation (2.81) would be equally valid, and there is no single correct way to combine several Δ's. Also, the acceptable value of Δ floats from 10 to 1000 depending on personal taste. So clearly, this (and any other) quantification of naturalness has to be treated with care. In the following we will assume $\Delta \leq 10$.

In SUSY, the tree-level mass of the Z boson (2.25) reduces to

$$m_Z^2 = -2(m_{H_u}^2 + |\mu|^2) + \dots \tag{2.82}$$

in the limit where $\tan\beta$ is large. We have $\Delta[\mu] \sim 2\mu^2/m_Z^2$ and, consequently, naturalness requires μ to be low, $\mu \leq 200$ GeV so that we expect higgsinos to be naturally light. At the one-loop level, the most important loop correction to m_{H_u} comes from the stop mass and is given by

$$\delta m_{H_u}^2 = -\frac{3y_t^2}{4\pi^2} m_{\tilde{t}}^2 \ln\left(\frac{\Lambda_{\text{UV}}}{m_{\tilde{t}}}\right) \tag{2.83}$$

where Λ_{UV} represents the UV cut-off. This correction cannot be too large which constrains $m_{\tilde{t}}$ to be of the order of 400 GeV for a cut-off $\Lambda_{\text{UV}} \sim 10$ TeV. A similar reasoning for the winos leads to an expected wino mass of the order of 1 TeV. Then, finally, at the two-loop level, the loop-corrections to the top squark have to be taken into account. The main corrections come from the gluino and naturalness constrains the mass of the gluino to be less than twice the stop mass [59].

Given that naturalness requires stops with a mass of at most 400 GeV and gluinos with a mass below 800 GeV, it becomes clear that reconciling naturalness, mSUGRA or mGMSB and the collider constraints discussed in sections 2.3.2 and 2.3.3 becomes hard and, as a consequence, the minimal realizations of supersymmetry became less and less attractive. There is however a whole plethora of supersymmetric models left to be looked for. The many possibilities combined with the lack of any experimental indications of where to go, demand a more model-independent approach in the experimental search for supersymmetry. To this end, the attention has shifted towards simplified models.

2.4.2 Simplified models and their experimental constraints

Simplified models are motivated by the observation that many supersymmetric theories would lead to similar signatures at colliders. If R-parity is conserved, the LSP is stable and, therefore, the collider signatures are largely determined by the supersymmetric particles at the bottom of the mass spectrum. For collider physics, it is often sufficient to assume that only a hand-full of supersymmetric particles have masses within the experimentally reachable range, the other sparticles are assumed to be too heavy and effectively decoupled, they are irrelevant for collider studies. Simplified models are widely used in experimental analyses and make it possible to set limits in a model-independent way.

The exclusion limits in the plane of the masses of the stop and the lightest neutralino obtained in the context of simplified models are shown in figure 2.3. The part underneath the curves is excluded at 95% Confidence Level. Clearly, also in the simplified model approach, there is little room left for 400 GeV stops as required by naturalness arguments.[5] In figure 2.4, we show an overview of the limits on the sparticle masses. We see that gluinos are experimentally bound to have masses above roughly 1 TeV, electroweak gauginos cannot be lighter than about 400 GeV and sleptons should have a mass above 300 GeV.

Given that no sign of supersymmetry has been observed so far, if SUSY is realized in Nature, it has to be hiding somewhere and we have to abandon some of the simplifications we made and look at more complicated theories which might cause SUSY to evade detection. In this thesis, we went along this road.

[5] In the region where the neutralino and stop mass are comparable, the limits are less stringent. The gaps correspond to the regions where stop-pair production is very similar to top-pair production and/or where the decay length of the stops becomes to large.

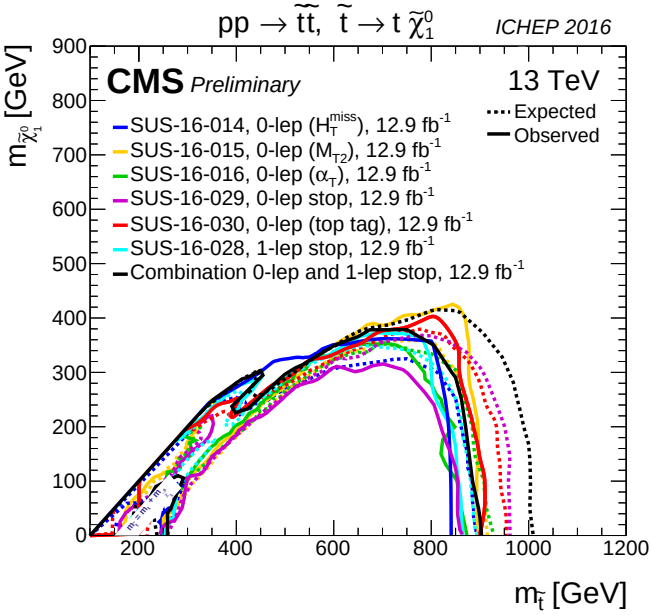

Figure 2.3: The exclusion limits at 95% Confidence Level are shown in the $m_{\tilde{t}_1}$-$m_{\tilde{\chi}_1^0}$ mass plane, the parts underneath the curves are excluded. Figure taken from [60].

In chapter 4 we will study a simplified model motivated from GGM that was overlooked so far. In chapter 5 we will investigate the implications of having two instead of one SUSY-breaking sector in gauge mediation and in chapter 6 we will revisit the flavour-violating terms in the soft masses of the squarks. But first, we will introduce collider physics and the phenomenological tools that will be used later in chapter 3.

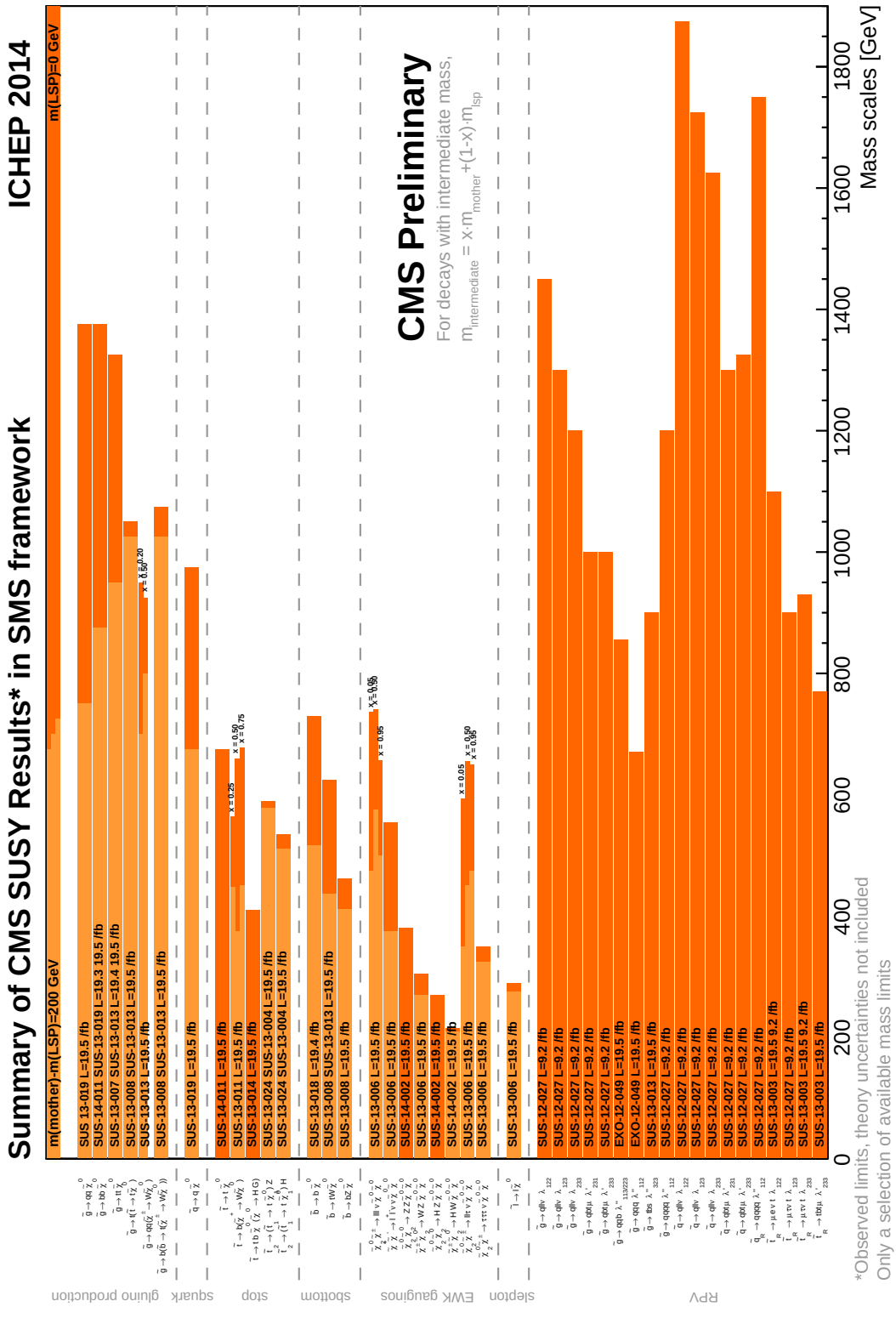

Figure 2.4: An overview of the limits on the masses of supersymmetric particles within the simplified-model approach. Figure taken from [60].

Chapter 3

Collider phenomenology

In chapter 1 and 2, we introduced the Standard Model and supersymmetry and discussed their experimental constraints without providing much detail on the experimental set-up. In this chapter, we will explain how quantum field theories are confronted with experiment, focussing in particular on collider experiments. Colliders study the particles and their interactions by colliding two particles with high energy on each other. Due to the high energy of this collision, other particles are produced which then pass through detectors. This way of studying the physics of the Standard Model and beyond has proven to be very successful.

Collider physics certainly owes a large part of this success to the development of simulation tools which make an efficient confrontation of a theory with experimental results feasible. We will discuss the basics of collider physics and introduce the colliders relevant for this work in section 3.1. Section 3.2 is devoted to the simulation tools. As the development of phenomenological tools was also a part of this thesis, I will also briefly touch upon my own contribution, ASperGe, in section 3.2.6.

3.1 Colliders

3.1.1 Basics of collider physics

When two particles collide, the probability for a certain process to occur, is given by its cross section σ, usually expressed in femtobarn fb ($1\text{b} = 10^{-28}\text{m}^2$). The number of events per second $d\text{N}/d\text{t}$ produced by the collider, depends on the instantaneous luminosity $\mathcal{L}$ of the collider as

$$\frac{d\text{N}}{d\text{t}} = \mathcal{L} \times \sigma. \tag{3.1}$$

Not all the events are stored and observed by the detectors. Since there are too many events to record all the information, only the events that pass certain

trigger criteria are selected[1] and it is also possible that an event falls outside the region covered by the detectors. We can correct for this by introducing the efficiency ϵ. The total number of recorded events N that took place during a certain running period of the collider, can then be estimated as

$$\mathrm{N} = \mathrm{L} \times \sigma \times \epsilon \tag{3.2}$$

where $\mathrm{L} = \int \mathcal{L} d\mathrm{t}$ denotes the integrated luminosity.

The cross section depends on the centre-of-mass energy $\sqrt{s}$ of the collision which is defined as

$$s = (p_1 + p_2)^2 \tag{3.3}$$

where p_1 and p_2 denote the four-momenta of the two colliding particles. A high centre-of-mass energy is crucial to probe new physics at high energy scales and depends largely on the collider design which can be linear or circular.

In a linear collider, the particles pass only once through the accelerating facilities and, therefore, the energy-gradient has to be very high which makes it technically hard to design a linear collider with a centre-of-mass energy in the TeV-range. In a circular collider, on the contrary, the energy of the particles can be gradually increased with each revolution. However, a charged particle following a circular path looses energy due to synchrotron radiation. For each revolution, the energy ΔE lost due to synchrotron radiation is

$$\Delta E \sim \frac{E^4}{Rm^4} \tag{3.4}$$

where R denotes the radius of the accelerator and E and m respectively the energy mass of the beam particle. Accelerating to a higher and higher energy therefore becomes increasingly more difficult. Moreover, we see that heavier particles will loose less energy: at the same beam energy, a proton will loose 8×10^{12} times less energy per revolution than an electron which is approximately 2000 times lighter. Circular hadron colliders will therefore typically collide at a higher centre-of-mass energy than their lepton equivalents which makes them well-suited to probe new, high-energy ranges.

However, an important drawback of hadron colliders comes from the internal structure of the hadrons, the processes of our interest result from the hard scattering of the constituent partons (the quarks and gluons) of the hadron. Their precise initial energy and hence the centre-of-mass energy of the hard scattering is a priori unknown. Moreover, since hadrons and their constituent partons are strongly interacting, they will give rise to large QCD backgrounds which will complicate the analysis. Since leptons are fundamental particles, lepton colliders

[1] At the time of writing, the LHC is colliding protons at a centre-of-mass energy of 13 TeV and the instantaneous luminosity at the CMS and ATLAS experiments is about $10^{34}\mathrm{cm}^{-2}s^{-1}$. Since the total proton-proton cross section at this energy is about 100 mb [61], we expect $\mathcal{O}(10^9)$ events per second.

produce clean collisions with a well-defined centre-of-mass energy which makes them ideal for precision measurements. Lepton and hadron colliders therefore both have their benefits and drawbacks and we will briefly describe two examples of each.

3.1.2 Lepton colliders

The Large Electron-Positron collider (LEP)

The Large Electron-Positron collider (LEP) was a circular electron-positron collider installed at the CERN laboratory (European Organisation for Nuclear Research), located near Geneva on the border between Switzerland and France. With its circumference of 26.7 km, it is the largest circular electron-positron collider built so far. Collisions were achieved at four interaction regions around which detectors were constructed, these correspond to the four LEP-experiments ALEPH, DELPHI, L3 and OPAL. LEP operated from 1989 to 2000 with a centre-of-mass energy ranging from 91 to 209 GeV and mainly contributed to the precision measurements of the parameters in the Standard Model, in particular the masses, partial and total widths and couplings of the W and Z boson [35].

The International Linear Collider (ILC)

The International Linear Collider (ILC) is a future linear electron-positron collider. The Technical Design Report was published in 2013 and currently the possibilities to build the ILC in Japan are being investigated. The ILC would have a centre-of-mass energy of 500 GeV and is mainly designed to study the origin and nature of the Brout-Englert-Higgs field [62, 63].

3.1.3 Hadron colliders

The Tevatron

The Tevatron was operational from about 1987 to September 2011 and was a circular proton-antiproton collider with a centre-of-mass energy of about $\sqrt{s} = 2$ TeV, has a circumference of 6.3 km and is located at the Fermi National Accelerator Laboratory (Fermilab) near Chicago. The collisions took place at the two interaction points around which the CDF and D0 experiments were built. Each experiment collected about 10 fb^{-1} of data and their main achievement was the discovery of the top quark in 1995 [64, 65].

The Large Hadron Collider

The Large Hadron Collider (LHC) [66] was built at the CERN laboratory near Geneva, in the 26.7 km tunnel that previously housed LEP. The LHC is mainly

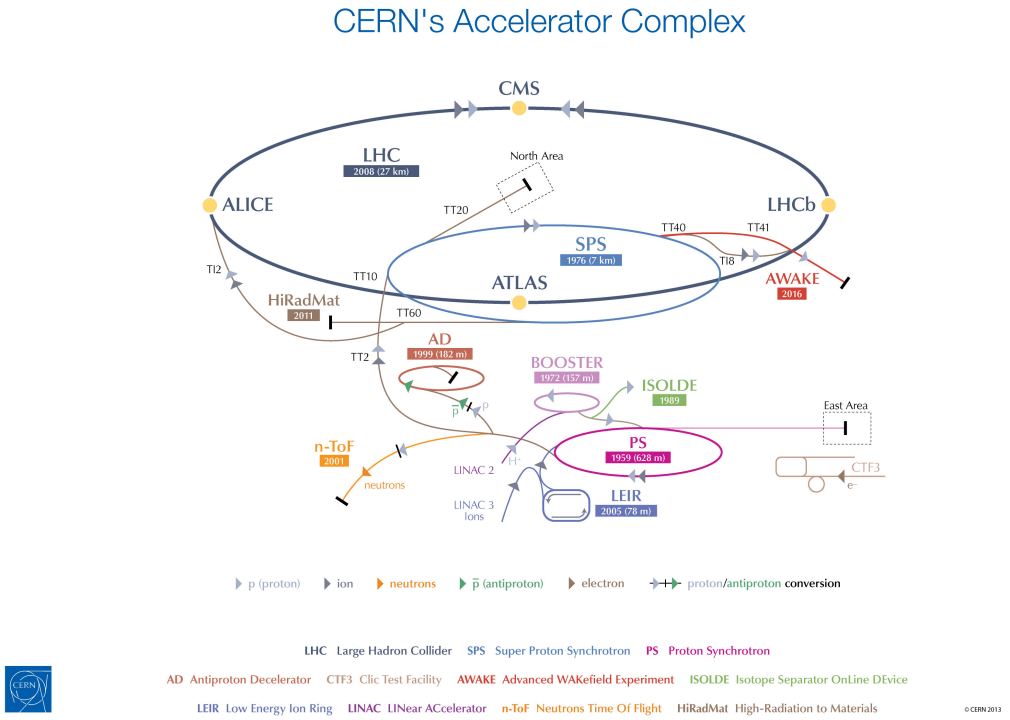

Figure 3.1: The LHC accelerator complex at CERN [67].

designed to perform proton-proton collisions at a centre-of-mass energy of $7-14$ TeV and is currently the world's largest particle accelerator. The accelerating complex of the LHC is shown in figure 3.1. As for LEP, there are four interaction regions around which experiments are conducted.

CMS [68] and ATLAS [69] are the two general-purpose experiments with a rather broad physics programme. They were designed to search for the Brout-Englert-Higgs boson as well as for physics beyond the Standard Model and their main difference lies in their magnet system. Having two similar experiments allows for cross-checks crucial to confirm potential discoveries. ALICE [70] is a detector designed to study the quark-gluon plasma that can be created in heavy-ion collisions and, finally, LHCb [71] mainly investigates B-mesons to understand the matter-antimatter asymmetry in the universe.

The timeline of the LHC, including the future plans for the high-luminosity LHC (HL-LHC), is shown in figure 3.2. After collecting about 30 fb^{-1} at $7-8$ TeV during the Run 1, the LHC was prepared to perform collisions at $13-14$ TeV during the first long shutdown (LS1). In June 2015, the LHC successfully performed the first collisions ever at 13 TeV and started taking data. At this centre-of-mass energy, the LHC will collect about 270 fb^{-1} of data by 2022 after which the HL-LHC will be installed during LS3. The HL-LHC will still collide at 14 TeV, but its luminosity will be 5 to 7 times higher which will lead to a total

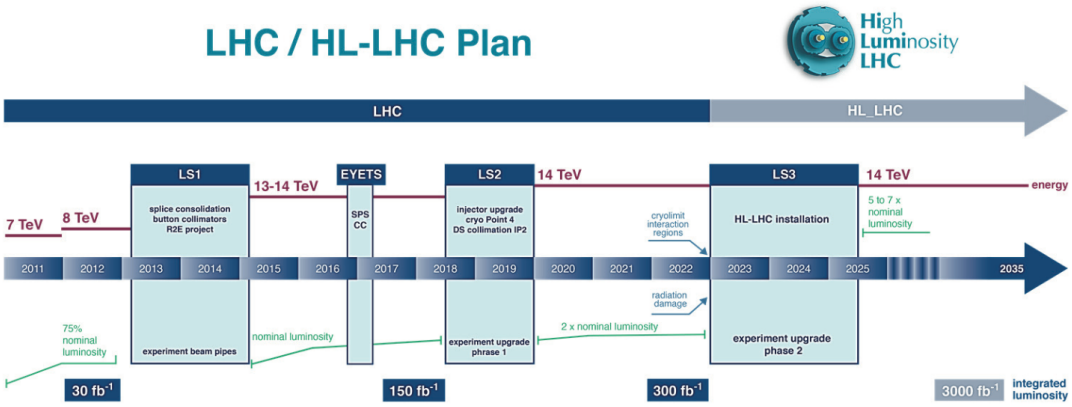

Figure 3.2: The timeline of the LHC and its future successor, the high-luminosity LHC (HL-LHC). The lower line indicates the luminosity while the centre-of-mass energy of the collisions is shown by the upper line. The first, second and third shutdowns are denoted by LS1 − 3 while EYETS stands for the Extended Year End Technical Stop, both serve to prepare the LHC for the next period of data taking [72].

integrated luminosity of 3000 fb^{-1} by 2035 [72].

At the moment of writing, we just entered Run 2 and the LHC has performed very well up to now: on the 4th of July 2012, CMS [23] and ATLAS [22] announced the discovery of the Brout-Englert-Higgs boson which resulted in 2013 in a Nobel Prize for François Englert [3] and Peter Higgs [5], two of the theorists who independently predicted its existence about 50 years before, in 1964. However, despite a couple of suggestive excesses of which one will be discussed in chapter 4, no sign of physics beyond the Standard Model has been found in the $7 - 8$ TeV data set of Run 1. Also the first analyses of the 13 TeV data of Run 2 did not yield any sign of new physics up to now.

3.1.4 Detectors

Detectors consist of several layers of instruments which allow us to measure the energy and momentum of the particles. We will only provide a brief overview of the features that are important here and we will restrict ourselves to the ATLAS and CMS detectors. More details can be found in [68–71] or [27].

The momentum of electrically charged particles is measured in the tracker. The particles move through a strong magnetic field which causes their path to bend and the momentum of the particles can be derived from the curvature of their trajectory. The trajectories are measured very precisely by means of silicon pixels and silicon strip detectors which leads to accurate knowledge of the momentum.

Calorimeters absorb the particles and measure their energy deposition as

well as their direction. The energy of electrons and photons is measured in the electromagnetic calorimeter, ECAL for short, whereas the hadronic calorimeter, the HCAL, measures the energy of strongly interacting particles.

Muons leave a trace in the tracker, but will fly through the calorimeters. The muon chambers are usually constructed behind the ECAL and HCAL and serve to track the muons with a higher precision. The only known particles that escape detection are the neutrinos. Since they are electrically neutral, they do not leave a trace in the tracker and since they only interact weakly they also will not be absorbed in the calorimeters.

3.1.5 The coordinate system and kinematical variables

The origin of the coordinate system is always chosen at the interaction point. The x-axis is directed radially towards the centre of the LHC while the y-axis points upwards. The z-axis is then aligned with the beam direction and is chosen such as to make a right-handed coordinate system. The (x, y)-plane is referred to as the transverse plane, the transverse momentum $p_T = \sqrt{p_x^2 + p_y^2}$ and the transverse energy $E_T = \sqrt{p_T^2 + m^2}$ of a particle are obtained from the projection of its four-momentum on this plane.

In spherical coordinates, the azimuthal angle ϕ is measured in the (x, y)-plane from the x-axis whereas the polar angle θ is measured from the z-axis. The pseudorapidity η

$$\eta = -\ln\left(\tan\left[\theta/2\right]\right) \tag{3.5}$$

is however more commonly used in particle physics because, contrary to θ, differences in η are invariant under Lorentz boosts along the beam direction. This feature is especially useful in hadron colliders where the boost along the z-axis is unknown due to the internal structure of the hadrons. The angular separation between two particles is defined as

$$\Delta R = \sqrt{(\Delta\eta)^2 + (\Delta\phi)^2} \tag{3.6}$$

and is invariant under Lorentz-boosts along the z-axis as well.

3.2 Simulation tools for colliders

At this point, it might not be so clear how collider experiments can be connected with the Lagrangian densities we constructed in chapters 1 and 2. Indeed, the path from a quantum field theory to the interpretation of experimental results is rather long and involves many steps. A whole research community has been working on collider phenomenology and, as a result, dedicated software programs have been developed for every stage of the calculation. A schematic overview of a hadron-hadron collision is shown in figure 3.3, in the following we will discuss and illustrate every step in the computation.

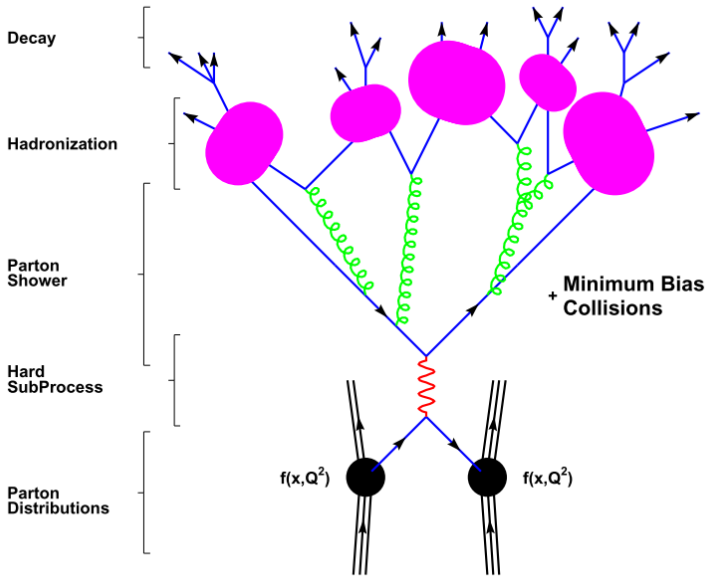

Figure 3.3: A schematic overview of a hadron-hadron collision showing the hard scattering, the hadronization and the showering [73].

3.2.1 The QCD factorization theorem and parton distribution functions

In a hadron-hadron collision, the actual process of interest is the hard scattering interaction between the partons inside the hadrons which is shown on the bottom of figure 3.3. The hadronic cross section can be calculated from the QCD factorization theorem which dictates that the hadronic cross section σ of two hadrons with four-momentum P_1 and P_2 is related to the partonic cross section $\hat{\sigma}_{ij}$ of two partons i and j with four-momentum $p_1 = x_1 P_1$ and $p_2 = x_2 P_2$ by

$$\sigma(P_1, P_2) = \sum_{i,j} \int_0^1 dx_1 dx_2 f_{1,i}(x_1, \mu_F) f_{2,j}(x_2, \mu_F) \hat{\sigma}_{ij}(p_1, p_2, \mu_F) \tag{3.7}$$

where we integrate over the four-momentum fractions $x_{1,2}$ of the partons and where the sum goes over all the partons i, j inside the hadrons. $f_{h,i}(x, \mu_F)$ denotes the Parton Distribution Function (PDF) and, at leading order, this function quantifies the probability to find a parton i carrying a four-momentum fraction x in a hadron h at the factorization scale μ_F. The factorization scale is the scale at which the hadron is probed, this can for example be the momentum transfer in deep inelastic scattering. The PDFs of the partons arise from non-perturbative effects, they have to be measured experimentally and PDFs at different factorization scales are related to each other by renormalization-group running, more specifically the Dokshitzer-Gribov-Lipatov-Altarelli-Parisi

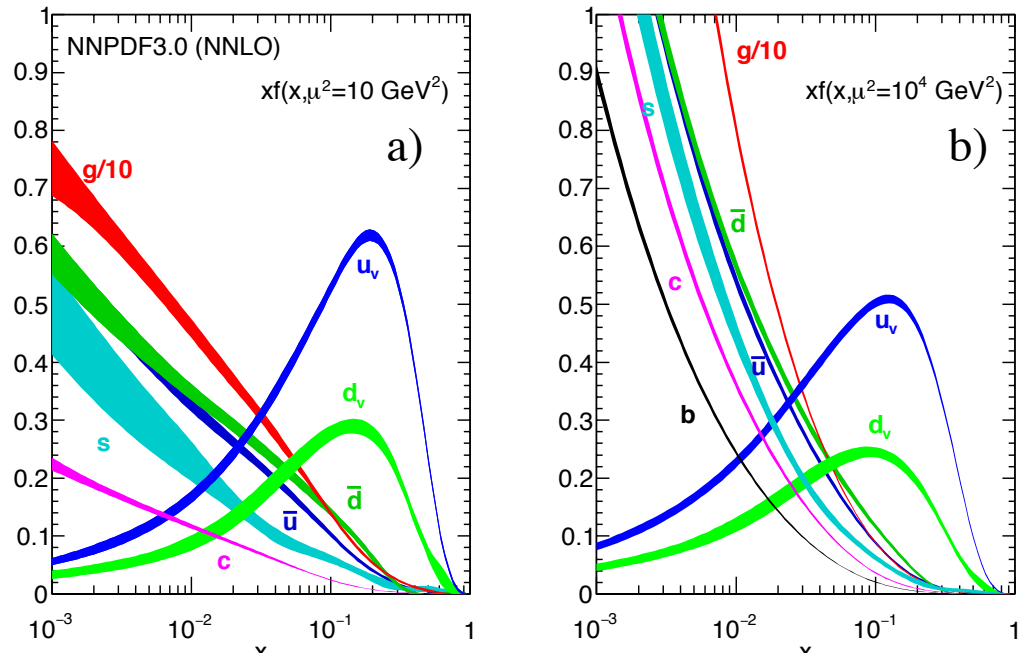

Figure 3.4: The NNPDF3.0 [77] parton distribution functions for $\mu_F^2 = 10$ GeV^2 (left) and $\mu_F^2 = 10^4$ GeV^2 (right). Figure taken from the Particle Data Group [27] review 2016.

(DGLAP) equations [74–76]. The best choice of the parametrization of the PDF and the loop-order of the DGLAP equations depends on the process under study and, consequently, many PDF sets are available. Figure 3.4 shows the NNPDF3.0 PDF [77] set at two different factorization scales.

Once the PDFs are known, the only missing piece to calculate the hadronic cross section in equation 3.7 is the partonic cross section as a measure for the probability for the hard scattering to occur.

3.2.2 The hard subprocess

The partonic cross section of a hard scattering process can be calculated from perturbation theory and all the information we need is contained in the Lagrangian density. After extracting the Feynman rules from the Lagrangian and drawing all the possible Feynman diagrams leading to the process of interest, we can write down the helicity amplitudes and the matrix elements $\mathcal{M}$ which will then lead to the partonic cross section after integrating over the phase space $d\Phi$ of the final state particles. More specifically, we have

$$\hat{\sigma}_{ij} = \frac{1}{2\hat{s}} \int |\mathcal{M}_{ij}|^2 d\Phi \tag{3.8}$$

where $\hat{s} = x_1 x_2 s$ denotes the partonic centre-of-mass energy.

Suppose we want to study a simplified model in which the only supersymmetric particles in reach of the LHC are the lightest stop and the lightest neutralino. The stops can be produced in pairs and will always decay to the lightest neutralino and a top. As a first step we will use the FeynRules package to extract the Feynman rules.

Model building – FeynRules

FeynRules [78,79] is a Mathematica package designed to automatically compute the Feynman rules starting from a Lagrangian implemented by the user. All gauge symmetries, fields and parameters as well as the gauge- and Lorentz-invariant Lagrangian density have to be specified in the model file.

For details on the syntax and mode implementation, we refer to the FeynRules manual. In our example, we can simply use the model file of the MSSM [80] which is publicly available on the FeynRules website [81]. Loading the FeynRules package and model file into a Mathematica notebook, then allows us to compute the Feynman rules of the model. The Feynman rule for the vertex connecting the up-type squark (su), up-type quark (uq) and gluino (go) can for example be obtained as

$$\left\{\left\{\left\{\bar{\text{uq}}, 1\right\}, \{\text{go}, 2\}, \{\text{su}, 3\}\right\},\right.$$
$$\left. i\sqrt{2}g_s(\text{RR}^u)^*_{\text{i}_3,\text{f}_1} P_{-\text{s}_1,\text{s}_2} T^{\text{a}_2}_{\text{m}_1,\text{m}_3} - i\sqrt{2}g_s(\text{RL}^u)^*_{\text{i}_3,\text{f}_1} P_{+\text{s}_1,\text{s}_2} T^{\text{a}_2}_{\text{m}_1,\text{m}_3}\right\}$$

where the index i runs over the up-type squarks while f, s, a and m respectively represent the generation, Lorentz, adjoint and fundamental colour indices. RR^u and RL^u denote the first and last three columns of the squark mixing matrix, $P_\pm = \frac{1\pm\gamma^5}{2}$ are the chiral projection operators and T^a represent the generators of the strong interaction in the fundamental representation. For a top quark and a purely right-handed stop this reduces to

$$i\sqrt{2}g_s \frac{1-\gamma^5}{2} T^a. \tag{3.9}$$

After fully implementing our theory in FeynRules, we can move on to calculating the cross section. FeynRules provides specific interfaces that export the model and its Feynman rules to Feynman-diagram or matrix-element generators like CalcHep/CompHep [82–85], FeynArts/FormCalc [86–89] and Whizard/O'Mega [90,91]. A more generic interface is provided by the Universal FeynRules Output, also known as the UFO-format [92], which is currently used by Aloha [93], Gosam [94,95], Herwig++ [96], MadAnalysis 5 [97] and MadGraph5_aMC@NLO [98]. We will focus on MadGraph5_aMC@NLO (MG5_aMC for short) in the following.

Event generation – MG5_aMC

After specifying a certain process in terms of the initial and final state particles, MG5_aMC generates all the Feynman diagrams contributing to the process and the computer codes necessary to evaluate the matrix elements. The latter is achieved by calling a helicity amplitude function library, either the HELAS subroutines [99] or ALOHA. The MADEVENT package then uses this code to generate events and calculate the requested cross section and decay widths.

To calculate the cross section for stop-pair production at the LHC at leading order (LO), we start MG5_aMC and type

```
generate p p > t1 t1~
```

where `t1` and `t1~` denote the lightest stop and its antiparticle. The generated Feyman diagrams are shown in figure 3.5 and 3.6, they all arise from the strong interaction and therefore, the cross section of stop-pair production does not depend on the left-right mixing of the stops. After setting the parameters such as the stop mass, centre-of-mass energy, PDF and the factorization and renormalization scale, the `launch`-command calls MADEVENT and starts the event generation. We choose $\sqrt{s} = 8$ or 13 TeV and the CTEQ6L1 [100] PDF set. For each $\sqrt{s}$, we scanned over the stop masses $m_{\tilde{t}}$ while fixing $\mu_F = \mu_R = m_{\tilde{t}}$. The result is shown in figure 3.7.

For more precise results, we would have to generate the events at the next-to-leading order (NLO) or, less precisely, we could simply rescale the number of events with the ratio of the NLO cross section over the LO cross section, the K-factor. We will adopt the latter approach. The higher-order calculation of the cross section (next-to-leading order (NLO) + next-to-leading logarithm (NLL)) as obtained by the LHC SUSY Cross Section Working Group [101, 102] is also shown in figure 3.7 and the K-factor in our case is about $1.7 - 1.8$.

If $m_{\tilde{t}} = 500$ (1000) GeV, MG5_aMC predicts the production-cross-section of stop pairs at the LHC to be about 47.1 (0.17) and 308.3 (3.3) fb at $\sqrt{s} = 8$ and 13 TeV respectively. Consequently, at leading order, we expect about 940 (3) stop pairs in the $20\,\text{fb}^{-1}$ data-set collected in Run 1 at 8 TeV while the $100\,\text{fb}^{-1}$ of data that will be collected during Run 2 should contain about 31000 (330) stop pairs. For the corresponding higher-order yields, we have to multiply these numbers by the K-factor. How many of these stop pairs will be detected depends, among others, on the decay of the stops.

In our simplified model, the stop will always decay to a top quark and the lightest neutralino `n1` after which the top quark decays to a bottom quark and a W boson. The W boson can decay hadronically or leptonically and we will focus on the semileptonic decay channel, *i.e.* one of the two W bosons decays leptonically while the other decays hadronically. This decay channel occurs in 28% of the cases and we generate this process inside MG5_aMC as

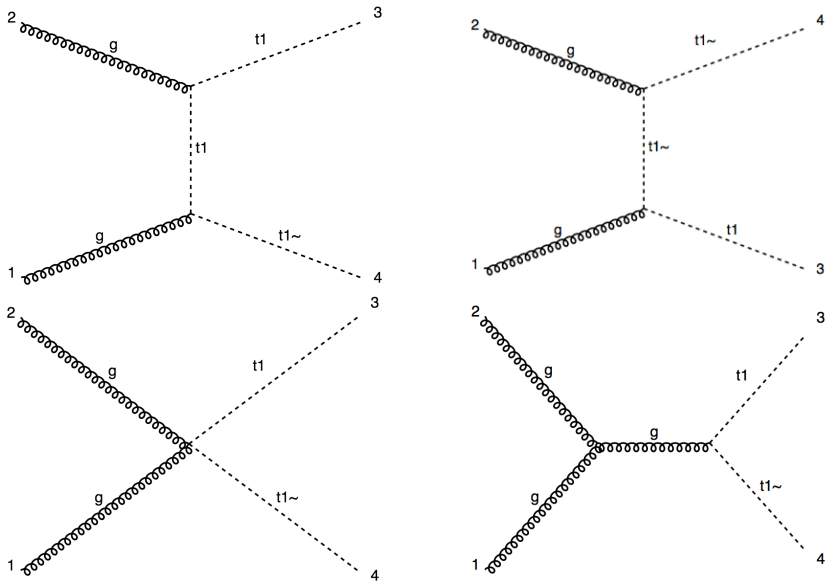

Figure 3.5: All the Feynman diagrams with gluon-gluon initial state contributing to stop-pair production, generated with MG5_aMC.

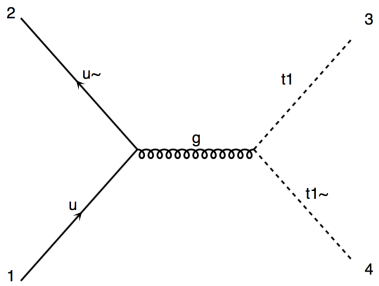

Figure 3.6: The Feynman diagrams with quark-anti-quark initial state contributing to stop-pair production, generated with MG5_aMC.

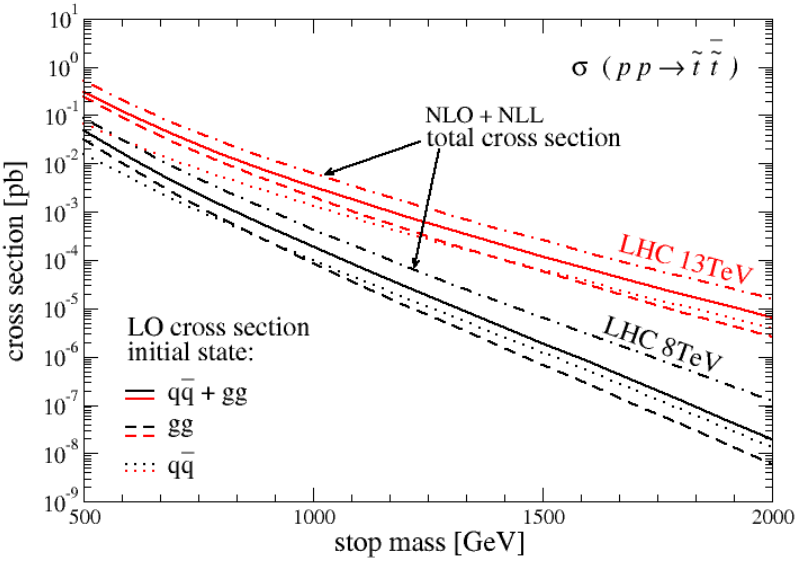

Figure 3.7: The cross section of the pair production of left-handed stops at the LHC at $\sqrt{s} = 8$ and 13 TeV in function of the stop mass $m_{\tilde{t}}$. We obtained the LO cross section with MG5_aMC with $\mu_F = \mu_R = m_{\tilde{t}}$ using the CTEQ6L1 PDF sets. The NLO + NLL cross section is taken from the LHC SUSY Cross Section Working Group [101, 102].

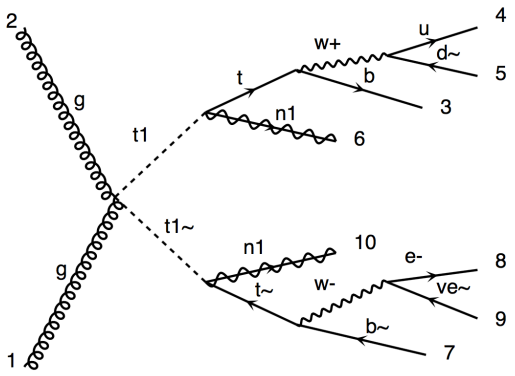

Figure 3.8: One of the Feynman diagrams contributing to the production of semileptonically decaying stop-pairs at the LHC, generated with MG5_aMC.

```
generate p p > t1 t1~, (t1 > n1 w+ b, w+ > j j), \
(t1~ > n1 w- b~, w- > l- vl~)
```

where we used the multiparticles `j` which represents all first and second generation quarks and `l-` which stands for the electrons and muons. We assumed the stops and the W bosons to be on-shell, the top quarks can be off-shell as well. Issuing

```
add process p p > t1 t1~, (t1 > n1 w+ b, w+ > l+ vl), \
(t1~ > n1 w- b~, w- > j j)
```

in a shell adds the other half of the decay channel. Figure 3.8 shows one of the diagrams as such generated by MG5_aMC. Since the width of the top squark depends on the left-right mixing of the stops and the mixing of the lightest neutralino, we ask MG5_aMC to calculate its width by setting the stop width to `AUTO` in the parameter card. The `launch` command then starts the event generation, yielding the cross section of the hard scattering process as well as the parton-level events.

In our illustration, we fix $m_{\tilde{t}} = \mu_F = \mu_R = 500$ GeV and $m_{\chi_1^0} = 130$ GeV. We fix the lightest neutralino to be fully bino-like and generate two samples at $\sqrt{s} = 8$ TeV, one with left- and one with right-handed stops. The black lines in figure 3.9 show the parton level p_T distribution of the leptons we obtained. Clearly, the left-right mixing of the stops has an influence on the kinematical distributions.

This effect has for example been studied in [103] and is due to the polarization of the top. Since a bino connects stops and tops with the same chirality, a right-handed stop decaying to a bino-like neutralino, will result in a right-handed or positively polarized top which then decays to a lepton flying in the forward direction, *i.e.* in the direction in of the momentum of the top. On the contrary, a left-handed stop decaying to a bino-like neutralino will decay to a left-handed

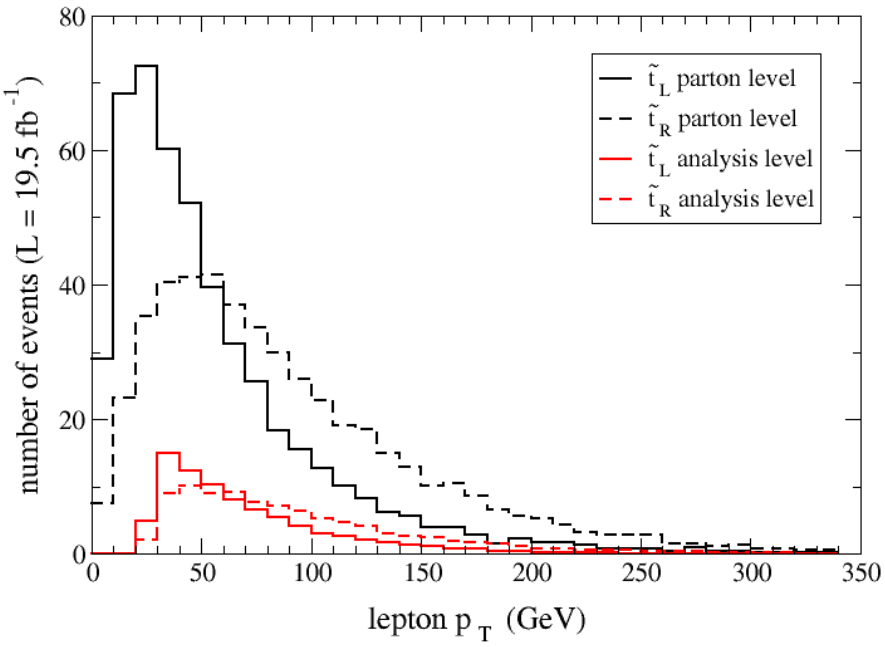

Figure 3.9: The p_T distribution of the leptons coming from left- or right-handed stop pairs with mass $m_{\tilde{t}} = 500$ GeV. Each stop decays to a top and bino-like neutralino, the tops then decay to a bottom quark and a W boson. One of the two W bosons decays leptonically while the other decays to hadrons. The black and red lines respectively show the p_T distribution at parton- and analysis level. We ran the CMS search for stop pairs in the single lepton final state [104] recasted within MadAnalysis 5 [105] (*cfr.* section 3.2.4) and show the number of events expected at the LHC for $\sqrt{s} = 8$ TeV and L = 19.5fb^{-1}.

or negatively polarized top which will result in a lepton emitted in the backward direction. For a lighest neutralino which is mainly bino-like, we therefore expect the lepton resulting from the decay of a right-handed stop to be more energetic than the one from a left-handed stop.

The p_T distribution we obtained with MG5_aMC shown in figure 3.9 meets our expectations and is additionally in agreement with figure 12 in [103].

3.2.3 The parton shower and hadronization

We now generated the hard subprocess of interest at the parton level. The partons of the initial hadrons and the strongly interacting decay products will result in initial and final state QCD radiation. As is shown in figure 3.3, the parton will radiate until its energy is lowered to the non-perturbative regime of

QCD, the parton is said to undergo a parton shower. When partons move into the non-perturbative regime, they will hadronize. Quarks and gluons produced in the collision will therefore result in a large number of particles in the detector, referred to as jets. The parton shower and hadronization can for example be simulated by HERWIG++, SHERPA or PYTHIA [106, 107]. In our example we used PYTHIA to shower the b-quarks, as this program can easily be called inside MG5_aMC. For more details on the parton shower and hadronization, we refer to the corresponding manuals or [108]. Since leptons are not so much affected by the parton shower, the p_T distributions of the leptons after showering will not differ much from the parton level distributions shown in figure 3.9.

3.2.4 Detector simulation and experimental analysis

After the parton shower and hadronization, the particles pass through the detector. As was described in section 3.1.4, a detector consists of the tracker, the electromagnetic and hadronic calorimeter and the muon chambers and their response to the particles flying through has to be simulated. For a detailed detector simulation, GEANT 4 [109] can be used. This package is however computationally intensive and simplified parametrizations of the detectors were for example implemented in the DELPHES 3 [110] fast-simulation package. DELPHES 3 simulates the detector response and reconstructs the physics objects. The hadrons have to be clustered into jets and several jet-clustering algorithms have been designed to this end. DELPHES 3 relies on the FASTJET [111] package for jet clustering.

With the reconstructed objects, we use the MADANALYSIS 5 [97, 112] framework to simulate the experimental analyses and investigate if and how the process under study will contribute. CHECKMATE [113] has been developed with the same purpose as MADANALYSIS 5 and can be used alternatively. MADANALYSIS 5 has two working modes: the normal interaction mode and the expert mode. The interaction mode allows the user to quickly impose selection cuts and make plots of the observables and was used to make figure 3.9 while the expert mode is well-suited for the detailed implementation of experimental analyses. MADANALYSIS 5 can process parton- and hadron- as well as detector-level events and DELPHES 3 or FASTJET can be easily called within MADANALYSIS 5 for detector simulation or jet clustering. MADANALYSIS 5 also has a database of publicly available validated experimental analyses [114, 115] which currently contains 19 analyses of the CMS and ATLAS experiments that can be used at will by the user.

For our semileptonically decaying stops, the CMS search for stop-pair production in the single-lepton final state at $\sqrt{s} = 8$ TeV [104] is especially relevant. Using the publicly available MADANALYSIS 5 implementation of this analysis [105], it is now straightforward to check whether the previously used reference point ($m_{\tilde{t}} = 500$ GeV, $m_{\chi_1^0} = 130$ GeV) of our simplified model is still allowed. To this

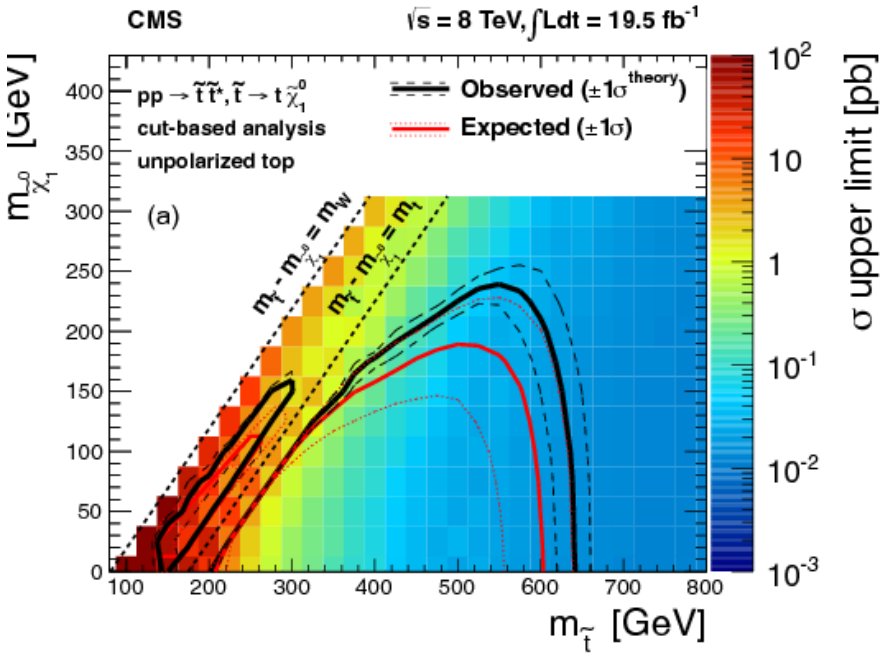

Figure 3.10: CMS exclusion plot in the plane of the stop mass $m_{\tilde{t}}$ and the mass of the lightest neutralino $m_{\tilde{\chi}_1^0}$. The parts of the parameter space underneath the curves are excluded. Taken from the CMS-search for stop pair production in the single-lepton final state [104].

end, we use MG5_aMC to generate unpolarized stop pairs (*i.e.* stops consisting of an equal left- and right-handed component) at $\sqrt{s} = 8$ TeV and let Pythia perform the parton shower and hadronization. Starting MadAnalysis 5 in the reconstruction mode by typing `.\bin\ma5 -R`, issuing

```
set main.recast = on
import [path-to-sample] as sample
set sample.xsection = [xsec in pb]
submit
```

where the square brackets have to be filled by the user, and indicating which experimental analyses we would like to run, will then start the detector simulation with Delphes or DelphesMA5tune (a Delphes-version adjusted for MadAnalysis 5) depending on the chosen analysis. For each analysis, MadAnalysis 5 then generates the cut-flow tables and histograms as well as the expected and observed upper limits on the cross section and the 95% confidence-level (CL) exclusion limits for each signal region.

Our leading-order (LO) sample is sufficient for our purposes, but in order to obtain realistic exclusion limits, we need the cross section up to a higher-order in perturbation theory. The ratio of higher-order cross section over the one at LO is called the K-factor and can be used for rescaling.

The next-to-leading-order and next-to-leading-log (NLO+NLL) cross section at $\sqrt{s} = 8$ TeV for the production of stop pairs with $m_{\tilde{t}} = 500$ GeV can be found at the webpage of the LHC SUSY Cross Section Working Group [101, 102] and reads 85.6 fb. Multiplying with the branching ratio for the semileptonic decays, we get $\sigma(\text{semileptonic stop-pair}) = 24.6$ fb. Using this information, MadAnalysis 5 shows that there are several signal regions in which our signal is excluded at 99% CL or higher. We can therefore conclude that our simplified model in which all SUSY particles are very heavy and decoupled except the top-squark and the lightest neutralino, is excluded for $m_{\tilde{t}} = 500$ GeV and $m_{\chi_1^0} = 130$ GeV. This is in agreement with the CMS-exclusion plot shown in figure 3.10.

We can now come back to the p_T distributions of the leptons for the left- and right-handed stops at the analysis level. They are shown by the red lines in figure 3.9. The difference in the p_T distribution which was clearly visible at the parton level, more or less disappeared after applying the analysis.

3.2.5 Introducing stop-scharm mixing

Suppose now that the lightest squark is not a pure stop, but a mixture of a stop and scharm. How would the limits from the aforementioned CMS search change? To investigate this, we assume that the lightest squark $\tilde{q}$ has a mass of 500 GeV and mixes the right-handed top and charm squark as $\tilde{q} = \tilde{t}_R \cos\alpha + \tilde{c}_R \sin\alpha$. The stop and scharm states will always decay as $\tilde{t}_R \to t\tilde{\chi}_1^0$ and $\tilde{c}_R \to c\tilde{\chi}_1^0$.

We generated the Monte Carlo samples for $pp \to \tilde{q}\bar{\tilde{q}}$ at $\sqrt{s} = 8$ TeV with MG5_aMC for various mixing angles between 0 and $\pi/2$. In addition to the Feynman diagrams shown in figure 3.5 and 3.6, the scharm states could also be produced from charm-anticharm initial states through a t-channel gluino. However, apart from being suppressed due to the high gluino mass in our simplified model, this process is additionally suppressed by the PDF: as can be seen from the PDFs shown in figure 3.4, the fraction of the proton momentum carried by the initial-state charms is usually too low for this channel to contribute. The K-factor could possibly depend on the mixing angle, but the difference would anyway be small [116] and we therefore assume the cross section to be independent of the mixing angle.

Using MadAnalysis 5, we calculated the expected and observed 95% CL upper limits on the cross section, the results are shown in figure 3.11. We also show the NLO+NLL MSSM prediction for the cross section, our simplified model is excluded if this cross section is higher than the upper limits. We see that, the larger the charm content of the squark, the higher the upper limit becomes. This is as expected: contrary to the top quark which can give rise to a lepton and a b-jet, a final-state charm will just be observed as a jet. Since the CMS search requires one lepton and a b-jet, a squark pair with a large charm content is less likely to pass the event selection and we expect the limit to be lower. As soon as the mixing angle becomes larger than roughly 40 degrees, our simplified model

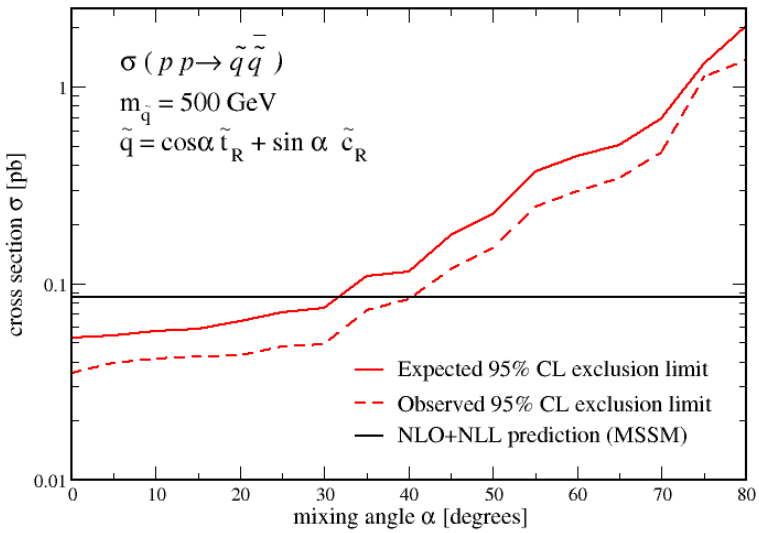

Figure 3.11: The expected and observed 95% CL upper limits on the cross section for the pair production of squarks mixing stop and scharm in function of the mixing angle. Limits obtained for the CMS search for stop-pair production in the single-lepton final state [104] using MadAnalysis 5 [105].

is no longer excluded by this search.

In this regime, we expect the LHC searches for multijets and missing energy, with or without charm-tagging, to become relevant and we can wonder what the overall impact of flavour mixing on the squark limits would be if we combine all the searches. This question was investigated in [117] and we show two plots of interest in figure 3.12. These figures show the sensitivity of four LHC searches to the signatures of a simplified model containing a gluino and the two lightest squarks which are a mixture between a right-handed stop and scharm. Their mass difference is 500 GeV, $\sin\theta_{23}^R = 0$ corresponds to a lightest squark which is purely stop-like and our scenario roughly corresponds to gluino masses which are much higher than the mass of the lightest squark. The coloured regions are excluded, *red and yellow* correspond to the exclusion due to the multijet analyses of ATLAS (ATLAS-SUSY-2013-04 [118]) and CMS (CMS-SUS-13-012 [119]) respectively, *blue* corresponds to the CMS search for stops in single lepton events we considered in our example (CMS-SUS-13-011 [104]) while *green* corresponds to an ATLAS search using charm-tagging to set limits on scharm-pair production (ATLAS-SUSY-2014-03 [120]).

Similar to the conclusion of our illustrative example, we can conclude that, whereas the CMS search for stop-pair production in the single lepton final state (blue) is very relevant if the lightest squark is mainly stop-like (left-hand side in

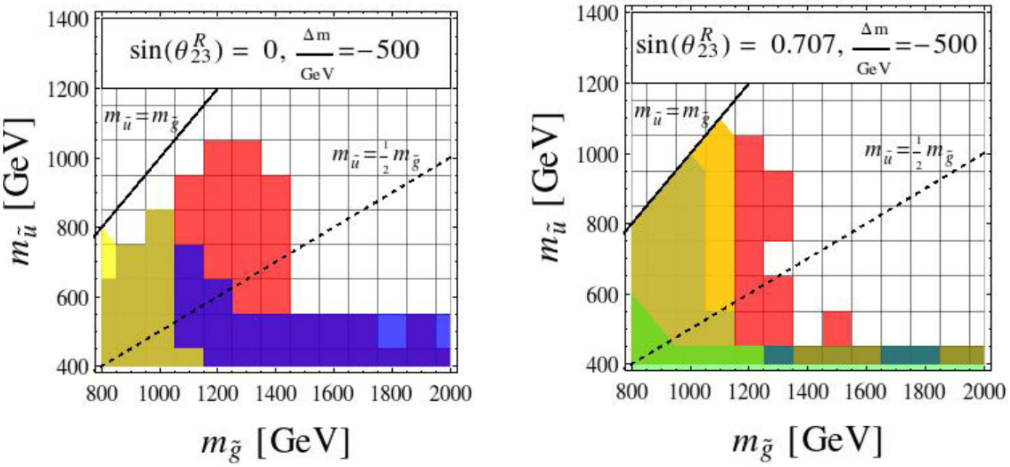

Figure 3.12: The sensitivity of four LHC searches to squark pair production. The coloured regions are excluded and the colour coding as well as more details are explained in the text. Taken from figure 9 in [117].

figure 3.12), this is no longer the case if the scharm component becomes dominant (right-hand side in figure 3.12). In that case the multilepton searches and the search for scharm-pair production take over and the limit on the gluino mass is not influenced by introducing flavour mixing. For very heavy gluinos, however, the limit on the lightest squarks is slightly softer.

3.2.6 Supersymmetric mass spectra with ASperGe

So far, we just studied a simplified model and we assumed the chosen mass spectrum and mixing could also be realised within a theory. Given the mass matrix of the up-type squarks (see equation 2.58), we can now ask ourselves which values for the SUSY parameters correspond to a scenario where the lightest squark has mass 500 GeV and is a mixture of top and charm squarks with. To make this connection, we can use an extension of the FeynRules package, ASperGe [121], dedicated to the automatic, numerical diagonalisation of mass matrices associated with any Lagrangian associated with any quantum field theory.

After implementing the model including the description of the mixings in the FeynRules model file, ASperGe extracts the mass matrices and writes the results to a numerical code which can then diagonalise the matrix numerically. The code provided by ASperGe can be used in itself, but it can also be called inside FeynRules or MadGraph to calculate and update the mass and mixing parameters of a certain model. Mass matrix diagonalisation is one of the steps necessary to calculate the SUSY mass spectrum starting from the UV input parameters in for example mSUGRA, as is for example done in the SUSY mass spectrum generators SOFTSUSY [49], SPheno [50] or SuSpect [51] we

mentioned already before in section 2.3. ASperGe could be part of a model-independent mass spectrum generator based on FeynRules.

However, we will just use the diagonalisation module of the MSSM generated by ASperGe to show that scenarios in which the lightest squark mixes the right-handed stop and scharm and has a mass of 500 GeV while the other squarks are decoupled are indeed possible within the low-energy parametrization of the MSSM. The soft squark masses $\widehat{M}^2_{\tilde{U}}$ are the most important parameters determining the masses and mixing of the right-handed up-type squarks. We take the entries related to the second and third generation as $(\widehat{M}^2_{\tilde{U}})_{22} = 700\,000\ \text{GeV}^2$, $(\widehat{M}^2_{\tilde{U}})_{33} = 560\,000\ \text{GeV}^2$ and $(\widehat{M}^2_{\tilde{U}})_{23} = (\widehat{M}^2_{\tilde{U}})_{32} = 370\,000\ \text{GeV}^2$ and set the remaining off-diagonal terms to zero while the diagonal terms are taken to be $10^7\ \text{GeV}^2$. If we additionally set $\widehat{T}_c = \widehat{T}_t = \mu = 0$ GeV to avoid left-right mixing, ASperGe indeed yields a lightest squark mixing the right-handed top and charm squarks with a mixing angle of 40° and a mass of about 500 GeV while the other squark masses are 1 TeV or larger. It should however be noted that a scenario in which the other, orthogonal state mixing the right-handed stop and scharm is also at the bottom of the spectrum, is more natural within the parametrization of the MSSM. An analysis in which both states are included, would be completely analogous to the illustrative example presented here.

Part II

Searching for unconventional signatures of supersymmetry

In Part I, we explained how the known fundamental particles and interactions are described within the Standard Model and we introduced supersymmetry to meet at least some of the shortcomings of the SM. We then showed how theoretical models within high-energy physics, such as the SM or SUSY, can be confronted with experimental observations at particle colliders and we illustrated how phenomenological simulation tools facilitate connecting theory and experiment.

We also discussed the current status of SUSY and we saw that not a single supersymmetric particle has been observed so far which puts natural SUSY under pressure. However, up to now collider searches for SUSY mainly focussed on minimal realisations of SUSY. Supersymmetry, however, encompasses a very broad class of models and it is important to get a more comprehensive overview of the SUSY phenomenology in order to ensure that we did not overlook anything. In Part II, we investigate how we can go beyond minimal SUSY, to which extent this is still allowed and how it would change the SUSY phenomenology.

In chapter 4, we investigate a GGM-inspired simplified model featuring a bino-like neutralino, the right-handed sleptons and the very light gravitino at the bottom of the spectrum. Part of this simplified model, namely the case in which the right-handed selectron and smuon are lighter than the stau, has escaped attention up to now and can lead to interesting multilepton signatures. In particular, we show that they can explain a, not yet significant, excess observed in a CMS search for three or more leptons while satisfying other constraints from multilepton searches.

In chapter 5 we have a closer look at the SUSY-breaking mechanism. Usually one assumes there is only one SUSY-breaking sector, however, there is no real motivation why this should be the case. In this chapter, we abandon this assumption and study the phenomenology of GMSB with two SUSY-breaking sectors. There will be one goldstino for each SUSY-breaking sector, one linear combination of them will be eaten by the gravitino while the remaining fields give rise to the pseudo-goldstino. The pseudo-goldstino can acquire a mass in between the mass of the light gravitino and the lightest of the remaining SUSY particles which, as we will see, can considerably change the collider signatures.

In chapter 6, we revisit the minimal-flavour violating paradigm which was introduced in chapter 2 in the context of the pMSSM. We investigate to which extent non-minimal flavour violation (NMFV) in the squark sector is still allowed by low-energy flavour observables such as meson mixing and the constraint coming from the Higgs boson. We use the Markov Chain Monte Carlo scanning technique and see there is still room left for NMFV in the squark sector. We also observe that the lightest squarks within NMFV are typically not the third generation squarks, as is the case in the usual SUSY scenarios.

Clearly, the work presented in this thesis is not the end of the story and there remains a lot of room for further investigation. In chapter 7 we summarize our findings and discuss the remaining open questions that can be studied in the

future.

Chapter 4

Multilepton signals of gauge-mediated supersymmetry breaking at the LHC

Even though the LHC has not delivered any conclusive evidence for physics beyond the Standard Model yet, some searches did observe 2-3σ deviations from the Standard Model predictions. They do not reach the 5σ significance needed to claim a discovery, but still they might give a hint of where to go. One of these excesses was observed in the CMS search for anomalous production of events with three or more leptons. In this chapter, based on the work presented in reference [122], we will investigate the collider signatures of a GGM-inspired simplified model and show that we can provide an explanation for the observed excess, while satisfying other existing experimental constraints. These models also give rise to final states with more than four leptons which offers alternative channels in which they can be probed. We estimate the corresponding production rates at the LHC.

We begin this chapter with an introduction in section 4.1. In section 4.2 we then construct the simplified models of interest and confront them with collider searches in section 4.3. Our findings are summarized in section 4.4.

4.1 Introduction

In this chapter, we consider the framework of gauge-mediated SUSY breaking in its general formulation (GGM) where it is possible to construct models in which all the coloured superpartners are heavy but some (or all) of the electroweak superpartners are light. One benefit of this kind of spectrum is that a 125 GeV Higgs boson can be easily accommodated by means of multi-TeV top squarks.

We focus on models in which the three generations of right-handed sleptons, together with the nearly massless gravitino, are in the low mass region of the

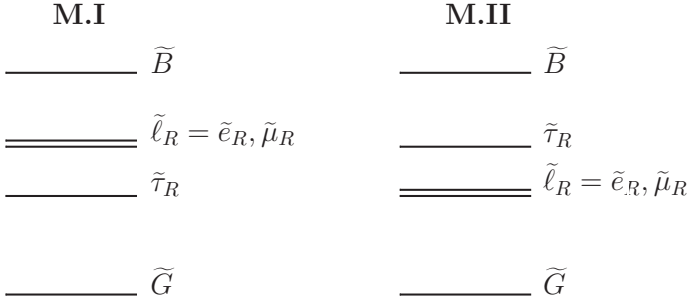

Figure 4.1: Mass spectra for our simplified model of type **M.I** (left) and **M.II** (right). In **M.I** scenarios, the stau $\tilde{\tau}_R$ is the NLSP and the right-handed selectron/smuon $\tilde{\ell}_R$ are co-NNLSP. In models of class **M.II**, the situation is reversed.

superpartner spectrum. Such models can be probed at the LHC by analyzing events originating from the pair-production of sleptons that decay promptly into lepton-rich final states with missing transverse energy $\not{E}_T$ carried by gravitinos.

We show that some of these GGM models can provide an explanation for a possible anomalous production of events with four leptons recently observed by the CMS collaboration [123, 124]. We also discuss the compatibility with the constraints extracted from the dilepton+$\not{E}_T$ searches at both LEP and LHC experiments, as well as from other LHC multilepton searches. We finally propose, for the model that fits the data best, additional signatures that could be searched for using both data from the previous LHC runs and future data from the run at a centre-of-mass energy of $\sqrt{s} = 13$ TeV.

4.2 Theoretical framework and benchmark scenarios

We consider a class of GGM models where the selectron and smuon (generically referred to as sleptons in the following), as well as the stau, lie in the low-mass range of the superparticle spectrum. As for any scenario with gauge-mediated SUSY breaking, the lightest supersymmetric particle (LSP) is the gravitino, whose typical mass is $\mathcal{O}$(eV) for SUSY-breaking scales of $\mathcal{O}$(100 TeV).

Adopting a bottom-up approach for new physics, we investigate the phenomenology of a simplified model in which we extend the SM field content by adding a nearly massless gravitino $\tilde{G}$, a pair of mass-degenerate right-handed sleptons $\tilde{\ell}_R = \tilde{e}_R, \tilde{\mu}_R$ and a (for simplicity, non-mixed) stau $\tilde{\tau}_R$. In addition, we also include the lightest neutralino state, considered to be bino-like and heavier than both the sleptons and the stau. All the remaining superpartners are assumed heavy and effectively decoupled. Similar scenarios were considered in [125, 126].

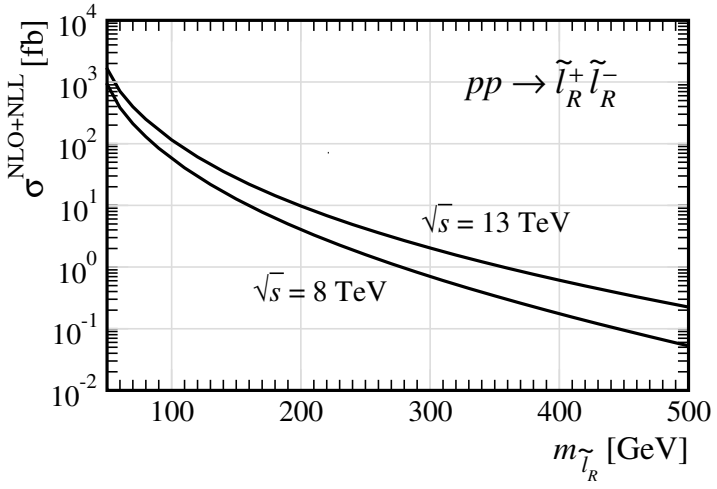

Figure 4.2: Right-handed slepton/stau pair-production cross section at the LHC, for a single flavour, as a function of the slepton mass.

In this simplified model, two possible hierarchies can be realized in the slepton/stau sector. As presented in figure 4.1, we consider both of these and denote by **M.I** scenarios where the stau is the next-to-lightest superparticle (NLSP) and sleptons the next-to-next-to-lightest superpartners (NNLSP), and by **M.II** scenarios with an inverted hierarchy, with the sleptons being co-NLSP and the stau the NNLSP. While models of type **M.I** are typical in GGM (even in minimal gauge mediation), models of type **M.II** can be realized when the soft masses for both Higgs fields at the UV scale are allowed to receive extra, non-gauge mediated, contributions [127, 128].

Slepton pairs are produced via the electroweak Drell-Yan process[1] and the production cross section of a right-handed slepton/stau pair at the LHC, for $\sqrt{s} = 8$ TeV and 13 TeV, as computed by Resummino [129–133] is shown in figure 4.2. Since the cross section steeply falls with increasing slepton mass [134], we consider slepton and stau masses only up to 300 GeV, a range above which it is unlikely that the LHC at $\sqrt{s} = 8$ TeV is sensitive.

For both types of scenarios, the NLSP universally decays into a gravitino and the corresponding SM partner,

$$\tilde{\tau}_R \to \tau \tilde{G} \quad (\mathbf{M.I}); \qquad \tilde{\ell}_R \to \ell \tilde{G} \quad (\mathbf{M.II}). \tag{4.1}$$

Generally speaking, the decay width of a SUSY particle $\widetilde{X}$ to its SM partner X

[1]Drell-Yan production of slepton pairs occurs in hadron-hadron collisions if a quark from one hadron annihilates with a corresponding anti-quark of the other hadron to form a virtual photon or Z boson which then consequently decays to two sleptons.

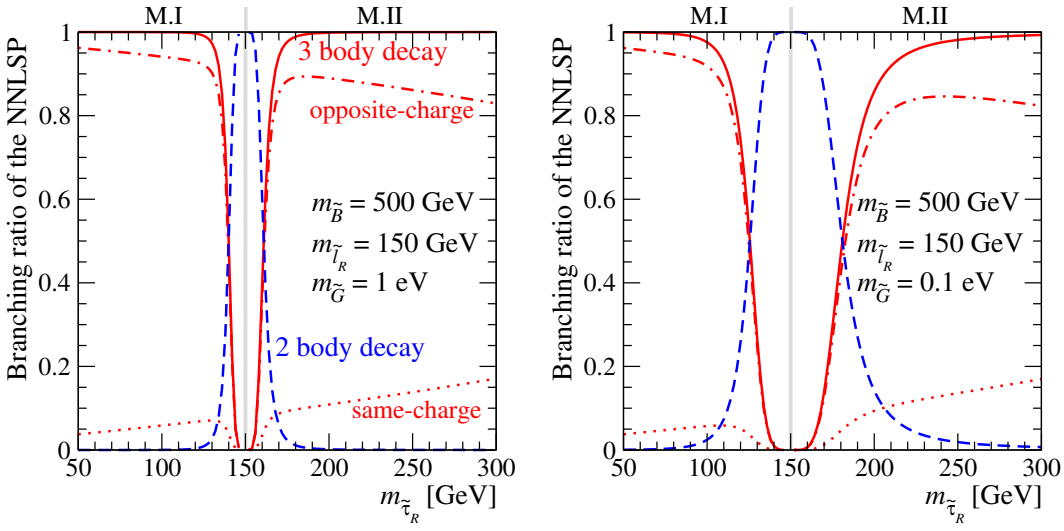

Figure 4.3: Branching ratio of the NNLSP as a function of the stau mass for two different choices of the gravitino mass, $m_{\tilde{G}} = 1$ eV (left) and 0.1 eV (right), where the bino and slepton masses are fixed at 500 GeV and 150 GeV, respectively. The dashed blue line corresponds to the two-body decay to the gravitino, while the solid red line indicates the total three-body decay branching ratio. The red dashed-dotted and dotted lines represent the opposite-charge and same-charge three-body decays, respectively, as explained in the text.

and a gravitino $\widetilde{G}$ depends on the gravitino mass and is given by [54]

$$\Gamma(\widetilde{X} \to X\widetilde{G}) \simeq \frac{m_{\widetilde{X}}^5}{16\pi \langle F \rangle^2} \simeq \frac{m_{\widetilde{X}}^5}{16\pi \left(\sqrt{3} M_P m_{3/2}\right)^2} \tag{4.2}$$

where we assumed $m_X \ll m_{\widetilde{X}}$ and from which we can estimate the decay length as $L \simeq \frac{\hbar c}{\Gamma}$. If we require the sleptons and staus to decay promptly (*i.e.* $L <$ 0.1 mm), the width has to be large and the gravitino mass can not be too high. We impose the gravitino mass to be lower than 10 eV.

Concerning the NNLSP, the analogous two-body decay competes with possible three-body decay modes via an off-shell bino,

$$\tilde{\ell}_R \to \ell\tau\tilde{\tau}_R \;\; (\mathbf{M.I}); \qquad \tilde{\tau}_R \to \tau\ell\tilde{\ell}_R \;\; (\mathbf{M.II}) \; . \tag{4.3}$$

Figure 4.3 presents, for two different choices of the gravitino mass $m_{\tilde{G}} = 1$ eV (left) and 0.1 eV (right), the NNLSP two-body and three-body branching ratios when fixing the bino mass to 500 GeV, the slepton mass $m_{\tilde{\ell}_R}$ to 150 GeV and when varying the stau mass $m_{\tilde{\tau}_R}$. When $m_{\tilde{\tau}_R} < m_{\tilde{\ell}_R}$ (**M.I**), we display the decay modes of the slepton, whereas when $m_{\tilde{\tau}_R} > m_{\tilde{\ell}_R}$ (**M.II**) the ones of the stau. The three-body decay is found dominant except in the region where the NNLSP and NLSP are close in mass ($m_{\tilde{\tau}_R} \approx m_{\tilde{\ell}_R}$). This result is robust under variations of the bino mass. In contrast to other SUSY scenarios, our models exhibit a suppression of the two-body decay mode of the NNLSP into the LSP by the SUSY-breaking scale. As will be shown below, this is a key feature to get agreement with data.

We briefly notice that the three-body decay distinguishes between the different charge channels, *i.e.*, the NLSP can have either the opposite charge of the NNLSP ($\tilde{\ell}_R^- \to \ell^-\tau^-\tilde{\tau}_R^+$) or the same ($\tilde{\ell}_R^- \to \ell^-\tau^+\tilde{\tau}_R^-$) [125], denoted by dashed-dotted and dotted lines in figure 4.3. Generically, the more the bino is off-shell, the more the opposite charge channel dominates. Since the dominance of one channel with respect to the other is very much dependent on whether the sleptons are right- or left-handed, on the amount of stau mixing and on the nature of the neutralino, a detailed analysis of these effects might give us a way of probing non-trivial properties of the spectrum. However, the current LHC statistics is too low to allow for this analysis and we leave it for further investigation.

4.3 Multilepton signals at the LHC

Recently the CMS collaboration reported a slight excess in events with three electrons or muons (out of which one opposite-sign same flavour lepton pair can be formed) and one hadronically decaying tau, in the category with a Z-veto, low hadronic activity and no jet issued from the fragmentation of a b-quark [123]. With 19.5 fb^{-1} of collisions at $\sqrt{s} = 8$ TeV, the number of observed (expected)

Selection 4 Lepton Results		E_T^{miss}	$N(\tau_h)=1$, $N_{b-jets}=0$ obs	exp
OSSF1 $H_T < 200$	off-Z	(100,∞)	3	0.6 ± 0.24
OSSF1 $H_T < 200$	off-Z	(50,100)	4	2.1 ± 0.5
OSSF1 $H_T < 200$	off-Z	(0,50)	15	7.5 ± 2

Figure 4.4: The observed and expected number of events for the categories of the CMS analysis [124] with four or more leptons featuring the excess. For more details we refer to reference [124].

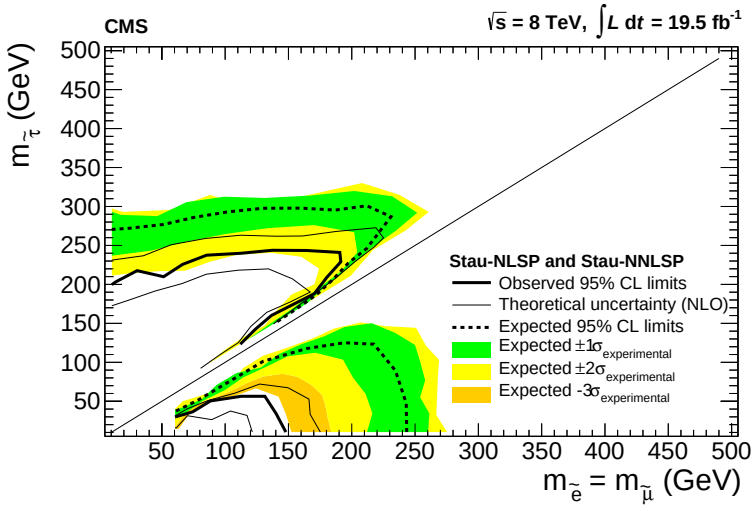

Figure 4.5: The 95% confidence level upper limits for the stau-(N)NLSP scenarios (corresponding to our **M.I** and **M.II** scenarios without bino) in the stau versus the slepton mass plane. The region to the left and below the contours is excluded. The discrepancy between the observed and expected limits is due to the excesses shown in figure 4.4. Figure taken from [124].

events in this category is 15 (7.5±2), 4 (2.1±0.5) and 3 (0.6±0.24) for the three regions $\not{E}_T < 50$ GeV, $\not{E}_T \in [50, 100]$ GeV and $\not{E}_T > 100$ GeV, respectively. The corresponding table and exclusion plot are shown in figure 4.4 and 4.5.

Motivated by this result, we investigate the contributions arising from slepton and stau pair production for models of class **M.I** and **M.II**. To display our results, we fix the bino and gravitino masses to 500 GeV and 1 eV, respectively, and scan the slepton and stau masses from 50 GeV to 300 GeV. Within our choice of parameters, the NNLSP dominantly decays via its three-body mode in most of the $(m_{\tilde{\ell}_R}, m_{\tilde{\tau}_R})$ mass plane. This allows for a possible enhancement of the production rates of final states comprised of $4\tau + 2\ell + \not{E}_T$ and $2\tau + 4\ell + \not{E}_T$ for **M.I** and **M.II** scenarios, respectively, as depicted in figure 4.6. The actual final state lepton multiplicity however depends on the number of leptonically decaying

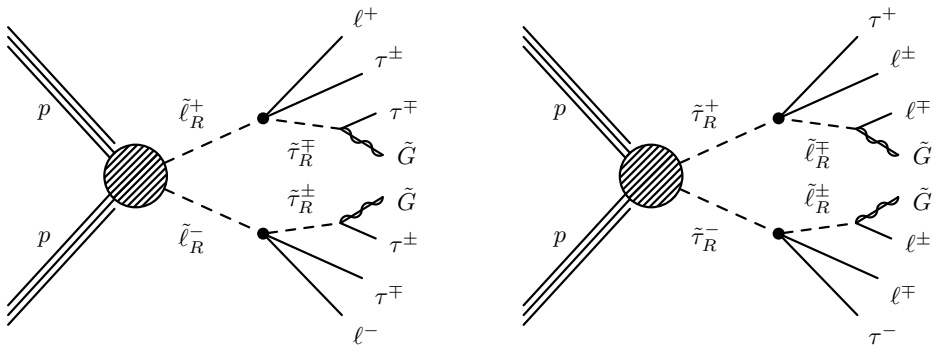

Figure 4.6: Diagrams leading to multilepton production in association with missing energy in scenarios of type **M.I** (left) and **M.II** (right).

taus.

4.3.1 Simulation

For our SUSY signal simulation, we use the goldstino model [135, 136] implemented in the FeynRules package [78, 80] and export it to a UFO library [92] which has been linked to MadGraph 5 [137]. The generated parton-level events have then been processed by Pythia [106] for parton showering and hadronization, Tauola [138] for tau decays and by Delphes [139] for detector simulation using the recent CMS detector description of [140]. We have analyzed 19.5 fb^{-1} of events describing NNLSP pair production at the LHC, running at $\sqrt{s} = 8$ TeV, with MadAnalysis 5 [97]. Generated events have been reweighted using signal cross sections predicted by Resummino at the next-to-leading order and next-to-leading logarithmic accuracy, as shown in figure 4.2. This results in typical K-factors of about 1.2 for the scanned mass range.

For event selection, we follow the CMS multilepton analysis of [123] and base our results on an investigation of the properties of isolated electron and muon candidates whose transverse-momentum p_T is greater than 10 GeV and pseudorapidity $|\eta|$ is smaller than 2.4. We enforce lepton isolation by imposing the amount of transverse activity in a cone of radius $R = \sqrt{\Delta\varphi^2 + \Delta\eta^2} = 0.3$ centered on the lepton, φ being the azimuthal angle with respect to the beam direction, to be less than 15% of the lepton p_T. Additionally, we impose the leading lepton (electron or muon) transverse momentum to satisfy $p_T > 20$ GeV and include efficiencies of 95%, 93% and 90% to simulate the effects of the double-electron, electron-muon and double-muon triggers relevant for the considered final state topologies. Finally, events featuring a pair of opposite-sign same flavour (OSSF) leptons whose invariant-mass is smaller than 12 GeV are rejected. While leptonically-decaying taus are accounted for as the electrons or muons in which they decay into, hadronically-decaying taus τ_h are reconstructed as such and we

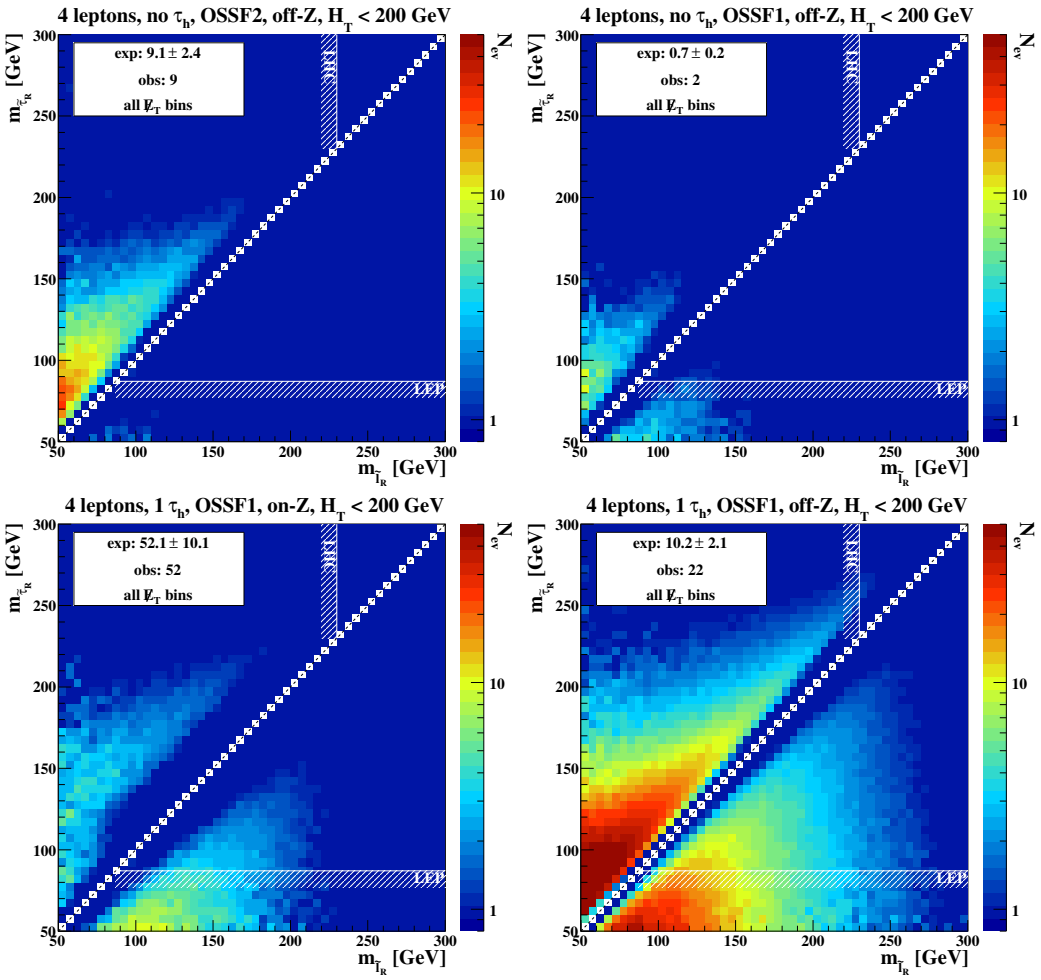

Figure 4.7: The number of signal events in the $(m_{\tilde{\ell}_R}, m_{\tilde{\tau}_R})$ plane for some representative categories, after summing $\not{E}_T$ bins. The numbers of expected and observed events are also presented [123], as well as LEP and LHC bounds from direct slepton searches.

demand their visible p_T to be greater than 20 GeV and their pseudorapidity to fulfill $|\eta| < 2.3$.

The CMS analysis classifies events as having H_T greater or less than 200 GeV as well as counting the number of b-tagged jets in the final states for which we employ the b-tagging algorithm described in [140]. The H_T variable is defined as the scalar sum of the transverse energy of all isolated reconstructed jets (not including hadronic tau contributions) with $p_T > 30$ GeV and $|\eta| < 2.5$, for which we use an anti-k_T algorithm whose radius parameter is fixed to $R = 0.5$ [141], as implemented in the FastJet package [111], and we consider a jet as isolated only if no electron, muon or tau lies within a cone of radius $R = 0.3$ centered on the jet. Concerning signal events, the hadronic activity mainly arises from

initial state radiation so that H_T is always found smaller than 200 GeV and the number of b-jets is rarely above zero. This feature is actually welcome since the CMS experiment does not see any excess in the regions where $H_T > 200$ GeV or $N_{\text{b-jets}} \geq 1$.

After applying the above requirements, events with at least three leptons are selected, where at most one of them is a hadronic tau. Further categories are made by classifying each event in terms of the maximum number of opposite-sign same flavour (OSSF) lepton pairs. Final state signatures predicted by both **M.I** and **M.II** models contain at least one OSSF lepton pair in most of the parameter space, which is again a welcome feature since the bins with zero OSSF lepton pairs do not exhibit any excess. The 'on-Z' region is populated if at least one OSSF lepton pair has an invariant mass in the Z-window $|m_{\ell^+\ell^-} - m_Z| < 15$ GeV while in the 'off-Z' region, each OSSF dilepton invariant mass lies outside the Z-window.

4.3.2 Results

After summing the $\not{E}_T$ bins, we have six categories for both the four lepton and the three lepton cases. We focus our discussion mainly on the four lepton channels since in the three leptons ones, the expected background is so large that the contributions from our signal region, characterized by a small yield, are always in agreement with the expectation within the statistical precision.

For illustrative purposes, in figure 4.7 we show four categories out of the possible six for the four lepton case, displaying the number of signal events in the $(m_{\tilde{\ell}_R}, m_{\tilde{\tau}_R})$ mass plane. We also quote the numbers of expected and observed events from table 2 in the CMS note [123]. The lower half plane, with $m_{\tilde{\tau}_R} < m_{\tilde{\ell}_R}$, corresponds to the **M.I** models, while the upper half plane, with $m_{\tilde{\tau}_R} > m_{\tilde{\ell}_R}$, corresponds to the **M.II** models.

In the category with two 'off-Z' OSSF lepton pairs, corresponding to the first panel of figure 4.7, the CMS analysis finds good agreement with the SM expectation. While models of class **M.I** do not give rise to any signal events in this category, the **M.II** models that are best compatible with the data in this category are those with $m_{\tilde{\tau}_R} \gtrsim 150$ GeV, *i.e.* those that give rise to very few signal events. The category with one 'off-Z' pair of OSSF leptons and no hadronic tau is shown as the second panel of figure 4.7. For very low stau masses, **M.I** scenarios can populate this bin with events featuring at least two leptonically decaying taus. By comparing with the first panel of the figure, we observe that out of the four leptons, **M.I** models generally predict, in the absence of hadronic taus, that one single OSSF lepton pair can be formed, whereas two OSSF lepton pairs are rather expected in **M.II** models. In the third panel of figure 4.7, we turn to the four lepton category including one hadronic tau and where one single OSSF lepton pair can be formed and lies in the Z-window. All scanned **M.I** and **M.II** scenarios predict number of events lying comfortably

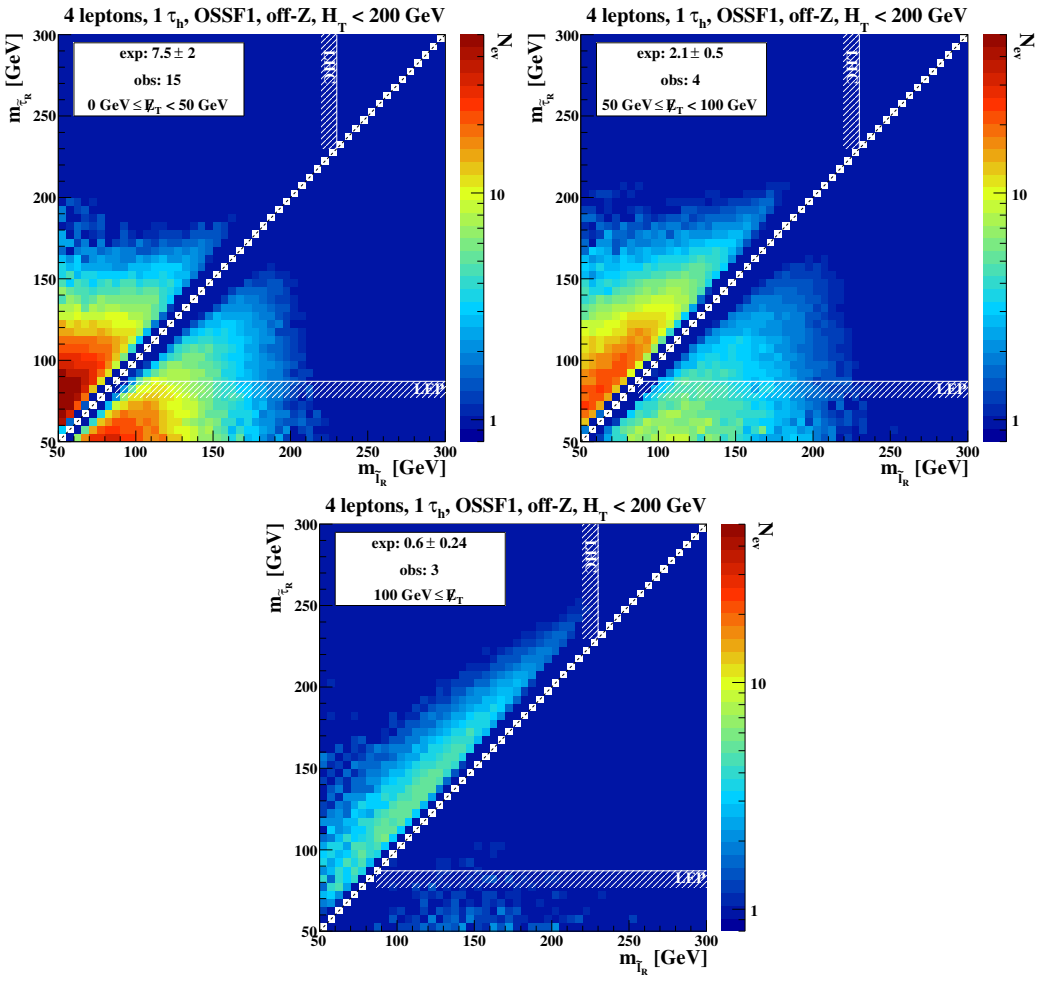

Figure 4.8: The same as in figure 4.7, but for the category where the excess events are observed. We show the results for different $\not\!\!E_T$ bins.

within 1σ variation of the SM expectation. The last panel of figure 4.7 shows the four lepton category including one hadronic tau and one OSSF lepton pair whose invariant mass is not compatible with the Z-boson mass. This category corresponds to the observed excess and both types of signal scenarios can provide good candidates for explaining it.

In figure 4.8, we display the precise distribution of our signal in the different $\not\!\!E_T$ bins corresponding to the last panel of figure 4.7. Scenarios of class **M.I** do not populate the bin with $\not\!\!E_T > 100$ GeV, unless in a narrow region where the stau is very light. Performing a χ^2 fit restricted to the three bins displayed in the figure for both class of models, the best benchmark scenarios are given by

$$\begin{aligned}
&\textbf{M.I}: \; m_{\tilde{\ell}_R} = 140 \text{ GeV}, \; m_{\tilde{\tau}_R} = 50 \text{ GeV}, \quad \chi^2_{\text{exc.}} = 1.22 \; ; \\
&\textbf{M.II}: m_{\tilde{\ell}_R} = 50 \text{ GeV}, \quad m_{\tilde{\tau}_R} = 140 \text{ GeV}, \; \chi^2_{\text{exc.}} = 2.28 \; .
\end{aligned}$$

Both models end up providing an explanation for the excess. However, as detailed below, experimental constraints arising from direct NLSP pair production exclude all **M.II** candidates explaining the excess, and have also non-trivial consequences on the best fit for **M.I** models.

In **M.II** models, where the right-handed sleptons are co-NLSP, current bounds on the slepton mass apply, $m_{\tilde{\ell}_R} > 230$ GeV [142,143]. These bounds are extracted from slepton pair production and subsequent decay into a lepton and a gravitino (a nearly massless LSP). As indicated in both figures 4.7 and 4.8, this excludes the entire region of the **M.II** parameter space possibly relevant for explaining the CMS excess. On the other hand, for **M.I** scenarios in which the right-handed stau is the NLSP, the most stringent constraints are those set by LEP experiments, $m_{\tilde{\tau}_R} > 87$ GeV [144], as the corresponding LHC searches have a too low sensitivity [145, 146]. Consequently, **M.I** models still provide viable candidates for explaining the excess.

The point of the **M.I** parameter space ending up to be the best fit of the three bins with the excess becomes, after accounting for LEP limits on the stau mass,

$$m_{\tilde{\ell}_R} = 145 \text{ GeV}, \; m_{\tilde{\tau}_R} = 90 \text{ GeV}, \; \chi^2_{\text{exc.}} = 2.42 \; ,$$

where $m_{\tilde{\tau}_R}$ lies at the edge of the excluded region. The significance of our best fit scenario is found reduced as signal contributions to the low missing energy bin of figure 4.8 are smaller for larger stau masses. As a crosscheck of our reasoning, we perform a global fit on the **M.I** parameter space including all four lepton categories. Not surprisingly, the same best fit benchmark point with $m_{\tilde{\tau}_R} = 90$ GeV and $m_{\tilde{\ell}_R} = 145$ GeV is obtained.

4.3.3 Confronting with other searches

Focusing from now on on the best fit point, we briefly comment on other signatures that it induces and which could be probed through other multilepton searches at the LHC. Firstly, CMS searches for R-parity violating (RPV) SUSY in leptonic final states are not expected to be sensitive to such models as it requires four electrons or muons in the final states [147]. Such a signature is suppressed in the framework of **M.I** models (as already shown on the first panel of figure 4.7) as it requires at least two of the taus to decay leptonically.

Secondly, the ATLAS collaboration has recently performed a multilepton search which features one signal region, dubbed 'SR1noZ', that might be relevant for models of class **M.I** [148]. This analysis has been designed for RPV SUSY searches and requires exactly three electrons or muons and at least one tau. An extended Z-veto is demanded so that events with a lepton pair, triplet or quadruplet whose invariant mass lies within a 20 GeV interval centered on the Z-boson mass are rejected. The search strategy additionally requires either a selection on the missing energy $\not{E}_T > 100$ GeV or on the effective mass, defined

$N(\ell)$	$N(\tau_h)$	N_{events}(8 TeV)	N_{events}(13 TeV)
4	2	22.5	223
5	0	0.074	0.79
5	1	1.7	14.7
5	2	7.4	76.1
6	0	0	0
6	1	0.075	0.66
6	2	1.0	7.89
> 6	0	0.038	13.9

Table 4.1: Number of multilepton events N_{events} predicted by the scenario that fits the CMS excess best (**M.I** model, $m_{\tilde{\ell}} = 145$ GeV, $m_{\tilde{\tau}} = 90$ GeV). The third column corresponds to 19.5 fb^{-1} of LHC collisions at $\sqrt{s} = 8$ TeV and the fourth column to 100 fb^{-1} of LHC collisions at $\sqrt{s} = 13$ TeV. Moreover, $N(\ell)$ denotes the total number of charged leptons and $N(\tau_h)$ how many of these are hadronically-decaying taus.

as the sum of the missing energy and of all the transverse momenta of the reconstructed final state objects (leptons, hadronic taus, jets), $m_{\text{eff}} > 400$ GeV. On the one hand, our signal does not populate the $\not{E}_T > 100$ GeV category as shown on figure 4.8. On the other hand, the tail of the effective mass distribution for our best benchmark point has been found to only extend up to about 350 GeV, which can be heuristically understood as most of the reconstructed final state objects come from the decay of a slepton pair with an invariant mass of about 300 GeV. This ATLAS search is therefore expected to be insensitive to our benchmark.

Lastly, the ATLAS collaboration has recently performed an investigation of ditau events [149], making use of a dedicated trigger on two reconstructed hadronic taus. This analysis could be relevant in our case since the signal is likely to populate bins with two hadronic taus, as shown in table 4.1. However, these taus are always accompanied by extra electrons or muons issued from NNLSP three-body decays, so that no hint in the ATLAS signal regions, which also include a veto on additional leptons, is foreseen.

4.3.4 Suggestions for future analyses

Let us finally discuss how some of the existing searches can be optimized to improve their sensitivity for signal scenarios of class **M.I**. As an illustrative example, we show in table 4.1 that our best fit point is considerably contributing to final states with two hadronically decaying taus plus either two or three electrons or muons. In particular, predicting a considerably large number of events featuring three electrons or muons shows that the lepton abundance in the final state

can be considerably enhanced by the leptonically decaying taus, even though the associated branching fraction is reduced. For these reasons we point out that an optimized search strategy for **M.I** models should impose selections on the lepton multiplicity as inclusive as possible, as already suggested in the context of optimizing Tevatron searches for gauge mediation scenarios [126]. Moreover, one peculiar feature of our benchmark scenario is the presence of at least two hadronically decaying taus which are hard enough to be reconstructed. We therefore suggest an effective search dedicated to **M.I** scenarios that could be made by combining triggers on two hadronically decaying taus with a binning on the number of extra leptons in the final state.

4.4 Summary

We have investigated the phenomenology of models involving light charged sleptons, realized within the framework of general gauge-mediated supersymmetry breaking. Motivated by the recent CMS observation of an excess in multilepton events, we have demonstrated that some of these models can not only provide an explanation for the excess but also explain why no hint of new physics has been found in other leptonic searches by both the ATLAS and CMS collaborations. We have shown that the model that best fits the data, and which is compatible with all current experimental constraints, involves right-handed selectrons and smuons of 145 GeV and a right-handed stau of 90 GeV. Finally, we proposed new investigations in multileptonic channels that could probe this type of GGM models and further constrain them in the future.

Chapter 5

Collider signatures of goldstini in gauge mediation

Since the most straightforward realizations of low-scale supersymmetry become less and less attractive, we have to broaden our view and consider also more general, unconventional realizations of supersymmetry and their signatures at colliders. In this chapter, we work in the framework of gauge mediation and assume there are two hidden SUSY-breaking sectors instead of only one. As we will see, the corresponding collider signatures are less energetic, softer, and more structured compared to standard gauge mediation. The work presented in this chapter is based on the work presented in reference [135].

This chapter is organized as follows: After further introducing the project in section 5.1, we provide the theoretical background behind gauge mediation with two SUSY-breaking sectors in section 5.2. In section 5.3 and 5.4 we then consider the two most common simplified models within GMSB (namely, where the gravitino is the lightest and the neutralino or stau the next-to-lightest SUSY particle) and investigate how a second SUSY-breaking sector would modify their appearance at colliders. We summarize our work in section 5.5.

5.1 Introduction

In the coming years we will receive the final verdict from the LHC experiments as to whether low-energy supersymmetry is present or not in Nature. So far, both ATLAS and CMS experiments have not seen any signal of SUSY yet and imposed strong bounds on the masses of coloured superpartners [60, 150]. In this chapter, we will work in the framework of gauge mediation where the SUSY-breaking effects are communicated to the observable sector by gauge interactions and gravity effects are subleading. A subclass of these models, namely those with

a light neutralino and a low SUSY-breaking scale, have already been constrained by the search for prompt photons plus missing energy [151–155]. Given that the most straightforward searches have not yielded any results yet, it is important at this stage to consider broadening the class of models to assure we are not missing anything.

Due to the large spectrum of possible SUSY theories, the collider searches shifted from theory-dependent studies to the more general simplified model approach (*cfr.* section 2.4.2). However, even within the general framework of simplified models, it is important to keep exploring less conventional avenues to make sure we get the most out of the current searches. When breaking supersymmetry, one usually assumes there is only one SUSY-breaking sector. There is, however, no real theoretical motivation why this should be the case. In this chapter, we will investigate the collider signatures of gauge mediation with more than one SUSY-breaking hidden sector interacting with the observable sector.

The possibility of having more than one SUSY-breaking hidden sector was first mentioned in [156] after which the theoretical formulation and phenomenology were further investigated in [157, 158] and later in [159–165]. If there are multiple SUSY-breaking sectors, each sector will give rise to a goldstino and, consequently, there will be multiple goldstini. A linear combination of the goldstini is eaten by the gravitino while the remaining fields give rise to light, neutral, spin one-half particles, the pseudo-goldstini. In our work, we will consider a set-up where there are only two decoupled hidden sectors and hence only one pseudo-goldstino, but the analysis can be trivially extended to the more general case and the qualitative features of the model are unchanged.

Contrary to the goldstino which is always massless, the pseudo-goldstino will obtain a tree-level mass of twice the gravitino mass due to supergravity effects and will additionally acquire a mass from radiative corrections ranging from 1 to 100 GeV. Since in gauge mediation the gravitino is very light, the mass of the pseudo-goldstino will be dominated by its radiative corrections [166]. If the pseudo-goldstino is the next-to-lightest supersymmetric particle (NLSP), it can only decay through a three-body decay to the gravitino and two SM particles and naturally has a long lifetime. The pseudo-goldstino can also be relevant for dark matter studies but we will refrain from considering cosmology in our work.[1] For our collider studies, we just assume that the pseudo-goldstino escapes the detector and, therefore, we are left with two invisible particles at the bottom of the spectrum. The next-to-next-to-lightest supersymmetric particle (NNLSP) is hence the lightest observable supersymmetric particle, referred to as LOSP, and will be very important in studying collider signatures.

In gauge mediation, the SUSY-breaking scale can be very low. Consequently, the gravitino LSP can be almost massless (*cfr.* equation (2.71)) implying that

[1] See *e.g.* [161, 166] for consideration on the pseudo-goldstino lifetime and its relevance for cosmology.

it behaves as the massless true goldstino (denoted by G) up to a very high level of accuracy. Yet, the LOSP decays predominantly through other channels, namely those containing the massive pseudo-goldstino (denoted by G'). One of the consequences of this fact is that it softens the spectra of the final states. We investigate those effects for the two most common scenarios where the LOSP is either a neutralino or a stau.

In the case of a neutralino LOSP (denoted by χ) the most accessible signature arises when χ is mostly a gaugino, promptly decaying into a photon and a (pseudo)-goldstino. The final state will contain photons and missing energy. A mostly gaugino χ can also decay into a Z boson and we will analyze these two situations in detail. In the case of the stau LOSP (denoted by $\tilde{\tau}$), lepton number conservation requires the staus to be created in pairs and the final state contains two taus and missing energy.

In the spirit of simplified models, our analysis is independent from many detailed features of the spectrum of superpartners. When forced to pick specific values for sparticle masses and mixing angles we will choose those used in common benchmark points [167] such as SPS8 (χ LOSP) and SPS7 ($\tilde{\tau}$ LOSP), in order to make a comparison with the standard gauge-mediated models. It should also be emphasized that although the points based on a minimal GMSB model have been constrained by the Tevatron [168, 169] and by the LHC [155], the multiple goldstini scenario eases the constraints due to the softer final spectrum.

5.2 GGM with two susy-breaking sectors

5.2.1 General formalism

The purpose of this section is to derive the relevant couplings of the (pseudo)-goldstino. We consider a set-up where there are two completely decoupled hidden sectors, each communicating to the supersymmetric Standard Model (SSM) through gauge interactions. In other words, each sector is a model of gauge mediation on its own. Each sector will then have a goldstino, G_1 and G_2 respectively, coupling to the SSM particles in a way dictated by the universal low-energy effective action of the goldstino, applied to each sector. If F_1 and F_2 are the respective SUSY-breaking scales of each sector, and $F = \sqrt{F_1^2 + F_2^2}$, then the true and pseudo-goldstino are respectively given by

$$G = \frac{1}{F}(F_1 G_1 + F_2 G_2), \tag{5.1}$$

$$G' = \frac{1}{F}(-F_2 G_1 + F_1 G_2). \tag{5.2}$$

For definiteness, we will always assume $F_1 > F_2$. It has been shown in [166] that, while G can be considered massless to all effects, G' acquires radiatively a

mass that is of the order of GeV if the scales in the two hidden sectors are of the same order. Moreover, when there is a hierarchy in the SUSY-breaking scales $F_1 \gg F_2$, the mass is enhanced to

$$m_{G'} \sim \frac{F_1}{F_2}\,\text{GeV}. \tag{5.3}$$

Since the exact expression for $m_{G'}$ is very much model dependent, for phenomenological purposes it should be taken as a free parameter, recalling that it will reasonably fall in the 1–100 GeV range. We will always assume that G' is the NLSP, *i.e.* it is lighter than the LOSP otherwise its presence is virtually impossible to detect.

The couplings of G and G' to the SSM particles can be derived by considering the couplings of G_1 and G_2, each as if it were the only source of SUSY breaking. The physical processes we are interested in involve only vertices with at most one (pseudo)-goldstino so we will not have to deal with the intricacies of the full (pseudo)-goldstino Lagrangian. We start by considering the couplings to a generic observable sector whose chiral and vector multiplets we denote by $\Phi \ni (\phi, \psi_\alpha, F_\phi)$ and $\mathcal{W}_\alpha \ni (\lambda_\alpha, A_\mu, D)$ respectively (gauge and flavour indices suppressed). After discussing the general features in this language, we present the explicit couplings in the context of the SSM, which are slightly more involved due to the additional presence of electroweak symmetry breaking (EWSB).

Let us begin by considering the true goldstino G, whose coupling at the linear level is fully understood since the seminal work of the '70s [170]. It is well known that there are two equivalent ways of writing the linear coupling of G to the matter fields. One is the derivative coupling to the supercurrent

$$\mathcal{L}_\partial = \frac{1}{F}(\partial_\mu G^\alpha J^\mu_\alpha + \text{h.c.}), \tag{5.4}$$

where, in the conventions of [171]

$$J^\mu = \sigma^\nu \bar\sigma^\mu \psi D_\nu \phi^* - i\sigma^\mu \bar\psi F_\phi + i\frac{1}{2\sqrt{2}}\sigma^\nu \bar\sigma^\rho \sigma^\mu \bar\lambda F_{\nu\rho} + \frac{1}{\sqrt{2}}\sigma^\mu \bar\lambda D. \tag{5.5}$$

The other action is the non-derivative coupling obtained from the previous one by integrating by parts and using the equation of motion to obtain $\Delta_\alpha = \partial_\mu J^\mu_\alpha|_{\text{e.o.m.}}$

$$\mathcal{L}_{\not\partial} = -\frac{1}{F}(G^\alpha \Delta_\alpha + \text{h.c.}). \tag{5.6}$$

Since the non-conservation of the supercurrent is entirely due to the presence of supersymmetry-breaking soft terms, the expression for Δ_α must be a function of the latter.

Let us consider the most general soft SUSY-breaking terms, namely:

$$\mathcal{L}_{\text{soft}} = -\frac{1}{2}m_\lambda \lambda\lambda - \frac{1}{2}m_\lambda^* \bar{\lambda}\bar{\lambda} - U(\phi, \phi^*), \tag{5.7}$$

where U is a (at most cubic) gauge invariant function of the scalars, containing for instance the sfermion soft masses and the $B\mu$ term and m_λ are the Majorana masses for the gauginos. The divergence of the supercurrent is now

$$\partial_\mu J^\mu_\alpha = \Delta_\alpha = \frac{m_\lambda}{2\sqrt{2}}\sigma^\mu\bar{\sigma}^\nu\lambda_\alpha F_{\mu\nu} - i\frac{m_\lambda}{\sqrt{2}}\lambda_\alpha D - \psi_\alpha\frac{\partial U}{\partial\phi} \tag{5.8}$$

from which the coupling follows using (5.6). This expression is valid regardless of whether the gauge symmetry is spontaneously broken or not (see for instance [172] for a complete treatment in the MSSM). The form of (5.6) can also easily be derived from a superspace formulation of the broken SUSY theory, in terms of the goldstino superfield X.

The derivative and non-derivative actions are completely equivalent, of course, but some issues are easier to investigate in one formalism than in the other. It turns out that it is the non-derivative action that is more directly generalized to the pseudo-goldstino case. This can be seen in various ways but perhaps the easiest argument comes by looking at the leading high energy behaviour of the $2 \to 2$ scattering amplitudes involving a goldstino. The action (5.4) contains terms of dimension six and one would expect the tree-level unpolarized squared amplitudes to scale like s^2 where $\sqrt{s}$ is the centre-of-mass energy. This is not what happens however since SUSY ensures that the leading order behaviour cancels between the different contributions. This must be so since (5.4) is equivalent to (5.6) which contains terms of dimension at most five and yields a scaling of order s.

The same scaling must occur for the pseudo-goldstino since, after all, at tree level it is a linear combination of two decoupled goldstini, but now the relative coefficients between the various terms in the action are no longer fixed by SUSY. Using the non-derivative action ensures that the high energy behaviour is preserved. One can of course use the equations of motion "backwards" and rewrite the non-derivative action in terms of the same type of terms that appear in the derivative action but with different relative coefficients. In the process however one also picks up dimension six contact terms schematically like $G\lambda\psi\psi$ that once again cancel the s^2 behaviour. Thus it is clearly more convenient to work with (5.6).

In order to derive the couplings of the pseudo-goldstino, let us start at tree level with the two fields G_h $(h = 1, 2)$ that are the goldstini of the respective hidden sectors contained in the superfields X_h. For each goldstino-gaugino-gauge boson vertex, we have

$$\frac{1}{2}\int d^2\theta \frac{m_{\lambda(h)}}{F_h} X_h \mathcal{W}^2 \supset \frac{m_{\lambda(h)}}{2\sqrt{2}F_h}\lambda\sigma^\mu\bar{\sigma}^\nu G_h F_{\mu\nu}. \tag{5.9}$$

For the goldstino-fermion-sfermion vertex, we have

$$\int d^4\theta \frac{m^2_{\phi(h)}}{F_h^2} X_h X_h^\dagger \Phi\Phi^\dagger \supset \frac{m^2_{\phi(h)}}{F_h} G_h \psi\phi^*. \tag{5.10}$$

The terms (5.9) and (5.10) correspond to the first and last terms in (5.8) inserted into (5.6), the last one with $U = m^2_\phi \phi^*\phi$. We ignore further vertices that do not contribute to the processes of interest but a full treatment can be found in [173].

Rotating to the G, G' basis, we obtain the couplings

$$\frac{m_\lambda}{2\sqrt{2}F}\lambda\sigma^\mu\bar\sigma^\nu G F_{\mu\nu} + K_\lambda \frac{m_\lambda}{2\sqrt{2}F}\lambda\sigma^\mu\bar\sigma^\nu G' F_{\mu\nu} \tag{5.11}$$

and

$$\frac{m^2_\phi}{F} G\psi\phi^* + K_\phi \frac{m^2_\phi}{F} G'\psi\phi^*, \tag{5.12}$$

where $m_\lambda = m_{\lambda(1)} + m_{\lambda(2)}$ and $m^2_\phi = m^2_{\phi(1)} + m^2_{\phi(2)}$, and the factors K_λ and K_ϕ are the ratios between the coupling of the pseudo-goldstino to the one of the true goldstino. Their expressions are

$$K_\lambda = -\frac{m_{\lambda(1)}}{m_\lambda}\frac{F_2}{F_1} + \frac{m_{\lambda(2)}}{m_\lambda}\frac{F_1}{F_2}, \tag{5.13}$$

$$K_\phi = -\frac{m^2_{\phi(1)}}{m^2_\phi}\frac{F_2}{F_1} + \frac{m^2_{\phi(2)}}{m^2_\phi}\frac{F_1}{F_2}, \tag{5.14}$$

where in general there will be different coefficients for each gauge group and matter multiplet. In some specific models, there can be relations or bounds between K_λ and K_ϕ. However, in the phenomenological set-up, one assumes that these two parameters are free. In any case, below we will use couplings of G' only to a very limited set of (s)particles. The interesting case will be when $K_\lambda, K_\phi \gg 1$. Note however that both cannot be larger than F_1/F_2, hence they are limited to be somewhat smaller than 10^3. (If F_1/F_2 is too large, the above picture is no longer valid because the SUSY-breaking vacuum of the second sector is destabilized [166].)

5.2.2 Pseudo-goldstino couplings in the SSM

We now specialize to the case where the observable sector is a SUSY extension of the SM. A couple of technical issues arise since one must also rotate to the physical bases of mass eigenstates of the observable sector after EWSB. More generally the (pseudo)-goldstini will also mix with the particles in the observable sector carrying the same quantum numbers but it is possible to treat this mixing to first order in the SUSY-breaking parameter.

Let us begin with the coupling of the neutralino to the G/G' and the photon. This involves an element of the neutralino mixing matrix, essentially proportional to how much the neutralino is the would-be photino. More precisely for the goldstino there is a factor (see *e.g.* [171])

$$a_\gamma = N_{11}^* \cos\theta_W + N_{12}^* \sin\theta_W, \tag{5.15}$$

where N_{11}^* and N_{12}^* are the mixing angles between the lightest neutralino and the bino and wino respectively. For the pseudo-goldstino, we can multiply the above by a factor K_γ that can be larger than one as discussed above. The relevant part of the Lagrangian is thus

$$\mathcal{L}_{\chi G\gamma} + \mathcal{L}_{\chi G'\gamma} = \frac{a_\gamma m_\chi}{2\sqrt{2}F}\chi\sigma^\mu\bar\sigma^\nu G F_{\mu\nu} + \frac{K_\gamma a_\gamma m_\chi}{2\sqrt{2}F}\chi\sigma^\mu\bar\sigma^\nu G' F_{\mu\nu}. \tag{5.16}$$

The coupling of the goldstino and the pseudo-goldstino to the neutralino and the Z boson is slightly more subtle. Standard computations, such as in [174], use the goldstino couplings in derivative form. After EWSB, there are two such couplings:

$$\mathcal{L}_\partial = i\frac{a_{Z_T}}{2\sqrt{2}F}\bar\chi\bar\sigma^\mu\sigma^\nu\bar\sigma^\rho\partial_\mu G F_{\nu\rho} - \frac{a_{Z_L} m_Z}{\sqrt{2}F}\chi\sigma^\mu\bar\sigma^\nu\partial_\mu G Z_\nu + \text{h.c.}, \tag{5.17}$$

where

$$a_{Z_T} = -N_{11}^* \sin\theta_W + N_{12}^* \cos\theta_W, \tag{5.18}$$

$$a_{Z_L} = N_{13}^* \cos\beta - N_{14}^* \sin\beta. \tag{5.19}$$

N_{13}^* and N_{14}^* are the higgsino components of the lightest neutralino, and $\tan\beta$ is the ratio of the vacuum expectation values of the two higgs doublets.[2] The notation follows from the notable fact that the first and second term respectively couple only transverse and longitudinal components of the Z to a massless goldstino.

Integrating by parts and using the equations of motion, one obtains the following terms in the non-derivative Lagrangian:

$$\mathcal{L}_{\chi GZ} = \frac{a_{Z_T} m_\chi + a_{Z_L} m_Z}{2\sqrt{2}F}\chi\sigma^\mu\bar\sigma^\nu G F_{\mu\nu} + i\frac{m_Z(a_{Z_T} m_Z + a_{Z_L} m_\chi)}{\sqrt{2}F}\bar\chi\bar\sigma^\mu G Z_\mu + \text{h.c.} \tag{5.20}$$

It might seem at first that the second term in the Lagrangian above cannot be reproduced using (5.8). This term appears because after EWSB there are off-diagonal mass terms involving the goldstino and the neutralinos. The mass

[2] Although we do not consider the decay into higgs, we will nonetheless treat the decay into Z exactly by including the contribution of the longitudinal component.

eigenstates have then to be shifted by $\mathcal{O}(1/F)$ terms mixing the goldstino with the neutralinos. Eventually the term above arises from the neutralino gauge couplings, and its precise form follows from using the equations leading to the EWSB vacuum (for a discussion, also including the pseudo-goldstino, see [163]).

The pseudo-goldstino couplings to the Z boson will be of the form above, with however some model-dependent factors in front of each term. Since there are two independent terms in (5.20), there will be two independent coefficients and we choose to associate them directly to the rescaling of the a_{Z_T} and a_{Z_L} coefficients:[3]

$$\mathcal{L}_{\chi G' Z} = \frac{K_{Z_T} a_{Z_T} m_\chi + K_{Z_L} a_{Z_L} m_Z}{2\sqrt{2}F} \chi \sigma^\mu \bar{\sigma}^\nu G' F_{\mu\nu} + i \frac{m_Z (K_{Z_T} a_{Z_T} m_Z + K_{Z_L} a_{Z_L} m_\chi)}{\sqrt{2}F} \bar{\chi} \bar{\sigma}^\mu G' Z_\mu + \text{h.c.} \quad (5.21)$$

We now move on to the couplings of the stau. Even in this case the general formula (5.12) requires some well known modifications after EWSB. Namely, the presence of a SUSY contribution to the tau mass makes the coefficient in the action depend on the difference of the masses in the multiplet. The large soft off-diagonal corrections to the stau mass matrix require rotating from the gauge eigenbasis $\tilde{\tau}_L, \tilde{\tau}_R$ to the mass eigenbasis $\tilde{\tau}, \tilde{\tau}'$. For the couplings to the first two families these effects can be neglected. We focus only on the LOSP $\tilde{\tau} = \cos\theta_{\tilde{\tau}}\, \tilde{\tau}_L + \sin\theta_{\tilde{\tau}}\, \tilde{\tau}_R$ and write the Lagrangian as

$$\mathcal{L}_{\tilde{\tau} G \tau} + \mathcal{L}_{\tilde{\tau} G' \tau} = \frac{m_{\tilde{\tau}}^2 - m_\tau^2}{F} \left(\cos\theta_{\tilde{\tau}}\, G \tau_L + \sin\theta_{\tilde{\tau}}\, G^\dagger \tau_R \right) \tilde{\tau}^* + \frac{m_{\tilde{\tau}}^2 - m_\tau^2}{F} \left(K_{\tau_L} \cos\theta_{\tilde{\tau}}\, G' \tau_L + K_{\tau_R} \sin\theta_{\tilde{\tau}}\, G'^\dagger \tau_R \right) \tilde{\tau}^* + \text{h.c.},$$

where we have set $P_{L/R}\tau = \tau_{L/R}$. Once again, we treat the coefficients K_{τ_L} and K_{τ_R} as free parameters.

5.3 The case of the neutralino LOSP

We begin our analysis by considering the case where the neutralino χ is the LOSP. For this we use the Lagrangians (5.16), (5.20) and (5.21).

[3] One could have also chosen to rescale each Lorentz invariant term in (5.20) independently but this would obscure the comparison in the simulation.

5.3.1 Decays of the neutralino

The partial widths for neutralino decay into a photon and a (pseudo)-goldstino are:

$$\Gamma(\chi \to \gamma G) = \frac{a_\gamma^2 m_\chi^5}{16\pi F^2}, \tag{5.22}$$

$$\Gamma(\chi \to \gamma G') = \frac{K_\gamma^2 a_\gamma^2 m_\chi^5}{16\pi F^2}\left(1 - \frac{m_{G'}^2}{m_\chi^2}\right)^3. \tag{5.23}$$

We could also write $F = \sqrt{3} m_{3/2} M_p$ in the denominators above, with the mass of the gravitino (*i.e.* the true goldstino) $m_{3/2}$ and the reduced Planck mass $M_p = 2.43 \times 10^{18}$ GeV.

For a rather massive pseudo-goldstino, the factor between parenthesis can be significantly smaller than 1, though it is always of $\mathcal{O}(1)$ barring any fine-tuning of $m_{G'}$ against m_χ. Hence the branching ratios can be of the same order if $K_\gamma = \mathcal{O}(1)$, or we can have a neutralino decaying almost exclusively to the pseudo-goldstino if $K_\gamma \gg 1$. For instance we can have $K_\gamma \sim 100$ and then the decay rate of the neutralino is going to be 10^4 times larger with respect to a single sector scenario.

In order for the neutralino to decay inside the detector, its total width cannot be too small. A rough order of magnitude of the bound is $\Gamma_{\text{tot}} \gtrsim 10^{-16}$ GeV. For a single sector scenario and $m_\chi \sim 200$ GeV, it would translate to $\sqrt{F} \lesssim 10^3$ TeV (see *e.g.* [39]), but in our case the constraint is more flexible due to the presence of the K_γ factor.

We now list the partial widths for the decay of the neutralino into a Z boson and a goldstino or a pseudo-goldstino. For the goldstino, using either (5.17) or (5.20), one obtains the classic result [174]

$$\Gamma(\chi \to ZG) = \frac{(2a_{Z_T}^2 + a_{Z_L}^2) m_\chi^5}{32\pi F^2}\left(1 - \frac{m_Z^2}{m_\chi^2}\right)^4. \tag{5.24}$$

For the pseudo-goldstino, the decay rate is given by

$$\Gamma(\chi \to ZG') = \frac{\beta}{16\pi m_\chi}|\mathcal{M}|^2, \tag{5.25}$$

where $\beta \equiv \beta(\frac{m_Z^2}{m_\chi^2}, \frac{m_{G'}^2}{m_\chi^2})$ with

$$\beta(a,b) = (1 + a^2 + b^2 - 2a - 2b - 2ab)^{1/2} \tag{5.26}$$

is the usual phase space factor and the spin summed and averaged amplitude

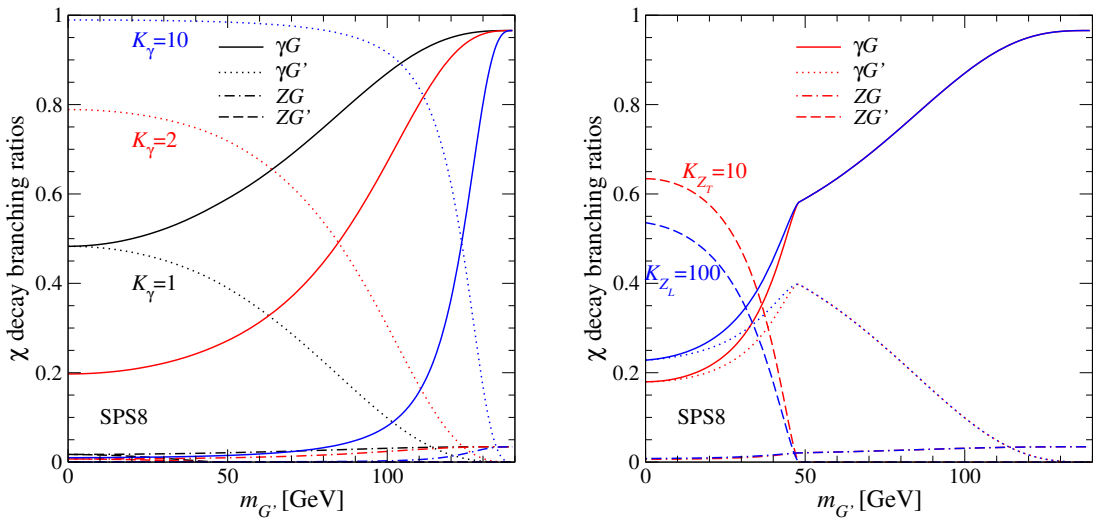

Figure 5.1: Branching ratios for the lightest neutralino decay into a (pseudo)-goldstino and a photon or Z at the SPS8 benchmark point. On the left the coupling of the pseudo-goldstino to the photon is gradually enhanced, while on the right the case of enhanced coupling of the pseudo-goldstino to the Z boson is shown.

squared is

$$
\begin{aligned}
|\mathcal{M}|^2 = \frac{1}{2F^2}\Big\{&(m_\chi^2 - m_Z^2)^3(2K_T^2 + K_L^2) + 6m_{G'}m_Z(m_\chi^2 - m_Z^2)^2 K_T K_L \\
&+ m_{G'}^2(m_\chi^2 - m_Z^2)\left[(-4m_\chi^2 - m_Z^2)K_T^2 + (-2m_\chi^2 + m_Z^2)K_L^2 - 6m_\chi m_Z K_T K_L\right] \\
&- 6m_{G'}^3 m_Z\left[m_\chi m_Z(K_T^2 + K_L^2) + (m_\chi^2 + m_Z^2)K_T K_L\right] \\
&+ m_{G'}^4\left[(2m_\chi^2 + m_Z^2)K_T^2 + (m_\chi^2 + 2m_Z^2)K_L^2 + 6m_\chi m_Z K_T K_L\right]\Big\}\,,
\end{aligned}
$$

where $K_T \equiv K_{Z_T} a_{Z_T}$ and $K_L \equiv K_{Z_L} a_{Z_L}$. The decay channel is open only when $m_{G'} < m_\chi - m_Z$.

We note that, upon setting $K_\gamma = K_{Z_T} = K_{Z_L} = 1$, the decay rates to a pseudo-goldstino slightly differ from those to a massive spin-3/2 gravitino, as detailed for instance in [175].

In figure 5.1 we plot the branching ratios for the lightest neutralino decay for varying pseudo-goldstino mass and for various values of K_γ, K_{Z_T} and K_{Z_L}. The remaining relevant SUSY parameters are taken at the SPS8 benchmark point as calculated by SOFTSUSY [49]. Namely, we have $m_G\,(= m_{3/2}) = 4.74$ eV, $m_\chi = 139.2$ GeV, $N_{11} = 0.99$, $N_{12} = -0.031$, $N_{13} = 0.124$, $N_{14} = -0.048$ and $\tan\beta = 14.5$. In general, the partial widths for decay into Z bosons are very much suppressed with respect to the ones for decay into photons, except when K_{Z_T} and/or K_{Z_L} are the only large factors. In the following we will not assume this. Also, the partial width for decay into higgses is negligible at the SPS8 point. See [163] for a different set-up where this is not the case.

It is obvious that the neutralino total width will always be exceedingly small, *e.g.* $\Gamma_{\rm tot} \sim 10^{-12}$ GeV for $K_\gamma = K_{Z_T} = K_{Z_L} = 1$, compared to m_χ, so that we can safely place ourselves in the narrow width approximation (NWA) in all processes of interest with an intermediate neutralino. In the next sub-sections we will discuss observable signatures involving the production and decay of neutralinos. Thus, the (differential) cross sections will be proportional to the square of the amplitudes for production of neutralinos, and to the branching ratios for their decay.

5.3.2 Goldstini and single-photon production in e^+e^- collisions

We now perform an analytic computation with the purpose of highlighting the differences with respect to the single sector case and the role played by the extra parameters K_λ and K_ϕ, characterizing the pseudo-goldstino couplings. For simplicity, in this subsection only, we stick to the case where the neutralino is a pure photino, *i.e.* $a_\gamma = 1$ and $a_{Z_T} = a_{Z_L} = 0$.

There are three kinds of diagrams contributing to this process, as in figure 5.2. In the s-channel, the intermediate particle is a photon, since the neutralino is pure photino. Note also that there is another s-channel diagram with the outgoing arrows reversed. (We are using the two-component notation of [171].) In the t- and u-channels, the intermediate particle is either of the right- and left-handed selectrons. We assume here that the factor K_ϕ is the same for both selectrons.

The couplings of the (pseudo)-goldstino have been reviewed in section 5.2 and for a pure photino neutralino they are (see (5.11) and (5.12))

$$\mathcal{L}_{G'} \supset K_\lambda \frac{m_\chi}{2\sqrt{6} M_p m_{3/2}} \lambda \sigma^\mu \bar{\sigma}^\nu G' F_{\mu\nu} + K_\phi \frac{m_{\tilde{e}}^2}{\sqrt{3} M_p m_{3/2}} G' \psi \phi^*, \tag{5.27}$$

where $m_{3/2} = F/\sqrt{3}M_p$ is the gravitino mass, $m_{\tilde{e}}$ is the right and left selectron mass (we have neglected the mass of the electron with respect to the mass of the

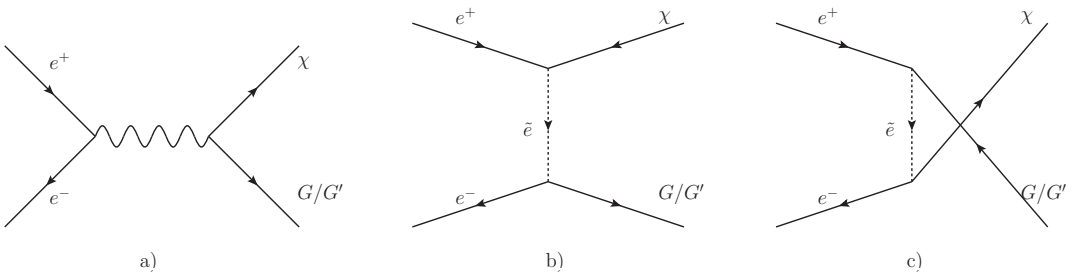

Figure 5.2: All diagrams contributing to $e^+e^- \to \chi G/G'$: a) s-channel, b) t-channel and c) u-channel.

selectrons) and finally $m_\chi \equiv m_\lambda$. The other couplings needed for the computation can be gathered from *e.g.* [171].

Note that in the amplitude squared all diagrams actually interfere due to the mass of the pseudo-goldstino. The computation is thus more involved than the one for a massless goldstino [176, 177]. The differential cross section for production of a photino and a pseudo-goldstino reads

$$d\sigma_{e^+e^-\to\chi G'} = \frac{1}{2s}|\mathcal{M}|^2\, d\Phi_2 \tag{5.28}$$

with the spin summed and averaged amplitude squared

$$\begin{aligned}
|\mathcal{M}|^2 = \\
&\frac{e^2}{3M_p^2 m_{3/2}^2}\left\{\frac{K_\lambda^2 m_\chi^2}{s}\left(2tu - m_\chi^2(t+u) + 2m_{G'}m_\chi s + m_{G'}^2(2m_\chi^2 - t - u)\right)\right. \\
&+ K_\phi^2 m_{\tilde e}^4\left(\frac{(t-m_{G'}^2)(t-m_\chi^2)}{(t-m_{\tilde e}^2)^2} + \frac{(u-m_{G'}^2)(u-m_\chi^2)}{(u-m_{\tilde e}^2)^2} + \frac{2m_{G'}m_\chi s}{(t-m_{\tilde e}^2)(u-m_{\tilde e}^2)}\right) \\
&\qquad - 2K_\lambda K_\phi m_\chi m_{\tilde e}^2\left(\frac{m_\chi(t-m_{G'}^2) + m_{G'}(t-m_\chi^2)}{t-m_{\tilde e}^2}\right. \\
&\qquad\qquad \left.\left. + \frac{m_\chi(u-m_{G'}^2) + m_{G'}(u-m_\chi^2)}{u-m_{\tilde e}^2}\right)\right\},
\end{aligned} \tag{5.29}$$

where e is the electromagnetic coupling constant. We refer to *e.g.* [27] concerning kinematics. One can check that in the limit $m_{G'} \to 0$ and $K_\lambda = K_\phi = 1$ this reproduces the result reported in [177]. Plugging $|\mathcal{M}|^2$ in (5.28) and integrating over $\cos\theta$ we get the total cross section.

It is interesting to note that the above amplitude is slightly different depending on the relative sign of the respective (real) Majorana masses of the neutralino LOSP and the pseudo-goldstino. This relative sign is model dependent.

It should be stressed that the cross section scales with $K_{\lambda,\phi}^2/m_{3/2}^2$. In the spirit of [177–181], LEP bounds on such cross sections can be translated into upper bounds on $K/m_{3/2}$, or alternatively on K at a given value of $m_{3/2}$. (Here K is for simplicity a common value for K_λ and K_ϕ.) Roughly, we get $K < 10^{4-5}(m_{3/2}/\text{eV})$, which allows us some elbow room. Note that in the case of the single true goldstino production, *i.e.* with $K_\lambda = K_\phi = 1$, the cross section is very small, unless the gravitino mass is of order $10^{-5} - 10^{-4}$ eV [177]. In the case of the pseudo-goldstino, instead, the cross section can be enhanced by the couplings K_λ and K_ϕ while keeping the gravitino mass to standard values for gauge mediation scenarios, *i.e.* $m_{3/2} \sim$ eV.

To exemplify the physics of this process, and in particular the dependence on the pseudo-goldstino parameters, in figure 5.3 we plot the total cross section as a function of the pseudo-goldstino mass for some values of the parameters K_λ and

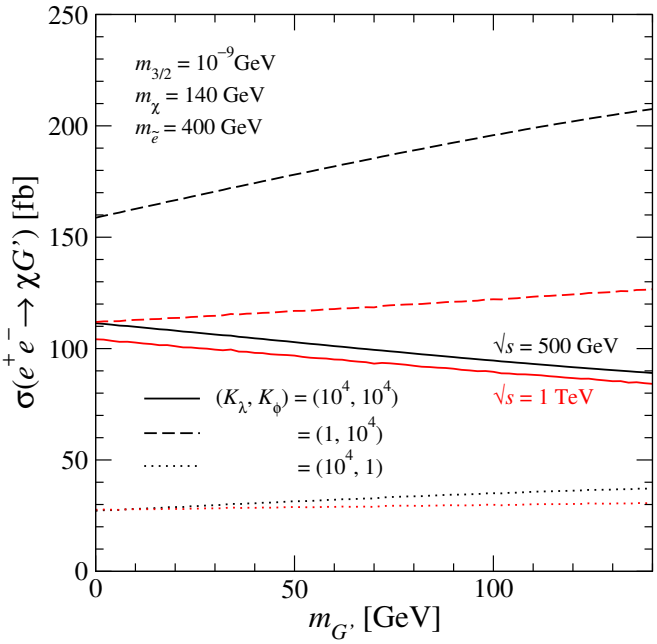

Figure 5.3: Total cross section of $e^+e^- \to \chi G'$ at $\sqrt{s} = 500$ GeV (black lines) and 1 TeV (red lines) as a function of the pseudo-goldstino mass, for various values of K_λ and K_ϕ.

K_ϕ. Here we consider a photino LOSP and take the masses as $m_{3/2} = 10^{-9}$ GeV, $m_\chi = 140$ GeV and $m_{\tilde{e}_R} = m_{\tilde{e}_L} = 400$ GeV.

There is a destructive interference between the diagrams and thus the cross section for large K_ϕ turns out to be greater than the cross section when both K_λ and K_ϕ are large. We notice that rather large values of K_λ and K_ϕ are required to obtain the cross section around $\mathcal{O}(10^{2-3})$ fb with the eV order gravitino mass, while such large values are not favoured by the stability of the SUSY-breaking vacuum as mentioned before.

One can also easily see that in these cases the emitted photons can be significantly softer than in usual gauge mediation scenario, since the pseudo-goldstino has a non negligible mass. Moreover, similar to the discussions in [182], the photon energy distribution can tell us about the masses of the neutralino and pseudo-goldstino as we will explicitly see in the next section. On the other hand, different K factors would give different photon angular distributions.

All the results presented here can be obtained numerically running MadGraph 5 [137] simulations adapted to the (pseudo)-goldstino scenario (building on [136]), having implemented the model using FeynRules [78, 80, 92]. This provides also a non trivial test of our FeynRules implementation, which we will use afterwards to simulate pp collisions.

5.3.3 Goldstini and di-photon production in e^+e^- collisions

The production of two neutralinos will lead to a di-photon plus missing energy signature, which is evidence for the processes

$$e^+e^- \to \gamma\gamma GG, \qquad e^+e^- \to \gamma\gamma GG', \qquad e^+e^- \to \gamma\gamma G'G'. \tag{5.30}$$

The total cross section ($\sigma^{\rm LO}_{e^+e^-\to\chi\chi} \sim 177$ fb at $\sqrt{s} = 500$ GeV at SPS8) is similar to the single sector case, since the couplings that can be enhanced in the pseudo-goldstino scenario only appear in the decay of the neutralinos. However the photon spectrum, and in particular the edges of the energy distribution, is sensitive to the mass of G', both if the branching ratios are comparable or if the decay to G' is favoured.

In figure 5.4, the distributions of the leading photon energy (left) and of the missing invariant mass (right) for $e^+e^- \to \chi\chi \to \gamma\gamma + \not{E}$ at $\sqrt{s} = 500$ GeV are shown. To obtain both plots, we applied a cut on the energy and the rapidity of the photons, $E_\gamma > 15$ GeV and $|\eta_\gamma| < 2$, as the minimal cuts for the detection of photons. In addition, we imposed the invisible invariant mass cut $M_{\rm inv} > 100$ GeV to remove the SM $(Z \to \nu\bar{\nu})\gamma\gamma$ background. The remaining background comes from the t-channel W-exchange process, and this can be reduced by using the polarized $e^\pm$ beams.

Besides the reference point $m_{G'} = 0$ with $K_\gamma = 1$ (for which we have essentially two indistinguishable copies of a light goldstino), we take two different pseudo-goldstino masses, 85 GeV and 125 GeV, with different couplings as in the following table:

1a.	$m_{G'} = 85$ GeV	with $K_\gamma = 1$	$[B(\chi \to \gamma G') \sim 0.2]$
1b.	$m_{G'} = 85$ GeV	with $K_\gamma = 2$	$[B(\chi \to \gamma G') \sim 0.5]$
1c.	$m_{G'} = 85$ GeV	with $K_\gamma = 10$	$[B(\chi \to \gamma G') \sim 1]$
2a.	$m_{G'} = 125$ GeV	with $K_\gamma = 10$	$[B(\chi \to \gamma G') \sim 0.5]$
2b.	$m_{G'} = 125$ GeV	with $K_\gamma = 100$	$[B(\chi \to \gamma G') \sim 1]$

Here, we keep $K_{Z_T} = K_{Z_L} = 1$, and hence the decay modes into Z are negligible; see also figure 5.1 for the branching ratios. We have also run the simulations for $m_{G'} = 10$ GeV with $K_\gamma = 1, 2$ and 10, for which the branching ratio is respectively 0.5, 0.8 and 1, but we found distributions essentially overlapping with the massless one.

The edges of the energy distributions allow to determine both the mass of the neutralino LOSP and of the pseudo-goldstino. A simple generalization of the massless goldstino case discussed in [174] gives the following expression for the minimal and maximal energy of each emitted photon:

$$E_\gamma^{\rm max,min} = \frac{\sqrt{s}}{4}\left(1 - \frac{m_{G'}^2}{m_\chi^2}\right)\left(1 \pm \sqrt{1 - \frac{4m_\chi^2}{s}}\right). \tag{5.31}$$

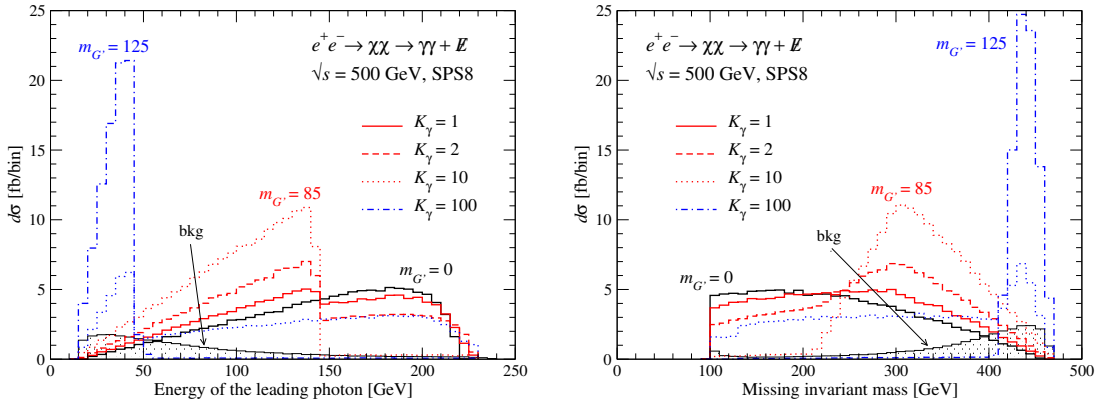

Figure 5.4: The distributions of the leading photon energy (left) and of the missing invariant mass (right) for $e^+e^- \to \chi\chi \to \gamma\gamma + \not{E}$ at $\sqrt{s} = 500$ GeV, where the pseudo-goldstino mass is fixed at 85 GeV (red) and 125 GeV (blue). The $m_{G'} = 0$ case (black) is also shown as the reference point as well as the SM background.

In this case, it is difficult to determine the minimal edges due to the detector cut. On the other hand, the $E_\gamma^{\max}$ is rather clear although the edge of the high energy region is smeared by the missing invariant mass cut. It is interesting to note that, unless the branching ratio is not close to unity, we can find the two $E_\gamma^{\max}$ edges with $m_{G'} \neq 0$ and $m_{G'} = 0$, which can determine both m_χ and $m_{G'}$. Moreover, we can also determine the branching ratio from the shape of the distributions, *i.e.* the information on the coupling.

5.3.4 Goldstini production in pp collisions

We now turn to consider the processes which are relevant to the LHC.

Similar to the process $e^+e^- \to \chi G'$ in section 5.3.2, the cross section of $pp \to \chi G'$ is proportional to $K^2/m_{3/2}^2$ and could be enhanced by the factor K. However, rather large K values of $\mathcal{O}(10^{4-5})$ are needed to obtain a visible cross section for an eV-order gravitino, leading to a bound for the K values by the $\gamma + \not{E}_T$ events at the Tevatron [183] similar to the LEP bound discussed above. We note that at the parton level the amplitudes are the same as the ones studied in the previous section after replacing the incoming electrons with the quarks.[4]

The clean $\gamma\gamma + \not{E}_T$ signal is given by the neutralino LOSP pair production. However, the cross section is too small ($\sigma^{\rm LO}_{pp\to\chi\chi} \sim 0.3\,(1.2)$ fb at $\sqrt{s} = 7\,(14)$ TeV at SPS8) to be significant over the SM background.[5] It is worth to emphasize

[4]Note that only in this process, and the following one, we would need to specify some squark masses. These can also be easily extracted from SPS8, however as we will argue the most interesting process that we study in more details does not involve intermediate coloured superpartners.

[5]It is well known that the NLO QCD corrections enhance the LO cross section by a factor of 1.3-1.4 for $\sqrt{s} = 14$ TeV [134]. It is also interesting to note that gg collisions can give a certain

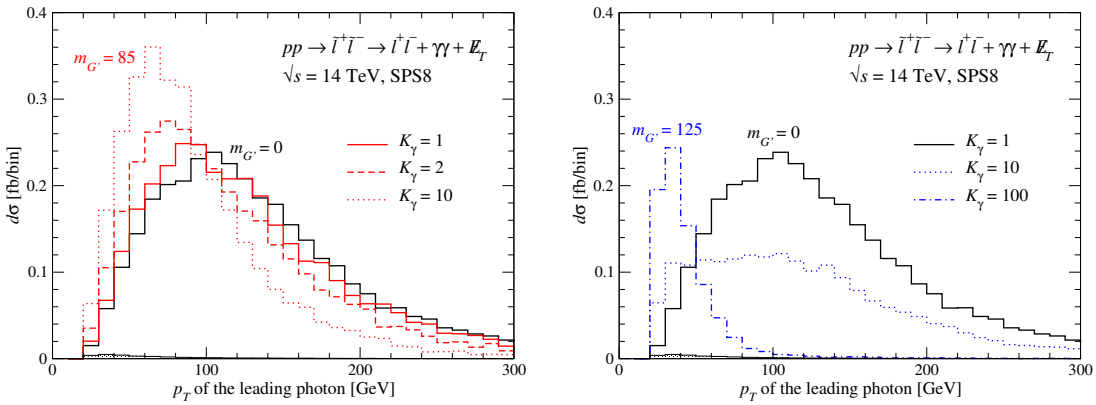

Figure 5.5: The p_T distributions of the leading photon for $pp \to \tilde{l}^+\tilde{l}^- \to l^+l^- + \gamma\gamma + \not{E}_T$ at $\sqrt{s} = 14$ TeV for $m_{G'} = 85$ GeV (left) and 125 GeV (right). The $m_{G'} = 0$ case is also shown as a reference with black lines.

again that the emitted photons associated with a pseudo-goldstino are softer than those with a true goldstino, which makes it difficult to apply some cuts to enhance the signal over the background. In other words, the experimental constraints for the SPS8 point in the standard minimal GMSB model as well as for general gauge mediation [55] (*e.g.* [185–189]) could be eased in the multiple goldstini scenario.

Among the exclusive processes with at most two extra particles in the final state, the cleanest one is the one where the two photons and missing energy are accompanied by two leptons. By far the main contribution to the signal comes from the pair production of sleptons, which subsequently decay into a lepton and the neutralino LOSP, $pp \to \tilde{l}^+_{R/L}\tilde{l}^-_{R/L} \to l^+l^- + \gamma\gamma + \not{E}_T$ ($l = e, \mu$). The electron and muon pairs give the same contributions due to the degeneracies between the first two slepton families. The Standard Model background is completely negligible compared to the signal of new physics.

The signal cross section is 1.1 (3.3) fb at $\sqrt{s} = 7$ (14) TeV at SPS8, where the slepton masses are $m_{\tilde{l}_{R/L}} = 180.2/358.2$ GeV and we employ the CTEQ6L1 PDFs [100] with the factorization scale chosen as $\mu = (m_{\tilde{l}_R} + m_{\tilde{l}_L})/2$.[6] Here, the leptons and photons are required to have $p_T > 20$ GeV, $|\eta| < 2.5$, and $R_{ll,\gamma\gamma} > 0.4$, where p_T and η are the transverse momentum and the pseudorapidity of a final-state particle, respectively, and R_{ij} describes the separation of the two particles in the plane of the pseudorapidity and the azimuthal angle.

Because of the peculiarities of hadronic collisions, raising the centre-of-mass

contribution to the neutralino pair production through one loop [184]. The corresponding amplitudes are suppressed by the loop factor, while they are enhanced because of the larger gluon PDF, and also because all (s)quarks can run in the loop.

[6]The NLO cross section is about 1.35 times larger than the LO one at $\sqrt{s} = 14$ TeV [134,190]. The gluon fusion contribution to the slepton pair productions has been also studied in [191,192].

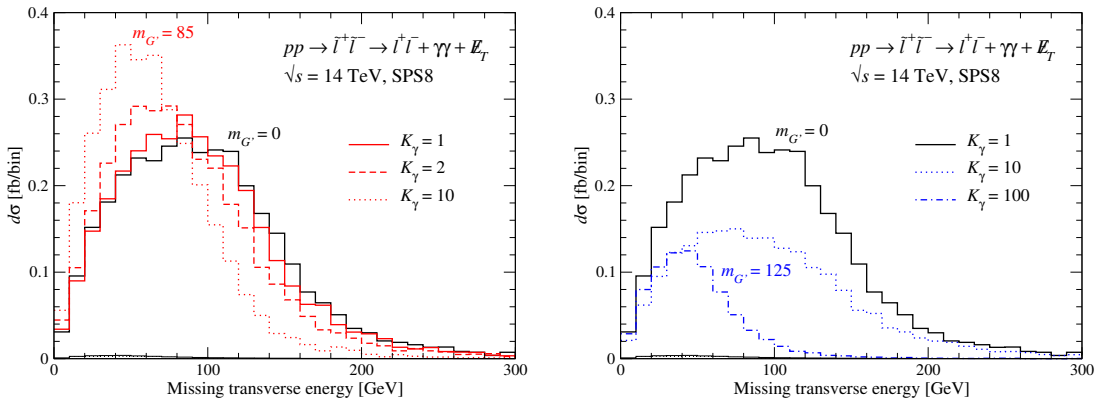

Figure 5.6: The same as figure 5.5, but the missing transverse energy distribution.

energy from 7 TeV to 14 TeV increases the total cross section but does not alter significantly the shape of the distributions. Therefore, we present the results only for the 14 TeV LHC here. In Figs. 5.5 and 5.6, the distributions of the p_T of the leading photon and of the transverse missing energy are shown, respectively, where the same benchmark points are taken as in Sec. 5.3.3. The SM background is invisibly small. The two plotted variables show different shapes with respect to the standard goldstino scenario ($m_{G'} = 0$) depending on the mass and the coupling of the pseudo-goldstino. This fact could in principle be used to extract the masses and the couplings by using techniques explained in [193–196]. We note that in the case of $m_{G'} = 125$ GeV the signal cross section is largely reduced by the experimental cuts, especially for large K_γ. This is due to the fact that, for more massive pseudo-goldstino, the emitted photons will be softer, and hence more excluded by the kinematical cuts.

Before closing the section, we note that the production cross sections of the coloured SUSY particles at SPS8 are small due to their large masses in the TeV range. In general, although we have presented the exclusive signals without jets here, the inclusive search is also interesting, we leave this for future work.

5.4 The case of the stau LOSP

We now move on to the case where the $\tilde{\tau}$ is the LOSP, and use the Lagrangian (5.22) to study it. The effect of the coefficients K_{τ_L} and K_{τ_R} is that of enhancing the G' production.

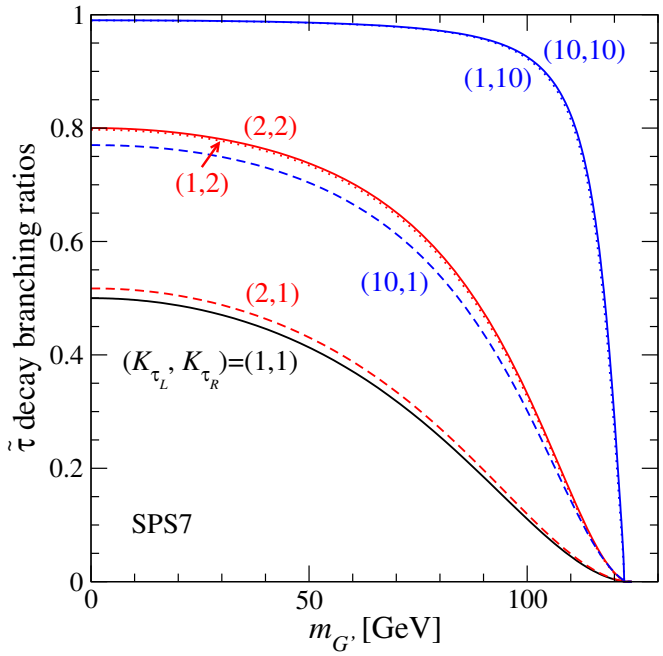

Figure 5.7: Branching rations of $\tilde{\tau} \to \tau G'$ at the SPS7 benchmark point, for various values of K_{τ_L} and K_{τ_R}.

5.4.1 Decays of the stau

The decay amplitude squared for the process $\tilde{\tau} \to \tau G'$ can be easily computed in terms of the coefficients in the Lagrangian yielding

$$|\mathcal{M}|^2 = \left(\frac{m_{\tilde{\tau}}^2 - m_\tau^2}{F}\right)^2 \big((K_{\tau_L}^2 \cos^2\theta_{\tilde{\tau}} + K_{\tau_R}^2 \sin^2\theta_{\tilde{\tau}})(m_{\tilde{\tau}}^2 - m_{G'}^2 - m_\tau^2) + 4K_{\tau_L} K_{\tau_R} \sin\theta_{\tilde{\tau}} \cos\theta_{\tilde{\tau}}\, m_{G'} m_\tau\big). \tag{5.32}$$

The width can be written as

$$\Gamma(\tilde{\tau} \to \tau G') = \frac{\beta}{16\pi m_{\tilde{\tau}}} |\mathcal{M}|^2 \tag{5.33}$$

with $\beta \equiv \beta(\frac{m_\tau^2}{m_{\tilde{\tau}}^2}, \frac{m_{G'}^2}{m_{\tilde{\tau}}^2})$ as in (5.26). Notice that the width depends not only on the magnitude but also on the ratio of the coefficients K_{τ_L} and K_{τ_R}. The well known expression for the true goldstino case is obtained from the above by simply setting $K_{\tau_L} = K_{\tau_R} = 1$ and $m_{G'} = 0$.

For illustration we plot the branching ratios of the decay $\tilde{\tau} \to \tau G'$, choosing the stau mass and mixing angle given by the SPS7 benchmark point, namely $m_{\tilde{\tau}} = 124.0$ GeV and $\cos\theta_{\tilde{\tau}} = 0.154$. The smallness of $\cos\theta_{\tilde{\tau}}$ at the SPS7 point makes the branching ratio largely independent from K_{τ_L} but this would of course change for a different mixing angle.

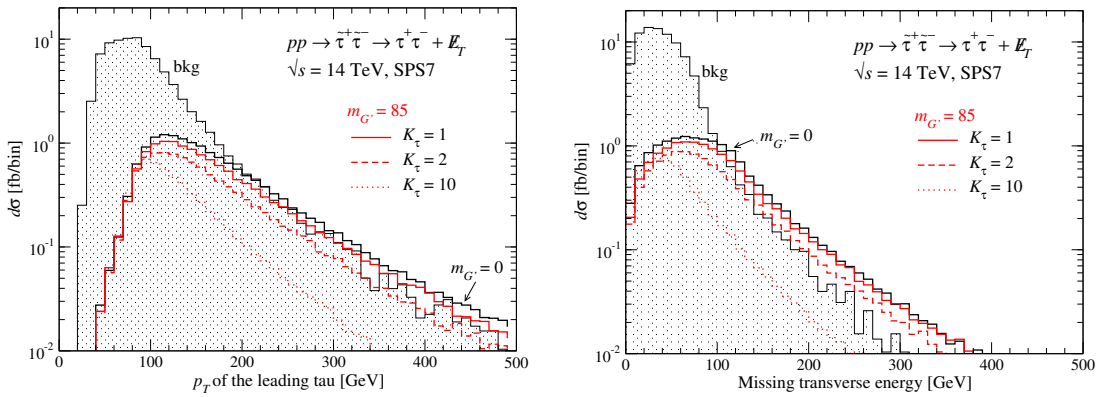

Figure 5.8: The distributions of p_T of the leading tau (left) and of the missing transverse energy (right) for $pp \to \tilde{\tau}^+\tilde{\tau}^- \to \tau^+\tau^- + \not{E}_T$ at $\sqrt{s} = 14$ TeV for $m_{G'} = 85$ GeV. The $m_{G'} = 0$ case (black) is also shown as the reference point as well as the SM background.

The total width of the stau LOSP at SPS7, where $m_G (= m_{3/2}) = 0.76$ eV, is of the order of 10^{-10} GeV for $K_{\tau_L} = K_{\tau_R} = 1$, and hence the stau will decay promptly into the detector. Scenarios with long lived staus could also be envisioned, with even the possibility of stopping them and then measuring their decays. In that case the branching ratio and the mass of the invisible particle(s) should be more directly accessible. We will not delve further on this scenario.

5.4.2 Goldstini and di-tau production

We now turn to stau production at colliders and subsequent decay into taus and (pseudo)-goldstini. Though we could first consider stau pair production at e^+e^- colliders, we will omit this rather straightforward exercise. In the neutralino LOSP scenario, the benefit of this set-up was the ability to infer the neutralino and pseudo-goldstino masses from the energy distribution of the emitted photons. In the present case the same considerations are practically harder to achieve because of the difficulties inherent in tau reconstruction. We thus proceed to consider directly the case of hadron colliders.

The process we are interested in is $pp \to \tilde{\tau}^+\tilde{\tau}^- \to \tau^+\tau^- + \not{E}_T$. The lighter stau-pair production cross section at SPS7 is 41 fb at $\sqrt{s} = 14$ TeV,[7] while the irreducible SM background $\tau^+\tau^-\nu\bar{\nu}$, mainly coming from Z and W pair productions, is ten times larger with the minimal cuts $p_{T_\tau} > 20$ GeV, $|\eta_\tau| < 2.5$, and $R_{\tau\tau} > 0.4$. Since the background is located in the low tau-tau invariant mass region, we impose the additional cut $M_{\tau\tau} > 150$ GeV in the analyses below. Figure 5.8 shows the distributions of the p_T of the leading tau and of the missing transverse energy for the following benchmark points covering different branching

[7] See footnote 6, and also [197] for more details on the stau-pair production.

	$m_{G'}=0$	$m_{G'}=85$			background
		$K_\tau=1$	$K_\tau=2$	$K_\tau=10$	
σ [fb]	15.5	13.2	10.1	5.9	86.4
s/b	0.18	0.15	0.12	0.07	
S (100 (30) fb^{-1})	5.1 (2.8)	4.4 (2.4)	3.4 (1.8)	2.0 (1.1)	

Table 5.1: Cross sections for the signals and the background. The significance S in (5.34) is calculated with an integrated luminosity of 100 (30) fb^{-1} and a di-tau detection efficiency $A = 0.1$.

ratios for stau decays into G or G':

1a. $m_{G'} = 85$ GeV with $K_{\tau_L} = K_{\tau_R} = 1$ $[B(\tilde{\tau} \to \tau G') \sim 0.2]$
1b. $m_{G'} = 85$ GeV with $K_{\tau_L} = K_{\tau_R} = 2$ $[B(\tilde{\tau} \to \tau G') \sim 0.5]$
1c. $m_{G'} = 85$ GeV with $K_{\tau_L} = K_{\tau_R} = 10$ $[B(\tilde{\tau} \to \tau G') \sim 1]$

The reference point $m_{G'} = 0$, *i.e.* the standard goldstino scenario, is also shown by a black solid line. As in the neutralino LOSP scenario, a sizable branching ratio of stau decays to pseudo-goldstini has an impact on the shape of the distribution, once again making the spectrum softer. Another noticeable fact is that the new physics signal becomes dominant especially for high missing transverse energy only when the stau decays to true goldstinos are significant. Therefore, the pseudo-goldstini scenario makes it harder to achieve enough significance for its observation.

In order to quantify the sensitivity of the missing transverse energy cut, in tables 5.1 and 5.2 we list the cross sections, signal (s) over background (b) and significances (S) for our benchmarks, without and with a cut on $\not{E}_T$ at 100 GeV respectively. Taking into account the branching ratio of the hadronic tau decays, $B(\tau_{had}) = 0.648$ [198], and the efficiency of the hadronic tau identification, $\epsilon = 0.5$ [199,200], we assume the di-tau detection efficiency $A = (B(\tau_{had}) \times \epsilon)^2 \sim 0.1$. We use the signal significance defined as [201]

$$S = \sqrt{2((s+b)\ln(1+s/b) - s)}. \tag{5.34}$$

We observe that for 100 fb^{-1} of integrated luminosity, a satisfactory significance can be achieved for most of our benchmarks, especially for $\not{E}_T > 100$ GeV. However, in the $K_\tau = 10$ case, *i.e.* in the case of the heavy pseudo-goldstino with the enhanced coupling, the cut on $\not{E}_T$ does not improve the significance of the signal.

Finally we note that, although we took $K_{\tau_L} = K_{\tau_R}$ for simplicity, tau polarization may be exploited to determine the case that the two coefficients are different, $K_{\tau_L} \neq K_{\tau_R}$ [202].

	$m_{G'} = 0$	$m_{G'} = 85$			background
		$K_\tau = 1$	$K_\tau = 2$	$K_\tau = 10$	
σ [fb]	5.6	4.8	3.4	0.9	3.5
s/b	1.59	1.36	0.95	0.25	
S (100 (30) fb^{-1})	7.9 (4.3)	6.9 (3.8)	5.0 (2.7)	1.4 (0.8)	

Table 5.2: The same as Table 5.1, but with the additional $\not{E}_T > 100$ GeV cut.

5.5 Summary

Motivated by the persisting absence of any sign of low-scale supersymmetry at colliders, we abandon the most straightforward SUSY scenarios. In this chapter, we extended usual gauge-mediation to include a second hidden SUSY-breaking sector and analyzed how this modifies the expected collider signatures.

We first considered the case of a gaugino-like neutralino LOSP and showed that the decay modes of the LOSP into a photon or Z boson and a pseudo-goldstino can be significant. We studied in detail the goldstini phenomenology in the photon(s) plus missing energy signals in e^+e^- and pp collisions. Our aim was to provide clues to interpret prompt photon plus missing energy signals at the LHC. We found that the resulting photon spectrum is typically softer and differs in shape compared to the standard gauge-mediation scenario with only one hidden sector.

We then proceeded to consider the case of a stau LOSP. Similarly to the previous case, the stau can significantly decay into a tau and a pseudo-goldstino. We studied a possible tau pair plus missing energy signal at the LHC, again finding that the pseudo-goldstino scenario leads to an altered shape in the tau energy distributions. The signature however seems more promising in the neutralino LOSP scenario, not only because photons have cleaner experimental features than taus, but also because the SM background is virtually absent in the process that we studied.

We performed our analyses at two particular benchmark points (SPS8 for χ LOSP and SPS7 for $\tilde{\tau}$ LOSP) to make a comparison with the standard gauge mediation model and we emphasize that the precise experimental signatures do depend on the parameters related to the second SUSY-breaking sector, namely the pseudo-goldstino mass and its couplings. However, we also observed rather model-independent features. In particular, due to the mass of the pseudo-goldstino, the SM decay products of a decaying LOSP will generically have a lower energy compared to the usual gauge-mediation scenarios. In this way such a scenario evades most experimental bounds that tend to exclude gauge-mediated scenarios.

In our work, we restricted ourselves to the case in which the LOSP is a gaugino-like neutralino or a stau. There are however many more possibilities such as a higgsino-like neutralino (as studied in [203, 204]) or coloured LOSP

which could lead to interesting collider signatures. Our goldstini model can be easily extended to other benchmark points and LOSP scenarios due to the implementation into an event generator, MadGraph 5.

Chapter 6

Non-minimally flavour-violating supersymmetry

Another interesting unconventional road to study supersymmetry, can be found when questioning the minimal-flavour violating (MFV) paradigm which we introduced in the context of the pMSSM (*cfr.* section 2.2.4). In this chapter we will abandon MFV and allow for more general flavour mixing in the squark sector. This opens up a large parameter space. If we want to study the phenomenology of a theory with many free parameters, the first step is scouting the parameter space. What is still possible given the current experimental constraints? What are typical values for the parameters? The project presented in this chapter, based on the work presented in [205, 206], gives a good example of how this can be done. gives a good example of how this can be done. We will see that non-minimally flavour violating (NMFV) supersymmetry is still allowed by the constraints from flavour observables as well as the constraint on the Higgs mass. We will also show that within NMFV, unlike the usual MFV scenarios, the lightest squarks are often not the top or bottom squark.

After further introducing the project in section 6.1, we motivate and specify the choice of our parameter space in section 6.2. In section 6.3 we describe the Markov Chain Monte Carlo technique that we use to probe the parameter space. We present the results in section 6.4 and four benchmark scenarios are proposed in section 6.5. We summarize our findings in section 6.6.

6.1 Introduction

We introduced supersymmetry in chapter 2 as a well motivated extension of the Standard Model of particle physics. Many search channels have been investigated at colliders and in particular [60, 150] at the Large Hadron Collider, the LHC. Since no signal of supersymmetry has been found so far, the results have been interpreted either in terms of limits on specific set-ups like constrained

versions of the Minimal Supersymmetric Standard Model (MSSM) or in terms of simplified model spectra inspired by the MSSM. As a result, either supersymmetric particles are constrained to reside at scales that are not reachable in proton-proton collisions at a centre-of-mass energy of 8 TeV, or the spectrum must present specific properties that allow the superpartners to evade detection as in the case of compressed supersymmetric spectra or non-minimal realizations of supersymmetry. In the project presented in this chapter, we follow this latter guiding principle and explore to which extent deviations from the minimal flavour-violation paradigm are allowed by current data.

We introduced minimally flavour-violating (MFV) supersymmetry in the context of the pMSSM in section 2.2.4 as a way to avoid undesirable flavour-violating effects. In MFV, all the flavour properties of the model stem from the diagonalization of the Yukawa (and hence the mass) matrices yielding different mass and gauge eigenbases for the (s)quarks and (s)leptons. The misalignment of the two bases and corresponding flavour-violating effects are therefore completely determined by the CKM and PMNS matrices.

MFV does avoid the strong constraints coming from low-energy flavour observables, but accomplishes this in a rather rough way and a more subtle treatment of FV is in place. Moreover, there is no theoretical motivation for the flavour structure of a supersymmetric model to be the same as in the Standard Model. New sources of flavour violation could be allowed when, for instance, supersymmetry is embedded in a Grand Unified framework [207]. The soft supersymmetry-breaking mass and trilinear coupling matrices of the sfermions could therefore comprise non-diagonal flavour-violating entries that are not related to the CKM and PMNS matrices. This set-up is referred to as non-minimally flavour-violating (NMFV) supersymmetry.

We consider the most general mixings between second and third generation squarks. Any non-CKM induced mixing with the first generation is ignored as a result of constraints imposed by kaon data [208]. Choosing a phenomenological approach, we model the flavour-violating effects under investigation by a set of 19 free parameters defined at the TeV scale and identify the regions of the parameter space that are favoured in light of current data by means of the Markov Chain Monte Carlo parameter scanning technique.

6.2 Motivation, theoretical set-up and parameter space

In this section we will introduce the parametrization of NMFV in supersymmetry we adopted and discuss the state of the art of the experimental and phenomenological studies to motivate our choices for the parameter space.

6.2.1 Parametrizing NMFV in the squark sector

When we discussed the mass spectrum of the supersymmetric particles in the MSSM in section 2.2.3, we obtained the mass matrix for the up- and down-type squarks in the super-CKM bases $(\tilde{u}_L, \tilde{c}_L, \tilde{t}_L, \tilde{u}_R, \tilde{c}_R, \tilde{t}_R)$ and $(\tilde{d}_L, \tilde{s}_L, \tilde{b}_L, \tilde{d}_R, \tilde{s}_R, \tilde{b}_R)$ as

$$\mathcal{M}^2_{\tilde{u}} = \begin{pmatrix} V_{\text{CKM}} \widehat{M}^2_{\tilde{Q}} V^\dagger_{\text{CKM}} + m_u^2 + D_{\tilde{u},L} & \frac{v_u}{\sqrt{2}} \widehat{T}^\dagger_u - m_u \frac{\mu}{\tan\beta} \\ \frac{v_u}{\sqrt{2}} \widehat{T}_u - m_u \frac{\mu^*}{\tan\beta} & \widehat{M}^2_{\tilde{U}} + m_u^2 + D_{\tilde{u},R} \end{pmatrix} \tag{6.1}$$

and

$$\mathcal{M}^2_{\tilde{d}} = \begin{pmatrix} \widehat{M}^2_{\tilde{Q}} + m_d^2 + D_{\tilde{d},L} & \frac{v_d}{\sqrt{2}} \widehat{T}^\dagger_d - m_d \mu \tan\beta \\ \frac{v_d}{\sqrt{2}} \widehat{T}_d - m_d \mu^* \tan\beta & \widehat{M}^2_{\tilde{D}} + m_d^2 + D_{\tilde{d},R} \end{pmatrix} \tag{6.2}$$

For the precise definition of the symbols we refer to the discussion around equations (2.58) and (2.59). In the MSSM, each of the four elements in the squark mass matrices correspond to a diagonal 3×3 matrix and is therefore flavour diagonal.

If we want to abandon minimally flavour-violating supersymmetry in the squark sector, we can do so by introducing non-diagonal terms in the soft mass matrices $\widehat{M}^2_{\tilde{Q},\tilde{U},\tilde{D}}$ and/or the trilinear coupling matrices $\widehat{T}_{u,d}$. Following the standard prescriptions [209], we normalize the off-diagonal terms with respect to the diagonal soft masses as

$$\begin{aligned} (\delta_{LL})_{ij} &= \frac{(\widehat{M}^2_{\tilde{Q}})_{ij}}{(\widehat{M}_{\tilde{Q}})_{ii}(\widehat{M}_{\tilde{Q}})_{jj}} \,, \quad (\delta^u_{RR})_{ij} = \frac{(\widehat{M}^2_{\tilde{U}})_{ij}}{(\widehat{M}_{\tilde{U}})_{ii}(\widehat{M}_{\tilde{U}})_{jj}} \,, \quad \left(\delta^d_{RR}\right)_{ij} = \frac{(\widehat{M}^2_{\tilde{D}})_{ij}}{(\widehat{M}_{\tilde{D}})_{ii}(\widehat{M}_{\tilde{D}})_{jj}} \,, \\ (\delta^u_{RL})_{ij} &= \frac{v_u}{\sqrt{2}} \frac{(\widehat{T}_u)_{ij}}{(\widehat{M}_{\tilde{U}})_{ii}(\widehat{M}_{\tilde{Q}})_{jj}} \,, \qquad (\delta^u_{LR})_{ij} = \frac{v_u}{\sqrt{2}} \frac{(\widehat{T}^\dagger_u)_{ij}}{(\widehat{M}_{\tilde{Q}})_{ii}(\widehat{M}_{\tilde{U}})_{jj}} \,, \\ \left(\delta^d_{RL}\right)_{ij} &= \frac{v_d}{\sqrt{2}} \frac{(\widehat{T}_d)_{ij}}{(\widehat{M}_{\tilde{D}})_{ii}(\widehat{M}_{\tilde{Q}})_{jj}} \,, \qquad \left(\delta^d_{LR}\right)_{ij} = \frac{v_d}{\sqrt{2}} \frac{(\widehat{T}^\dagger_d)_{ij}}{(\widehat{M}_{\tilde{Q}})_{ii}(\widehat{M}_{\tilde{D}})_{jj}} \,. \end{aligned} \tag{6.3}$$

where $i, j = 1 \ldots 3$ and $i < j$. The lower half of the soft mass matrices is then completely determined by requiring hermiticity so that NMFV is parametrized by 21 dimensionless, possibly complex, δ's that can be constrained by experimental data. Note that the trilinear coupling matrices do not have to be hermitian so that $(\delta^u_{RL})_{ij}$ and $(\delta^u_{LR})_{ij}$ can be different.

6.2.2 Constraints from flavour physics

Meson oscillations and rare meson decays are very sensitive to new physics and strongly constrain any flavour violating interactions. Mesons are particles made of two quarks. Kaons, for example, consist of a strange quark and a quark of

the first generation (u or d). We will discuss the kaon system and corresponding observables a bit more in detail.

The neutral kaons K^0 and $\bar{K}^0$ have respective quark content $d\bar{s}$ and $\bar{d}s$ and under CP, charge conjugation combined with parity, they transform as CP $|K^0\rangle = -\left|\bar{K}^0\right\rangle$ and CP $\left|\bar{K}^0\right\rangle = -|K^0\rangle$. The neutral kaons are hence clearly no CP-eigenstates. It is however straightforward to construct CP-odd and CP-even eigenstates as $K_O = \frac{1}{\sqrt{2}}\left(|K^0\rangle - \left|\bar{K}^0\right\rangle\right)$ and $K_E = \frac{1}{\sqrt{2}}\left(|K^0\rangle + \left|\bar{K}^0\right\rangle\right)$ and we can write the physical states $K_{L/S}$ as

$$|K_L\rangle = \frac{1}{\sqrt{1+|\epsilon_K|^2}}\left(|K_O\rangle + \epsilon_K |K_E\rangle\right) \tag{6.4}$$

$$|K_S\rangle = \frac{1}{\sqrt{1+|\epsilon_K|^2}}\left(\epsilon_K |K_O\rangle + |K_E\rangle\right). \tag{6.5}$$

If CP were an exact symmetry of Nature, ϵ_K would vanish. However, it has been shown experimentally that ϵ_K is small but different from zero and is given by [210]

$$\epsilon_K = (2.228 \pm 0.29^{\text{th}} \times 10^{-3}). \tag{6.6}$$

The physical eigenstates are therefore no CP-eigenstates and the level of CP-violation is quantified by ϵ_K.

When K_L and K_S evolve in time, they can oscillate into one another and the period of their oscillation is related to their mass splitting $\Delta M_K = m_{K_L} - m_{K_S}$ which has been measured to be [210]

$$\Delta M_K = (3.484 \pm 0.006) \times 10^{-12}\ \text{MeV}. \tag{6.7}$$

In non-minimally flavour violating supersymmetry, non-zero $(\delta_{LL})_{12}$, $(\delta^d_{RR})_{12}$ or $(\delta^d_{LR})_{12}$ would imply processes like the ones shown in figure 6.1. These diagrams contribute to the calculation of ΔM_K and ϵ_K and are strongly constrained by experiment.

In a similar way, the electrically neutral $D^0 = \bar{c}u$, $B^0_d = d\bar{b}$ and $B^0_s = s\bar{b}$ mesons mix with their antiparticles and experimental constraints on $D\bar{D}$-mixing put limits on $(\delta_{LL})_{12}$, $(\delta^u_{RR})_{12}$ and $(\delta^u_{LR})_{12}$, $B_d\bar{B}_d$-oscillations constrain the 13-mixing and the $B_s\bar{B}_s$ system limits the 23-mixing. Depending on the experimental and theoretical precision, the constraints will be more or less strong and the NMFV parameters mixing the first and second/third generation appear to be the most strongly constrained [208, 209, 211]. In our study, we therefore restrict ourselves to the 23-mixing.

6.2.3 State of the art

In recent years, the consequences of non-minimal flavour violation in the squark sector have been investigated in various areas, we provide here an, unavoidably

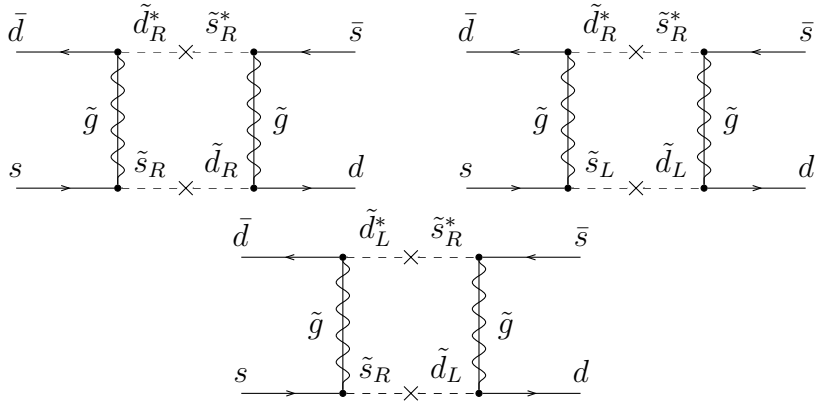

Figure 6.1: A sample from the supersymmetric contributions to $K\bar{K}$-mixing, related to $(\delta_{LL})_{12}$, $(\delta^d_{RR})_{12}$ and $(\delta^d_{LR})_{12} \neq 0$.

incomplete, overview. NMFV effects on low-energy observables such as rare decays (see *e.g.* reference [212] and references therein) or electroweak precision parameters [213] have been considered, and the potential signatures at the LHC have been investigated. Recently also the contributions to the mass of the lightest SUSY Higgs-boson have been obtained [214].

Due to the complexity of the problem, the studies presented in [215–220] and more recently [221], chose to focus on a couple of MFV reference scenarios and investigate what happens if they turn on one or at most two NMFV parameters at the time. They scan over the one- or two-dimensional parameter space and study the impact on the branching ratios for flavour-violating decays while imposing constraints from low-energy flavour observables, electroweak precision, cosmology and/or direct collider searches. These studies give an idea of the allowed magnitude of the NMFV couplings, they all conclude that NMFV is not excluded and can be relevant for colliders.

Instead of investigating the impact of NMFV only in a limited set of reference points, one can also take a UV-complete SUSY model, add flavour-violating parameters at the low scale and check which parts of the NMFV SUSY parameter space are still allowed by experiment. This has for example been done for the CMSSM, minimal gauge mediation and models with minimal anomaly-mediated SUSY breaking in [43, 222–224]. They considered left-left and right-right mixing between the second and third generation squarks and found that, compared to MFV, the constraints in the NMFV case are stronger, especially for large left-left mixing. There are however still large regions of the parameter space that are left unconstrained.

Whereas the work in the two previous paragraphs introduced their NMFV parameters at the electroweak scale without questioning whether they can be realized in a UV-complete theory, the studies in [225] and [226] showed that NMFV can be realized in the Minimal R-symmetric Supersymmetric Model as

well as in gauge mediation.

Apart from describing the constraints on the NMFV parameters, the previously mentioned works also showed that NMFV might lead to interesting collider signatures and has to be taken into account when interpreting the limits on the masses of the supersymmetric particles set by the experiments. This can have important consequences for naturalness. As was explained in chapter 2, the persisting absence of any sign of SUSY at colliders, puts naturalness, one of the main motivations for SUSY, under pressure. Allowing for NMFV in the squark sector and in particular introducing mixing between the right-handed charm and top squark can slightly reduce the experimental bound on the stop and gluino mass. This improves the current situation of naturalness and can meanwhile lead to interesting signatures at colliders [117, 227].

All the aforementioned results studying the viability of NMFV, have been derived under the restriction that only few off-diagonal elements of the squark mass matrices are non-zero, and that at most two of them are varied at the same time. One would however generally expect that several of the flavour-violating entries could be non-vanishing, especially if the flavour structure is generated by some mechanism at a higher scale. A comprehensive study of the most general NMFV configuration in the MSSM, where all flavour-violating Lagrangian terms are taken into account and confronted to current data and theoretical constraints, is in order. A first step in this direction is achieved with the work presented in this chapter.

6.2.4 Choice of the parameters

We start from the 22-dimensional parametrization of the pMSSM discussed in section 2.2.4. We extend the squark flavour sector and simplify the slepton and gaugino sector. As for the pMSSM, the diagonal soft masses of the first and second generation are degenerate while the third generation is kept separate,

$$\left(\widehat{M}_{\tilde{Q}}\right)_{11} = \left(\widehat{M}_{\tilde{Q}}\right)_{22} \equiv M_{\tilde{Q}_{1,2}} \qquad \left(\widehat{M}_{\tilde{Q}}\right)_{33} \equiv M_{\tilde{Q}_3} \tag{6.8}$$

$$\left(\widehat{M}_{\tilde{U}}\right)_{11} = \left(\widehat{M}_{\tilde{U}}\right)_{22} \equiv M_{\tilde{U}_{1,2}} \qquad \left(\widehat{M}_{\tilde{U}}\right)_{33} \equiv M_{\tilde{U}_3} \tag{6.9}$$

$$\left(\widehat{M}_{\tilde{D}}\right)_{11} = \left(\widehat{M}_{\tilde{D}}\right)_{22} \equiv M_{\tilde{D}_{1,2}} \qquad \left(\widehat{M}_{\tilde{D}}\right)_{33} \equiv M_{\tilde{D}_3}. \tag{6.10}$$

Unlike the pMSSM however, in NMFV the soft masses in the squark sector can be off-diagonal as well and we extend the squark flavour sector with the 21 dimensionless NMFV couplings introduced in 6.2.1. However, as detailed in section 6.2.2, any mixing involving one of the first generation squarks is strongly constrained by low-energy flavour observables and we restrict ourselves to mixing between the second and third generation squarks leaving us with the seven

dimensionless quantities

$$\delta_{LL} = \frac{(\widehat{M}^2_{\tilde{Q}})_{23}}{(\widehat{M}_{\tilde{Q}})_{22}(\widehat{M}_{\tilde{Q}})_{33}} \ , \quad \delta^u_{RR} = \frac{(\widehat{M}^2_{\tilde{U}})_{23}}{(\widehat{M}_{\tilde{U}})_{22}(\widehat{M}_{\tilde{U}})_{33}} \ , \quad \delta^d_{RR} = \frac{(\widehat{M}^2_{\tilde{D}})_{23}}{(\widehat{M}_{\tilde{D}})_{22}(\widehat{M}_{\tilde{D}})_{33}} \ ,$$
$$\delta^u_{RL} = \frac{v_u}{\sqrt{2}} \frac{(\widehat{T}_u)_{23}}{(\widehat{M}_{\tilde{U}})_{22}(\widehat{M}_{\tilde{Q}})_{33}} \ , \qquad \delta^u_{LR} = \frac{v_u}{\sqrt{2}} \frac{(\widehat{T}^\dagger_u)_{23}}{(\widehat{M}_{\tilde{Q}})_{22}(\widehat{M}_{\tilde{U}})_{33}} \ ,$$
$$\delta^d_{RL} = \frac{v_d}{\sqrt{2}} \frac{(\widehat{T}_d)_{23}}{(\widehat{M}_{\tilde{D}})_{22}(\widehat{M}_{\tilde{Q}})_{33}} \ , \qquad \delta^d_{LR} = \frac{v_d}{\sqrt{2}} \frac{(\widehat{T}^\dagger_d)_{23}}{(\widehat{M}_{\tilde{Q}})_{22}(\widehat{M}_{\tilde{D}})_{33}} \ . \tag{6.11}$$

The slepton sector is defined in a flavour-conserving fashion, implying diagonal soft mass matrices. Since we are mainly interested in the squark sector, we do not expect details in the slepton sector to have much influence and we simplify the soft masses as

$$\left(\widehat{M}_{\tilde{L}}\right)_{11} = \left(\widehat{M}_{\tilde{L}}\right)_{22} = \left(\widehat{M}_{\tilde{L}}\right)_{33} = \left(\widehat{M}_{\tilde{E}}\right)_{11} = \left(\widehat{M}_{\tilde{E}}\right)_{22} = \left(\widehat{M}_{\tilde{E}}\right)_{33} = M_{\tilde{l}}. \tag{6.12}$$

In addition, the gaugino sector is chosen to be determined by a single parameter, the bino mass M_1. The wino and gluino tree-level masses M_2 and M_3 are then obtained by making use of a relation inspired by Grand-Unified theories,

$$M_1 = \frac{1}{2} M_2 = \frac{1}{6} M_3 \ . \tag{6.13}$$

The trilinear couplings of the squarks as well as the sleptons are defined proportional to the Yukawa couplings as

$$\widehat{T}_u \equiv A_u \, \widehat{y}_u \qquad \widehat{T}_d \equiv A_d \, \widehat{y}_d \qquad \widehat{T}_e \equiv A_e \, \widehat{y}_e. \tag{6.14}$$

We neglect the first and second generation Yukawa couplings so that only the trilinear coupling parameters related to the third generation squarks and sleptons are considered as free parameter. We then simplify the parameter space as

$$A_t = A_b = A_\tau \equiv A_f \tag{6.15}$$

so that the trilinear couplings are determined by one single parameter. All flavour-conserving trilinear sfermion interactions with the Higgs bosons are consequently driven by a single input parameter A_f. Finally, the Higgs sector is parametrized in terms of the μ parameter, $\tan\beta$ and the pole mass of the pseudoscalar Higgs boson m_A.

This leaves us with 19 parameters which fully determine our NMFV model and hence the squared mass matrices of the squarks $\mathcal{M}^2_{\tilde{u}}$ and $\mathcal{M}^2_{\tilde{d}}$ defined in equations (2.58) and (2.58). These are the mass matrices written in the super-CKM bases $(\tilde{u}_L, \tilde{c}_L, \tilde{t}_L, \tilde{u}_R, \tilde{c}_R, \tilde{t}_R)$ and $(\tilde{d}_L, \tilde{s}_L, \tilde{b}_L, \tilde{d}_R, \tilde{s}_R, \tilde{b}_R)$. The fields in these

bases are however not the propagating, physical fields. The physical squark states $\tilde{u}_i$ and $\tilde{d}_i$ (with $i = 1, \ldots, 6$) are obtained by diagonalizing $\mathcal{M}^2_{\tilde{u}}$ and $\mathcal{M}^2_{\tilde{d}}$ according to

$$\text{diag}\big(m^2_{\tilde{q}_1}, m^2_{\tilde{q}_2}, \ldots, m^2_{\tilde{q}_6}\big) \;=\; \mathcal{R}_{\tilde{q}} \mathcal{M}^2_{\tilde{q}} \mathcal{R}^\dagger_{\tilde{q}} \qquad \text{for} \quad q = u, d \; . \tag{6.16}$$

By convention the mass eigenstates are taken ordered such that $m^2_{\tilde{q}_1} < \cdots < m^2_{\tilde{q}_6}$. The 6×6 rotation matrices $\mathcal{R}_{\tilde{u}}$ and $\mathcal{R}_{\tilde{d}}$ carry the information about the flavour decomposition of the squarks,

$$\begin{aligned} \big(\tilde{u}_1 \;\; \tilde{u}_2 \;\; \tilde{u}_3 \;\; \tilde{u}_4 \;\; \tilde{u}_5 \;\; \tilde{u}_6\big)^t &= \mathcal{R}_{\tilde{u}} \big(\tilde{u}_L \;\; \tilde{c}_L \;\; \tilde{t}_L \;\; \tilde{u}_R \;\; \tilde{c}_R \;\; \tilde{t}_R\big)^t \\ \big(\tilde{d}_1 \;\; \tilde{d}_2 \;\; \tilde{d}_3 \;\; \tilde{d}_4 \;\; \tilde{d}_5 \;\; \tilde{d}_6\big)^t &= \mathcal{R}_{\tilde{d}} \big(\tilde{d}_L \;\; \tilde{s}_L \;\; \tilde{b}_L \;\; \tilde{d}_R \;\; \tilde{s}_R \;\; \tilde{b}_R\big)^t \end{aligned} \tag{6.17}$$

and their different entries directly appear in couplings of the squarks to the other particles (see *e.g.* references [218, 222]).

The parameter space we specified up to now, consists of 16 soft supersymmetry-breaking parameters and three parameters related to the Higgs sector. In addition to these 19 SUSY parameters, we also have to specify the parameters of the Standard Model. The QCD interaction strength is computed from the value of the strong coupling constant at the Z-pole $\alpha_s(m_Z)$, while we choose as three independent electroweak inputs the electromagnetic coupling constant evaluated at the Z-pole $\alpha(m_Z)$, the Fermi constant G_F and the Z-boson mass m_Z. The fermion sector is defined by the pole mass of the top quark m_t^{pole}, the $\overline{\text{MS}}$ mass of the bottom (charm) quark m_b (m_c) evaluated at the m_b (m_c) scale and the $\overline{\text{MS}}$ masses of the three lightest quarks evaluated at a scale of 2 GeV. Finally, we include the masses of the electron (m_e), the muon (m_μ) and the tau (m_τ) in our parametrisation and we calculate the CKM matrix using the Wolfenstein parameters λ^{CKM}, A^{CKM}, $\bar{\rho}^{\text{CKM}}$ and $\bar{\eta}^{\text{CKM}}$. In our parameter scan, we will fix all Standard Model parameters except $\alpha_s(m_Z)$, m_t^{pole} and $m_b(m_b)$, which we allow to vary according a Gaussian around their experimentally measured value. The total parameter space we want to probe is hence 22-dimensional.

6.3 Probing the parameter space

If we want to get a representative idea of a n-dimensional parameter space using a grid scan, the number of points we have to scan scales like x^n where x stands for the number of points per parameter, which quickly becomes too time and computing-power consuming for a high-dimensional parameter space. In section 6.2.1 we saw that our NMFV supersymmetric model has 19 free parameters which is too much to be suitable for a gridscan and we will rely on Markov chains instead.

6.3.1 The Markov Chain Monte Carlo scanning technique

The Markov Chain Monte Carlo (MCMC) scanning technique [228–230] probes the parameter space guided by the likelihood of the points. It is based on Bayesian statistics and provides us with a set of points of which the distribution is proportional to the likelihood. Consequently, we get an idea of the parameter regions preferred by experiment and we can select benchmark scenarios from the points with the highest likelihood. This will be explained in more detail in the following.

Bayesian inference

Assume a certain model, or hypothesis H, is the true theory of Nature and we would like to know what the experimental observations, the data D, can tell us about the set of parameters Θ in this theory. In other words, we want to calculate the probability distribution $P(\Theta|D,H)$ of the parameters Θ assuming the model H is correct, after imposing the experimental data D. Bayes' theorem tells us that $P(\Theta|D,H)$, referred to as the *posterior* in the following, is proportional to

$$P(\Theta|D,H) \sim P(D|\Theta,H)P(\Theta,H). \tag{6.18}$$

where $P(D|\Theta,H) \equiv \mathcal{L}(D)$ is the likelihood to observe the data D assuming H and Θ and $P(\Theta,H) \equiv \pi(\Theta)$ is called the *prior*. The prior encodes everything we know about the parameters before imposing D. This includes constraints from earlier experimental observations as well as from theory. The posterior distribution can be obtained using the Metropolis algorithm [230].

The Metropolis algorithm

The Metropolis algorithm draws a sample from a distribution provided we are able to calculate a function proportional to this distribution. The algorithm relies on Markov chains: it walks through the parameter space and every next step depends solely on the current state and the likelihoods of both points. The algorithm goes as follows:

1. Draw a point Θ_1 in the parameter space from the prior distribution. Set $\Theta_1 = \Theta_{\text{old}}$.

2. Choose a new point Θ_{new} in the neighbourhood of Θ_{old}. For each supersymmetric parameter, we draw a point from a Gaussian distribution around Θ_{old} with standard deviation or width $w = 5\%$ of the scanned range. The width is chosen to optimize the convergence of the sample obtained in the scan to the distribution we are probing.[1]

[1] For more details, we refer to appendix B.2.

3. Suppose we want to include m measurements D_i where $i \in 1 \dots m$ and we set $\mathcal{L}_{\rm i}(\Theta) = P(\Theta|D_i, H)$. We then define the likelihood of a point as $\mathcal{L}(\Theta) = \prod_{i=1}^{m} \mathcal{L}_{\rm i}$ and calculate the ratio

$$R = \frac{\mathcal{L}(\Theta_{\rm new})}{\mathcal{L}(\Theta_{\rm old})}. \tag{6.19}$$

4. Accept $\Theta_{\rm new}$ with a probability $\min(R, 1)$. If the point is accepted, set $\Theta_{\rm old} = \Theta_{\rm new}$. Otherwise, just proceed to the next step.

5. Start the procedure again from point 2 until the sample of parameter points is likely to have converged.

We applied the Metropolis algorithm on equation (6.18) to obtain the posterior distributions of our 19 supersymmetric parameters. The posterior distributions for the SUSY parameters can be calculated as soon as we know the likelihood and the prior.

The prior

The prior distribution of the parameters quantifies the initial belief of what the distribution should look like and is clearly not always well defined. Several choices for the prior are possible and the final posterior distribution can depend on this choice. This may seem worrying, but prior dependence in itself is not necessarily a problem. If the results strongly depend on the prior, it rather indicates that the experimental constraints are not strong enough to state anything conclusive about the model and more measurements are needed. If we would be interested in the true posterior distribution of the parameters, we would have to check whether the final results depend on the choice of prior.

In our study, we only considered one kind of prior and consequently, we do not claim that our posterior distributions are the true distributions. It is however still possible to get an idea of the influence of the measurements on the most likely parameter values by looking at the difference between the prior and posterior distributions. This is why we will always show the posteriors together with the prior, it is the difference between the two that matters.

The parameter space we want to probe contains 19 NMFV supersymmetric and 3 Standard Model parameters, the total parameter space is hence 22-dimensional and every parameter has its own prior. The prior of the SM parameters is chosen to be a Gaussian around the experimentally measured value while the supersymmetric parameters are drawn from a prior which is flat over the scanned parameter range. However, all the points entering the scan should yield theoretically viable models, there should not be any tachyons in their spectrum and electroweak symmetry has to be successfully broken. Moreover, if the model is to provide a dark matter candidate, the lightest supersymmetric particle (LSP)

should be the lightest neutralino. We include all these theoretical requirements in the theoretical prior $\pi_{\text{th}}(\Theta)$. The total prior is then given by

$$\pi(\Theta) = \pi_{\text{th}}(\Theta) \times \prod_{i=1}^{22} \pi_i(\theta_i) \tag{6.20}$$

where $\Theta = \{\theta_1 \dots \theta_{22}\}$ and $\pi_i(\theta_i)$ respectively denote a point in the parameter space and the prior corresponding to point i in the parameter space.

Convergence

Parameter scans based on MCMC algorithms are often subject of discussion. Not only because of the prior dependence explained in the previous section, but also because proving that the posterior distributions converged to the true distributions has been a long-standing problem which, unfortunately, remains unsolved. It is not possible to prove that the scan has converged. If the chains get stuck in a local instead of a global maximum, the distributions will definitely be different. In our case, this also means that the points with maximal likelihood which we will use to set-up our benchmark scenarios might not be the true maxima. This has to be kept in mind when looking at the results.

However, even though we will never be able to prove convergence of the scan, we can still do as much as we can to avoid bias of any kind. First of all, it is clear that including the first points of the chains would introduce a bias, the number of points it takes to remove this bias, is called the burn-in length. We solve this problem by removing the first 15% of each chain.

Additionally, we can run convergence tests on the chains. Even though they can not ensure whether the chains converged, they do provide necessary criteria that have to be fulfilled. Several tests have been designed, we ran the convergence test of Gelman and Rubin [231] and we showed that all the chains passed the test. Details on the convergence test of Gelman and Rubin as well as the results of for scan are provided in appendix B.1.

Interpretation of MCMC results

In principle, the posterior distribution of parameter values indicate the real probability distribution of the parameters given constraints from experimental data. However, the distribution can still depend on the choice of the prior and one has to be careful when interpreting the results too strictly. Nevertheless, comparing the posterior and prior distributions does show how the data influences the likelihood distribution of the parameter and can be used to get an idea of what a 'typical NMFV scenario' would be like.

Studying the impact of every observable separately also shows which experimental constraints are the most stringent. Finally, if the chains converged, the

Parameter	Value	Parameter	Value
$\alpha^{-1}(m_Z)$	127.934	m_e	510.9989 keV
m_Z	91.1876 GeV	m_μ	105.6583 MeV
G_F	1.16637×10^{-5} GeV^{-2}	m_τ	1.77699 GeV
$m_c^{\overline{\rm MS}}(m_c)$	1.25 GeV	$\lambda^{\rm CKM}$	0.2272
$m_s^{\overline{\rm MS}}(2\text{ GeV})$	120 MeV	$A^{\rm CKM}$	0.818
$m_u^{\overline{\rm MS}}(2\text{ GeV})$	3 MeV	$\bar{\rho}^{\rm CKM}$	0.221
$m_d^{\overline{\rm MS}}(2\text{ GeV})$	7 MeV	$\bar{\eta}^{\rm CKM}$	0.34

Table 6.1: The fixed part of the Standard Model sector of our NMFV MSSM parameter space.

points with the highest likelihood in the sample also represent the regions in parameter space that are the most likely given the experimental constraints and can be used to define benchmark points to further study NMFV supersymmetry.

6.3.2 Specifying the parameter space

For our exploration of the NMFV MSSM, we start by fixing the Standard Model parameters to the values provided in the review of the Particle Data Group [210], as shown in table 6.1. We then allow $\alpha_s(m_Z)$, $m_t^{\rm pole}$ and $m_b^{\overline{\rm MS}}(m_b)$ to vary according to Gaussian profiles with their measured central values and uncertainties taken as expectation value and square-root of the variance, as shown in Table 6.2. This table also shows the intervals over which the 19 supersymmetric parameters will be allowed to vary in our study.

Before moving on to scanning the parameter space, we need to know how we to confront a single point to experiment. The next section explains which experimental measurements are relevant and how we can calculate their predictions for a given point in the parameter space.

6.3.3 Experimental constraints

The masses and flavour-violating mixings of the superpartners can be indirectly probed by numerous flavour physics constraints, the anomalous magnetic moment of the muon as well as by the properties of the recently discovered Standard-Model-like Higgs boson. In our MCMC scanning procedure, we additionally impose the lightest superpartner to be the lightest neutralino, so that it could be a phenomenologically viable dark matter candidate. We dedicate the rest of this section to a brief description of all observables that have been considered in the scan and that are summarised in table 6.3.

Parameter	Scanned range	Parameter	Scanned range
$\alpha_s(m_Z)$	$\mathcal{N}(0.1184, 0.0007)$	$\tan\beta$	[10, 50]
m_t^{pole}	$\mathcal{N}(173.3, 1.3928)$ GeV	μ	[100, 850] GeV
$m_b(m_b)$	$\mathcal{N}(4.19, 0.12)$ GeV	m_A	[100, 1600] GeV
$M_{\tilde{Q}_{1,2}}$	[300, 3500] GeV	M_1	[100, 1600] GeV
$M_{\tilde{Q}_3}$	[100, 3500] GeV	$M_{\tilde{\ell}}$	[100, 3500] GeV
$M_{\tilde{U}_{1,2}}$	[300, 3500] GeV	δ_{LL}	[-0.8, 0.8]
$M_{\tilde{U}_3}$	[100, 3500] GeV	δ^u_{RR}	[-0.8, 0.8]
$M_{\tilde{D}_{1,2}}$	[300, 3500] GeV	δ^d_{RR}	[-0.8, 0.8]
$M_{\tilde{D}_3}$	[100, 3500] GeV	δ^u_{LR}	[-0.5, 0.5]
A_f	[-10000, 10000] GeV	δ^u_{RL}	[-0.5, 0.5]
	or $\lvert A_f\rvert < 4\max\{M_{\tilde{q}}, M_{\tilde{\ell}}\}$	δ^d_{LR}	[-0.05, 0.05]
		δ^d_{RL}	[-0.05, 0.05]

Table 6.2: Supersymmetric and Higgs sectors of our NMFV MSSM parameter space, as well as varying Standard Model parameters. $\mathcal{N}(\mu, \sigma)$ denotes a Gaussian profile with an expectation value μ and square root of the variance σ.

NMFV squark mixing involving third generation squarks is by construction very sensitive to constraints arising from B-physics observables. In particular, B-meson rare decays and oscillations are expected to play an important role as the Standard Model contributions are loop-suppressed. Although we only consider squark mixing between the second and third generations, we also include constraints arising from observables related to the kaon sector. Even if not present at the scale at which we calculate the supersymmetric spectrum (*i.e.* the electroweak symmetry breaking scale), squark mixings with the first generation are induced by the non-vanishing CKM matrix and renormalisation-group running so that kaon physics observables (calculated at a different scale) are also relevant for extracting constraints on the NMFV MSSM parameter space.

We focus on the branching ratios associated with the rare $B \to X_s\gamma$, $B \to K^*\mu\mu$, $B \to X_s\mu\mu$ and $B_u \to \tau\nu$ decays, as well as on the forward-backward asymmetry (AFB) arising in $B \to K^*\mu\mu$ decays. The associated predictions are calculated with the SuperIso package [237, 238]. In addition, we compute the neutral B-meson mass difference ΔM_{B_s}, the branching ratio associated with the $B_s \to \mu^+\mu^-$, $K^0 \to \pi^0\nu\nu$ and $K^+ \to \pi^+\nu\nu$ decays and the kaon parameter ϵ_K with the SPheno code [50, 239]. We furthermore employ SPheno for the estimation of the supersymmetric contributions to the anomalous magnetic moment

Observable	Experimental result	Likelihood function
$\mathrm{BR}(B \to X_s\gamma)$	$(3.43 \pm 0.22) \times 10^{-4}$ [232]	Gaussian
$\mathrm{BR}(B_s \to \mu\mu)$	$(2.8 \pm 0.7) \times 10^{-9}$ [233]	Gaussian
$\mathrm{BR}(B \to K^*\mu\mu)_{q^2\in[1,6]\ \mathrm{GeV}^2}$	$(1.7 \pm 0.31) \times 10^{-7}$ [234]	Gaussian
$\mathrm{AFB}(B \to K^*\mu\mu)_{q^2\in[1.1,6]\ \mathrm{GeV}^2}$	$(-0.075 \pm 0.036) \times 10^{-7}$ [235]	Gaussian
$\mathrm{BR}(B \to X_s\mu\mu)_{q^2\in[1,6]\ \mathrm{GeV}^2}$	$(0.66 \pm 0.88) \times 10^{-6}$ [236]	Gaussian
$\mathrm{BR}(B \to X_s\mu\mu)_{q^2>14.4\ \mathrm{GeV}^2}$	$(0.60 \pm 0.31) \times 10^{-6}$ [236]	Gaussian
$\mathrm{BR}(B_u \to \tau\nu)/\mathrm{BR}(B_u \to \tau\nu)_{\mathrm{SM}}$	1.04 ± 0.34 [210]	Gaussian
ΔM_{B_s}	$(17.719 \pm 3.300)\ \mathrm{ps}^{-1}$ [210]	Gaussian
ϵ_K	$(2.228 \pm 0.29^{\mathrm{th}}) \times 10^{-3}$ [210]	Gaussian
$\mathrm{BR}(K^0 \to \pi^0\nu\nu)$	$\leq 2.6 \times 10^{-8}$ [210]	1 if yes, 0 if no
$\mathrm{BR}(K^+ \to \pi^+\nu\nu)$	$1.73^{+1.15}_{-1.05} \times 10^{-10}$ [210]	Two-sided Gaussian
Δa_μ	$(26.1 \pm 12.8) \times 10^{-10}$ $[e^+e^-]$ [210]	Gaussian
m_h	125.5 ± 2.5 GeV [22, 23]	1 if yes, 0 if no
Lightest supersymmetric particle	Lightest neutralino	1 if yes, 0 if no

Table 6.3: Constraints imposed in our scan of the NMFV MSSM parameter space. The constraint concerning the nature of the LSP is part of the theoretical prior while the other constraints are taken into account in the posterior distribution.

of the muon a_μ[2] and for a calculation of the lightest Higgs boson mass m_h. The data transfer between SPheno and SuperIso is achieved through the Flavour Les Houches Accord standard [240], and the Wilson coefficients for all hadronic observables are calculated in SPheno (at the scale $Q = 160$ GeV) and SuperIso (at a scale $Q = m_W$) from the values of the running coupling constants and the supersymmetric masses and parameters that have been evaluated with SPheno.

We now briefly collect all references where the formulas that have been employed for the calculation of the considered observables can be found, and we indicate which NMFV MSSM parameters are mainly constrained by each of these observables. The calculation of the $B \to X_s\gamma$ branching ratio is mainly based on the results of [241–243], while those of the $B \to X_s\mu^+\mu^-$ and $B \to K^*\mu^+\mu^-$ branching ratios respectively follow [244–247] and [248–253]. All three decays are sensitive to the left-left and to the left-right squark mixing parameters.

In the case of the $B_s \to \mu^+\mu^-$ branching ratio, the formulas of [254] have been used. For large values of $\tan\beta$, the pseudoscalar Higgs boson contribution gives a sizeable deviation from the Standard Model expectation so that when non-minimal flavour violation in the squark sector is allowed, this observable mainly restricts left-right mixing parameters [255]. Additionally, it is also sensitive to δ_{LL} and δ^d_{RR} when the gluino is not too heavy [256]. For the B-meson oscillation parameter ΔM_{B_s}, we use the formulas of [255,257] with the hadronic parameters $\bar{P}_1^{LR} = -0.71$, $\bar{P}_2^{LR} = -0.9$, $\bar{P}_1^{SLL} = -0.37$ and $\bar{P}_1^{SLL} = -0.72$. The NMFV contributions are mainly sensitive to the $\delta_{LL}\delta^d_{RR}$, $\delta^d_{LR}\delta^d_{RL}$ and $\delta^u_{LR}\delta^u_{RL}$ products, the relative suppression and enhancement of their contributions being driven by the ratio of the chargino over the gluino mass [215, 255].

In the kaon sector, the ϵ_K observable is estimated by combining the formulas of [255, 258], the loop-contributions being evaluated with $\eta_{tt} = 0.5$, $\eta_{ct} = 0.47$ and $\eta_{cc} = 1.44$ [259]. In addition, we fix all hadronic parameters at the scale $Q = 2$ GeV as $B_1^{VLL} = 0.61, B_1^{SLL} = 0.76, B_2^{SLL} = 0.51, B_1^{LR} = 0.96$ and $B_2^{LR} = 1.2$ [258], and we set the decay constant f_K to 155.8 MeV. The quantity ϵ_K is not directly sensitive to a single NMFV MSSM parameter but will allow us to constrain $\delta_{LL,13}\delta^d_{RR,23}$ and $\delta_{LL,23}\delta^d_{RR,13}$ products (recalling that first generation squark mixings are generated by renormalisation-group running). On different lines, the branching ratios associated with the rare $K^+ \to \pi^+\nu\nu$ and $K_L \to \pi^0\nu\nu$ decays are calculated from the formulas given in [260] with $\kappa_L = 2.1310^{-11}$, $\kappa_+ = 5.1610^{-11}$ and $P_c = 0.39$. These observables mainly constrain the product $\delta^u_{LR,13}\delta^{u*}_{LR,23}$ as well as higher-order combinations of δ-parameters that in particular appear in gluino/down-type squark box-contributions [260, 261].

In all the calculations described above, we have used the results of [262] for calculating chirally-enhanced interaction strengths that include *e.g.* the re-

[2]Imposing predictions for a_μ to agree with the related measured values leads to a preference for a lighter slepton mass spectrum. This can indirectly imply constraints on the NMFV MSSM parameters *via* the flavour observables that involve sleptons.

summation of loop-induced holomorphic coupling effects when $\tan\beta$ and/or the sfermion-Higgs trilinear couplings are large.

As we allow for relatively light sleptons, charginos and neutralinos, we calculate the supersymmetric contributions to the anomalous magnetic moment of the muon by using the formulas of [263]. The related impact in terms of constraints on our NMFV MSSM parameter space depends on the higgsino/gaugino nature of the lighter charginos and neutralinos.

Finally, the calculation of the Higgs boson mass includes the complete one-loop contribution that embeds all possible flavour structures and that is obtained by extending the formulas of [264]. For the two-loop corrections, we have made use of the formulas of [265–270] where generation mixing is neglected so that only third generation mass parameters in the super-CKM basis are used as input parameters. Although flavour effects can shift the Higgs mass by a few GeV at the one-loop level, in particular when the product $\delta^u_{LR}\delta^u_{RL}$ is large [214, 220, 271], the two-loop effects are expected to be of one order of magnitude smaller so that ignoring the associated flavour mixing is expected to be a reasonable approximation.

6.4 Results

The analysis of the results of the Markov Chain Monte Carlo scan presented in the previous sections gives us information on the regions of parameter space that are favoured by the experimental data shown in table 6.3. The influence of a specific experimental result on a given parameter can be studied by comparing its theoretical prior distribution to the posterior one that is derived after imposing the related constraint. The prior distributions of all parameters are obtained from a uniform random scan in which we ignore scenarios that exhibit tachyons, where the electroweak symmetry is not successfully broken and where the lightest neutralino is not the lightest supersymmetric particle. We hence include about 1.5×10^6 theoretically accepted set-ups. The posterior distributions are then computed on the basis of our MCMC scan in which all the experimental constraints, except, at this initial state, the one on the Higgs boson mass, are imposed. This scan consists of 100 chains of 6000 scenarios in which the first 900 ones (the burn-in length) are removed. The constraint on the Higgs boson mass is eventually imposed and the final posterior distributions include about 100 000 points. To estimate the importance of each observable separately, we have run a separate MCMC scan consisting of 100 chains of 2000 scenarios for each observable. After removing the burn-in length, 170 000 points remain. For each scan, the convergence test of Gelman and Rubin has been verified [231].

Although we are mainly interested in the non-minimally flavour-violating parameters defined in equation (6.11), we first also discuss for completeness the flavour-conserving parameters of our model description.

6.4.1 Flavour-conserving parameters

We start the discussion with the twelve flavour-conserving parameters of our NMFV MSSM description. Figure 6.2 shows their probability density distributions over the respective parameter ranges. In each panel, we display the theoretical prior (yellow area) as well as the posterior distribution (solid line), which shows the impact of all constraints given in table 6.3 together.

The prior distribution of the gaugino mass parameter M_1 is centred at relatively low values of $M_1 \sim 400$ GeV and may reach values ranging up to about 1000 GeV. When imposing all considered experimental constraints, the distribution is shifted by about 100 GeV to higher values. This feature can be traced to the chargino contributions to the $B_s \to \mu\mu$ branching ratio and to the neutral B-meson mass difference ΔM_{B_s}, as we have fixed the ratios of the gaugino mass parameters M_1 and M_2 so that chargino effects are connected to M_1.

For the trilinear coupling parameter A_f, the prior distribution is centred around zero. Large values of A_f are indeed often rejected since they can induce a large left-right squark mixing implying tachyonic states. Imposing the experimental constraints drastically changes the shape of the distribution and leads to two peaks corresponding to $|A_f| \sim 3000$ GeV. This feature is induced by the Higgs boson mass requirement that necessitates, in order to be satisfied, a relatively large splitting of the masses of the squarks exhibiting the largest stop component $m_{\tilde{q}_1}$ and $m_{\tilde{q}_2}$. More precisely, the flavour-conserving formula for the leading contributions to the Higgs mass,

$$m_h^2 \;=\; m_Z^2 \cos^2 2\beta + \frac{3g^2 m_t^4}{8\pi m_W^2}\left[\log\frac{M_{\rm SUSY}^2}{m_t^2} + \frac{X_t^2}{M_{\rm SUSY}^2}\left(1 - \frac{X_t^2}{12 M_{\rm SUSY}^2}\right)\right] \;, \quad (6.21)$$

where $X_t = A_t - \mu/\tan\beta$ and $M_{\rm SUSY}^2 = m_{\tilde{q}_1} m_{\tilde{q}_2}$, stays approximatively valid in the NMFV regime, so that peaks defined by $|X_t| \sim \sqrt{6} M_{\rm SUSY}$ are expected (see *e.g.* reference [270] and references therein).

Moving on with the slepton mass parameter $M_{\tilde{\ell}}$, we observe a peak centred at around 600 GeV after imposing all experimental constraints. This is mainly inferred by the anomalous magnetic moment of the muon requirement that strongly depends on the slepton sector properties. Turning to the Higgs sector (second line of figure 6.2), the prior distribution of the μ-parameter shows a preference for low values while its posterior distribution slightly peaks around $\mu \sim 200$ GeV due to the $B_s \to \mu\mu$, Δa_μ and ΔM_{B_s} constraints which all depend on the chargino and neutralino sector. Next, the $\tan\beta$ parameter tends towards lower values both in its prior and posterior distributions, the favourite values being pushed to satisfy $12 \lesssim \tan\beta \lesssim 18$. Finally, the posterior distribution of the mass of the pseudoscalar Higgs boson m_A is shifted towards higher values with respect to its prior distribution. This results from the interplay of most considered observables for which low values of m_A would induce too large Higgs contributions.

The last two lines of figure 6.2 concern the soft squark mass parameters. Low

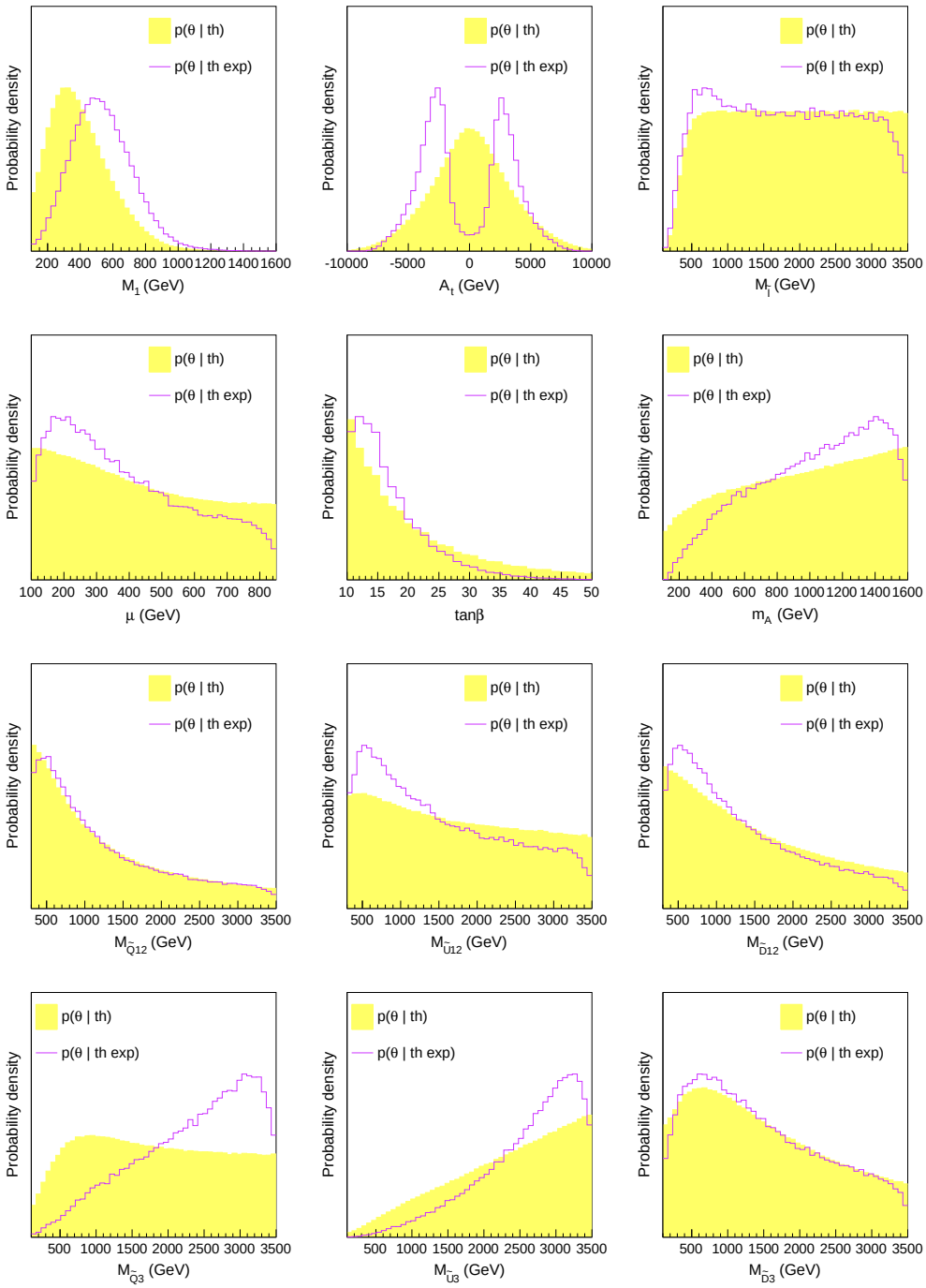

Figure 6.2: The one-dimensional prior (yellow histogram) and posterior (violet curve) distributions of the parameters of our NMFV MSSM description. The prior only incorporates theoretical inputs while the posterior distribution shows the impact of all experimental observations listed in table 6.3. The probability density on the y-axis is shown on a linear scale.

values are preferred for the first and second generation squark masses $M_{\tilde{Q}_{1,2}}$, $M_{\tilde{U}_{1,2}}$ and $M_{\tilde{D}_{1,2}}$, a feature that is mostly caused by the Higgs boson. This behaviour can be understood from the limiting case in which $M^2_{\tilde{Q}_{1,2}} \simeq M^2_{\tilde{U}_{1,2}} \simeq M^2_{\tilde{D}_{1,2}} \equiv \tilde{m}^2$. The one-loop corrections to m_h that are proportional to δ^u_{LR} are here approximately given by [214]

$$\Delta m_h^2 = \frac{3v_u^4}{8\pi^2(v_d^2+v_u^2)}\left[\frac{(T_u)^2_{23}}{\tilde{m}^2}\left(\frac{Y_t^2}{2}-\frac{(T_u)^2_{23}}{12\tilde{m}^2}\right)\right] , \tag{6.22}$$

while the corresponding contributions of down-type squarks are obtained by replacing T_u by T_d, Y_t by Y_b and by exchanging v_u and v_d. In our parameterisation,

$$\left(\widetilde{T}_u\right)_{23} = \frac{\sqrt{2}}{v_u}\delta^u_{LR} M_{\tilde{Q}_{1,2}} M_{\tilde{U}_3} \tag{6.23}$$

so that for non-zero δ^u_{LR}, the Higgs boson becomes tachyonic if $\tilde{m}^2$ is too large. Similarly, the requirement of a physical solution for the electroweak vacuum also favours lower values for $M_{\tilde{Q}_{1,2}}$. The distributions of the third-generation mass parameters $M_{\tilde{Q}_3}$ and $M_{\tilde{U}_3}$ prefer in contrast larger values due to ΔM_{B_s} and the mass of the Higgs boson constraints. Finally, both the prior and posterior distributions of the right-handed down-type squark mass $M_{\tilde{D}_3}$ prefer lower values and are in this case very similar.

6.4.2 Flavour-violating parameters

We now turn to the analysis of the constraints that are imposed on the seven non-minimally flavour-violating parameters $\delta^q_{\alpha\beta}$ that are at the centre of interest of the present analysis. The corresponding prior and posterior distributions are displayed in figure 6.3, and we detail the impact of the most important observables on figure 6.4, figure 6.5 and figure 6.6.

The theoretical constraints on any additional stop-scharm mixing in the left-left sector (δ_{LL}) are relatively mild such that an almost flat behaviour is observed (see figure 6.3). The δ_{LL} parameter is then mainly constrained by the B-meson oscillation parameter ΔM_{B_s} (which favours smaller absolute values of δ_{LL}) and the branching ratio for the $B_s \to \mu\mu$ decay (which causes a slight preference to positive values), as shown in figure 6.4. Values ranging up to $|\delta_{LL}| = 0.8$ can nevertheless be reached, but this simultaneously requires large values for other δ quantities so that cancellations between the different contributions to the considered observables occur (see section 6.4.3). In a similar way, the prior distributions of the parameters δ^u_{RR} and δ^d_{RR} show a mild preference for low absolute values. The posterior distribution of the δ^u_{RR} parameter does not differ much from its prior distribution so that δ^u_{RR} is not sensitive to the experimental constraints under study. In contrast, the B-meson oscillation parameter ΔM_{B_s} restricts the posterior distribution of δ^d_{RR} to be narrower while the $B_s \to \mu\mu$

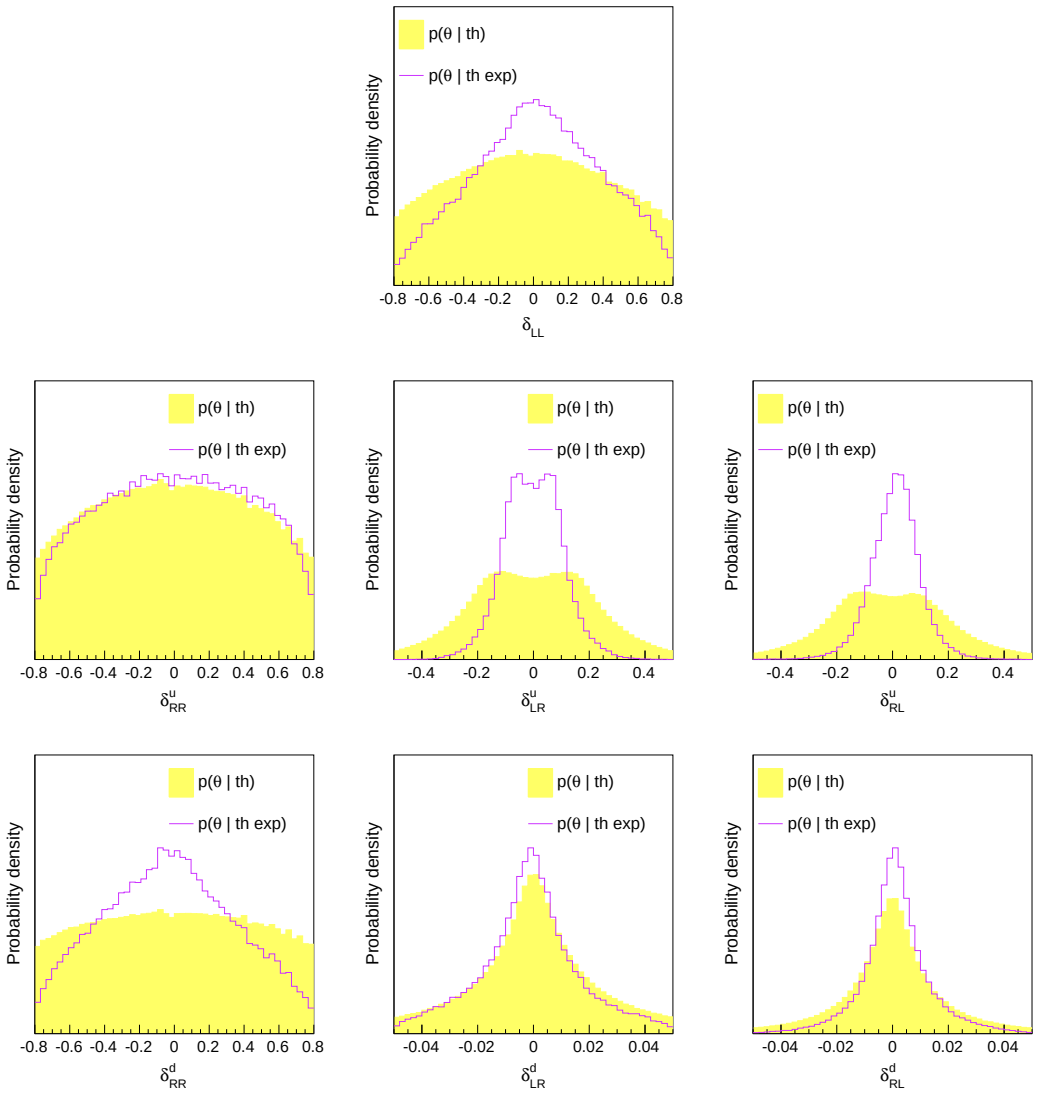

Figure 6.3: Same as figure 6.2 in the case of the flavour-violating input parameters of our NMFV MSSM description.

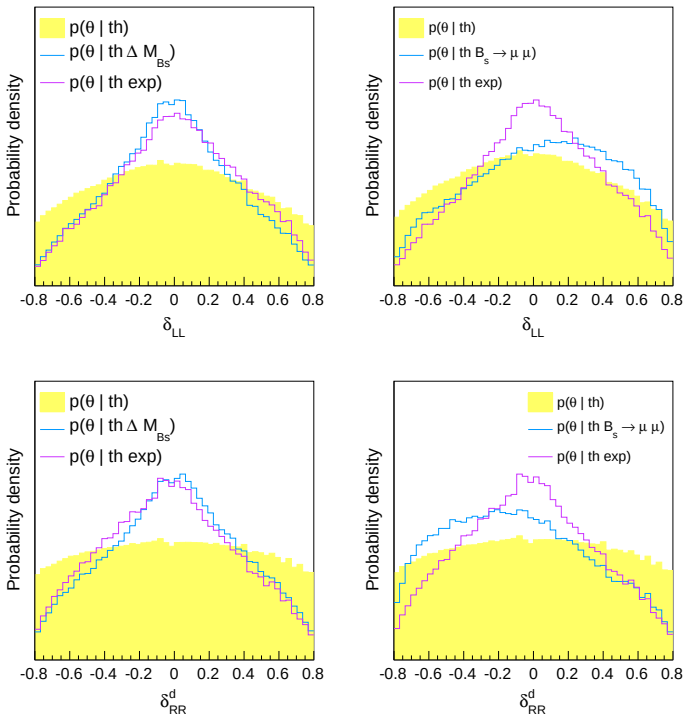

Figure 6.4: The same as figure 6.2. The blue curve shows the most relevant observables constraining the δ_{LL} (upper panel) and δ^d_{RR} (lower panel) parameters.

branching ratio implies a preference to negative values (see figure 6.4). However, the full explored range of $-0.8 \lesssim \delta^{u,d}_{RR} \lesssim 0.8$ stays accessible in the context of both right-right mixing parameters.

The flavour-violating left-right and right-left elements of the up-type squark mass matrix (δ^u_{LR} and δ^u_{RL}) turn out to be mainly constrained by the necessity to incorporate a Higgs boson with a mass of about 125 GeV, as can be seen in figure 6.5. The posterior distribution of δ^u_{LR} exhibits two peaks at $|\delta^u_{LR}| \sim 0.05$ and is restricted to $-0.15 \lesssim \delta^u_{LR} \lesssim 0.15$. Theoretically, this behaviour is expected from equation (6.23). The δ^u_{RL} parameter however receives extra constraints stemming from the BR($B_s \to \mu\mu$) observable (see figure 6.5) so that the posterior distribution peaks around zero and has a maximal value of $|\delta^u_{RL}| \sim 0.2$. We recall that the two parameters δ^u_{LR} and δ^u_{RL} are independent and induce different mixing patterns. More precisely, δ^u_{LR} describes a $\tilde{c}_L$–$\tilde{t}_R$ mixing, while δ^u_{RL} corresponds to mixing between the $\tilde{c}_R$ and $\tilde{t}_L$ eigenstates. The impact of the constraints and the resulting distributions are therefore different and directly related to the structure of the chargino-squark-quark and neutralino-squark-quark interactions.

In the down-type squark sector, the prior distributions of the δ^d_{LR} and δ^d_{RL} mixing parameters show a clear peak for values close to zero. Large values are

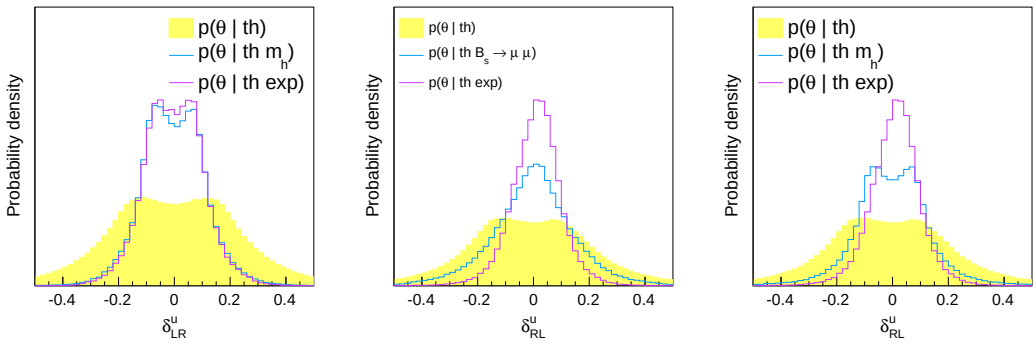

Figure 6.5: The same as figure 6.4, showing the most relevant observables constraining the δ^u_{LR} (left panel) and δ^u_{RL} (centre and right panel) parameters.

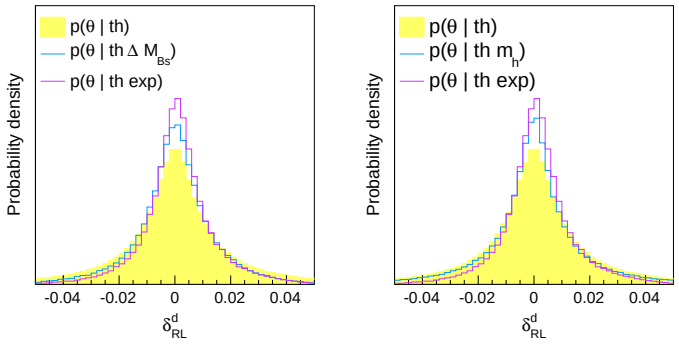

Figure 6.6: The same as figure 6.4, showing the most relevant observables constraining the δ^d_{RL} parameter.

often discarded as they imply large off-diagonal terms in the $M_{\tilde{d}}$ mass matrix so that the resulting spectrum likely contains tachyons. Both parameters are hardly constrained by any of the observables under consideration and we only observe minor effects. The posterior distribution of δ^d_{LR} slightly prefers negative values, and the posterior distribution of δ^d_{RL} is slightly narrower, when both distributions are compared to their respective prior. This mostly results from an interplay of all observables, although but for the δ^d_{RL} case, the B-meson oscillation observable ΔM_{B_s} and the Higgs boson mass requirement play a non-negligible role (see figure 6.6).

We now illustrate the global distribution of all NMFV parameters. To this

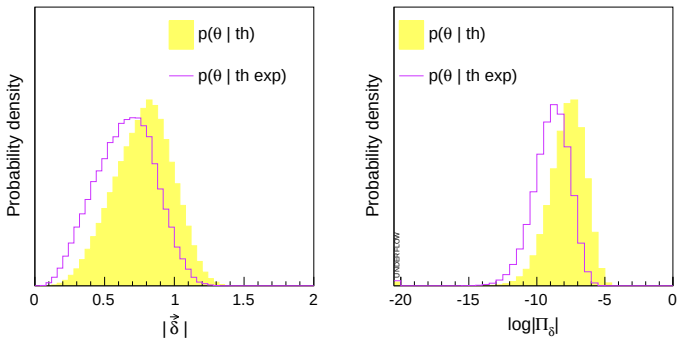

Figure 6.7: The one-dimensional prior (yellow histogram) and posterior (violet curve) distributions of the quantities $|\vec{\delta}|$ and $\log|\Pi_\delta|$ defined in equation (6.24). The probability density is shown on a linear scale.

end, we introduce the quantities

$$|\vec{\delta}| = \left[\left(\delta_{LL}\right)^2 + \left(\delta^u_{RR}\right)^2 + \left(\delta^d_{RR}\right)^2 + \left(\delta^u_{LR}\right)^2 + \left(\delta^u_{RL}\right)^2 + \left(\delta^d_{LR}\right)^2 + \left(\delta^d_{RL}\right)^2\right]^{1/2} ,$$
$$\log|\Pi_\delta| = \log\left|\delta_{LL}\delta^u_{RR}\delta^d_{RR}\delta^u_{LR}\delta^u_{RL}\delta^d_{LR}\delta^d_{RL}\right| . \tag{6.24}$$

The former, $|\vec{\delta}|$, corresponds to the norm of a vector whose components are the seven NMFV parameters. Its value gives a measure of how far a given benchmark is situated from the minimally flavour-violating set-up where $|\vec{\delta}| = 0$. The maximum value that can be reached in our scan is $|\vec{\delta}| \approx 1.56$. The second quantity, $\log|\Pi_\delta|$, corresponds to the logarithm of the absolute value of the product of the seven NMFV parameters. The case where all NMFV parameters are maximum corresponds to $\log|\Pi_\delta| \approx -3.5$. In figure 6.7, we show the prior and posterior distributions of these two quantities. All scanned points feature $|\vec{\delta}| > 0$ so that at least one of the NMFV parameters is sizeable and non-vanishing. The second quantity is in general large and negative so that at least one of the NMFV parameters has to be small. However, since the distribution shows a peak around $\log|\Pi_\delta| \approx -7$ it is clear that a large fraction of the scanned points exhibit seven non-vanishing (with some sizeable) NMFV parameters.

6.4.3 Correlations within the flavour-violating parameters

Having discussed the distribution of single parameters, it is interesting to investigate possible correlations between different NMFV quantities. A correlation indicator between two parameters x and y can be computed as

$$r = \frac{\sum_{i=1}^n (x_i - \bar{x})(y_i - \bar{y})}{\sqrt{\sum_{i=1}^n (x_i - \bar{x})^2}\sqrt{\sum_{i=1}^n (y_i - \bar{y})^2}} , \tag{6.25}$$

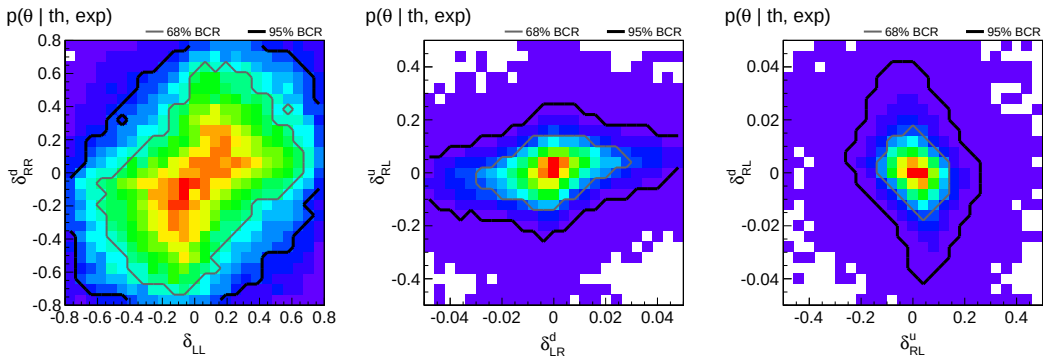

Figure 6.8: Two-dimensional distributions of the mostly correlated pairs of NMFV parameters after including all constraints. The red colour indicates the highest and dark purple the lowest likelihood. The grey and black lines respectively indicate the 68% and 95% Bayesian Credibility Regions (BCR).

where the sum runs over all the points (x_i, y_i) of the sample and $\bar{x}$ and $\bar{y}$ are the mean values of the two parameters. The correlation factor is vanishing when there is no correlation, while $r = \pm 1$ indicates a linear correlation with the exception of the case in which the sampled points lie on a line parallel to one of the x and y axes. We restrict our analysis to the NMFV parameters. The correlation indicators have been computed for any pair out of the seven NMFV parameters and the results are shown in table 6.4 when one only accounts for the theoretical prior (second column) and after imposing the full set of constraints (last column). The correlations are found not particularly pronounced with all r-values being close to zero.

We illustrate the correlations between different NMFV parameters on figure 6.8. We however only focus on cases where the correlation indicator is above $|r| > 0.25$, namely on the $(\delta_{LL}, \delta^d_{RR})$, $(\delta^d_{LR}, \delta^u_{RL})$ and $(\delta^u_{RL}, \delta^d_{RL})$ pairs. This shows that scenarios in which several NMFV parameters are non-zero (and even significantly large) simultaneously are still allowed by current low-energy flavour and Higgs data.

6.4.4 Squark masses and flavour decomposition

We discuss in this section the distributions of the masses of the squarks, their flavour decomposition and the mass differences between states relevant for the LHC phenomenology of NMFV MSSM models. Figure 6.9 shows the prior and posterior distributions for the up-type squark masses. The shapes of the distributions for the two lightest states $\tilde{u}_1$ and $\tilde{u}_2$ are very similar and they both peak at about 800–1000 GeV. The two lightest up-type states $\tilde{u}_1$ and $\tilde{u}_2$, that are mostly of the first and second generation (see figure 6.10), are in general relatively close in mass. This is due to the choice of common mass parameters

Parameters	th	th + exp
$(\delta_{LL}, \delta^d_{RR})$	-0.003	0.270
$(\delta^d_{LR}, \delta^u_{RL})$	0.007	0.267
$(\delta^u_{RL}, \delta^d_{RL})$	-0.000	-0.254
$(\delta^d_{RR}, \delta^u_{RL})$	-0.002	0.185
$(\delta_{LL}, \delta^u_{RL})$	0.009	-0.158
$(\delta^u_{RR}, \delta^u_{RL})$	0.003	-0.037
$(\delta_{LL}, \delta^u_{LR})$	0.002	-0.031
$(\delta^d_{RR}, \delta^d_{LR})$	-0.021	-0.028
$(\delta^d_{LR}, \delta^d_{RL})$	-0.001	0.027
$(\delta_{LL}, \delta^d_{LR})$	-0.002	0.023
$(\delta_{LL}, \delta^d_{RL})$	-0.024	0.013
$(\delta^u_{LR}, \delta^d_{LR})$	-0.006	-0.012
$(\delta^u_{RR}, \delta^u_{LR})$	0.003	0.010
$(\delta^u_{RR}, \delta^d_{RL})$	-0.000	-0.010
$(\delta^d_{RR}, \delta^d_{RL})$	-0.002	-0.008
$(\delta^u_{LR}, \delta^u_{RL})$	0.002	-0.007
$(\delta^u_{RR}, \delta^d_{RR})$	0.001	-0.006
$(\delta^u_{RR}, \delta^d_{LR})$	0.000	-0.003
$(\delta^d_{RR}, \delta^u_{LR})$	-0.001	0.002
$(\delta^u_{LR}, \delta^d_{RL})$	0.000	0.000

Table 6.4: The correlation coefficient r defined in equation (6.25) for all pairs of NMFV parameters. The parameter pairs are ordered by their correlation indicators when taking into account all imposed constraints ('th+exp'). We also display the indicator values when only the theoretical prior is imposed ('th').

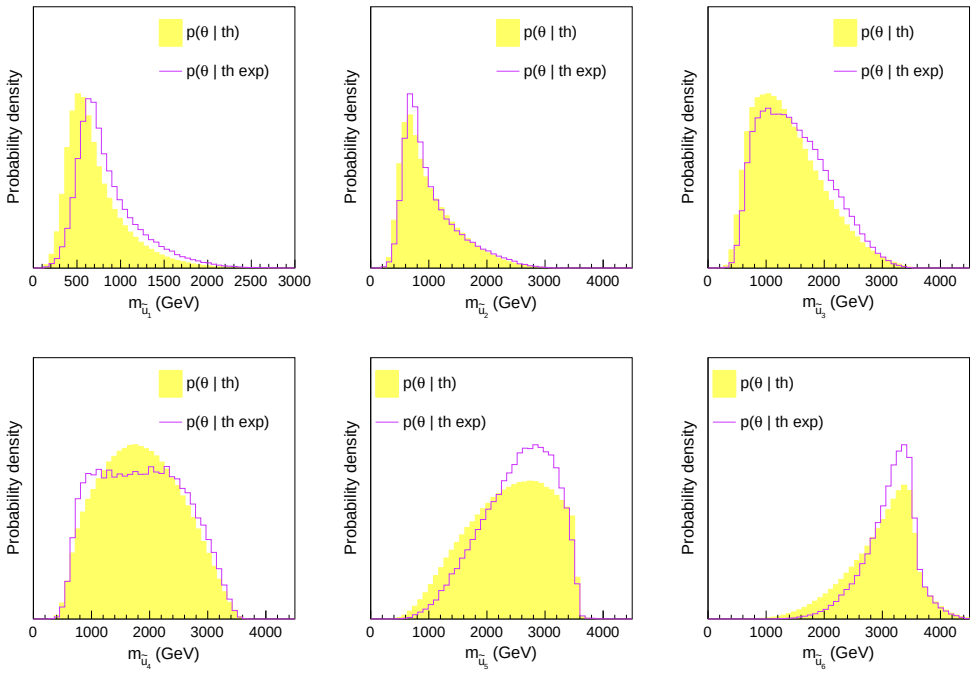

Figure 6.9: One-dimensional prior (yellow histogram) and posterior (violet curve) distributions of the masses of the six up-type squarks. The probability density is shown on a linear scale.

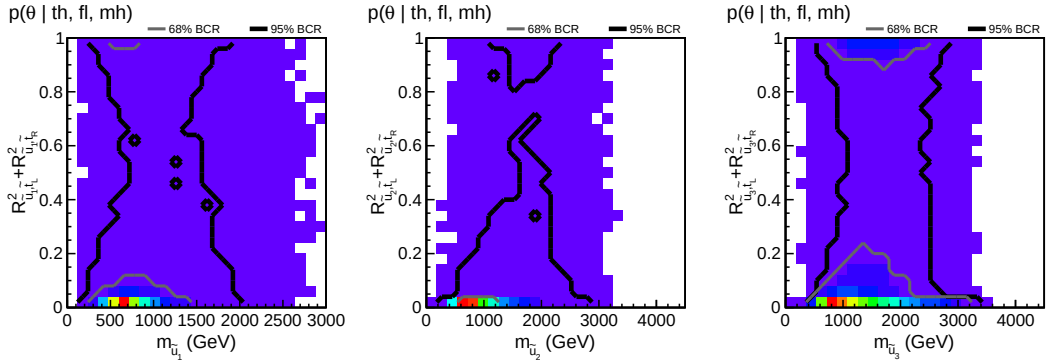

Figure 6.10: Resulting correlations between the stop flavour content and the masses of the three lightest up-type squarks after imposing all experimental constraints mentioned in table 6.3. The red colour indicates the highest and dark purple the lowest likelihood. The grey and black lines respectively indicate the 68% and 95% Bayesian Credibility Regions (BCR).

for the first and second generation squarks. The heavier $\tilde{u}_3$, $\tilde{u}_4$ and $\tilde{u}_5$ states exhibit more spread distributions, the masses ranging from 1 to 3.5 TeV. Finally, the heaviest state $\tilde{u}_6$ is barely reachable at the LHC, with a mass lying in general

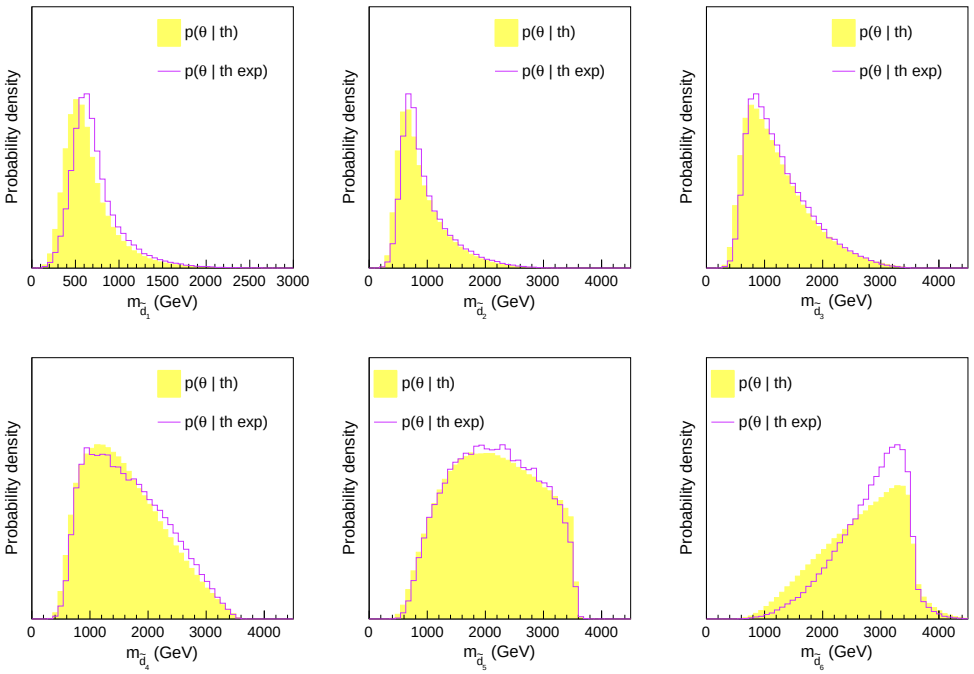

Figure 6.11: Same as figure 6.9 for the down-type squark sector.

above 2 TeV. Although the considered experimental constraints affect all NMFV supersymmetric parameters, the associated effects on the mass eigenvalues is at the end only mild, the mass distributions being only slightly shifted towards higher values.

From a phenomenological point of view, it is interesting to examine the flavour (in particular the stop) content of the six up-type squarks. The posterior distribution of the stop content of the three lightest up-type squarks is depicted in figure 6.10 and shown in correlation with the respective squark mass. The lighter states $\tilde{u}_1$, $\tilde{u}_2$, $\tilde{u}_3$ (and also $\tilde{u}_4$) are mainly not stop-like, *i.e.* they have a significant up or charm component. Most scanned scenarios indeed exhibit a charm-dominated lightest $\tilde{u}_1$ squark, while $\tilde{u}_2$ is mostly dominated by its up component. This contrasts with usual flavour-conserving MSSM set-ups where the lightest squark state is typically a stop. This feature can be traced to the first and second generation soft masses that are driven to lower values as explained in section 6.4.1, whilst the third generation squark masses are pushed towards higher values by the flavour constraints. Furthermore, even in the presence of large trilinear terms, the lightest states are still found to be up-like or charm-like.

Similar conclusions hold for the sector of the down-type squarks. We show their masses in figure 6.11 and selected flavour decompositions in figure 6.12. The three lighter states exhibit comparable distributions, peaking as for the up-type squarks at about 800–1000 GeV. The mass distributions of the $\tilde{d}_4$ and $\tilde{d}_5$ states

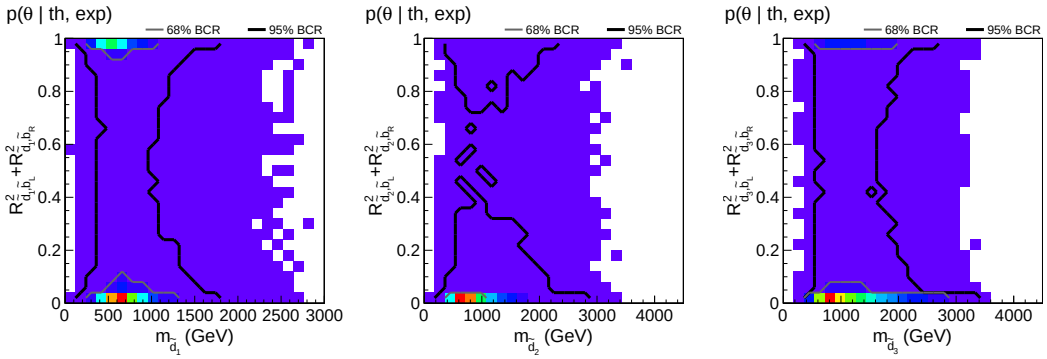

Figure 6.12: Resulting correlations between the sbottom flavour content and the masses of the three lightest down-type squarks after imposing all experimental constraints mentioned in table 6.3. The red colour indicates the highest and dark purple the lowest likelihood. The grey and black lines respectively indicate the 68% and 95% Bayesian Credibility Regions (BCR).

feature distributions with a larger spread, and the one of heaviest $\tilde{d}_6$ squark is peaking at about 3 TeV, although masses of about 1 TeV are predicted for a small subset of scenarios. Flavour mixing in the down-type squark sector is generally less pronounced than for the up-type squarks, as illustrated on figure 6.12 where we depict the correlations between the sbottom content and the masses of the lighter down-type squarks. A majority of scenarios include light down-like and strange-like squark states and there is only a small number of parameter points where $\tilde{d}_1$ and $\tilde{d}_2$ contain a sizeable sbottom content.

In figure 6.13, we show the correlations between the masses of the lightest squark states and the one of the lightest neutralino. For most ($\sim 95\%$) viable points, the mass difference is well above 50 GeV, which is a favorable condition for collider searches as the spectrum is not compressed. A considerable number ($\sim 40\%$) of parameter points features $\tilde{u}_1$ masses of about 500 – 1000 GeV together with neutralino masses of the order of 150 – 400 GeV. Such mass configurations are likely to be ruled out by Run I LHC data. This is accounted for in the next section, where we include collider constraints on the NMFV MSSM set-up and define benchmark scenarios suitable for searches at the LHC Run II.

6.5 Benchmark scenarios

In this section, we identify an ensemble of benchmark scenarios capturing typical features of the parameter space regions favoured by the constraints previously investigated. We have ordered all acceptable parameter set-ups according to their likelihood and selected four scenarios among the best ones. Our selection is aimed to cover different phenomenological properties of the NMFV MSSM and to be relevant for future LHC searches. The input parameters corresponding to

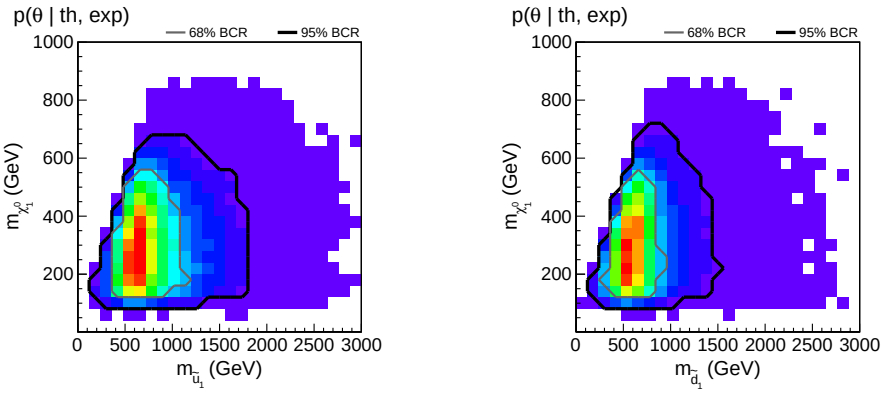

Figure 6.13: Correlations between the lightest neutralino mass and the lightest up-and down-type squark masses. The grey and black lines respectively indicate the 68% and 95% Bayesian Credibility Regions (BCR).

the benchmark scenarios of our choice are indicated in table 6.5.

The values stated in this table are rather precise and we can wonder how stable our reference scenarios would be under small variations of the parameters. As we can see from the 1D posterior distributions shown in figures 6.2 and 6.3, all the reference points are situated in a well-populated part of the parameter space. This suggests they can be stable. However, since the dependence of the low-energy observables on the parameters is rather complicated and hard to predict, we would need a detailed analysis studying the stability of the reference points to state anything more concrete.[3]

In figure 6.14, we present the mass spectra of the four selected scenarios and depict the flavour content of the different squark eigenstates. We finally show in tables 6.6–6.8 the branching ratios related to the dominant decay modes of the squarks ligther than about 1 TeV. Additionally, we have verified that the electroweak vacuum is stable for all selected points by using the programme `Vevacious` [272]. We now briefly outline the main characteristics of the four proposed benchmark scenarios.

Scenario I

This benchmark point presents one up-type and two down-type squarks with masses below 1 TeV. The lightest up-type squark is mostly stop-like, although it contains a small scharm component, and has a mass of 831 GeV which implies a sizeable production cross section at the LHC. In the sector of the down-type squarks, the two lightest states are almost purely sbottom-like with masses of 763 GeV and 854 GeV respectively. Since only the heaviest neutralino and

[3]We presented an example of such an analysis for a different set of reference points based on a grid scan of a more restricted parameter space in [205].

Parameter	I	II	III	IV
$\alpha_s(m_Z)$	$1.187 \cdot 10^{-1}$	$1.194 \cdot 10^{-1}$	$1.176 \cdot 10^{-1}$	$1.176 \cdot 10^{-1}$
m_t^{pole}	176.00 GeV	175.53 GeV	173.53 GeV	174.02 GeV
$m_b(m_b)$	4.10 GeV	4.24 GeV	4.28 GeV	4.10 GeV
$M_{\tilde{Q}_{1,2}}$	1192.7 GeV	2288.2 GeV	637.7 GeV	753.2 GeV
$M_{\tilde{Q}_3}$	883.7 GeV	425.3 GeV	3483.0 GeV	2662.7 GeV
$M_{\tilde{U}_{1,2}}$	2412.6 GeV	1757.7 GeV	934.0 GeV	984.7 GeV
$M_{\tilde{U}_3}$	2344.3 GeV	2753.8 GeV	2862.2 GeV	2010.6 GeV
$M_{\tilde{D}_{1,2}}$	2295.1 GeV	551.6 GeV	1331.1 GeV	882.7 GeV
$M_{\tilde{D}_3}$	843.8 GeV	713.5 GeV	901.8 GeV	670.5 GeV
A_f	-2424.1 GeV	1807.3 GeV	1586.3 GeV	-2833.4 GeV
$\tan\beta$	17.4	21.1	29.2	34.0
μ	615.7 GeV	772.8 GeV	508.1 GeV	442.7 GeV
m_A	1334.5 GeV	1300.3 GeV	1294.8 GeV	1431.0 GeV
M_1	474.5 GeV	315.3 GeV	525.2 GeV	390.0 GeV
$M_{\tilde{\ell}}$	2466.5 GeV	1552.5 GeV	3396.7 GeV	2813.4 GeV
δ_{LL}	$1.4 \cdot 10^{-1}$	$-4.6 \cdot 10^{-2}$	$3.7 \cdot 10^{-1}$	$5.9 \cdot 10^{-1}$
δ^u_{RR}	$1.7 \cdot 10^{-1}$	$2.2 \cdot 10^{-1}$	$7.3 \cdot 10^{-1}$	$6.0 \cdot 10^{-1}$
δ^d_{RR}	$1.4 \cdot 10^{-1}$	$-1.4 \cdot 10^{-1}$	$-2.9 \cdot 10^{-1}$	$-7.5 \cdot 10^{-1}$
δ^u_{LR}	$9.2 \cdot 10^{-2}$	$3.5 \cdot 10^{-2}$	$1.7 \cdot 10^{-1}$	$1.0 \cdot 10^{-1}$
δ^d_{LR}	$-3.9 \cdot 10^{-2}$	$-3.6 \cdot 10^{-3}$	$-6.1 \cdot 10^{-3}$	$4.6 \cdot 10^{-3}$
δ^u_{RL}	$-9.7 \cdot 10^{-2}$	$1.4 \cdot 10^{-2}$	$-9.9 \cdot 10^{-2}$	$-7.2 \cdot 10^{-2}$
δ^d_{RL}	$-7.6 \cdot 10^{-4}$	$-1.4 \cdot 10^{-2}$	$-1.2 \cdot 10^{-3}$	$1.6 \cdot 10^{-3}$

Table 6.5: Definition of four benchmark points suitable for phenomenological studies of the NMFV MSSM.

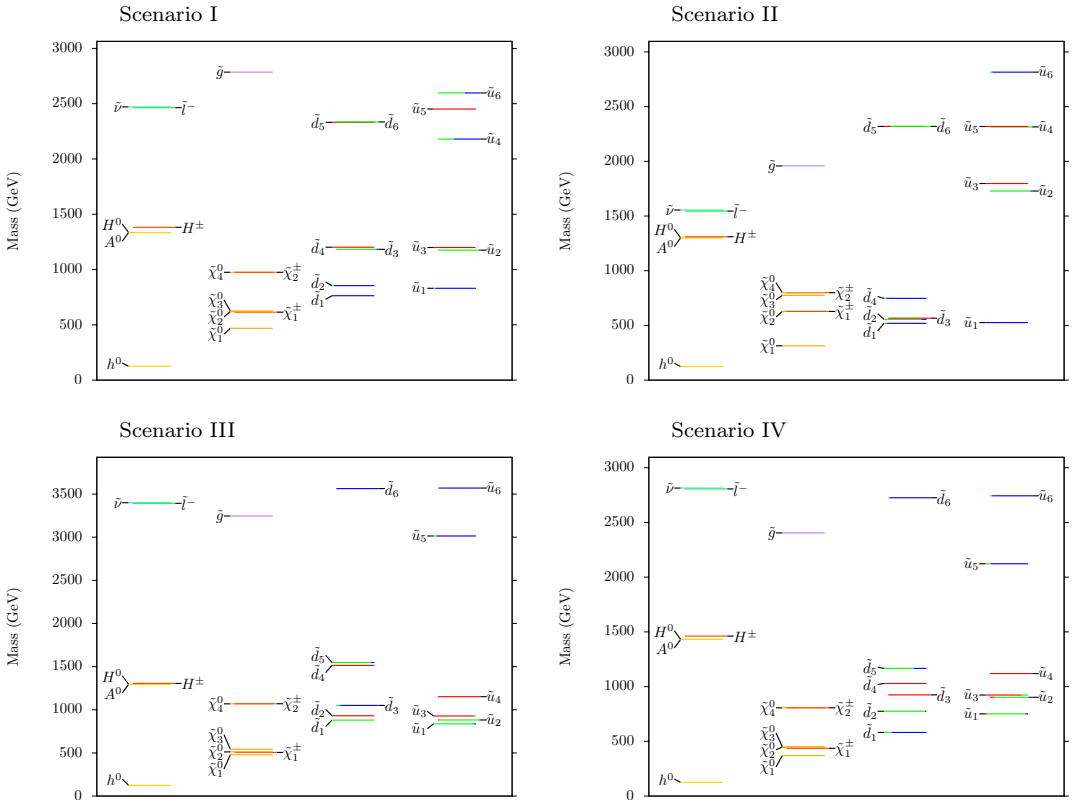

Figure 6.14: Mass spectra of the benchmark scenarios defined in table 6.5. The colour code that has been employed for depicting the squark eigenstates indicates their flavour content: the {red, green, blue} colour corresponds to the {first, second, third} generation flavours.

Decay	I	II	III	IV
$\tilde{u}_1 \to t\tilde{\chi}_1^0$	0.14	0.99	0.06	0.09
$\tilde{u}_1 \to c\tilde{\chi}_1^0$		0.01	0.24	0.07
$\tilde{u}_1 \to t\tilde{\chi}_2^0$	0.24		0.11	
$\tilde{u}_1 \to t\tilde{\chi}_3^0$	0.43		0.06	0.26
$\tilde{u}_1 \to t\tilde{\chi}_3^0$				0.07
$\tilde{u}_1 \to c\tilde{\chi}_3^0$			0.27	0.10
$\tilde{u}_1 \to b\tilde{\chi}_1^+$	0.19		0.24	0.22
$\tilde{u}_1 \to s\tilde{\chi}_1^+$			0.02	0.17
$\tilde{u}_1 \to W^+\tilde{d}_1$				0.02
$\tilde{u}_2 \to t\tilde{\chi}_1^0$			0.07	0.04
$\tilde{u}_2 \to c\tilde{\chi}_1^0$			0.22	0.32
$\tilde{u}_2 \to t\tilde{\chi}_2^0$			0.08	0.09
$\tilde{u}_2 \to t\tilde{\chi}_3^0$			0.09	0.11
$\tilde{u}_2 \to c\tilde{\chi}_3^0$			0.35	0.06
$\tilde{u}_2 \to b\tilde{\chi}_1^+$			0.11	0.21
$\tilde{u}_2 \to s\tilde{\chi}_1^+$			0.09	
$\tilde{u}_2 \to W^+\tilde{d}_2$				0.06
$\tilde{u}_2 \to Z^0\tilde{u}_1$				0.05
$\tilde{u}_2 \to h^0\tilde{u}_1$				0.02
$\tilde{u}_3 \to c\tilde{\chi}_1^0$			0.03	0.09
$\tilde{u}_3 \to u\tilde{\chi}_1^0$			0.03	0.03
$\tilde{u}_3 \to t\tilde{\chi}_2^0$				0.02
$\tilde{u}_3 \to t\tilde{\chi}_3^0$				0.02
$\tilde{u}_3 \to c\tilde{\chi}_3^0$			0.05	0.02
$\tilde{u}_3 \to u\tilde{\chi}_3^0$			0.45	0.09
$\tilde{u}_3 \to c\tilde{\chi}_4^0$				0.01
$\tilde{u}_3 \to u\tilde{\chi}_4^0$				0.15
$\tilde{u}_3 \to b\tilde{\chi}_1^+$			0.01	0.05
$\tilde{u}_3 \to d\tilde{\chi}_1^+$			0.41	0.01
$\tilde{u}_3 \to d\tilde{\chi}_2^+$				0.33
$\tilde{u}_3 \to W^+\tilde{d}_2$				0.01
$\tilde{u}_3 \to Z^0\tilde{u}_1$				0.02

Table 6.6: Branching ratios associated with the dominant decay modes of the up-type squarks lighter than about 1 TeV for the benchmark points defined in table 6.5. Branching ratios below 1% are not indicated.

chargino states are heavier than the three lightest squark states, various decay channels are open so that the real challenge for future LHC analyses would be to become sensitive to flavour-violating branching ratios of a few percents. In this scenario, the electroweak vacuum is long-lived and has a lifetime larger than the age of the Universe.

Decay	I	II	III	IV
$\tilde{d}_1 \to b\tilde{\chi}_1^0$	0.73	0.84		0.35
$\tilde{d}_1 \to s\tilde{\chi}_1^0$		0.16	0.40	0.09
$\tilde{d}_1 \to b\tilde{\chi}_2^0$	0.15		0.01	0.30
$\tilde{d}_1 \to s\tilde{\chi}_2^0$			0.02	
$\tilde{d}_1 \to b\tilde{\chi}_3^0$	0.12			0.25
$\tilde{d}_1 \to s\tilde{\chi}_3^0$			0.05	
$\tilde{d}_1 \to t\tilde{\chi}_1^-$			0.42	
$\tilde{d}_1 \to c\tilde{\chi}_1^-$			0.09	
$\tilde{d}_2 \to b\tilde{\chi}_1^0$	0.04	0.05		0.02
$\tilde{d}_2 \to s\tilde{\chi}_1^0$				0.24
$\tilde{d}_2 \to d\tilde{\chi}_1^0$			0.70	
$\tilde{d}_2 \to b\tilde{\chi}_2^0$				0.04
$\tilde{d}_2 \to s\tilde{\chi}_2^0$	0.04	0.95		
$\tilde{d}_2 \to d\tilde{\chi}_2^0$			0.03	
$\tilde{d}_2 \to d\tilde{\chi}_2^0$			0.08	
$\tilde{d}_2 \to b\tilde{\chi}_3^0$				0.04
$\tilde{d}_2 \to s\tilde{\chi}_3^0$	0.04			0.02
$\tilde{d}_2 \to t\tilde{\chi}_1^-$	0.87			0.51
$\tilde{d}_2 \to c\tilde{\chi}_1^-$				0.09
$\tilde{d}_2 \to u\tilde{\chi}_1^-$			0.15	
$\tilde{d}_2 \to W^-\tilde{u}_1$			0.03	
$\tilde{d}_2 \to Z^0\tilde{d}_1$				0.02
$\tilde{d}_2 \to h^0\tilde{d}_1$				0.02

Table 6.7: Branching ratios associated with the dominant decay modes of the down-type squarks lighter than about 1 TeV for the benchmark points defined in table 6.5. Branching ratios below 1% are not indicated.

Decay	I	II	III	IV
$\tilde{d}_3 \to d\tilde{\chi}_1^0$		1.00		0.16
$\tilde{d}_3 \to d\tilde{\chi}_3^0$				0.01
$\tilde{d}_3 \to d\tilde{\chi}_4^0$				0.25
$\tilde{d}_3 \to u\tilde{\chi}_1^-$				0.07
$\tilde{d}_3 \to c\tilde{\chi}_2^-$				0.02
$\tilde{d}_3 \to u\tilde{\chi}_2^-$				0.48
$\tilde{d}_4 \to b\tilde{\chi}_1^0$		0.42		
$\tilde{d}_4 \to s\tilde{\chi}_1^0$		0.03		
$\tilde{d}_4 \to d\tilde{\chi}_1^0$				0.83
$\tilde{d}_4 \to d\tilde{\chi}_3^0$				0.17
$\tilde{d}_4 \to W^-\tilde{u}_1$		0.27		
$\tilde{d}_4 \to Z^0\tilde{d}_1$		0.13		
$\tilde{d}_4 \to h^0\tilde{d}_1$		0.13		
$\tilde{d}_4 \to h^0\tilde{d}_2$		0.01		

Table 6.8: Branching ratios associated with the dominant decay modes of the down-type squarks lighter than about 1 TeV for the benchmark points defined in table 6.5. Branching ratios below 1% are not indicated.

Scenario II

In this scenario, only the lightest of the up-type squarks is expected to lie within the reach of LHC, with a mass of 526 GeV. It is almost a pure stop state with a small charm component. Since the only lighter superpartner is the lightest neutralino, it will preferably decay into a $\tilde{\chi}_1^0 t$ system. There are four down-type squarks lying below 1 TeV, their masses being 519 GeV, 555 GeV, 566 GeV and 747 GeV. These four states are admixtures of all three flavours and their dominant decay modes include in particular final states containing the next-to-lightest neutralino or the lightest chargino. Contrary to the scenario I, the branching ratios related to flavour-violating decays can reach up to 16 percents, which make them possibly testable at the LHC. Moreover, the fourth down-type squark has sizeable branching ratios for decays into the lightest up-type squark and a W boson as well as into the lightest down-type squark and either a Z boson or a Higgs boson. Although many squarks are very light, this scenario evades all LHC Run I constraints thanks to a heavy lightest neutralino of 315 GeV. Moreover, the vacuum has been found to be stable.

Scenario III

This benchmark point features numerous squark mass eigenstates in the reach of the LHC. It indeed exhibits three up-type squarks with masses of 836 GeV, 882 GeV and 928 GeV, and three down-type squarks with masses of 880 GeV, 931 GeV and 1050 GeV. The stop-like states are here the heaviest ones, and the up-type squark states reachable at LHC only contain up and charm flavours. Similarly, the heavier $\tilde{d}_3$ and $\tilde{d}_6$ down-type squarks are the only ones containing a sbottom component. This feature is the direct consequence of the lower values that are favoured for the $M_{\tilde{Q}_{1,2}}$, $M_{\tilde{U}_{1,2}}$ and $M_{\tilde{D}_{1,2}}$ parameters, when compared to the values that are favoured by the third-generation soft parameters $M_{\tilde{Q}_3}$, $M_{\tilde{U}_3}$ and $M_{\tilde{D}_3}$. Equivalently, this can be seen as an implication of allowing for flavour-violating entries in the squark mass matrices (see section 6.4.1). In addition, all gauginos except the heaviest neutralino and chargino feature lower masses, so that a variety of decay channels are open. Finally, we found a direction in which, for extremely large field excitations, the electroweak vacuum is unbounded from below. This situation is similar to the case of the Standard Model [273, 274], and higher order corrections to the scalar potential would be needed to make a conclusive statement.

Scenario IV

Our last scenario features numerous squark states as well as a complete electroweakino spectrum below 1 TeV. More precisely, the lighter up-type squarks have masses of 751 GeV, 902 GeV and 923 GeV, while the lighter down-type squark masses are of 582 GeV, 775 GeV and 924 GeV. In addition, three other

states are not too far above 1 TeV with masses of 1119 GeV ($\tilde{u}_4$), 1029 GeV ($\tilde{d}_4$) and 1167 GeV ($\tilde{d}_5$). The two lightest up-type squarks consist in this case of a mixture of all three flavours (with a dominant charm content), which leads to interesting decay patterns, as shown in tables 6.6–6.8. Similarly to scenario I, this scenario exhibits a long-lived electroweak vacuum with a lifetime larger than the age of the Universe.

6.6 Summary

We have studied non-minimal flavour-violation in the MSSM by allowing for flavour mixing between the second and third generation squarks. We have used a Markov Chain Monte Carlo scanning technique to explore the underlying parameter space and imposed a set of experimental constraints arising from B-meson and kaon physics and the anomalous magnetic moment of the muon. We have additionally enforced the model to accommodate a light Higgs boson with a mass of 125 GeV.

First and second generation soft squark masses are theoretically restricted to low values in order to avoid tachyons in the Higgs sector. As a consequence, the lighter squarks are often not the stop and sbottom ones, which contrasts with scenarios of the usual minimally flavour-violating MSSM. Requiring a theoretically consistent Higgs sector and a light Higgs boson of about 125 GeV similarly restrict the left-right and right-left flavour-violating squark mixing parameters $\delta^{u,d}_{LR/RL}$ to be small. In contrast, the δ_{LL} and δ^{d}_{RR} NMFV parameters are mainly constrained by neutral B-meson oscillations, and the rare $B_s \to \mu\mu$ decay mainly influences δ^{u}_{RL}. All other NMFV parameters are left unconstrained by the considered experimental observations.

In view of the recently started second LHC run, we have used our MCMC scan results to propose four benchmark scenarios allowed by current data that exhibit distinct features and that are suitable for future analyses of NMFV effects in the MSSM. In most proposed scenarios, several squarks have masses close to 1 TeV so that they should be reachable within the next few years.

Chapter 7

Summary and outlook

Elementary particle physics aims at answering the question 'What is matter made of?' and, to this end, particle colliders such as the Large Hadron Collider (LHC) have been designed. The LHC collides protons with a very high energy onto each other which allows us to probe matter at distance scales of the order $\mathcal{O}(10^{-16})$ meter. At these small scales, matter is made up of only a limited number of elementary particles which are well described within the Standard Model of particle physics. The Standard Model is formulated as a quantum field theory and is a very successful theory. One of its biggest and most recent successes is the prediction and discovery of the Brout-Englert-Higgs (BEH) boson at the LHC.

However, we also know that the Standard Model has its limitations. Results from the Planck space observatory have shown that the matter described within the Standard Model covers only about 5% of all the matter and energy content in the universe. The remaining matter and energy is called dark matter/energy and cannot be incorporated within the Standard Model. Also, the SM describes only three of the four fundamental forces. Every attempt to formulate a quantum field theory of gravity resulted in a theory which is not renormalizable and, therefore, lacks any predictive power. We therefore know that new physics should enter at the scale where quantum gravitational effects become important, namely at the Planck scale, $\mathcal{O}(10^{19})$ GeV.

The huge energy range between the electroweak scale of the SM ($\mathcal{O}(10^2)$ GeV) and the Planck scale does not only suggest there is some other physics in between, it also creates problems within the Standard Model. The radiative corrections to the mass of the BEH boson depend quadratically on the cut-off scale, *i.e.* the scale up to which the theory is valid. If the Standard Model would be valid up to the Planck scale, this cut-off scale is the Planck scale and, consequently, we would expect the mass of the BEH boson to be naturally large. To explain the experimentally observed BEH-boson mass of 125 GeV, the radiative corrections would have to be cancelled by tuning the parameters within the Standard Model very accurately. This seems, however, very unnatural. Even if there would be

some new physics entering at a higher scale, the quadratic sensitivity remains and a certain amount of tuning would be required. This is referred to as the fine-tuning problem of the SM.

These, and other, arguments motivate us to keep searching for physics beyond the Standard Model (BSM). Many candidates for BSM physics have been formulated and, currently, supersymmetry is one of the most attractive extensions of the Standard Model. Supersymmetry is a symmetry relating fermions and bosons. Every particle within the Standard Model is hence predicted to have a supersymmetric partner with a spin differing by 1/2. Supersymmetry is the only way in which gravity could be incorporated in a quantum field theory and, if we assume R-parity conservation, the lightest supersymmetric particle (LSP) is stable and can be a candidate for dark matter. Additionally, as long as the masses of the SM particles and their superpartners do not differ too much, it solves the fine-tuning problem.

If supersymmetry would be an exact symmetry of Nature, the SM particles and their SUSY partners would have the same mass and the implications of SUSY should have been observed already experimentally, at colliders or through low-energy observables such as B-meson mixing. However, no sign of SUSY has been observed so far and SUSY partners with the same mass are experimentally excluded. A mass difference between the SM particles and their SUSY partners can be accomplished if supersymmetry is spontaneously broken, but still we have to be careful not to reintroduce the fine-tuning problem. Since the latest experimental results impose high mass limits on, especially, the coloured superpartners, SUSY seems to become more and more fine-tuned and less natural.

However, SUSY encompasses a broad class of theories and up to now, mainly the minimal versions of SUSY have been studied. In order to get a complete overview of the status of SUSY, it is crucial to also study less minimal supersymmetric models. In this thesis, we went beyond minimal SUSY and we presented a phenomenological study of non-minimal SUSY models.

7.1 Multilepton signals of gauge-mediated supersymmetry breaking at the LHC

Since the LHC is a hadron machine, the cross section for strong production is typically much larger than the cross section for electroweak processes. The cross section for electroweak slepton-pair production, for example, is about three orders of magnitude lower than the one for stop-pair production. As a consequence, the LHC has only recently been able to set limits on the slepton masses which are stronger than the LEP bounds. The data set of LHC Run 2 has, however, more potential with respect to electroweak production.

Even though the EW production channels are currently not the strongest point of the LHC, they did yield some interesting results. The CMS search

for anomalous production of events with three or more leptons, for example, did observe a deviation from the Standard Model prediction. They observed 22 events where they only expected 10 ± 2.4 in the category where they require three electrons or muons and one hadronically decaying tau out of which one opposite-sign same flavour lepton pair can be formed, they impose low hadronic activity and veto b-jets and leptons coming from the decay of a Z boson. Even though this corresponds to a 5σ deviation in this particular category, it only shows up in three out of 64 bins and, after we take into account the look-elsewhere effect, this deviation becomes less significant. It might however still give a hint for new physics. In chapter 4, we investigated whether we can explain the excess within supersymmetry.

We considered a GGM-inspired simplified model in which the bino-like neutralino, the three generations of right-handed sleptons and the gravitino are at the bottom of the spectrum. We choose the bino to be the heaviest, the selectron and smuon are mass degenerate while the right-handed stau can have a different mass and, since we work in gauge mediation, the gravitino is always the LSP. We fix the mass of the bino and gravitino to 500 GeV and 1 eV respectively, and let the masses of the NLSP and NNLSP vary in between 50 and 300 GeV. In this mass regime, the NLSP will always decay promptly to its SM partner and the gravitino while for the NNLSP the three-body decay through the off-shell bino will be dominant. The NNLSP stau, for example, will therefore dominantly decay as $\tilde{\tau}_R \to \tau l \tilde{l}_R$ where $l = e, \mu$. Due to this three-body decay, our simplified model will give rise to multilepton final states at the LHC which, as we have seen, is crucial to explain the excess. We scanned over the aforementioned parameters and found that our simplified model, with right-handed selectrons and smuons of mass 145 GeV and right-handed staus of mass 90 GeV, can explain the CMS results while satisfying other experimental constraints. We propose this as a benchmark scenario for further investigation.

Outlook

In order to further probe our best fit point, we investigated how many events with four or more electrons, muons and hadronically decaying taus we would expect in the data sets that are or will be collected at the LHC during Run 1 and 2. Even though we only produce two electrons/muons and four hadronically decaying taus, we saw that there can easily be 2-4 electrons or muons in the final state and our scenario is very likely to feature two hadronically decaying taus which are hard enough to be reconstructed. A multilepton search, as inclusive as possible, which requires two hadronically decaying taus with a binning on the number of electrons or muons would hence be ideal to probe our best fit scenario.

Another next step that could be made on the experimental side, lies in the limit on the staus. The right-handed stau in our best fit scenario is rather light and lies close to the LEP bound. One obvious way to probe our benchmark,

would be to try to improve this bound using the LHC data. However, tau leptons are hard to identify, and up to now, nor ATLAS [145], nor CMS [146] have been able to set limits on the stau mass.

In our work, we only recasted the CMS analysis featuring the excess [123] within MadAnalysis 5 and the other LHC searches that might be relevant, were only briefly considered. Moreover, the first $12 - 13\,\text{fb}^{-1}$ of data of the LHC Run 2 at $\sqrt{s} = 13$ TeV have been analysed and these results might be relevant for our best fit scenario. As an example, CMS recently presented a multilepton search for electroweak SUSY production in multilepton final states [275] in which no deviation from the Standard Model is observed. They searched for events featuring two, three or at least four leptons (electrons, muons, or hadronically decaying taus) and no b-jets in the final state and order their results according to the number of leptons, their invariant mass, E_T^{miss} and two more variables related to the transverse mass of the leptons. Our signal might contribute to many of the categories presented in this search, but to be sure about the exact expected yields, we would need to generate the simulated samples at 13 TeV and recast the analysis. We leave a detailed analysis of this and other possibly constraining searches such as [276] for future work.

Finally, the properties of the three-body decay of the NNLSP in our simplified model also deserve further investigation. The NNLSP will dominantly decay through the off-shell bino to the NLSP and two SM partners and the NNLSP and NLSP can have the same or opposite charge. In our set-up, the opposite-charge channel dominates over the one with the same charge. Generically, the branching ratios of the same- and opposite-charge decays depend on whether the sleptons are right- or left-handed, the mixing of the staus and on the nature of the neutralino. A detailed phenomenological analysis of these effects might allow us to probe the details of the superparticles in our spectrum. However, such a study would clearly require much more LHC data than is currently available and we suggest to postpone this investigation to more appropriate times.

7.2 Collider signatures of goldstini in gauge mediation

In order to account for the observed mass splitting between the SM particles and their superpartners, supersymmetry has to be broken. In section 2.3 we explained that SUSY breaking occurs in a hidden sector which does not interact directly or only very weakly with the visible sector. In gauge mediation, SUSY breaking is mediated to the visible sector through messenger particles charged under the SM gauge interactions. Usually, one assumes there is only one hidden SUSY-breaking sector, however, there is no theoretical motivation why this should be the case. We extended the usual scenario of gauge mediation with one SUSY-breaking sector to the case in which there are two hidden SUSY-breaking sectors

and we investigated how this would change the collider signatures.

Since each SUSY-breaking sector comes with a goldstino, there will be two goldstini instead of only one. One linear combination of them, the true goldstino G, is eaten by the gravitino while the remaining fields combine to form the pseudo-goldstino G'. While the true goldstino remains massless, the pseudo-goldstino can acquire a mass ranging from 1 to 100 GeV due to radiative corrections. As always in gauge mediation, the gravitino is the LSP and we assume the pseudo-goldstino to be the NLSP. The pseudo-goldstino is further assumed to have a long enough lifetime to decay outside the detector so that the collider signatures will be largely determined by the Lightest Observable Supersymmetric Particle (LOSP). We considered the two most common LOSPs, namely neutralino and stau, and showed that their coupling to G' and their SM partner can essentially be considered as free parameters. The LOSP can then decay to its SM partner and the (pseudo-)goldstino and we showed that, depending on the choice of the couplings and the pseudo-goldstino mass, the decay to G' can be significant.

We first considered the case in which the neutralino is the LOSP. The neutralino is assumed to be mainly gaugino-like and, consequently, it can decay to the photon or Z boson and the (pseudo)-goldstino. The decay to the Z boson is in most of the cases very much suppressed with respect to the decay to the photon. If the neutralino decay to $\gamma G/G'$ is prompt, neutralino production at colliders will give rise to final states consisting of photons and missing energy.

We first studied single- and di-photon production at e^+e^- colliders and we saw that the cross section for single-photon production $\sigma(e^+e^- \to \gamma G/G')$ can be enhanced depending on the choice of the parameters. The di-photon signal arises from the production and decay of a neutralino pair $e^+e^- \to \chi\chi \to \gamma\gamma + \not{E}$ and we showed that the energy distributions of the leading photon and the distributions of the missing invariant mass can differ significantly with respect to usual gauge mediation: the emitted photons can be much softer and both distributions can exhibit edges which can provide information on the couplings and mass of the pseudo-goldstino. In pp colliders, the cleanest signal comes from slepton-pair production $pp \to \tilde{l}^+_{R/L}\tilde{l}^-_{R/L} \to l^+l^- + \gamma\gamma + \not{E}_T$ where $l = e, \mu$ leading to a final state with two opposite-sign leptons, two photons and missing transverse energy. The Standard Model background is very low and we showed that the p_T- and $\not{E}_T$-distributions again differentiate between the couplings and mass of the pseudo-goldstino.

For the case in which the stau is the LOSP, we restricted ourselves to pp colliders and studied stau-pair production $pp \to \tilde{\tau}^+\tilde{\tau}^- \to \tau^+\tau^- + \not{E}_T$. Also here, the final state is found to be softer and more structured with respect to the one-sector case. However, compared to neutralino LOSP, the signal is less clean due to a higher SM background and the difficulties in reconstructing τ-leptons at colliders.

We performed our analysis on two particular benchmark points, SPS8 for

neutralino and SPS7 for stau LOSP, and the described experimental signatures do depend on the parameters related to the pseudo-goldstino. However, we also observed more model-independent features. In particular, due to the mass of the pseudo-goldstino, we expect the SM decay products of a decaying LOSP to have a lower energy compared to the usual gauge-mediation scenarios. Consequently, such a scenario evades most experimental bounds tending to exclude gauge-mediated scenarios.

Outlook

Since the publication of this work, the phenomenology of the goldstini scenario has been further investigated within the community. Our work was based solely on the implementation of the model in FeynRules and the event generation with MadGraph 5. We did impose the minimal detector cuts as well as some basic cuts at the analysis level to remove the background, but a detailed simulation of the detector and experimental analyses was lacking. The work presented in [277] extended our analysis of di-photon production at pp colliders to a more generic study of the parameters space and used MadAnalysis 5 to confronted it with an inclusive diphoton+$\not{E}_T$ search performed by the ATLAS collaboration. Additionally, they introduced a third SUSY-breaking sector and showed that this can result in cascades of the pseudo-goldstini leading to multiphoton final states.

We restricted ourselves to the cases in which the gaugino-like neutralino and stau are the LOSP. However, the case in which the neutralino LOSP has a large higgsino component is also worth to be studied and the same holds for a chargino LOSP. The collider signatures of these two cases have been studied in [204, 278, 279]. The goldstini scenario with a higgsino-like LOSP was also shown [280] to be able to explain a 3.0σ excess in events featuring a Z-peaked same-flavour opposite-sign lepton pair recently observed by the ATLAS collaboration. The LOSP could however also be a coloured SUSY particle and this case has not been investigated up to now.

We also would like to suggest that models like the one we have presented here, where the missing energy is carried away by two different particles, one rather massive and the other almost massless, and with similar couplings but with different strength, deserve to be considered in LHC data analysis.

7.3 General squark flavour mixing: constraints, phenomenology and benchmarks

The minimal flavour violation (MFV) paradigm of supersymmetry assumes that all flavour properties of the model stem from the diagonalization of the SM Yukawa matrices so that all flavour-violating effects are related to the CKM and PMNS matrices. In this project, we went beyond MFV and studied to which

extent non-minimal flavour violation (NMFV) in the squark sector is still allowed given the current indirect experimental constraints coming from the low-energy flavour-observables, the anomalous magnetic moment of the muon and the mass of the recently discovered BEH boson.

We adopted a phenomenological approach and start from a pMSSM-like parametrisation of the MSSM. Contrary to the MFV case, we now also allow for off-diagonal NMFV entries in the squark soft masses and trilinear couplings. Since any mixing involving the first generation squarks is strongly constrained by kaon-mixing, we only consider mixing between the second and third generation squarks which leaves us with 7 NMFV parameters. Contrary to most previous work on NMFV which only varies one or two NMFV parameters at a time, we allow all our NMFV parameters to vary at the same time. After slightly reducing the usual pMSSM parameter space, our NMFV model has 19 free parameters.

We probe this parameter space by means of the Markov Chain Monte Carlo (MCMC) scanning technique which probes the parameter space guided by the likelihood of the parameter points. Starting from a prior distribution quantifying theoretical constraints and the initial knowledge about the parameters, the MCMC yields a posterior distribution which is proportional to the real likelihood distribution based on the imposed theoretical and experimental constraints. Comparing the prior and posterior distributions gives insight in how the imposed experimental data can influence the likelihood distributions of the parameters.

We found that the typical mass spectrum of the squarks within NMFV supersymmetry can considerably differ from the one in MFV SUSY. Within NMFV the first and second generation soft squark masses are theoretically restricted to be rather low to avoid taychons in the Higgs sector. Consequently, the masses of the first two generations are pushed towards lower values and, unlike the usual MFV SUSY scenarios, the lightest squarks are generally not the third generation squarks. Requiring a theoretically consistent Higgs sector and a light Higgs boson with a mass of 125 GeV similarly restricts the left-right and right-left flavour-violating NMFV parameters $\delta^{u,d}_{LR/RL}$ to be small. On the other hand, the NMFV parameters δ_{LL} and δ^{d}_{RR} are mainly constrained by the neutral B-meson oscillations while the rare $B_s \to \mu\mu$ decay mainly influences δ^{u}_{RL}. All other NMFV parameters are left unconstrained by the considered experimental observations.

Based on the points with the highest likelihood in our scan, we selected four benchmark scenarios, allowed by the current data, which cover different phenomenological features of NMFV SUSY and can be relevant for future LHC searches.

Outlook

This work was only a first step towards a comprehensive study of NMFV in the squark sector. In our study, we restricted ourselves to indirect experimental constraints. Direct constraints from collider searches might however also have a

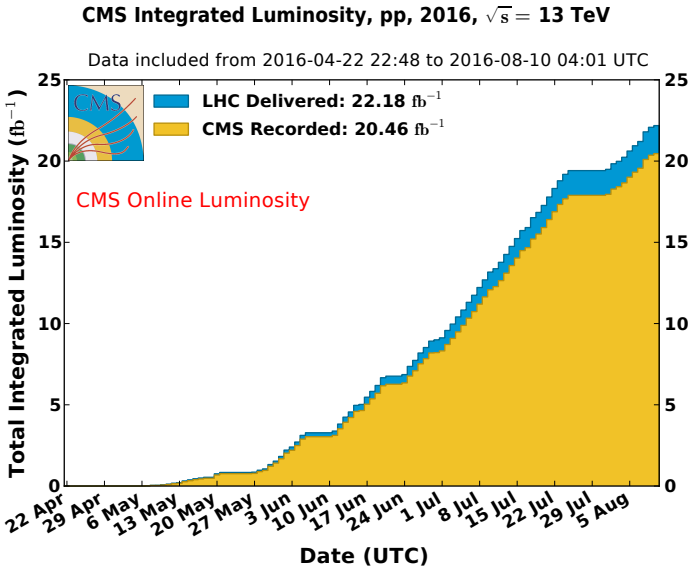

Figure 7.1: Cumulative luminosity measured online versus day delivered to (blue), and recorded by CMS (orange) during stable beams and for pp collisions at 13 TeV centre-of-mass energy in 2016. Figure and caption taken from [282].

large impact on the constraints on the parameter space and could be included in a next stage.

We could also improve the MCMC scan itself. It would be interesting to run a scan for different kinds of priors to see whether our results are robust. Also, we can wonder whether NMFV SUSY fits the data better compared to the usual MFV SUSY case and if the higher level of complexity due to the extra parameters is worth the improvement. This could be done by using an alternative implementation of MCMC scanning technique which also calculates the Bayesian evidence as is done for example in [281].

Finally, we would like to stress that flavour-violating effects can have important consequences for collider searches. For example (*cfr.* the references mentioned in section 6.2.3), FV effects can loosen the current experimental constraints on the stop mass, they can have an influence on the level of fine-tuning of the model and they can lead to signatures which are currently not probed at colliders. As we have shown in our work, indirect constraints still allow for flavour violation in the squark sector and it is therefore important to take FV effects on the collider signatures into account.

7.4 Overall outlook

The cumulative integrated luminosity at 13 TeV collected by the CMS experiment during the last three months is shown in figure 7.1 and we can see that the

LHC is performing very well. CMS and ATLAS each collected already about 20 fb^{-1} of data, more than the whole 8 TeV data set of Run 1. By the beginning of August 2016, ATLAS and CMS presented the first results on their 13 fb^{-1} dataset. A promising diphoton resonance at 750 GeV presented a few months earlier by both ATLAS and CMS [283,284] now appeared to be a mere statistical fluctuation [285,286] and no other sign of SUSY or any other physics beyond the Standard Model has been observed up to now. However, there remain many more analyses to be done and, as was demonstrated in this thesis, SUSY might still be hiding somewhere. The LHC will continue collecting data until the end of October 2016 after which there will be a technical stop to prepare for the next period of data taking. The dataset collected by then should give us an idea of the (hopefully new) physics within reach of the LHC.

7.5 Overview of my contributions

As a final conclusion, I can now come back to the overview of my publications and indicate my own contributions:

- A. Alloul, J. D'Hondt, K. De Causmaecker, B. Fuks and M. Rausch de Traubenberg, *Automated mass spectrum generation for new physics*, *Eur. Phys. J.* **C73** (2013) 2325, [arxiv:1301.5932]

  I am the author of ASperGe*, the numerical code performing numerical mass matrix diagonalisation and I also worked on the interfaces with* FeynRules *and* MadGraph5*. To complete this project, I participated in the* 2012 FeynRules *workshop in Mont Sainte-Odile and the* 2012 MadGraph *meeting in Natal.*

- J. D'Hondt, K. De Causmaecker, B. Fuks, A. Mariotti, K. Mawatari, C. Petersson and D. Redigolo, *Multilepton signals of gauge mediated supersymmetry breaking at the LHC*, *Phys. Lett.* **B731** (2014) 7-12, [arxiv:1310.0018]

  In this project, we all had more or less an equal contribution. I participated in a broad and deep discussion together with the other authors and I gave an oral presentation of this work at the SUSY2014 conference in Manchester.

- R. Argurio, K. De Causmaecker, G. Ferretti, A. Mariotti, K. Mawatari and Y. Takaesu, *Collider signatures of goldstini in gauge mediation*, *JHEP* **06** (2012) 096, [arxiv:1112.5058]

  I joined this project right after starting my PhD in the VUB phenomenology group in October 2011. While I was learning the basics of supersymmetric theories and collider phenomenology, I helped in practice with the analyses.

- K. De Causmaecker, B. Fuks, B. Herrmann, F. Mahmoudi, B. O'Leary, W. Porod, S. Sekmen and N. Strobbe, *General squark flavour mixing:*

constraints phenomenology and benchmarks, *JHEP* **11** (2015) 125, [arxiv:1509.05414]

I was one of the driving forces behind this project and my involvement in the development of the ideas was significant. I am the author of the MCMC code and I have done all the parameter scans by using the CERN and IIHE clusters. I also did the visualisation of the data, provided all the figures and wrote parts of the paper.

- G. Brooijmans et al., *Les Houches 2013: Physics at TeV Colliders: New Physics Working Group Report*, (2014), [arxiv:1405.1617]

  The preliminary results of the above project were presented in this report.

Appendices

Appendix A

Conventions

Throughout this thesis, we assume

$$\hbar \equiv \frac{h}{2\pi} = c = 1 \tag{A.1}$$

where h and c are respectively Planck's constant and the velocity of light. We also follow the Einstein summation convention: the sum over a repeated upper and lower index is always implicitly understood and we do not explicitly write the summation sign.

A.1 Lorentz indices

The Minkowski metric $g_{\mu\nu}$ and its inverse $g^{\mu\nu}$ are given by

$$g_{\mu\nu} = g^{\mu\nu} = \text{diag}(1, -1, -1, -1) \tag{A.2}$$

so that

$$g_{\mu\nu} g^{\nu\rho} = \delta_{\mu}{}^{\rho} \tag{A.3}$$

where the sum over repeated indices is implicitly understood. Summing over an upper and a lower index, as we did for the index ν in equation (A.3), is referred to as contracting indices. The Minkowski metric is used to define the norm of a four-vector x^μ as

$$x^2 \equiv x^\mu x_\mu = g_{\mu\nu} x^\mu x^\nu \tag{A.4}$$

and the group of transformations leaving this norm invariant is called the Lorentz group. Under a Lorentz transformation x^μ transforms as

$$x^\mu \to \Lambda^\mu{}_\nu x^\nu \tag{A.5}$$

which leaves $x^\mu x_\mu$ invariant so that

$$g_{\mu\nu} \Lambda^\mu{}_\alpha \Lambda^\nu{}_\beta = g_{\alpha\beta}. \tag{A.6}$$

As a consequence, contracting all Lorentz indices in an expression ensures that this expression will Lorentz invariant.

A.2 The Pauli matrices

The four-vectors $\sigma^\mu = (1, \sigma^i)$ and $\bar{\sigma}^\mu = (1, -\sigma^i)$ are built upon the Pauli matrices σ^i, $i = 1, 2, 3$, the unitary and hermitian 2×2 matrices given by

$$\sigma^1 = \begin{pmatrix} 0 & 1 \\ 1 & 0 \end{pmatrix}, \qquad \sigma^2 = \begin{pmatrix} 0 & -i \\ i & 0 \end{pmatrix}, \qquad \sigma^3 = \begin{pmatrix} 1 & 0 \\ 0 & -1 \end{pmatrix}. \tag{A.7}$$

We further define $\sigma^{\mu\nu}$ and $\bar{\sigma}^{\mu\nu}$ as

$$\sigma^{\mu\nu} = \frac{i}{4}\left(\sigma^\mu \bar{\sigma}^\nu - \sigma^\nu \bar{\sigma}^\mu\right) \qquad \text{and} \qquad \bar{\sigma}^{\mu\nu} = \frac{i}{4}\left(\bar{\sigma}^\mu \sigma^\nu - \bar{\sigma}^\nu \sigma^\mu\right). \tag{A.8}$$

A.3 The Gell-mann matrices

The Gell-mann matrices form one possible representation for the generators of SU(3). They are traceless and hermitian and are given

$$\lambda_1 = \begin{pmatrix} 0 & 1 & 0 \\ 1 & 0 & 0 \\ 0 & 0 & 0 \end{pmatrix} \qquad \lambda_2 = \begin{pmatrix} 0 & -i & 0 \\ i & 0 & 0 \\ 0 & 0 & 0 \end{pmatrix} \qquad \lambda_3 = \begin{pmatrix} 1 & 0 & 0 \\ 0 & -1 & 0 \\ 0 & 0 & 0 \end{pmatrix}$$

$$\lambda_4 = \begin{pmatrix} 0 & 0 & 1 \\ 0 & 0 & 0 \\ 1 & 0 & 0 \end{pmatrix} \lambda_5 = \begin{pmatrix} 0 & 0 & -i \\ 0 & 0 & 0 \\ i & 0 & 0 \end{pmatrix}$$

$$\lambda_6 = \begin{pmatrix} 0 & 0 & 0 \\ 0 & 0 & 1 \\ 0 & 1 & 0 \end{pmatrix} \qquad \lambda_7 = \begin{pmatrix} 0 & 0 & 0 \\ 0 & 0 & -i \\ 0 & i & 0 \end{pmatrix} \qquad \lambda_8 = \frac{1}{\sqrt{3}} \begin{pmatrix} 1 & 0 & 0 \\ 0 & 1 & 0 \\ 0 & 0 & -2 \end{pmatrix}.$$

Appendix B

The Markov Chain Monte Carlo scanning technique

B.1 The convergence test of Gelman and Rubin

When probing the parameter space using the Markov Chain Monte Carlo scanning technique, it is important to check whether the chains are converging. One of the necessary conditions for convergence, is the convergence test of Gelman and Rubin [231]. Their test is based on the Possible Scale Reduction Factor (PSRF) which should approach one if the chains are converging well. Suppose we perform a parameter scan over a parameter θ using m chains, each containing n points. Each parameter value is denoted by θ_i^t where $i \in 1 \ldots m$ and $t \in 1 \ldots n$ respectively specify the chain and the place within the chain. The simplest version of the PRSF can then be defined as

$$\text{PSRF} = \sqrt{\frac{n-1}{n} + \frac{m+1}{mn}\frac{B}{W}} \tag{B.1}$$

where B is the variance among the chains of the averages within the chain

$$B = \frac{1}{m-1}\sum_{i=1}^{m}\left(\bar{\theta}_i - \bar{\bar{\theta}}\right)^2 \tag{B.2}$$

and W is the average among the chains of the variances within the chain

$$W = \frac{1}{m}\sum_{i=1}^{m} s_i^2 \tag{B.3}$$

where the variance is given by

$$s_i^2 = \frac{1}{n-1}\sum_{t}^{n}\left(\theta_i^t - \bar{\theta}_i\right)^2. \tag{B.4}$$

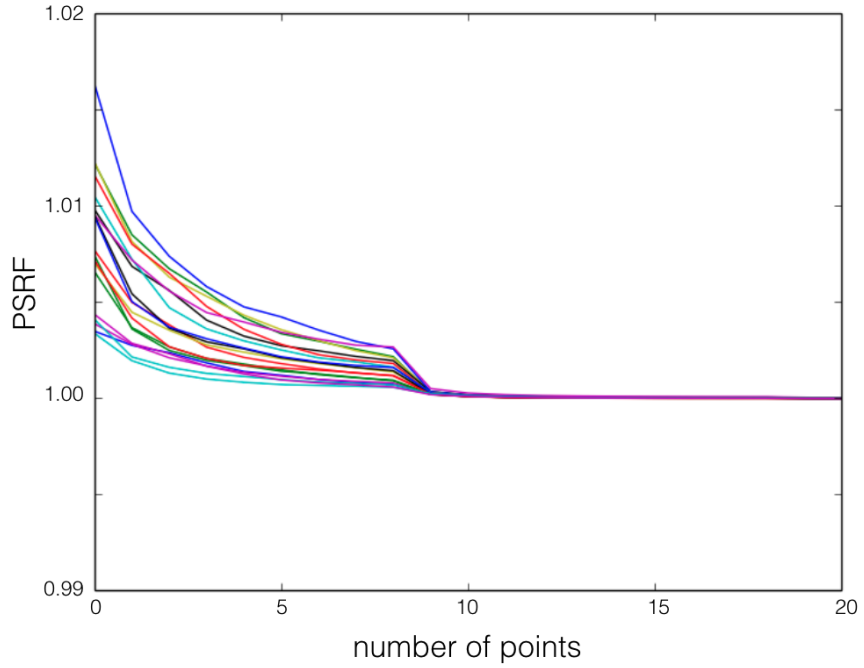

Figure B.1: The PSRF for the scan including all experimental observables after removing the burn-in length, *i.e.* the first 15% of the points. Every line corresponds to one input parameter. The PSRF for the scans including only one of the observables exhibits a similar behaviour.

The PSRF can be calculated at every iteration in the chain and and example is shown in figure B.1. For all variables it converges to one, as it should, and our MCMC passes the test. It should however be noted that this test is a necessary requirement for convergence but it is not sufficient, it not possible to prove that our final distributions converge to the real distributions.

B.2 Optimizing the Metropolis algorithm

In section 6.3.1, we discussed the Metropolis algorithm to perform an MCMC scan. In the second step of this algorithm, we choose the next point in the parameter space by drawing a point from a Gaussian distribution around the previous point. The standard deviation of this Gaussian distribution has to be chosen well in order to optimize the convergence of the sample.

Figure B.2 shows the PSRF of the input parameter $\tan\beta$ of a MCMC scan similar to the scan of which the results are presented in chapter 6 and compares the convergence for several choices of the standard deviation $w = 0.01$, 0.05 and 0.1. Choosing w too small, would imply that the scan risks to get stuck in a local minimum while a too large standard deviation becomes very inefficient: in the

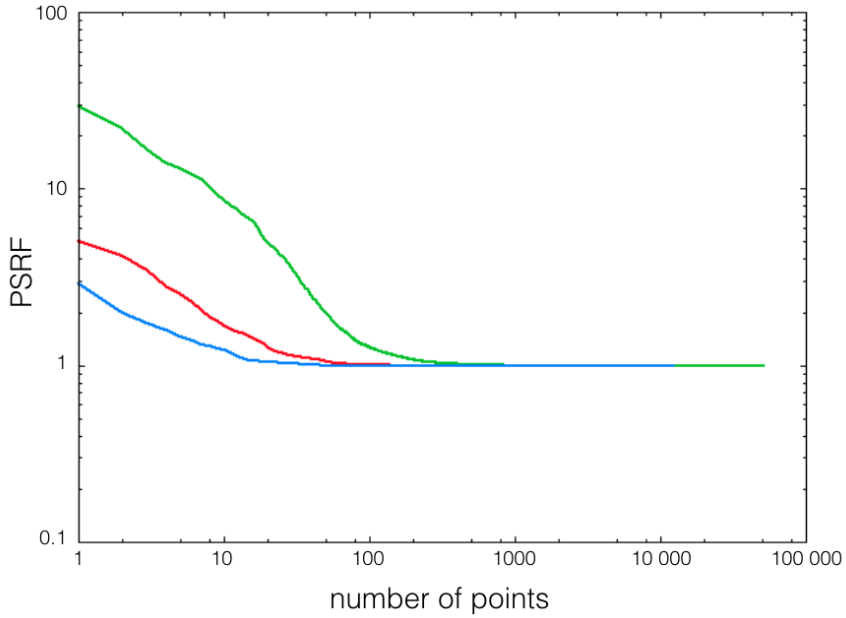

Figure B.2: The PSRF for $\tan\beta$ for three values of the standard deviation $w = 0.1$ (blue), 0.05 (red) and 0.01 (green).

limit where $w = 1$, we would need equally many points to probe the parameter space as we would need in a gridscan.

Indeed, we observed that the chains with a low standard deviation $w = 0.01$ had the tendency to get stuck in local maxima resulting in irregularities in the posterior distributions while, on the other hand, the chains with a large standard deviation $w = 0.1$ were very inefficient. The intermediate value $w = 0.05$ shows a good balance between the two extremes, this is the standard deviation we chose for our scan.

Bibliography

Bibliography

[1] Retrieved from `http://www.quantumdiaries.org/2014/03/14/the-standard-model-a-beautiful-but-flawed-theory/` on May 14, 2016.

[2] J. Goldstone, A. Salam and S. Weinberg, *Broken Symmetries*, *Phys. Rev.* **127** (1962) 965–970.

[3] F. Englert and R. Brout, *Broken Symmetry and the Mass of Gauge Vector Mesons*, *Phys. Rev. Lett.* **13** (1964) 321–323.

[4] P. W. Higgs, *Broken symmetries, massless particles and gauge fields*, *Phys. Lett.* **12** (1964) 132–133.

[5] P. W. Higgs, *Broken Symmetries and the Masses of Gauge Bosons*, *Phys. Rev. Lett.* **13** (1964) 508–509.

[6] G. S. Guralnik, C. R. Hagen and T. W. B. Kibble, *Global Conservation Laws and Massless Particles*, *Phys. Rev. Lett.* **13** (1964) 585–587.

[7] S. L. Glashow, *Partial Symmetries of Weak Interactions*, *Nucl. Phys.* **22** (1961) 579–588.

[8] S. Weinberg, *A Model of Leptons*, *Phys. Rev. Lett.* **19** (1967) 1264–1266.

[9] A. Salam, *Weak and electromagnetic interactions*, in *Elementary particle theory* (N. Svartholm, ed.), pp. 367–377, Almquist & Wiksell.

[10] M. Gell-Mann, *Symmetries of baryons and mesons*, *Phys. Rev.* **125** (1962) 1067–1084.

[11] M. Gell-Mann, *A Schematic Model of Baryons and Mesons*, *Phys. Lett.* **8** (1964) 214–215.

[12] D. J. Gross and F. Wilczek, *Ultraviolet Behavior of Nonabelian Gauge Theories*, *Phys. Rev. Lett.* **30** (1973) 1343–1346.

[13] D. J. Gross and F. Wilczek, *Asymptotically Free Gauge Theories. 1*, *Phys. Rev.* **D8** (1973) 3633–3652.

[14] D. J. Gross and F. Wilczek, *Asymptotically Free Gauge Theories. 2.*, *Phys. Rev.* **D9** (1974) 980–993.

[15] H. D. Politzer, *Reliable Perturbative Results for Strong Interactions?*, *Phys. Rev. Lett.* **30** (1973) 1346–1349.

[16] H. D. Politzer, *Asymptotic Freedom: An Approach to Strong Interactions*, *Phys. Rept.* **14** (1974) 129–180.

[17] N. Cabibbo, *Unitary Symmetry and Leptonic Decays*, *Phys. Rev. Lett.* **10** (1963) 531–533.

[18] M. Kobayashi and T. Maskawa, *CP Violation in the Renormalizable Theory of Weak Interaction*, *Prog. Theor. Phys.* **49** (1973) 652–657.

[19] B. Pontecorvo, *Inverse beta processes and nonconservation of lepton charge*, *Sov. Phys. JETP* **7** (1958) 172–173.

[20] Z. Maki, M. Nakagawa and S. Sakata, *Remarks on the unified model of elementary particles*, *Prog. Theor. Phys.* **28** (1962) 870–880.

[21] Gfitter Group collaboration, M. Baak, J. Cúth, J. Haller, A. Hoecker, R. Kogler, K. Mönig et al., *The global electroweak fit at NNLO and prospects for the LHC and ILC*, *Eur. Phys. J.* **C74** (2014) 3046, [1407.3792].

[22] ATLAS collaboration, G. Aad et al., *Observation of a new particle in the search for the Standard Model Higgs boson with the ATLAS detector at the LHC*, *Phys.Lett.* **B716** (2012) 1–29, [1207.7214].

[23] CMS collaboration, S. Chatrchyan et al., *Observation of a new boson at a mass of 125 GeV with the CMS experiment at the LHC*, *Phys.Lett.* **B716** (2012) 30–61, [1207.7235].

[24] *The Nobel Prize in Physics 2013*, retrieved from www.nobelprize.org on May 14, 2016.

[25] *GFitter: A Generic Fitter Project for HEP Model Testing*, retrieved from www.project-gfitter.web.cern.ch on May 14, 2016.

[26] J. Charles et al., *Current status of the Standard Model CKM fit and constraints on $\Delta F = 2$ New Physics*, *Phys. Rev.* **D91** (2015) 073007, [1501.05013].

[27] Particle Data Group collaboration, K. A. Olive et al., *Review of Particle Physics*, *Chin. Phys.* **C38** (2014) 090001.

[28] *CKMfitter*, retrieved from `http://ckmfitter.in2p3.fr/` on May 14, 2016.

[29] F. Zwicky, *On the Masses of Nebulae and of Clusters of Nebulae*, *Astrophys. J.* **86** (1937) 217–246.

[30] V. C. Rubin, N. Thonnard and W. K. Ford, Jr., *Rotational properties of 21 SC galaxies with a large range of luminosities and radii, from NGC 4605 /R = 4kpc/ to UGC 2885 /R = 122 kpc/*, *Astrophys. J.* **238** (1980) 471.

[31] Planck collaboration, P. A. R. Ade et al., *Planck 2015 results. XIII. Cosmological parameters*, `1502.01589`.

[32] Super-Kamiokande collaboration, Y. Fukuda et al., *Evidence for oscillation of atmospheric neutrinos*, *Phys. Rev. Lett.* **81** (1998) 1562–1567, [`hep-ex/9807003`].

[33] SNO collaboration, Q. R. Ahmad et al., *Direct evidence for neutrino flavor transformation from neutral current interactions in the Sudbury Neutrino Observatory*, *Phys. Rev. Lett.* **89** (2002) 011301, [`nucl-ex/0204008`].

[34] M. E. Peskin and D. V. Schroeder, *An Introduction to quantum field theory*. 1995.

[35] SLD Electroweak Group, DELPHI, ALEPH, SLD, SLD Heavy Flavour Group, OPAL, LEP Electroweak Working Group, L3 collaboration, S. Schael et al., *Precision electroweak measurements on the Z resonance*, *Phys. Rept.* **427** (2006) 257–454, [`hep-ex/0509008`].

[36] CMS collaboration, S. Chatrchyan et al., *Combined search for the quarks of a sequential fourth generation*, *Phys. Rev.* **D86** (2012) 112003, [`1209.1062`].

[37] ATLAS collaboration, *Search for pair production of heavy top-like quarks decaying to a high-p_{T} W boson and a b quark in the lepton plus jets final state in pp collisions at $\sqrt{s} = 8$ TeV with the ATLAS detector*, ATLAS-CONF-2013-060, 2013.

[38] O. Eberhardt, G. Herbert, H. Lacker, A. Lenz, A. Menzel, U. Nierste et al., *Impact of a Higgs boson at a mass of 126 GeV on the standard model with three and four fermion generations*, *Phys. Rev. Lett.* **109** (2012) 241802, [`1209.1101`].

[39] S. P. Martin, *A Supersymmetry primer*, `hep-ph/9709356`.

[40] A. Djouadi, *The Anatomy of electro-weak symmetry breaking. II. The Higgs bosons in the minimal supersymmetric model*, *Phys. Rept.* **459** (2008) 1–241, [hep-ph/0503173].

[41] S. R. Coleman and J. Mandula, *All Possible Symmetries of the S Matrix*, *Phys. Rev.* **159** (1967) 1251–1256.

[42] R. Haag, J. T. Lopuszanski and M. Sohnius, *All Possible Generators of Supersymmetries of the s Matrix*, *Nucl. Phys.* **B88** (1975) 257.

[43] B. Fuks, *Supersymmetry - When Theory Inspires Experimental Searches*. PhD thesis, U. Strasbourg, 2013. 1401.6277.

[44] P. Z. Skands et al., *SUSY Les Houches accord: Interfacing SUSY spectrum calculators, decay packages, and event generators*, *JHEP* **07** (2004) 036, [hep-ph/0311123].

[45] L. J. Hall, V. A. Kostelecky and S. Raby, *New Flavor Violations in Supergravity Models*, *Nucl. Phys.* **B267** (1986) 415–432.

[46] S. Dimopoulos and D. W. Sutter, *The Supersymmetric flavor problem*, *Nucl. Phys.* **B452** (1995) 496–512, [hep-ph/9504415].

[47] S. L. Glashow, J. Iliopoulos and L. Maiani, *Weak Interactions with Lepton-Hadron Symmetry*, *Phys. Rev.* **D2** (1970) 1285–1292.

[48] MSSM Working Group collaboration, A. Djouadi et al., *The Minimal supersymmetric standard model: Group summary report*, in *GDR (Groupement De Recherche) - Supersymetrie Montpellier, France, April 15-17, 1998*, 1998. hep-ph/9901246.

[49] B. C. Allanach, *SOFTSUSY: a program for calculating supersymmetric spectra*, *Comput. Phys. Commun.* **143** (2002) 305–331, [hep-ph/0104145].

[50] W. Porod, *SPheno, a program for calculating supersymmetric spectra, SUSY particle decays and SUSY particle production at e^+e^- colliders*, *Comput.Phys.Commun.* **153** (2003) 275–315, [hep-ph/0301101].

[51] A. Djouadi, J.-L. Kneur and G. Moultaka, *SuSpect: A Fortran code for the supersymmetric and Higgs particle spectrum in the MSSM*, *Comput. Phys. Commun.* **176** (2007) 426–455, [hep-ph/0211331].

[52] A. H. Chamseddine, R. L. Arnowitt and P. Nath, *Locally Supersymmetric Grand Unification*, *Phys. Rev. Lett.* **49** (1982) 970.

[53] ATLAS collaboration, G. Aad et al., *Summary of the searches for squarks and gluinos using $\sqrt{s} = 8$ TeV pp collisions with the ATLAS experiment at the LHC*, *JHEP* **10** (2015) 054, [1507.05525].

[54] G. F. Giudice and R. Rattazzi, *Theories with gauge mediated supersymmetry breaking*, *Phys. Rept.* **322** (1999) 419–499, [hep-ph/9801271].

[55] P. Meade, N. Seiberg and D. Shih, *General Gauge Mediation*, *Prog. Theor. Phys. Suppl.* **177** (2009) 143–158, [0801.3278].

[56] S. Dimopoulos, S. D. Thomas and J. D. Wells, *Sparticle spectroscopy and electroweak symmetry breaking with gauge mediated supersymmetry breaking*, *Nucl. Phys.* **B488** (1997) 39–91, [hep-ph/9609434].

[57] ATLAS collaboration, G. Aad et al., *Search for photonic signatures of gauge-mediated supersymmetry in 8 TeV pp collisions with the ATLAS detector*, *Phys. Rev.* **D92** (2015) 072001, [1507.05493].

[58] R. Barbieri and G. F. Giudice, *Upper Bounds on Supersymmetric Particle Masses*, *Nucl. Phys.* **B306** (1988) 63.

[59] N. Craig, *The State of Supersymmetry after Run I of the LHC*, in *Beyond the Standard Model after the first run of the LHC Arcetri, Florence, Italy, May 20-July 12, 2013*, 2013. 1309.0528.

[60] *http://twiki.cern.ch/twiki/CMSPublic/PhysicsResultsSUS* .

[61] N. Ellis and M. B. Gavela, eds., *1993 European School of High-Energy Physics, Zakopane, Poland, 12-25 Sep 1993: Proceedings*, 1994.

[62] H. Baer, T. Barklow, K. Fujii, Y. Gao, A. Hoang, S. Kanemura et al., *The International Linear Collider Technical Design Report - Volume 2: Physics*, 1306.6352.

[63] *ILC International Linear Collider*, retrieved from www.linearcollider.org/ILC on March 21, 2016.

[64] CDF collaboration, F. Abe et al., *Observation of top quark production in $\bar{p}p$ collisions*, *Phys. Rev. Lett.* **74** (1995) 2626–2631, [hep-ex/9503002].

[65] D0 collaboration, S. Abachi et al., *Observation of the top quark*, *Phys. Rev. Lett.* **74** (1995) 2632–2637, [hep-ex/9503003].

[66] L. Evans and P. Bryant, *LHC Machine*, *JINST* **3** (2008) S08001.

[67] F. Marcastel, *CERN's Accelerator Complex*, Oct, 2013, Retrieved from https://cds.cern.ch/record/1621583 on March 13, 2016.

[68] CMS collaboration, S. Chatrchyan et al., *The CMS experiment at the CERN LHC*, *JINST* **3** (2008) S08004.

[69] ATLAS collaboration, G. Aad et al., *The ATLAS Experiment at the CERN Large Hadron Collider*, *JINST* **3** (2008) S08003.

[70] ALICE collaboration, K. Aamodt et al., *The ALICE experiment at the CERN LHC*, *JINST* **3** (2008) S08002.

[71] LHCb collaboration, A. A. Alves, Jr. et al., *The LHCb Detector at the LHC*, *JINST* **3** (2008) S08005.

[72] L. Rossi and O. Brüning, *The High Luminosity Large Hadron Collider: the new machine for illuminating the mysteries of Universe*. Advanced series on directions in high energy physics. World Scientific, Hackensack, NJ, 2015.

[73] M. A. Dobbs et al., *Les Houches guidebook to Monte Carlo generators for hadron collider physics*, in *Physics at TeV colliders. Proceedings, Workshop, Les Houches, France, May 26-June 3, 2003*, pp. 411–459, 2004. hep-ph/0403045.

[74] Y. L. Dokshitzer, *Calculation of the Structure Functions for Deep Inelastic Scattering and e+ e- Annihilation by Perturbation Theory in Quantum Chromodynamics.*, *Sov. Phys. JETP* **46** (1977) 641–653.

[75] V. N. Gribov and L. N. Lipatov, *Deep inelastic e p scattering in perturbation theory*, *Sov. J. Nucl. Phys.* **15** (1972) 438–450.

[76] G. Altarelli and G. Parisi, *Asymptotic Freedom in Parton Language*, *Nucl. Phys.* **B126** (1977) 298–318.

[77] NNPDF collaboration, R. D. Ball et al., *Parton distributions for the LHC Run II*, *JHEP* **04** (2015) 040, [1410.8849].

[78] N. D. Christensen and C. Duhr, *FeynRules - Feynman rules made easy*, *Comput. Phys. Commun.* **180** (2009) 1614–1641, [0806.4194].

[79] A. Alloul, N. D. Christensen, C. Degrande, C. Duhr and B. Fuks, *FeynRules 2.0 - A complete toolbox for tree-level phenomenology*, *Comput. Phys. Commun.* **185** (2014) 2250–2300, [1310.1921].

[80] C. Duhr and B. Fuks, *A superspace module for the FeynRules package*, *Comput. Phys. Commun.* **182** (2011) 2404–2426, [1102.4191].

[81] *FeynRules – A mathematica package to calculate Feynman rules*, https://feynrules.irmp.ucl.ac.be/ as visited on May 22, 2016.

[82] A. Pukhov, *CalcHEP 2.3: MSSM, structure functions, event generation, batchs, and generation of matrix elements for other packages*, hep-ph/0412191.

[83] A. Belyaev, N. D. Christensen and A. Pukhov, *CalcHEP 3.4 for collider physics within and beyond the Standard Model*, *Comput. Phys. Commun.* **184** (2013) 1729–1769, [1207.6082].

[84] A. Pukhov, E. Boos, M. Dubinin, V. Edneral, V. Ilyin, D. Kovalenko et al., *CompHEP: A Package for evaluation of Feynman diagrams and integration over multiparticle phase space*, hep-ph/9908288.

[85] CompHEP collaboration, E. Boos, V. Bunichev, M. Dubinin, L. Dudko, V. Ilyin, A. Kryukov et al., *CompHEP 4.4: Automatic computations from Lagrangians to events*, *Nucl. Instrum. Meth.* **A534** (2004) 250–259, [hep-ph/0403113].

[86] T. Hahn and M. Perez-Victoria, *Automatized one loop calculations in four-dimensions and D-dimensions*, *Comput. Phys. Commun.* **118** (1999) 153–165, [hep-ph/9807565].

[87] T. Hahn, *Generating Feynman diagrams and amplitudes with FeynArts 3*, *Comput. Phys. Commun.* **140** (2001) 418–431, [hep-ph/0012260].

[88] T. Hahn, *FormCalc 6*, *PoS* **ACAT08** (2008) 121, [0901.1528].

[89] S. Agrawal, T. Hahn and E. Mirabella, *FormCalc 7*, *J. Phys. Conf. Ser.* **368** (2012) 012054, [1112.0124].

[90] M. Moretti, T. Ohl and J. Reuter, *O'Mega: An Optimizing matrix element generator*, hep-ph/0102195.

[91] W. Kilian, T. Ohl and J. Reuter, *WHIZARD: Simulating Multi-Particle Processes at LHC and ILC*, *Eur.Phys.J.* **C71** (2011) 1742, [0708.4233].

[92] C. Degrande, C. Duhr, B. Fuks, D. Grellscheid, O. Mattelaer and T. Reiter, *UFO - The Universal FeynRules Output*, *Comput. Phys. Commun.* **183** (2012) 1201–1214, [1108.2040].

[93] P. de Aquino, W. Link, F. Maltoni, O. Mattelaer and T. Stelzer, *ALOHA: Automatic Libraries Of Helicity Amplitudes for Feynman Diagram Computations*, *Comput. Phys. Commun.* **183** (2012) 2254–2263, [1108.2041].

[94] G. Cullen, N. Greiner, G. Heinrich, G. Luisoni, P. Mastrolia, G. Ossola et al., *Automated One-Loop Calculations with GoSam*, *Eur. Phys. J.* **C72** (2012) 1889, [1111.2034].

[95] G. Cullen, N. Greiner, G. Heinrich, G. Luisoni, P. Mastrolia, G. Ossola et al., *GoSam: A Program for Automated One-Loop Calculations*, *J. Phys. Conf. Ser.* **368** (2012) 012056, [1111.6534].

[96] M. Bahr et al., *Herwig++ Physics and Manual*, *Eur. Phys. J.* **C58** (2008) 639–707, [0803.0883].

[97] E. Conte, B. Fuks and G. Serret, *MadAnalysis 5, A User-Friendly Framework for Collider Phenomenology*, *Comput. Phys. Commun.* **184** (2013) 222–256, [1206.1599].

[98] J. Alwall, R. Frederix, S. Frixione, V. Hirschi, F. Maltoni, O. Mattelaer et al., *The automated computation of tree-level and next-to-leading order differential cross sections, and their matching to parton shower simulations*, *JHEP* **07** (2014) 079, [1405.0301].

[99] H. Murayama, I. Watanabe and K. Hagiwara, *HELAS: HELicity amplitude subroutines for Feynman diagram evaluations*, .

[100] J. Pumplin, D. R. Stump, J. Huston, H. L. Lai, P. M. Nadolsky and W. K. Tung, *New generation of parton distributions with uncertainties from global QCD analysis*, *JHEP* **07** (2002) 012, [hep-ph/0201195].

[101] C. Borschensky, M. Krämer, A. Kulesza, M. Mangano, S. Padhi, T. Plehn et al., *Squark and gluino production cross sections in pp collisions at* $\sqrt{s}$ *= 13, 14, 33 and 100 TeV*, *Eur. Phys. J.* **C74** (2014) 3174, [1407.5066].

[102] *LHC SUSY Cross Section Working Group*, https://twiki.cern.ch/twiki/bin/view/LHCPhysics/SUSYCrossSections as of May 2016.

[103] G. Belanger, R. M. Godbole, L. Hartgring and I. Niessen, *Top Polarization in Stop Production at the LHC*, *JHEP* **05** (2013) 167, [1212.3526].

[104] CMS collaboration, S. Chatrchyan et al., *Search for top-squark pair production in the single-lepton final state in pp collisions at* $\sqrt{s}$ *= 8 TeV*, *Eur. Phys. J.* **C73** (2013) 2677, [1308.1586].

[105] B. Dumont, B. Fuks and C. Wymant, *MadAnalysis 5 implementation of CMS-SUS-13-011: search for stops in the single lepton final state at 8 TeV*, 2014, doi:10.7484/INSPIREHEP.DATA.LR5T.2RR3.

[106] T. Sjostrand, S. Mrenna and P. Z. Skands, *PYTHIA 6.4 Physics and Manual*, *JHEP* **05** (2006) 026, [hep-ph/0603175].

[107] T. Sjöstrand, S. Ask, J. R. Christiansen, R. Corke, N. Desai, P. Ilten et al., *An Introduction to PYTHIA 8.2*, *Comput. Phys. Commun.* **191** (2015) 159–177, [1410.3012].

[108] A. Buckley et al., *General-purpose event generators for LHC physics*, *Phys. Rept.* **504** (2011) 145–233, [1101.2599].

[109] GEANT4 collaboration, S. Agostinelli et al., *GEANT4: A Simulation toolkit*, *Nucl. Instrum. Meth.* **A506** (2003) 250–303.

[110] DELPHES 3 collaboration, J. de Favereau, C. Delaere, P. Demin, A. Giammanco, V. Lemaître, A. Mertens et al., *DELPHES 3, A modular framework for fast simulation of a generic collider experiment*, *JHEP* **02** (2014) 057, [1307.6346].

[111] M. Cacciari, G. P. Salam and G. Soyez, *FastJet User Manual*, *Eur. Phys. J.* **C72** (2012) 1896, [1111.6097].

[112] E. Conte, B. Dumont, B. Fuks and C. Wymant, *Designing and recasting LHC analyses with MadAnalysis 5*, *Eur. Phys. J.* **C74** (2014) 3103, [1405.3982].

[113] M. Drees, H. Dreiner, D. Schmeier, J. Tattersall and J. S. Kim, *CheckMATE: Confronting your Favourite New Physics Model with LHC Data*, *Comput. Phys. Commun.* **187** (2014) 227–265, [1312.2591].

[114] B. Dumont, B. Fuks, S. Kraml, S. Bein, G. Chalons, E. Conte et al., *Toward a public analysis database for LHC new physics searches using MADANALYSIS 5*, *Eur. Phys. J.* **C75** (2015) 56, [1407.3278].

[115] *MadAnalysis 5 Public Analysis Database (PAD) for recasting LHC results*, http://madanalysis.irmp.ucl.ac.be/wiki/PublicAnalysisDatabase as visited on July 22, 2016.

[116] W. Beenakker, S. Brensing, M. n. Kramer, A. Kulesza, E. Laenen, L. Motyka et al., *Squark and Gluino Hadroproduction*, *Int. J. Mod. Phys.* **A26** (2011) 2637–2664, [1105.1110].

[117] M. Blanke, B. Fuks, I. Galon and G. Perez, *Gluino Meets Flavored Naturalness*, *JHEP* **04** (2016) 044, [1512.03813].

[118] ATLAS collaboration, G. Aad et al., *Search for new phenomena in final states with large jet multiplicities and missing transverse momentum at $\sqrt{s}$=8 TeV proton-proton collisions using the ATLAS experiment*, *JHEP* **10** (2013) 130, [1308.1841].

[119] CMS collaboration, S. Chatrchyan et al., *Search for new physics in the multijet and missing transverse momentum final state in proton-proton collisions at $\sqrt{s}$= 8 TeV*, *JHEP* **06** (2014) 055, [1402.4770].

[120] ATLAS collaboration, G. Aad et al., *Search for Scalar Charm Quark Pair Production in pp Collisions at $\sqrt{s} = 8$ TeV with the ATLAS Detector*, *Phys. Rev. Lett.* **114** (2015) 161801, [1501.01325].

[121] A. Alloul, J. D'Hondt, K. De Causmaecker, B. Fuks and M. Rausch de Traubenberg, *Automated mass spectrum generation for new physics*, *Eur. Phys. J.* **C73** (2013) 2325, [1301.5932].

[122] J. D'Hondt, K. De Causmaecker, B. Fuks, A. Mariotti, K. Mawatari, C. Petersson et al., *Multilepton signals of gauge mediated supersymmetry breaking at the LHC*, *Phys. Lett.* **B731** (2014) 7–12, [1310.0018].

[123] CMS collaboration, S. Chatrchyan et al., *Search for anomalous production of events with three or more leptons in pp collisions at $\sqrt{(}s) = 8$ TeV*, *Phys. Rev.* **D90** (2014) 032006, [1404.5801].

[124] CMS collaboration, *A search for anomalous production of events with three or more leptons using 19.5/fb of sqrt(s)=8 TeV LHC data*, CMS-PAS-SUS-13-002, 2013.

[125] S. Ambrosanio, G. D. Kribs and S. P. Martin, *Three body decays of selectrons and smuons in low-energy supersymmetry breaking models*, *Nucl. Phys.* **B516** (1998) 55–69, [hep-ph/9710217].

[126] J. T. Ruderman and D. Shih, *Slepton co-NLSPs at the Tevatron*, *JHEP* **11** (2010) 046, [1009.1665].

[127] J. L. Evans, D. E. Morrissey and J. D. Wells, *Higgs boson exempt no-scale supersymmetry and its collider and cosmology implications*, *Phys. Rev.* **D75** (2007) 055017, [hep-ph/0611185].

[128] P. Grajek, A. Mariotti and D. Redigolo, *Phenomenology of General Gauge Mediation in light of a 125 GeV Higgs*, *JHEP* **07** (2013) 109, [1303.0870].

[129] G. Bozzi, B. Fuks and M. Klasen, *Transverse-momentum resummation for slepton-pair production at the CERN LHC*, *Phys. Rev.* **D74** (2006) 015001, [hep-ph/0603074].

[130] G. Bozzi, B. Fuks and M. Klasen, *Threshold Resummation for Slepton-Pair Production at Hadron Colliders*, *Nucl. Phys.* **B777** (2007) 157–181, [hep-ph/0701202].

[131] G. Bozzi, B. Fuks and M. Klasen, *Joint resummation for slepton pair production at hadron colliders*, *Nucl. Phys.* **B794** (2008) 46–60, [0709.3057].

[132] B. Fuks, M. Klasen, D. R. Lamprea and M. Rothering, *Precision predictions for electroweak superpartner production at hadron colliders with Resummino*, *Eur. Phys. J.* **C73** (2013) 2480, [1304.0790].

[133] B. Fuks, M. Klasen, D. R. Lamprea and M. Rothering, *Revisiting slepton pair production at the Large Hadron Collider*, *JHEP* **01** (2014) 168, [1310.2621].

[134] W. Beenakker, M. Klasen, M. Kramer, T. Plehn, M. Spira and P. M. Zerwas, *The Production of charginos / neutralinos and sleptons at hadron colliders*, *Phys. Rev. Lett.* **83** (1999) 3780–3783, [hep-ph/9906298].

[135] R. Argurio, K. De Causmaecker, G. Ferretti, A. Mariotti, K. Mawatari and Y. Takaesu, *Collider signatures of goldstini in gauge mediation*, *JHEP* **06** (2012) 096, [1112.5058].

[136] K. Mawatari and Y. Takaesu, *HELAS and MadGraph with goldstinos*, *Eur. Phys. J.* **C71** (2011) 1640, [1101.1289].

[137] J. Alwall, M. Herquet, F. Maltoni, O. Mattelaer and T. Stelzer, *MadGraph 5 : Going Beyond*, *JHEP* **06** (2011) 128, [1106.0522].

[138] S. Jadach, Z. Was, R. Decker and J. H. Kuhn, *The tau decay library TAUOLA: Version 2.4*, *Comput. Phys. Commun.* **76** (1993) 361–380.

[139] S. Ovyn, X. Rouby and V. Lemaitre, *DELPHES, a framework for fast simulation of a generic collider experiment*, 0903.2225.

[140] J.-L. Agram, J. Andrea, E. Conte, B. Fuks, D. Gelé and P. Lansonneur, *Probing top anomalous couplings at the LHC with trilepton signatures in the single top mode*, *Phys. Lett.* **B725** (2013) 123–126, [1304.5551].

[141] M. Cacciari, G. P. Salam and G. Soyez, *The Anti-k(t) jet clustering algorithm*, *JHEP* **04** (2008) 063, [0802.1189].

[142] ATLAS collaboration, *Search for direct-slepton and direct-chargino production in final states with two opposite-sign leptons, missing transverse momentum and no jets in 20/fb of pp collisions at sqrt(s) = 8 TeV with the ATLAS detector*, ATLAS-CONF-2013-049, 2013.

[143] CMS collaboration, *Search for electroweak production of charginos, neutralinos, and sleptons using leptonic final states in pp collisions at 8 TeV*, CMS-PAS-SUS-13-006, 2013.

[144] OPAL collaboration, G. Abbiendi et al., *Searches for gauge-mediated supersymmetry breaking topologies in e+ e- collisions at LEP2*, *Eur. Phys. J.* **C46** (2006) 307–341, [hep-ex/0507048].

[145] ATLAS collaboration, G. Aad et al., *Search for the electroweak production of supersymmetric particles in $\sqrt{s}$=8 TeV pp collisions with the ATLAS detector*, *Phys. Rev.* **D93** (2016) 052002, [1509.07152].

[146] CMS collaboration, *Search for electroweak production of charginos in final states with two tau leptons in pp collisions at $\sqrt{s} = 8$ TeV*, CMS-PAS-SUS-14-022, 2016.

[147] CMS collaboration, *Search for RPV SUSY in the four-lepton final state*, CMS-PAS-SUS-13-010, 2013.

[148] ATLAS collaboration, *Search for supersymmetry in events with four or more leptons in 21 fb^{-1} of pp collisions at $\sqrt{s} = 8$ TeV with the ATLAS detector*, ATLAS-CONF-2013-036, 2013.

[149] ATLAS collaboration, *Search for electroweak production of supersymmetric particles in final states with at least two hadronically decaying taus and missing transverse momentum with the ATLAS detector in proton-proton collisions at $\sqrt{s} = 8$ TeV*, ATLAS-CONF-2013-028, 2013.

[150] *http://twiki.cern.ch/twiki/AtlasPublic/SupersymmetryPublicResults* .

[151] CDF collaboration, T. Aaltonen et al., *Search for Supersymmetry with Gauge-Mediated Breaking in Diphoton Events with Missing Transverse Energy at CDF II*, *Phys. Rev. Lett.* **104** (2010) 011801, [0910.3606].

[152] CMS collaboration, S. Chatrchyan et al., *Search for Supersymmetry in pp Collisions at $\sqrt{s} = 7$ TeV in Events with Two Photons and Missing Transverse Energy*, *Phys. Rev. Lett.* **106** (2011) 211802, [1103.0953].

[153] CMS collaboration, S. Chatrchyan et al., *Search for supersymmetry in events with a lepton, a photon, and large missing transverse energy in pp collisions at $\sqrt{s} = 7$ TeV*, *JHEP* **06** (2011) 093, [1105.3152].

[154] ATLAS collaboration, G. Aad et al., *Search for Diphoton Events with Large Missing Transverse Energy with 36 pb^{-1} of 7 TeV Proton-Proton Collision Data with the ATLAS Detector*, *Eur. Phys. J.* **C71** (2011) 1744, [1107.0561].

[155] ATLAS collaboration, G. Aad et al., *Search for diphoton events with large missing transverse momentum in fb^{-1} of 7 TeV proton–proton collision data with the ATLAS detector*, *Phys. Lett.* **B710** (2012) 519–537, [1111.4116].

[156] K. Benakli and C. Moura, *Brane-Worlds Pseudo-Goldstinos*, *Nucl. Phys.* **B791** (2008) 125–163, [0706.3127].

[157] C. Cheung, Y. Nomura and J. Thaler, *Goldstini*, *JHEP* **03** (2010) 073, [1002.1967].

[158] C. Cheung, J. Mardon, Y. Nomura and J. Thaler, *A Definitive Signal of Multiple Supersymmetry Breaking*, *JHEP* **07** (2010) 035, [1004.4637].

[159] N. Craig, J. March-Russell and M. McCullough, *The Goldstini Variations*, *JHEP* **10** (2010) 095, [1007.1239].

[160] M. McCullough, *Stimulated Supersymmetry Breaking*, *Phys. Rev.* **D82** (2010) 115016, [1010.3203].

[161] H.-C. Cheng, W.-C. Huang, I. Low and A. Menon, *Goldstini as the decaying dark matter*, *JHEP* **03** (2011) 019, [1012.5300].

[162] K. I. Izawa, Y. Nakai and T. Shimomura, *Higgs Portal to Visible Supersymmetry Breaking*, *JHEP* **03** (2011) 007, [1101.4633].

[163] J. Thaler and Z. Thomas, *Goldstini Can Give the Higgs a Boost*, *JHEP* **07** (2011) 060, [1103.1631].

[164] C. Cheung, F. D'Eramo and J. Thaler, *The Spectrum of Goldstini and Modulini*, *JHEP* **08** (2011) 115, [1104.2600].

[165] D. Bertolini, K. Rehermann and J. Thaler, *Visible Supersymmetry Breaking and an Invisible Higgs*, *JHEP* **04** (2012) 130, [1111.0628].

[166] R. Argurio, Z. Komargodski and A. Mariotti, *Pseudo-Goldstini in Field Theory*, *Phys. Rev. Lett.* **107** (2011) 061601, [1102.2386].

[167] B. C. Allanach et al., *The Snowmass points and slopes: Benchmarks for SUSY searches*, *Eur. Phys. J.* **C25** (2002) 113–123, [hep-ph/0202233].

[168] CDF collaboration, T. Aaltonen et al., *Search for Supersymmetry with Gauge-Mediated Breaking in Diphoton Events with Missing Transverse Energy at CDF II*, *Phys. Rev. Lett.* **104** (2010) 011801, [0910.3606].

[169] D0 collaboration, V. M. Abazov et al., *Search for diphoton events with large missing transverse energy in 6.3 fb^{-1} of $\mathbf{p\bar{p}}$ collisions at $\sqrt{\mathbf{s}} = \mathbf{1.96}$ TeV*, *Phys. Rev. Lett.* **105** (2010) 221802, [1008.2133].

[170] P. Fayet, *Mixing Between Gravitational and Weak Interactions Through the Massive Gravitino*, *Phys. Lett.* **B70** (1977) 461.

[171] H. K. Dreiner, H. E. Haber and S. P. Martin, *Two-component spinor techniques and Feynman rules for quantum field theory and supersymmetry*, *Phys. Rept.* **494** (2010) 1–196, [0812.1594].

[172] F. Luo, K. A. Olive and M. Peloso, *The Gravitino coupling to broken gauge theories applied to the MSSM*, *JHEP* **10** (2010) 024, [1006.5570].

[173] Z. Komargodski and N. Seiberg, *From Linear SUSY to Constrained Superfields*, *JHEP* **09** (2009) 066, [0907.2441].

[174] S. Ambrosanio, G. L. Kane, G. D. Kribs, S. P. Martin and S. Mrenna, *Search for supersymmetry with a light gravitino at the Fermilab Tevatron and CERN LEP colliders*, *Phys. Rev.* **D54** (1996) 5395–5411, [hep-ph/9605398].

[175] J. L. Feng, S. Su and F. Takayama, *Supergravity with a gravitino LSP*, *Phys. Rev.* **D70** (2004) 075019, [hep-ph/0404231].

[176] P. Fayet, *Lower Limit on the Mass of a Light Gravitino from e+ e- Annihilation Experiments*, *Phys. Lett.* **B175** (1986) 471.

[177] J. L. Lopez, D. V. Nanopoulos and A. Zichichi, *Single photon signals at LEP in supersymmetric models with a light gravitino*, *Phys. Rev.* **D55** (1997) 5813–5825, [hep-ph/9611437].

[178] D. A. Dicus and S. Nandi, *New collider bound on light gravitino mass*, *Phys. Rev.* **D56** (1997) 4166–4169, [hep-ph/9611312].

[179] A. Brignole, F. Feruglio and F. Zwirner, *Signals of a superlight gravitino at e+ e- colliders when the other superparticles are heavy*, *Nucl. Phys.* **B516** (1998) 13–28, [hep-ph/9711516].

[180] L3 collaboration, P. Achard et al., *Single photon and multiphoton events with missing energy in e^+e^- collisions at LEP*, *Phys. Lett.* **B587** (2004) 16–32, [hep-ex/0402002].

[181] DELPHI collaboration, J. Abdallah et al., *Photon events with missing energy in e+ e- collisions at s**(1/2) = 130-GeV to 209-GeV*, *Eur. Phys. J.* **C38** (2005) 395–411, [hep-ex/0406019].

[182] K. Mawatari, B. Oexl and Y. Takaesu, *Associated production of light gravitinos in e^+e^- and $e^-\gamma$ collisions*, *Eur. Phys. J.* **C71** (2011) 1783, [1106.5592].

[183] CDF collaboration, D. Acosta et al., *Limits on extra dimensions and new particle production in the exclusive photon and missing energy signature in $p\bar{p}$ collisions at $\sqrt{s} = 1.8$ TeV*, *Phys. Rev. Lett.* **89** (2002) 281801, [hep-ex/0205057].

[184] J. Yi, W.-G. Ma, L. Han, Z.-H. Yu and H. Pietschmann, *Pair production of neutralinos via gluon-gluon collisions*, *Phys. Rev.* **D62** (2000) 035006, [hep-ph/0003291].

[185] S. Abel, M. J. Dolan, J. Jaeckel and V. V. Khoze, *Phenomenology of Pure General Gauge Mediation*, *JHEP* **12** (2009) 001, [0910.2674].

[186] S. Abel, M. J. Dolan, J. Jaeckel and V. V. Khoze, *Pure General Gauge Mediation for Early LHC Searches*, *JHEP* **12** (2010) 049, [1009.1164].

[187] P. Meade, M. Reece and D. Shih, *Prompt Decays of General Neutralino NLSPs at the Tevatron*, *JHEP* **05** (2010) 105, [0911.4130].

[188] J. T. Ruderman and D. Shih, *General Neutralino NLSPs at the Early LHC*, *JHEP* **08** (2012) 159, [1103.6083].

[189] Y. Kats, P. Meade, M. Reece and D. Shih, *The Status of GMSB After 1/fb at the LHC*, *JHEP* **02** (2012) 115, [1110.6444].

[190] H. Baer, B. W. Harris and M. H. Reno, *Next-to-leading order slepton pair production at hadron colliders*, *Phys. Rev.* **D57** (1998) 5871–5874, [hep-ph/9712315].

[191] F. del Aguila and L. Ametller, *On the detectability of sleptons at large hadron colliders*, *Phys. Lett.* **B261** (1991) 326–333.

[192] F. Borzumati and K. Hagiwara, *Testing supersymmetry at the LHC through gluon-fusion production of a slepton pair*, *JHEP* **03** (2011) 103, [0912.0454].

[193] C. G. Lester and D. J. Summers, *Measuring masses of semiinvisibly decaying particles pair produced at hadron colliders*, *Phys. Lett.* **B463** (1999) 99–103, [hep-ph/9906349].

[194] D. R. Tovey, *On measuring the masses of pair-produced semi-invisibly decaying particles at hadron colliders*, *JHEP* **04** (2008) 034, [0802.2879].

[195] A. J. Barr and C. G. Lester, *A Review of the Mass Measurement Techniques proposed for the Large Hadron Collider*, *J. Phys.* **G37** (2010) 123001, [1004.2732].

[196] H.-C. Cheng and J. Gu, *Measuring Invisible Particle Masses Using a Single Short Decay Chain*, *JHEP* **10** (2011) 094, [1109.3471].

[197] J. M. Lindert, F. D. Steffen and M. K. Trenkel, *Direct stau production at hadron colliders in cosmologically motivated scenarios*, *JHEP* **08** (2011) 151, [1106.4005].

[198] Particle Data Group collaboration, K. Nakamura et al., *Review of particle physics*, *J.Phys.* **G37** (2010) 075021.

[199] CMS collaboration, *Tau identification in CMS*, CMS-PAS-TAU-11-001, 2011.

[200] ATLAS collaboration, *Reconstruction, Energy Calibration, and Identification of Hadronically Decaying Tau Leptons*, ATLAS-CONF-2011-077, 2011.

[201] G. Cowan, K. Cranmer, E. Gross and O. Vitells, *Asymptotic formulae for likelihood-based tests of new physics*, *Eur. Phys. J.* **C71** (2011) 1554, [1007.1727].

[202] S. Y. Choi, K. Hagiwara, Y. G. Kim, K. Mawatari and P. M. Zerwas, *tau polarization in SUSY cascade secays*, *Phys. Lett.* **B648** (2007) 207–212, [hep-ph/0612237].

[203] C. Petersson, A. Romagnoni and R. Torre, *Higgs Decay with Monophoton + MET Signature from Low Scale Supersymmetry Breaking*, *JHEP* **10** (2012) 016, [1203.4563].

[204] K.-i. Hikasa, T. Liu, L. Wang and J. M. Yang, *Pseudo-goldstino and electroweak gauginos at the LHC*, *JHEP* **07** (2014) 065, [1403.5731].

[205] G. Brooijmans et al., *Les Houches 2013: Physics at TeV Colliders: New Physics Working Group Report*, 1405.1617.

[206] K. De Causmaecker, B. Fuks, B. Herrmann, F. Mahmoudi, B. O'Leary, W. Porod et al., *General squark flavour mixing: constraints, phenomenology and benchmarks*, *JHEP* **11** (2015) 125, [1509.05414].

[207] F. Gabbiani and A. Masiero, *FCNC in Generalized Supersymmetric Theories*, *Nucl.Phys.* **B322** (1989) 235.

[208] M. Ciuchini, A. Masiero, P. Paradisi, L. Silvestrini, S. Vempati et al., *Soft SUSY breaking grand unification: Leptons versus quarks on the flavor playground*, *Nucl.Phys.* **B783** (2007) 112–142, [hep-ph/0702144].

[209] F. Gabbiani, E. Gabrielli, A. Masiero and L. Silvestrini, *A Complete analysis of FCNC and CP constraints in general SUSY extensions of the standard model*, *Nucl.Phys.* **B477** (1996) 321–352, [hep-ph/9604387].

[210] Particle Data Group collaboration, J. Beringer et al., *Review of Particle Physics (RPP)*, *Phys.Rev.* **D86** (2012) 010001.

[211] M. Ciuchini, E. Franco, D. Guadagnoli, V. Lubicz, M. Pierini, V. Porretti et al., *D - $\bar{D}$ mixing and new physics: General considerations and constraints on the MSSM*, *Phys. Lett.* **B655** (2007) 162–166, [hep-ph/0703204].

[212] M. Artuso, D. Asner, P. Ball, E. Baracchini, G. Bell et al., *B, D and K decays*, *Eur.Phys.J.* **C57** (2008) 309–492, [0801.1833].

[213] S. Heinemeyer, W. Hollik, F. Merz and S. Penaranda, *Electroweak precision observables in the MSSM with nonminimal flavor violation*, *Eur.Phys.J.* **C37** (2004) 481–493, [hep-ph/0403228].

[214] K. Kowalska, *Phenomenology of SUSY with General Flavour Violation*, *JHEP* **1409** (2014) 139, [1406.0710].

[215] T. Hurth and W. Porod, *Flavour violating squark and gluino decays*, *JHEP* **0908** (2009) 087, [0904.4574].

[216] A. Bartl et al., *Impact of squark generation mixing on the search for gluinos at LHC*, *Phys.Lett.* **B679** (2009) 260–266, [0905.0132].

[217] A. Bartl et al., *Impact of squark generation mixing on the search for squarks decaying into fermions at LHC*, *Phys.Lett.* **B698** (2011) 380–388, [1007.5483].

[218] M. Bruhnke, B. Herrmann and W. Porod, *Signatures of bosonic squark decays in non-minimally flavour-violating supersymmetry*, *JHEP* **1009** (2010) 006, [1007.2100].

[219] A. Bartl et al., *Flavour violating gluino three-body decays at LHC*, *Phys.Rev.* **D84** (2011) 115026, [1107.2775].

[220] A. Bartl, H. Eberl, E. Ginina, B. Herrmann, K. Hidaka et al., *Flavor violating bosonic squark decays at LHC*, *Int.J.Mod.Phys.* **A29** (2014) 1450035, [1212.4688].

[221] M. Arana-Catania, S. Heinemeyer and M. Herrero, *Updated Constraints on General Squark Flavor Mixing*, *Phys.Rev.* **D90** (2014) 075003, [1405.6960].

[222] G. Bozzi, B. Fuks, B. Herrmann and M. Klasen, *Squark and gaugino hadroproduction and decays in non-minimal flavour violating supersymmetry*, *Nucl.Phys.* **B787** (2007) 1–54, [0704.1826].

[223] B. Fuks, B. Herrmann and M. Klasen, *Flavour Violation in Gauge-Mediated Supersymmetry Breaking Models: Experimental Constraints and Phenomenology at the LHC*, *Nucl.Phys.* **B810** (2009) 266–299, [0808.1104].

[224] B. Fuks, B. Herrmann and M. Klasen, *Phenomenology of anomaly-mediated supersymmetry breaking scenarios with non-minimal flavour violation*, *Phys.Rev.* **D86** (2012) 015002, [1112.4838].

[225] G. D. Kribs, A. Martin and T. S. Roy, *Squark Flavor Violation at the LHC*, *JHEP* **06** (2009) 042, [0901.4105].

[226] M. Backović, A. Mariotti and M. Spannowsky, *Signs of Tops from Highly Mixed Stops*, *JHEP* **06** (2015) 122, [1504.00927].

[227] M. Blanke, G. F. Giudice, P. Paradisi, G. Perez and J. Zupan, *Flavoured Naturalness*, *JHEP* **1306** (2013) 022, [1302.7232].

[228] A. A. Markov, *Extension of the limit theorems of probability theory to a sum of variables connected in a chain.* reprinted in Appendix B of: R. Howard, *Dynamic Probabilistic Systems, volume 1: Markov Chains*, John Wiley and Sons, 1971.

[229] N. Metropolis, A. W. Rosenbluth, M. N. Rosenbluth, A. H. Teller and E. Teller, *Equation of state calculations by fast computing machines*, *J. Chem. Phys.* **21** (1953) 1087–1092.

[230] W. K. Hastings, *Monte Carlo Sampling Methods Using Markov Chains and Their Applications*, *Biometrika* **57** (1970) 97–109.

[231] A. Gelman and D. B. Rubin, *Inference from iterative simulation using multiple sequences*, *Statist. Sci.* **7** (11, 1992) 457–472.

[232] Heavy Flavor Averaging Group (HFAG) collaboration, Y. Amhis et al., *Averages of b-hadron, c-hadron, and τ-lepton properties as of summer 2014*, 1412.7515.

[233] LHCb, CMS collaboration, *Observation of the rare $B^0\_s \to \mu^+\mu^-$ decay from the combined analysis of CMS and LHCb data*, *Nature* **522** (2015) 68–72, [1411.4413].

[234] LHCb collaboration, R. Aaij et al., *Differential branching fraction and angular analysis of the decay $B^0 \to K^{*0}\mu^+\mu^-$*, *JHEP* **1308** (2013) 131, [1304.6325].

[235] LHCb collaboration, *Angular analysis of the $B^0 \to K^{*0}\mu^+\mu^-$ decay*, LHCb-CONF-2015-002, 2015.

[236] BaBar collaboration, J. Lees et al., *Measurement of the $B \to X_s\ell^+\ell^+-$ branching fraction and search for direct CP violation from a sum of exclusive final states*, *Phys.Rev.Lett.* **112** (2014) 211802, [1312.5364].

[237] F. Mahmoudi, *SuperIso: A Program for calculating the isospin asymmetry of $B \to K^*$ gamma in the MSSM*, *Comput.Phys.Commun.* **178** (2008) 745–754, [0710.2067].

[238] F. Mahmoudi, *SuperIso v2.3: A Program for calculating flavor physics observables in Supersymmetry*, *Comput.Phys.Commun.* **180** (2009) 1579–1613, [0808.3144].

[239] W. Porod and F. Staub, *SPheno 3.1: Extensions including flavour, CP-phases and models beyond the MSSM*, *Comput.Phys.Commun.* **183** (2012) 2458–2469, [1104.1573].

[240] F. Mahmoudi, S. Heinemeyer, A. Arbey, A. Bharucha, T. Goto et al., *Flavour Les Houches Accord: Interfacing Flavour related Codes*, *Comput.Phys.Commun.* **183** (2012) 285–298, [1008.0762].

[241] M. Misiak et al., *Estimate of $\mathcal{B}(\bar{B} \to X_s\gamma)$ at $O(\alpha_s^2)$*, *Phys. Rev. Lett.* **98** (2007) 022002, [hep-ph/0609232].

[242] M. Misiak and M. Steinhauser, *NNLO QCD corrections to the $\bar{B} \to X_s\gamma$ matrix elements using interpolation in m(c)*, *Nucl.Phys.* **B764** (2007) 62–82, [hep-ph/0609241].

[243] M. Misiak and M. Poradzinski, *Completing the Calculation of BLM corrections to $\bar{B} \to X_s\gamma$*, *Phys.Rev.* **D83** (2011) 014024, [1009.5685].

[244] Y.-B. Dai, C.-S. Huang and H.-W. Huang, *$B \to X_s\tau^+\tau^-$ in a two Higgs doublet model*, *Phys.Lett.* **B390** (1997) 257–262, [hep-ph/9607389].

[245] A. Ghinculov, T. Hurth, G. Isidori and Y. Yao, *The Rare decay $B \to X_s l^+ l^-$ to NNLL precision for arbitrary dilepton invariant mass*, *Nucl.Phys.* **B685** (2004) 351–392, [hep-ph/0312128].

[246] T. Huber, E. Lunghi, M. Misiak and D. Wyler, *Electromagnetic logarithms in $\bar{B} \to X_s l^+ l^-$*, *Nucl.Phys.* **B740** (2006) 105–137, [hep-ph/0512066].

[247] T. Huber, T. Hurth and E. Lunghi, *Logarithmically Enhanced Corrections to the Decay Rate and Forward Backward Asymmetry in $\bar{B} \to X_s\ell^+\ell^-$*, *Nucl.Phys.* **B802** (2008) 40–62, [0712.3009].

[248] M. Beneke, T. Feldmann and D. Seidel, *Systematic approach to exclusive $B \to V l^+ l^-$, $V\gamma$ decays*, *Nucl.Phys.* **B612** (2001) 25–58, [hep-ph/0106067].

[249] M. Beneke, T. Feldmann and D. Seidel, *Exclusive radiative and electroweak $b \to d$ and $b \to s$ penguin decays at NLO*, *Eur.Phys.J.* **C41** (2005) 173–188, [hep-ph/0412400].

[250] F. Kruger and J. Matias, *Probing new physics via the transverse amplitudes of $B^0 \to K^{*0}(\to K^-\pi^+)l^+l^-$ at large recoil*, *Phys.Rev.* **D71** (2005) 094009, [hep-ph/0502060].

[251] U. Egede, T. Hurth, J. Matias, M. Ramon and W. Reece, *New observables in the decay mode $\bar{B}_d \to \bar{K}^{*0}l^+l^-$*, *JHEP* **0811** (2008) 032, [0807.2589].

[252] U. Egede, T. Hurth, J. Matias, M. Ramon and W. Reece, *New physics reach of the decay mode $\bar{B} \to \bar{K}^{*0}\ell^+\ell^-$*, *JHEP* **1010** (2010) 056, [1005.0571].

[253] A. Khodjamirian, T. Mannel, A. Pivovarov and Y.-M. Wang, *Charm-loop effect in $B \to K^{(*)}\ell^+\ell^-$ and $B \to K^*\gamma$*, *JHEP* **1009** (2010) 089, [1006.4945].

[254] H. Dreiner, K. Nickel, W. Porod and F. Staub, *Full 1-loop calculation of $BR(B^0_{s,d} \to \ell\bar{\ell})$ in models beyond the MSSM with SARAH and SPheno*, *Comput.Phys.Commun.* **184** (2013) 2604–2617, [1212.5074].

[255] A. J. Buras, P. H. Chankowski, J. Rosiek and L. Slawianowska, *$\Delta M_{d,s}, B^0 d, s \to \mu^+\mu^-$ and $B \to X_s\gamma$ in supersymmetry at large* $\tan\beta$, *Nucl.Phys.* **B659** (2003) 3, [hep-ph/0210145].

[256] G. Isidori and A. Retico, *$B_{s,d} \to \ell^+\ell^-$ and $K_L \to \ell^+\ell^-$ in SUSY models with nonminimal sources of flavor mixing*, *JHEP* **0209** (2002) 063, [hep-ph/0208159].

[257] S. Baek, T. Goto, Y. Okada and K.-i. Okumura, *Muon anomalous magnetic moment, lepton flavor violation, and flavor changing neutral current processes in SUSY GUT with right-handed neutrino*, *Phys.Rev.* **D64** (2001) 095001, [hep-ph/0104146].

[258] A. J. Buras, S. Jager and J. Urban, *Master formulae for Delta F=2 NLO QCD factors in the standard model and beyond*, *Nucl.Phys.* **B605** (2001) 600–624, [hep-ph/0102316].

[259] S. Herrlich and U. Nierste, *The Complete $|\Delta S| = 2$ - Hamiltonian in the next-to-leading order*, *Nucl.Phys.* **B476** (1996) 27–88, [hep-ph/9604330].

[260] A. J. Buras, T. Ewerth, S. Jager and J. Rosiek, *$K^+ \to \pi^+\nu\bar{\nu}$ and $K(L) \to \pi^0\nu\bar{\nu}$ decays in the general MSSM*, *Nucl.Phys.* **B714** (2005) 103–136, [hep-ph/0408142].

[261] G. Colangelo and G. Isidori, *Supersymmetric contributions to rare kaon decays: Beyond the single mass insertion approximation*, *JHEP* **9809** (1998) 009, [hep-ph/9808487].

[262] A. Crivellin, L. Hofer and J. Rosiek, *Complete resummation of chirally-enhanced loop-effects in the MSSM with non-minimal sources of flavor-violation*, *JHEP* **1107** (2011) 017, [1103.4272].

[263] T. Ibrahim and P. Nath, *CP violation and the muon anomaly in N=1 supergravity*, *Phys.Rev.* **D61** (2000) 095008, [hep-ph/9907555].

[264] D. M. Pierce, J. A. Bagger, K. T. Matchev and R.-j. Zhang, *Precision corrections in the minimal supersymmetric standard model*, *Nucl.Phys.* **B491** (1997) 3–67, [hep-ph/9606211].

[265] G. Degrassi, P. Slavich and F. Zwirner, *On the neutral Higgs boson masses in the MSSM for arbitrary stop mixing*, *Nucl.Phys.* **B611** (2001) 403–422, [hep-ph/0105096].

[266] A. Brignole, G. Degrassi, P. Slavich and F. Zwirner, *On the $O(\alpha(t)^2)$ two loop corrections to the neutral Higgs boson masses in the MSSM*, *Nucl.Phys.* **B631** (2002) 195–218, [hep-ph/0112177].

[267] A. Brignole, G. Degrassi, P. Slavich and F. Zwirner, *On the two loop sbottom corrections to the neutral Higgs boson masses in the MSSM*, *Nucl.Phys.* **B643** (2002) 79–92, [hep-ph/0206101].

[268] A. Dedes, G. Degrassi and P. Slavich, *On the two loop Yukawa corrections to the MSSM Higgs boson masses at large* $\tan\beta$, *Nucl.Phys.* **B672** (2003) 144–162, [hep-ph/0305127].

[269] A. Dedes and P. Slavich, *Two loop corrections to radiative electroweak symmetry breaking in the MSSM*, *Nucl.Phys.* **B657** (2003) 333–354, [hep-ph/0212132].

[270] B. Allanach, A. Djouadi, J. Kneur, W. Porod and P. Slavich, *Precise determination of the neutral Higgs boson masses in the MSSM*, *JHEP* **0409** (2004) 044, [hep-ph/0406166].

[271] M. Arana-Catania, S. Heinemeyer, M. Herrero and S. Penaranda, *Higgs Boson masses and B-Physics Constraints in Non-Minimal Flavor Violating SUSY scenarios*, *JHEP* **1205** (2012) 015, [1109.6232].

[272] J. Camargo-Molina, B. O'Leary, W. Porod and F. Staub, **Vevacious***: A Tool For Finding The Global Minima Of One-Loop Effective Potentials With Many Scalars*, *Eur.Phys.J.* **C73** (2013) 2588, [1307.1477].

[273] G. Degrassi, S. Di Vita, J. Elias-Miro, J. R. Espinosa, G. F. Giudice et al., *Higgs mass and vacuum stability in the Standard Model at NNLO*, *JHEP* **1208** (2012) 098, [1205.6497].

[274] D. Buttazzo, G. Degrassi, P. P. Giardino, G. F. Giudice, F. Sala et al., *Investigating the near-criticality of the Higgs boson*, *JHEP* **1312** (2013) 089, [1307.3536].

[275] CMS collaboration, *Search for electroweak SUSY production in multilepton final states in pp collisions at sqrt(s)=13 TeV with 12.9/fb*, CMS-PAS-SUS-16-024, 2016.

[276] CMS collaboration, *Search for SUSY with multileptons in 13 TeV data*, CMS-PAS-SUS-16-022, 2016.

[277] G. Ferretti, A. Mariotti, K. Mawatari and C. Petersson, *Multiphoton signatures of goldstini at the LHC*, *JHEP* **04** (2014) 126, [1312.1698].

[278] T. Liu, L. Wang and J. M. Yang, *Higgs decay to goldstini and its observability at the LHC*, *Phys. Lett.* **B726** (2013) 228–233, [1301.5479].

[279] T. Liu, L. Wang and J. M. Yang, *Pseudo-goldstino and electroweakinos via VBF processes at LHC*, *JHEP* **02** (2015) 177, [1411.6105].

[280] S. P. Liew, A. Mariotti, K. Mawatari, K. Sakurai and M. Vereecken, *Z-peaked excess in goldstini scenarios*, *Phys. Lett.* **B750** (2015) 539–546, [1506.08803].

[281] S. S. AbdusSalam, B. C. Allanach, F. Quevedo, F. Feroz and M. Hobson, *Fitting the Phenomenological MSSM*, *Phys. Rev.* **D81** (2010) 095012, [0904.2548].

[282] *CMS Luminosity - Public Results*, retrieved from https://twiki.cern.ch/twiki/bin/view/CMSPublic/LumiPublicResults on July 26, 2016.

[283] *Search for resonances decaying to photon pairs in 3.2 fb^{-1} of pp collisions at $\sqrt{s}$ = 13 TeV with the ATLAS detector*, ATLAS-CONF-2015-081, 2015.

[284] CMS collaboration, *Search for new physics in high mass diphoton events in proton-proton collisions at 13TeV*, CMS-PAS-EXO-15-004, 2015.

[285] ATLAS collaboration, *Search for scalar diphoton resonances with 15.4 fb^{-1} of data collected at $\sqrt{s}$=13 TeV in 2015 and 2016 with the ATLAS detector*, ATLAS-CONF-2016-059, 2016.

[286] CMS collaboration, *Search for resonant production of high mass photon pairs using* $12.9\,\mathrm{fb}^{-1}$ *of proton-proton collisions at* $\sqrt{s} = 13$ TeV *and combined interpretation of searches at 8 and 13 TeV*, CMS-PAS-EXO-16-027, 2016.

Summary

Elementary particle physics aims at answering the question 'What are the fundamental building blocks of Nature and how do they interact?' It turns out that the constituents of all matter can be brought back to a rather small number of fundamental particles which are described in the Standard Model (SM) of particle physics. The SM describes most experimental observations very well and is considered to be a very successful theory. There remain, however, still some unanswered questions. The SM fails to explain neutrino oscillations, it does not offer a candidate for dark matter/energy, does not include gravity and exhibits an undesirable sensitivity to very small variations of some of its parameters. This motivates us to keep searching for physics Beyond the Standard Model (BSM).

The search for BSM was one of the main motivations to build the Large Hadron Collider (LHC) at the CERN laboratory in Geneva. The LHC performs proton-proton collisions at a very high energy in the hope of creating and observing new, unknown particles or phenomena. However, a huge amount of particles are created in each collision and searching for new physics is very much like searching for a needle in a haystack. It is crucial to have a good understanding of what we would expect to see at the LHC based on the SM or any other theory we might formulate. Particle physics phenomenology aims at facilitating this connection between theory and experiment and it is in this field of research that this thesis is situated. In particular, this work focusses on the phenomenology of a well-motivated BSM candidate, supersymmetry.

Supersymmetry (SUSY) predicts that for every particle of the SM, there exists an extra supersymmetric particle, its superpartner. Signs of supersymmetry have been sought for already for a long time, but not a single supersymmetric particle has yet been detected. However, supersymmetry encompasses a very broad class of models and up to now mainly the most straightforward realisations of SUSY have been studied. The lack of positive results motivates us to broaden our view and also search for less straightforward and less conventional signatures of supersymmetry. In this thesis we go beyond minimal SUSY, we study to which extent the current experimental data allow for this extension and how this would change the SUSY phenomenology. We follow three different approaches.

The first project starts with an experimental observation. Even though no conclusive evidence for new physics has been found, yet some hints for new

physics have been observed at the LHC. We look at one of those and show that it can be explained within a, rather unusual, supersymmetric set-up. The second project has a more theoretical origin. If SUSY were an exact symmetry of Nature, the SM particles and their SUSY partners would have equal masses. Since we did not observe any superpartner yet, this is clearly not the case and we know that SUSY has to be broken. We investigate an extension of the usual SUSY-breaking mechanism and find that such a scenario can soften the constraints on supersymmetry. In a third project we look at generation mixing between the superpartners of the quarks. Despite the strong experimental limits, we conclude generation mixing is still allowed. Moreover, we note that it influences the expectations about the nature of the lightest SUSY particle, which is relevant for experimental analyses.

We can hence conclude that less conventional supersymmetric scenarios can influence the interpretation of the current experimental limits and lead to signatures which are currently overlooked. It is therefore important to also take these scenarios into account, only then can we get a comprehensive view on supersymmetry and its constraints.

Samenvatting

De elementaire deeltjes fysica zoekt naar een antwoord op de vraag 'Wat zijn de fundamentele bouwstenen van de materie en hoe interageren ze?' Het blijkt dat alle materie is opgebouwd uit een beperkt aantal elementaire deeltjes, beschreven in het Standaard Model (SM) van de deeltjesfysica. Het SM wordt beschouwd als een succesrijke theorie aangezien het de meeste experimentele observaties met een grote nauwkeurigheid beschrijft. Sommige vragen blijven echter onbeantwoord. Het SM geeft geen verklaring voor neutrino oscillaties of donkere materie/energie, het omvat de zwaartekracht niet en is heel gevoelig voor een kleine verandering van sommige van de parameters zodat het ook vanuit theoretisch standpunt niet helemaal tevreden stelt. Dit motiveert ons om verder te zoeken naar nieuwe fysica voorbij het SM.

De zoektocht naar nieuwe fysica was één van de voornaamste motivaties voor het bouwen van een deeltjesversneller, de Large Hadron Collider (LHC), op het CERN, het onderzoekscentrum te Genève. De LHC botst protonen met hoge energie op elkaar in de hoop nieuwe, ongekende deeltjes te creëren en te observeren. Bij elke botsing wordt echter een enorm aantal deeltjes geproduceerd en zoeken naar nieuwe fysica heeft dus veel weg van het zoeken naar een naald in een hooiberg. Een goed begrip van wat we op basis van het SM, of een alternatieve theorie, verwachten te zien is bijgevolg cruciaal. Het onderzoeksdomein van de fenomenologie van de deeltjesfysica houdt zich bezig met deze connectie tussen theorie en experiment en dit is ook het onderwerp van deze thesis. In het bijzonder bestudeert dit werk de fenomenologie van supersymmetrie, een goed gemotiveerde kandidaat voor nieuwe fysica.

Supersymmetrie (SUSY) voorspelt dat er voor elk SM deeltje een extra supersymmetrisch deeltje bestaat, zijn superpartner. Hoewel er al lang in deeltjesversnellers naar een teken van SUSY gezocht wordt, werd tot op vandaag nog geen enkel supersymmetrisch deeltje waargenomen. Supersymmetrie omvat echter een heel brede waaier aan modellen en tot nog toe werden voornamelijk de meest voor de hand liggende modellen bestudeerd. Het uitblijven van een positief resultaat motiveert ons om onze blik te verruimen en ook te zoeken naar minder voor de hand liggende tekenen van supersymmetrie. In deze thesis kijken we verder dan de minimale realisaties van supersymmetrie, we onderzoeken in welke mate de huidige experimentele data die uitbreiding toelaat en hoe dit de fenomenologie

verandert. We doen dit vanuit drie verschillende invalshoeken.

Het eerste project begint bij een experimentele waarneming. Er is dan wel nog geen sluitend bewijs gevonden voor nieuwe fysica, dat neemt niet weg dat er wel een paar, weliswaar nog niet significante, hints for nieuwe fysica waargenomen werden bij de LHC. We bekijken één dergelijke waarneming en tonen aan dat die verklaard kan worden met behulp van een, eerder ongewoon, supersymmetrisch model. Een tweede project vindt zijn motivatie eerder in de theorie. Als SUSY een exacte symmetrie was van de natuur, dan zouden de SM deeltjes en hun superpartners dezelfde massa moeten hebben. Aangezien we nog geen enkele superpartner waargenomen hebben is dit duidelijk niet het geval zodat we weten dat SUSY gebroken moet zijn. We bekijken een uitbreiding van het gebruikelijke brekingsformalisme en vonden dat een dergelijk scenario de limieten op supersymmetrie kan verzachten. In een derde project onderzoeken we wat er gebeurt als we de generaties van de supersymmetrische partners van de quarks opmengen. Ondanks de sterke experimentele limieten concluderen we dat dit nog steeds toegestaan is. We merken bovendien op dat het opmengen van generaties een invloed heeft op de aard van de lichtste SUSY deeltjes, dit is van belang voor experimentele analyses.

We kunnen dus besluiten dat de interpretatie van de huidige experimentele limieten op supersymmetrie veranderen wanneer we minder conventionele SUSY scenarios bekijken. Het is dus van belang ook met deze scenarios rekening te houden, alleen zo kunnen we een correct en volledig beeld krijgen van supersymmetrie.

Acknowledgements

Thinking back about the past five years, makes me realize how much I received from the people surrounding me. It clearly takes much more than just one PhD student to finalize a PhD and I would like to use these last pages to express my gratitude to all of you. I tried to be complete but I apologize in advance for those I might have forgotten.

First of all, I would like to thank my promotor Jorgen D'Hondt for being such an enthusiastic, inspiring and creative supervisor. Thanks for the chances you gave me and for the always open door, I always left more optimistic than I came. I also owe a lot of gratitude to Kentarou Mawatari, Benjamin Fuks and Alberto Mariotti who shared my supervision. Thanks for all opportunities you gave me, for the guidance and the willingness to help me. Each of you taught me a different way of thinking and they all proved to be very useful. I owe special thanks to Benjamin and Michelangelo Mangano who gave me the opportunity to spend half a year at the department of Theoretical Physics at CERN and I am also grateful to Fabio Maltoni for his support and useful discussions. I also would like to thank Adam, Ben, Björn, Christoffer, Diego, Gabriele, Nadja, Nazila, Sezen, Riccardo, Werner and Yoshitaro for the very pleasant and fruitful collaborations during the past years.

The phenomenology group at the VUB is part of the IIHE as well as TENA and it was a true pleasure to join the activities of both research groups. I am very grateful to Marleen, Merel and Audrey for the always kind and efficient administrative support and for creating such a warm atmosphere at the institute. I really enjoyed the coffee breaks, team building activities, Christmas parties, barbecues, Sinterklaas-breakfasts, vastenavond-waffles and everything else... Thanks! These events would off course not have been so enjoyable without my all my colleagues at the IIHE/TENA. Thanks a lot for the nice and friendly atmosphere! I additionally would like to thank the IT-team, without the computing resources and IT-support at the IIHE, this work would not have been there, merci!

I would like to thank Tina, my former office mate, with whom I shared much more than merely an office. Thanks for the nice daily chats and the good times at summer schools and conferences. I also would like to thank my current office mates, Matthias V. and Dries. Onze vaak ietwat absurde conversaties en jullie steun en advies hebben me heel erg geholpen bij het afwerken van mijn doctoraat,

bedankt en ik wens jullie veel geluk verder! I would further like to thank Priscila, Pantelis and Bryan for the nice time at the VUB, Christine, Frederic, Jan, Michal, Matthijs, Rob and in particular Matthias S. for the good times at CERN and Céline, Claude, Olivier M. and in fact the whole MadGraph/FeynRules-team for the kind help and all the pleasant workshops and schools during the past years. Ook mijn collega's bij het lesgeven, zowel Ben Craps als het volledige TGT-team, zou ik graag bedanken. Het was een plezier met jullie samen te werken!

Dan rest mij nog een meer dan aanzienlijk wolkje dankbaarheid voor mijn familie en vrienden. Dank je wel, mama en papa, om er altijd voor mij te zijn, voor de morele steun en voor de duwtjes in de rug waar nodig. Dank je, zus, voor je eeuwige enthousiasme, onze poëtische reisjes en het ontwerp van de cover en tussenbladen, hiervoor zou ik ook graag Trui bedanken. Ook bedankt aan mijn twee broers, schoonzussen, neefjes, mijn metekindje en de rest van de familie voor alle fijne feestjes en familieweekends. Ik heb ook heel erg genoten van jullie enthousiaste bezoek aan CERN. Heel erg bedankt aan mijn huisgenoten in de Kasterlindenstraat, het was fijn door zo een grote verscheidenheid omringd te zijn, jullie maakten mijn stekje hier in Brussel tot een thuis. Ook bedankt aan Olivier D. voor de talloze theetjes, wandelingen, concerten en zoveel meer en aan Mateusz, Nadja, Pieter en Tine voor alles wat we de laatste jaren samen gedaan hebben.

Last but not least, I would like to thank the members of the jury for their careful reading and constructive questions and comments, I believe they improved my thesis a lot. I am also grateful to the VUB (GOA 'Supersymmetric models and their signatures at the Large Hadron Collider'), FWO Vlaanderen and the ERC grant 291377 for their financial support.